SCUOLA DI DOTTORATO
UNIVERSITÀ DEGLI STUDI DI MILANO-BICOCCA

Department of Medicine and Surgery
PhD program in Translational and Molecular Medicine
(DIMET) Cycle XXXV

Understanding T and NK cell reconstitution after allogeneic hematopoietic cell transplantation: a path to improve graft *versus* leukemia and minimize graft *versus* host disease

Surname: Rambaldi Name: Benedetta

Registration number: 710883

Tutor: Andrea Biondi

Co-tutor: Jerome Ritz

Coordinator: Andrea Biondi

ACADEMIC YEAR 2021/2022

To the "hopeless cases"

"Sydney Farber's entire purpose consist only of hopeless cases."

- *Medical World News,*

November 25, 1966

Table of Contents

Chapter 1

General introduction

Hematopoietic cell transplantation (HCT) represents a cardinal therapy for hematological malignancy otherwise incurable. The practice over the last decades has improved in term of safety, efficacy, and donor availability. However, patients still experience a considerable risk of disease recurrence and transplant related mortality, primarily due to graft versus host disease (GVHD) and infections (1).

The main actor of this complex cellular treatment is the donor immune system (IS) that has the role to recognize and kill the patient cancer cells and to protect the host from infections. Understanding the reconstitution of the transferred IS and the different dynamics is crucial to improve the outcome of patients undergoing HCT (2). Immune reconstitution (IR) after HCT, especially of the adaptive IS, is highly variable between patients and can take several months to even years. A timely and balanced IR is especially important for sustained graft-versus-leukemia (GVL) effects, protection against opportunistic infections, and survival chances after HCT. However, immune-suppressive drugs are often needed during the first months after transplant to induce immune-tolerance between the donor IS and the recipient. This is detrimental for avoiding GVHD, but it is also the cause of the induced immunocompromised status in the patient (3).

In this regards, T and NK cells represent two major players in the reconstitution of the new IS and in the protection against infection and disease recurrence, but they are also involved in the pathogenesis

of GVHD. Hence, there is a clear need to develop strategies to better predict, enhance, and modulate T- and NK-cell recovery and function after HCT.

Multiple variables may influence the T and NK-cell IR (4):

- Pre-transplant factors, such as cell source, cell dose, donor-recipient matching, graft manipulation and conditioning regimens.
- Peri-transplant factors, such as the nutritional status of the patient and the composition of the gut microbiome.
- Post-transplant factors, such as occurrence of GVHD, infections or relapse.

Several interventions can be done at different time to improve both T- and NK-cells reconstitution (4):

- Enhance the immune system using cytokine administration such as IL-2 or IL-15, to boost a specific cell subset, T regulatory cells (Treg) and NK ells respectively.
- Add cellular therapy for both GVHD (Treg infusions or mesenchymal stromal cells (MSC) infusion) and GVL (donor lymphocyte infusion (DLI), cytokine-induced memory-like (CIML) NK cells, cytokine-induced killer (CIK) cells or chimeric antigen receptor (CAR) T cell infusion).
- Use check-point inhibitor such as abatacept (CTLA4-Ig, anti CD80/CD86) and itolizumab (antiCD6 antibody) for GVHD prevention/treatment or sabatolimab (TIM3 inhibitor), nivolumab and pembrolizumab (PD-1 inhibitors) and atezolizumab (PD-L1 inhibitor) for the GVL enhancement.

In conclusion, a comprehensive knowledge of the dynamics of the IR after HCT is needed to approach and tailor novel strategy to improve patient's outcome after HCT.

Scope of the thesis

The aims pf my PhD thesis are:

- Performing a deep analysis of T and NK cells reconstitution after different HCT platforms in order to find new strategy to improve the transplant outcomes (GVL and GVHD).
- Exploring the activity of cytokine-induced memory-like (CIML) NK cells for the treatment of myeloid malignancies relapsing after HCT.
- Targeting the CD6-ALCAM pathway in T cells for the treatment of GVHD.

All these topics are discussing in the chapters of this thesis and represent the main objectives of the publications that I have produced during my PhD.

References

1. Copelan EA. Hematopoietic Stem-Cell Transplantation [Internet]. N. Engl. J. Med. 2006;354(17):1813–1826.
2. Ogonek J et al. Immune Reconstitution after Allogeneic Hematopoietic Stem Cell Transplantation [Internet]. Front. Immunol. 2016;7:507.
3. van den Brink MRM, Velardi E, Perales M-A. Immune reconstitution following stem cell transplantation [Internet]. Hematology 2015;2015(1):215–219.
4. de Koning C, Nierkens S, Boelens JJ. Strategies before, during, and after hematopoietic cell transplantation to improve T-cell immune

reconstitution [Internet]. Blood 2016;128(23):2607–2615.

Chapter 2

Key Aspects of the Immunobiology of Haploidentical Hematopoietic Cell Transplantation

Susanne H. C. Baumeister[1,2,3], **Benedetta Rambaldi**[3,4,5], Roman M. Shapiro[3,4] and Rizwan Romee [3,4]*

[1] Division of Pediatric Hematology-Oncology, Boston Children's Hospital, Boston, MA, United States, [2] Department of Pediatric Oncology, Dana-Farber Cancer Institute, Boston, MA, United States, [3] Harvard Medical School, Boston, MA, United States, [4] Division of Hematologic Malignancies, Dana-Farber Cancer Institute, Boston, MA, United States, [5] Bone Marrow Transplant Unit, Clinical and Experimental Sciences Department, ASST Spedali Civili, University of Pavia, Brescia, Italy

Frontiers in Immunology 2020 Feb 14;11:191

doi: 10.3389/fimmu.2020.00191. eCollection 2020.PMID: 32117310

Abstract

Hematopoietic stem cell transplantation from a haploidentical donor is increasingly used and has become a standard donor option for patients lacking an appropriately matched sibling or unrelated donor. Historically, prohibitive immunological barriers resulting from the high degree of HLA-mismatch included graft-vs.-host disease (GVHD) and graft failure. These were overcome with increasingly sophisticated strategies to manipulate the sensitive balance between donor and recipient immune cells. Three different approaches are currently in clinical use: (a) *ex vivo* T-cell depletion resulting in grafts with defined immune cell content (b) extensive immunosuppression with a T-cell replete graft consisting of G-CSF primed bone marrow and PBSC (GIAC) (c) T-cell replete grafts with post-transplant cyclophosphamide (PTCy). Intriguing studies have recently elucidated the immunologic mechanisms by which PTCy prevents GVHD. Each approach uniquely affects post-transplant immune reconstitution which is critical for the control of post-transplant infections and relapse. NK-cells play a key role in haplo-HCT since they do not mediate GVHD but can successfully mediate a graft-vs.-leukemia effect. This effect is in part regulated by KIR receptors that inhibit NK cell cytotoxic function when binding to the appropriate HLA-class I ligands. In the context of an HLA-class I mismatch in haplo-HCT, lack of inhibition can contribute to NK-cell alloreactivity leading to enhanced anti-leukemic effect. Emerging work reveals immune evasion phenomena such as copy-neutral loss of heterozygosity of the incompatible HLA alleles as one of the major mechanisms of relapse. Relapse and infectious complications remain the leading causes impacting overall survival and

are central to scientific advances seeking to improve haplo-HCT. Given that haploidentical donors can typically be readily approached to collect additional stem- or immune cells for the recipient, haplo-HCT represents a unique platform for cell- and immune-based therapies aimed at further reducing relapse and infections. The rapid advancements in our understanding of the immunobiology of haplo-HCT are therefore poised to lead to iterative innovations resulting in further improvement of outcomes with this compelling transplant modality.

INTRODUCTION

Allogeneic hematopoietic cell transplantation (HCT) remains a curative approach for many patients with malignant and non-malignant hematologic indications (1). However, timely availability of a suitable HLA-matched sibling donor (MSD) or adequately HLA-matched unrelated donor (MUD) remains a significant challenge in providing access to HCT. The likelihood of finding an optimal donor varies significantly among racial and ethnic groups with the chances of finding an appropriate donor ranging from 75% for whites of European descent to 16% for blacks of South or Central American descent (2). Although most candidates for HCT will have a donor or cord blood unit considered suitable (HLA-matched or minimally mismatched), even single allele mismatches negatively impact patient outcomes after HCT (3). Additionally, proceeding with an unrelated donor is a time- and cost- consuming process that can result in delay or suboptimal timing of HCT.

In contrast, haploidentical donors are available for >95% of patients in need of HCT (4). Biological children, parents, siblings, and frequently more distant family members who share one haplotype potentially qualify as donors (**Figure 1**). They can be readily identified and are typically available and motivated to donate bone marrow (BM) or peripheral blood stem cells (PBSC) to their family member in a timely fashion. This is particularly beneficial when unexpected events delay or expedite the need for HCT. Moreover, haploidentical donors can readily be tested in situations where there is concern for an underlying familiar predisposition syndrome and are typically available for a repeat stem cell collection, donor lymphocyte infusion or other cell therapeutic approaches which may be indicated if post-transplant complications such as graft failure, relapse, or infectious complications arise. Finally, if the selected family member had a poor stem cell mobilization for a PBSC graft or the optimal graft composition was not achieved then a different family member can be approached to serve as a haploidentical donor.

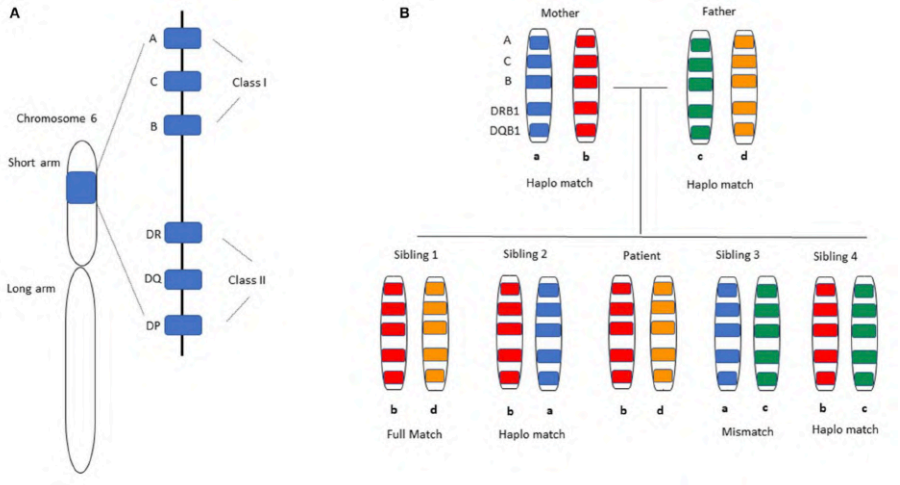

Figure 1. HLA-matching in Haplo-HCT. (A) Distribution of HLA alleles on chromosome 6. All HLA alleles exist on the short arm of the chromosome, specifically 6p21.3. The classical HLA classification system is used clinically for matching donors and recipients in the transplant setting. HLA class I alleles -A, -B, and -C are expressed on all nucleated cells and display antigen to CD8+ T-cells, while HLA Class II alleles -DR, -DQ, -DP are expressed on antigen-presenting cells and initiate a response by CD4+ T-cells. Not shown are the non-classical HLA Class I alleles -E, -F, -G, -H, -J that are also present on the same chromosome arm. (B) A representative inheritance pattern of HLA alleles is demonstrated. For a patient with HLA allele distribution (b) and (d) as shown in the middle, each sibling has a 25% chance of being a full match based on inheritance of the same maternal (b) and paternal (d) alleles as the patient. Each sibling has a 50% chance of being a haploidentical match by virtue of having inherited one identical allele (b) from the parents. The likelihood of having inherited neither of the parental alleles that were inherited by the patient is 25% (complete HLA-mismatch).

Historically, haploidentical HCT (haplo-HCT) was associated with high rates of graft vs. host disease (GVHD) and graft failure (5–7). With the introduction of efficient T-cell depletion (TCD) of the graft (8), haplo-HCT became feasible from a GVHD perspective. However, TCD led to an imbalance between host and donor T cells resulting in high rates of graft failure. This imbalance was overcome with the use of T-cell depleted "megadose" stem cell grafts (9, 10). Since then, nuanced *ex vivo* approaches to optimize the immunological composition of haploidentical grafts have been developed as outlined in this review.

A major milestone in promoting the wide-spread use and cost-efficient accessibility of haplo-HCT, including in resource-poor countries, was reached with the use of high-dose post-transplant cyclophosphamide (PTCy) to achieve *in vivo* attenuation of T cell alloreactivity (11). A different strategy using Granulocyte-colony

stimulating factor (G-CSF) mobilized bone marrow grafts with extensive immunosuppression has been similarly feasible (12). In addition, a special emphasis is being placed on using natural killer (NK) cells to harness both innate and adaptive immunity in haplo-HCT. NK cells are uniquely regulated by activating and inhibitory receptors and can mediate a critical graft-vs.-leukemia (GVL) effect, also referred to as NK-cell alloreactivity, without mediating GVHD (13–15).

These approaches have contributed to a surge in the use of haplo-HCT in recent years (16). Furthermore, dramatic advances in the field of adoptive immune cell transfer have been applied to the haplo-HCT platform whereby donors could be readily approached for additional cell collections to enhance immunity against infections and relapse (17, 18). As haplo- HCT evolves to refine and establish its role in the field of transplantation, it is critical to examine the immunobiological properties unique to haplo-HCT and the effect of *ex vivo* or *in vivo* graft manipulation on the immunological content and trajectory of immune reconstitution.

CHALLENGES OF THE HLA-BARRIER IN HAPLO-HCT

Early trials of T-cell-replete haplo-HCT were associated with poor outcomes due to a high incidence of GVHD and graft rejection, resulting in ∼10% long-term survival (5–7, 19, 20). In the setting of grafting across a haploidentical HLA barrier, ∼2% of donor T cells mediate alloreactive reactions resulting in GVHD while residual host T cells mount host-vs.-graft responses leading to graft rejection (21–23). The ability to overcome the problem of GVHD despite the large HLA-disparity in haplo-HCT was first demonstrated by Reisner and

colleagues with the successful transplantation of children with severe combined immunodeficiency (SCID) using T-cell depleted haploidentical grafts which differed at three major HLA loci (8). However, when this approach was extended to other indications in which a patient's underlying immune system is generally functional, the minimal T-cell content in the graft resulted in unopposed host- vs.-graft rejections and a high rate of graft failure. The latter was mediated by recipient anti-donor T lymphocyte precursors that survived the conditioning regimen (22, 24, 25), as well as anti-donor HLA antibodies (26) (**Figure 2**).

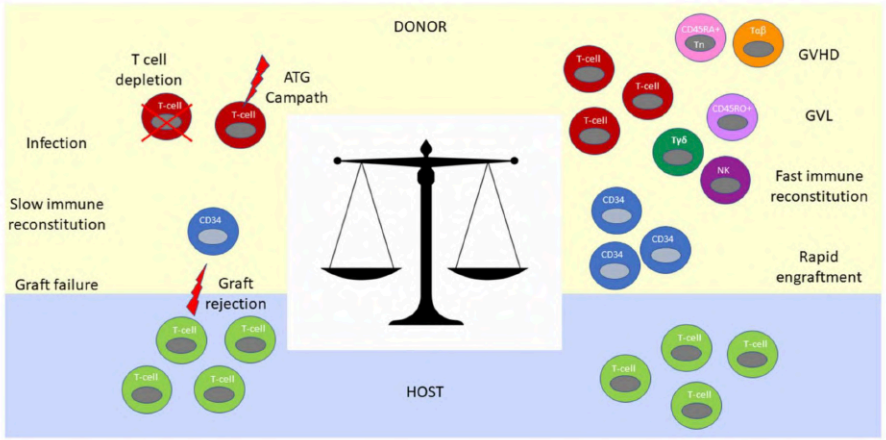

Figure 2. Immunological balance determines outcomes after haplo-HCT. The graft contains CD34+ and CD34− hematopoietic cells. CD34+ progenitor and stem cells are required for engraftment and reconstitution of the bone marrow after transplantation into the host. T cells in the graft facilitate neutrophil engraftment, immune reconstitution, post-transplant infectious immunity and exert GVL effect (Right). However, without an ex vivo (T cell depletion or CD34 positive selection) or in vivo (ATG or Campath) T cell depletion strategy, they mediate prohibitively severe GVHD (Right). In contrast, extensive T cell depletion from the graft results in an immunologic imbalance between residual host and donor T cells favoring graft rejection (Left). Extensive T cell depletion of the graft also results in slow immune

constitution, infections and poor GVL control. To achieve an optimal immunologic balance, novel graft manipulation approaches selectively deplete T cells involved in GVHD (CD45RA+ T cell and αβ- T cell depletion strategies), while maintaining beneficial immune cells such as NK cells and γδT cells in the graft.

A second breakthrough that paved the way toward the broad application of haplo-HCT was the use of "megadose" grafts, targeting the infusion of a stem cell product containing on the order of $\geq 10 \times 10^6$/kg $CD34^+$ hematopoietic stem cells while retaining the threshold dose of $\leq 4 \times 10^4$/kg T cells established in the SCID patients (9, 10, 27, 28). The underlying immunologic effect of megadose grafting was attributed to tolerance induction of host anti-donor cytotoxic T cell precursors by donor $CD34^+$ stem cells or by $CD34^+$ derived regulatory immune cells endowed with a "veto"-effect in a TNFα mediated mechanism (29, 30). Intensified myeloablative conditioning (MAC) with 8 Gy total body irradiation (TBI), thiotepa, rabbit anti-thymocyte globulin (ATG) and fludarabine (replacing cyclophosphamide after 1995) (31) to eliminate host T cells, followed by G-CSF mobilized megadose T-cell depleted PBSC grafts (initially using soybean agglutination and erythrocyte resetting and later immunomagnetic selection of $CD34^+$ HSCs) without any additional post-transplant immunosuppression was refined over the years (28, 32). This approach ultimately demonstrated primary engraftment in 95% of patients with acute leukemia ($n = 104$), with 6 of 7 patients who initially experienced graft failure engrafting successfully after second transplantation. Although acute and chronic GVHD were largely prevented, a significant non-relapse mortality (NRM) of 36.5% was observed

largely owing to post-transplant infections (27 of the 38 patients died of infectious complications) and substantial relapse risk. The 2-year event-free survival (EFS) probability among patients receiving transplantation in any complete remission (CR) was 47%, while the EFS for those transplanted in relapse was 4% (27).

Despite the tremendous advances toward clinical feasibility of haplo-HCT, these early studies embodied the challenge of achieving a sensitive immunologic balance during transplantation across haploidentical HLA-barriers. This challenge is reflective of the need for extensive T-cell depletion and immunosuppression to control GVHD on the one hand, and facilitation of engraftment, immune reconstitution, protection from infections, and prevention of relapse on the other (**Figure2**). This conundrum has fueled the iterative improvement of modulating immunity in the context of haplo-HCT as outlined below.

CURRENT HAPLO-HCT PLATFORMS

In vivo Haplo-HCT Strategies with Unmanipulated Stem Cell Grafts

Post-transplantation Cyclophosphamide (PTCy)

Post-transplantation high-dose cyclophosphamide (PTCy), when administered in a specific time-frame after graft infusion, efficiently attenuates alloreactive T cells from both donor and host and prevents GVHD and graft rejection. This immunological effect of PTCy was first observed in the 1960s in animal models of allogeneic skin grafts whereby cyclophosphamide administration within a window of up to 4 days after grafting delayed rejection (33). Subsequent

preclinical studies defined the role of PTCy in the setting of allogeneic HCT and showed the benefits of its use with respect to engraftment and GVHD (34–36). Importantly the concurrent immunosuppression of T cells with cyclosporine or steroids interfered with PTCy-tolerogenic effects (37, 38), indicating that high proliferative rates are critical for the PTCy immunomodulatory mechanism (39).

Initial mechanistic studies based on murine skin allografting models attributed the PTCy-effect to the selective depletion of alloreactive T cells. Based on these hypotheses, the presumed depletion was dependent on the heightened cytotoxic sensitivity of newly primed and highly proliferative alloreactive T cells (particularly $CD4^+$ T cells) at the peak of anti-host and anti- donor T cell expansion, aided by a favorable balance between effector T cells and regulator T cells (Tregs) as well as an additional intra-thymic clonal deletion of alloreactive T cell precursors (40–44). Suppressive immune cells were only felt to have an adjunct role in maintaining tolerance (45, 46). However, recent work by Kanakry and colleagues formally tested the putative immunologic mechanisms (selective destruction of alloreactive T cells, intra-thymic clonal deletion of alloreactive T cells and induction of suppressor T cells) in dedicated murine PTCy haplo-HCT models (47). These studies suggest that PTCy reduces $CD4^+$ T cell proliferation but does not eliminate alloreactive T cells and instead functionally impairs the T-cell response to alloantigens and induces the rapid and preferential recovery and expansion of regulatory T cells (Treg). Treg resistance to PTCy is based on their differential expression of aldehyde dehydrogenase (ALDH) (48). Evidence for the importance of the role of Tregs after PTCy is exemplified by the development of severe and

fatal GVHD in the context of Foxp3^{+} Treg depletion, as well as additional data showing that Tregs are required for PTCy-mediated protection against GVHD (49). Studies in thymectomized mice also suggested the dispensability of the thymus in this process (47). Advances in this active field of preclinical and clinical study are poised to further elucidate and facilitate adaption of the PTCy platform for different clinical scenarios. Increasing experience with this platform and the potential for PTCy-mediated bi-directional tolerance induction also lends itself to further exploration of this approach in the setting of combined solid organ and bone marrow transplantation (44).

The first clinical study of unmanipulated haplo-HCT with PTCy was conducted in the setting of non-myeloablative (NMA) conditioning with administration of PTCy at 50 mg/kg on day +3 and an added immunosuppressive regimen of mycophenolate mofetil (MMF) and tacrolimus starting on day +4 in 13 patients (50) (**Figures 3A**, **4C**). Subsequent prospective clinical trials, administering PTCy either on day +3 or on days +3 and +4, demonstrated rates of graft failure and GVHD comparable to those reported with reduced intensity conditioning (RIC) HLA-matched sibling and MUD HCTs with a trend toward a lower risk of extensive chronic GVHD among recipients of two doses of PTCy (50). These studies paved the way for the increased investigation and clinical use of haplo-HCT with PTCy (**Figure 3B**).

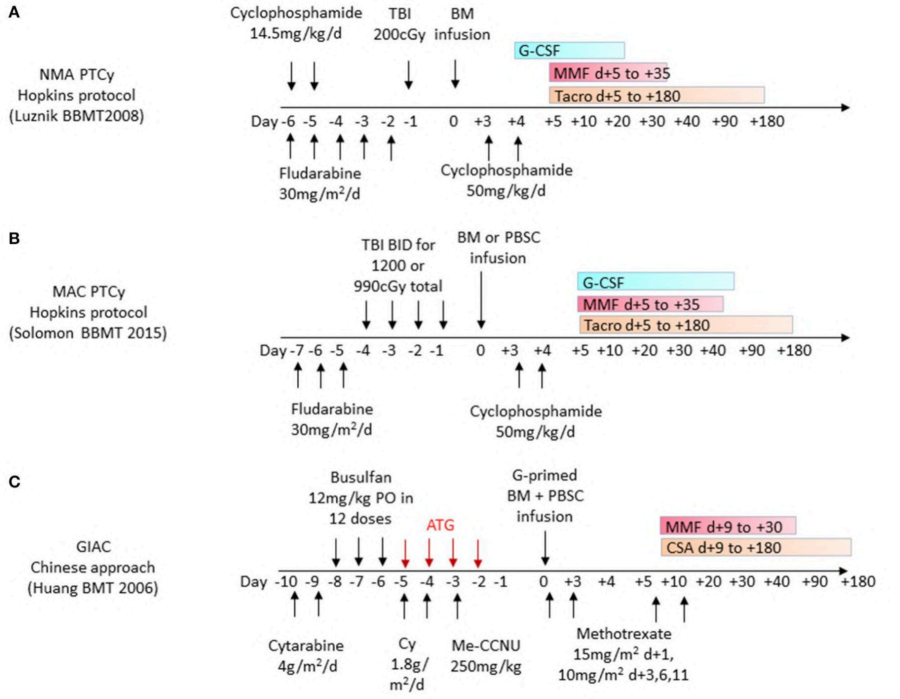

Figure 3. Frequently used haplo-HCT regimens. (A) Non-myeloablative (NMA) conditioning with administration of post-transplant cyclophosphamide (PTCy) as part of the Hopkins protocol for haplo-related donor HCT uses cyclophosphamide 50 mg/kg/day on days +3 and +4 and additional GVHD prophylaxis with oral MMF and tacrolimus (Tacro) starting on day +5. (B) Myeloablative conditioning (MAC) protocol with administration of post-transplant cyclophosphamide 50 mg/kg/day given on days +3 and +4 and additional GVHD prophylaxis with oral MMF and tacrolimus starting on day +5. (C) GIAC haplo-HCT protocol using a combination of G-CSF primed bone marrow (BM) and peripheral blood stem cells (PBSC) administered after a conditioning regimen including ATG on days −5 to −2. GVHD prophylaxis includes short-course Methotrexate in addition to MMF and cyclosporine (CSA).

GIAC Approach (G-CSF-Mobilization, Intensified Post-transplant Immunosuppression, ATG and Combination of PBSC and BM Allografts)

The GIAC approach using T-cell replete haploidentical grafts was pioneered at Peking University (12, 51). This approach uses ATG as part of the conditioning regimen, which affects recipient T cells and facilitates engraftment. Owing to its long half-life, it also exerts effects on donor T cells and therefore impacts GVHD and post-transplant immunity. The graft consists of a combination of G-CSF-primed bone marrow and PBSC, thereby combining the advantages of both elements. PBSC grafts contain 2–3-fold higher $CD34^+$ cells and a log-fold higher T cell dose than are typically contained in a steady-state bone marrow graft (52), and this has been shown to accelerate engraftment and decrease the relapse rate (**Figures 3C**, **4B**).

The higher T cell dose in PBSC grafts adversely affects chronic GVHD but not acute GVHD rates in unrelated donor HCT (53). Multiple mechanisms may contribute to why acute GVHD rates are not drastically higher despite the high T cell dose. These include preferential dendritic cell mobilization and T cell polarization (54, 55), attenuating effects on costimulatory molecules such as CD86 on APCs and CD28 on $CD4^+$ T cells (56, 57), as well as IL-10 mediated T-cell suppression by monocytes (58). Several studies underscored the benefit of utilizing G-CSF mobilized bone marrow, leading to less acute and chronic GVHD while maintaining engraftment rates comparable to PBSC (59) and have attributed these effects to differences in cytokine milieu, T-cell polarization and T-cell hypo- responsiveness (60–62).

In the initial study of 171 patients using GIAC, most of whom had ALL, AML, or CML, all patients engrafted with sustained full donor chimerism. The rates of leukemia-free survival and incidences of grade II-IV acute GVHD and extensive chronic GVHD were

comparable to MUD HCT (12, 53). A prospective multicenter study of AML patients has demonstrated that transplant outcomes with the GIAC strategy have also been comparable to MSD HCT (63). Although a modified approach using G-CSF primed haploidentical bone marrow and extensive GVHD prophylaxis has also been applied in Europe (64), the GIAC strategy has been used most extensively in China and therefore patients transplanted with this strategy represent a large cohort of haploidentical transplants HCT treated to date (65).

Haploidentical HCT with *ex vivo* T Cell Depletion or Anergy Induction Strategies

$CD34^+$ Cell Selection

The establishment of procedures for the *ex vivo* removal of T cells from the graft in the late 1970s by Reisner, O'Reilly and colleagues, represented a tremendous breakthrough toward the feasibility of utilizing haploidentical donors. In the initial approach, T cells were eliminated from the bone marrow by first rosetting with sheep red blood cells followed by differential soybean agglutination of residual T lymphocytes in the non-rosetting population. This yielded an un-agglutinated fraction containing a high proportion of colony-forming cells without any detectable T cell alloreactivity, and abrogated lethal GVHD in murine models (66, 67). This strategy was applied in the first clinically successful haploidentical HCT of an infant with AML, leading to sustained hematopoietic engraftment without GVHD until relapse occurred 11 weeks after HCT (68). Three infants with SCID were also treated with this approach of whom 2 had sustained engraftment and none developed GVHD (8).

$CD34^+$ selection, now in wide-spread use in TCD transplants, was first introduced in the 1990s. This process utilizes a $CD34^+$ directed antibody coupled to immunomagnetic beads to positively select $CD34^+$ cells and isolate them over a magnetic column. This effectively eliminates all other immune cells, including T-, B-, NK-cells, dendritic cells and monocytes from the graft (69, 70). This process was further refined with the use of micromagnetic beads, which had the advantages of high purity selection via attachment to single cells and safe infusion into patients (71). Aversa and colleagues of the Perugia group pioneered a novel haploidentical HCT platform incorporating an intensified conditioning regimen to eliminate host T cells and administering megadose T cell depleted grafts without additional post-grafting immunosuppression (28, 72). Handgretinger et al. tested this approach with G-CSF mobilized megadose PBSC grafts in 39 children lacking suitable donors and observed low rates of GVHD, but significant relapse and treatment-related mortality (TRM) (73). Investigators from Perugia further evaluated this system in adults with high- risk leukemia using megadose haplo-HCT, demonstrating 91% primary engraftment and low rates of GVHD without post- transplant GVHD prophylaxis (27) (**Figure 4A**, top panel).

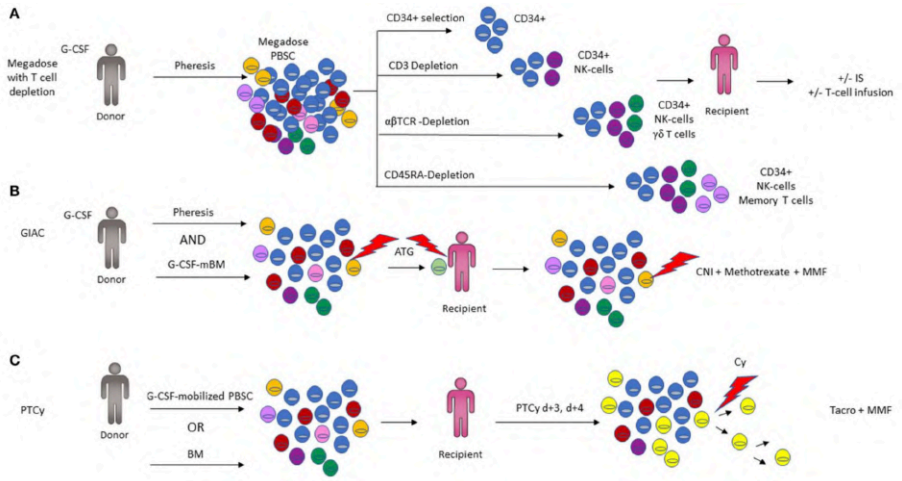

Figure 4. Comparison of the three major haplo-HCT platforms. (A) Four different ex vivo T-cell depletion protocols are shown, with the resulting cell composition in the graft. CD34-positive selection preferentially isolates the hematopoietic stem and progenitor fraction required for engraftment with minimal immune cell content (top panel). Depletion of CD3+ T-cells results in a graft composed predominantly of CD34+ and NK cells (2nd panel). Depletion of αβ-T cells depletes T cells involved in mediating GVHD but retains beneficial immune cells such as NK cells and γδ- T cells in the graft. CD45RA-Depletion removes naïve T cells including cells responsible for alloreactivity and GVHD, while retaining memory T cells including cells vital for immunity against infections (3rd panel). Additional immunosuppression (IS) and/or infusion of T-cell subsets may be employed post-transplant to optimize engraftment (3rd panel). (B) Representation of the GIAC protocol indicating a G-CSF primed bone marrow (BM) and peripheral blood stem cell (PBSC) graft, with ATG targeting T-cells derived from both the donor and recipient. GVHD prophylaxis with methotrexate, a calcineurin inhibitor (CNI), and MMF targets residual T cells (3rd panel). (C) Post-transplant cyclophosphamide (PTCy) functionally impairs actively proliferating recipient and graft derived T cells while favoring Treg recovery (color of cells corresponds to Figure 2; Tregs are depicted in bright yellow).

$CD3^+$ Cell Depletion

To improve post-transplant immune reconstitution, control of infections and prevention of relapse, further iterations of

immunomagnetic graft engineering were developed (74). This included the elimination of $CD3^+$ T cells and $CD19^+$ B cells using a negative immunomagnetic selection method to deplete these subsets from the graft. Stem cells, NK cells, myeloid precursors, monocytes, and other progenitor cells important for engraftment are preserved (75). This strategy maintains innate immunity in the graft while removing $CD3^+$ T cells capable of inducing GVHD. Depletion of $CD19^+$ B cells was introduced to reduce the risk of post-transplant lymphoproliferative disease (PTLD) (73) and GVHD (76). While the depletion of donor B-cells reduces the risk of PTLD, it does not address PTLD arising from residual host B cells. Instead, this can be addressed with the inclusion of rituximab or Campath (but not the T cell directed agents ATG or OKT3) into the conditioning regimen (77, 78). Several centers established $CD3^+/CD19^+$ depletion as a feasible approach for patients lacking a suitable donor, with excellent primary engraftment and reduced rates of GVHD correlating with the remaining $CD3^+$ cell/kg content of the graft. However, the low OS rate of 31% remains primarily attributable to infections and relapse, suggesting that further improvement of TCD haplo-HCT is needed (79, 80) (**Figure 4A**, second panel).

αβT-Cell/B-Cell Depletion

With emerging recognition of γδT cells (81), a yet more sophisticated approach was developed for GVHD prevention. In contrast to αβ-T-cell receptor (TCR) expressing T cells, γδ-TCR expressing T-cells are not implicated in mediating GVHD (82) but do exhibit important functions characteristic of innate immune recognition

and anti-tumor effects (83, 84). These cells represent 1–20% of all $CD3^+$ circulating T lymphocytes in human peripheral blood and the majority of resident T cells in skin and mucosa. Their TCR heterodimer consists of a γ and δ chain encoded by a limited repertoire of V, D, and J gene segments. The two major Vδ1 and Vδ2 subsets are distinguished based on their TCRδ composition. Whereas, $V\delta1^+$ cells are typically associated with a Vγ1/2/3/5/8 chain, the majority of $V\delta2^+$ T cells express an invariant TCR harboring Vγ9. The Vγ9δ2 TCR is expressed by the majority of peripheral γδ T cells, whereas γδ T cells including other Vδ elements are predominantly enriched at epithelial surfaces and the skin (81, 84). Analogous to NK cell biology, γδT cells are fine-tuned by activating and inhibitory receptors and recognize conserved non-peptide antigens that signal potential danger or cellular stress. The activating receptor NKG2D is broadly expressed in γδT cells and functions synergistically with the γδ-TCR as a costimulatory receptor (85, 86).

γδT cells have heterogenous functions, ranging from protection against intra- and extracellular pathogens or malignant cells to modulation of the immune response and tissue homeostasis. They contribute to pathogen clearance through the production of granulysin, defensins, and cytotoxic effector molecules such as perforin and granzymes (84). γδT cells secrete proinflammatory cytokines involved in protective immunity against viruses, intracellular pathogens (TNF-α and IFN-γ), extracellular bacteria, fungi (IL-17), and extracellular parasites (IL4, IL5, IL13), and have been shown to exhibit lytic activities against leukemia, lymphoma and carcinoma cells (87–89). Indeed, increased γδT-cell numbers after allogeneic HCT were

associated with a lower incidence of infections and improved disease-free survival (DFS) in several studies (90–92).

In a pediatric trial using αβ-T cell/B-cell depleted haplo-HCT, γδ-T cells were the predominant T-cell population in the initial weeks after transplantation, specifically expanded in response to CMV reactivation, and displayed cytotoxicity and degranulation when challenged with primary leukemia blasts *in vitro* (93). These effects were increased after exposure to zoledronic acid, suggesting that the anti-leukemic capacity of γδ-T cells could further be enhanced (94). Outcomes with the αβ-T cell/B-cell depleted haplo-HCT approach in which no additional GVHD prophylaxis was employed appear promising both in children with malignant (95) and non-malignant conditions (96), and when compared with MUD and MMUD HCTs in a retrospective analysis of children transplanted for acute leukemias (97). However, the high incidence of viral infections reported by some groups highlights the potential to further improve *ex vivo* T-cell depletion strategies (98) (**Figure 4A**, third panel).

CD45RA-Depletion

As our understanding of T cell differentiation status and phenotype has become increasingly sophisticated, so have approaches to tailor graft composition further (99, 100). αβ-T cells exist as distinct subsets that can be differentiated by cell surface phenotype: naïve (T_N), stem cell memory (T_{SCM}), effector (T_E), effector memory (T_{EM}), and central memory (T_{CM}). The $CD45RA^+CD62L^+$ T_N subset is antigen inexperienced, has a more diverse TCR repertoire than memory T cells and clonally expands following T cell priming to execute short-lived

effector functions. They ultimately differentiate into memory subsets, which is associated with downregulation of CD45RA and upregulation of CD45RO. Studies in mouse models demonstrated that T_N mediated severe GVHD, whereas T_{CM} induced milder GVHD and T_{EM} were devoid of GVH activity (101–105). Importantly memory T cells transferred infectious immunity and GVL activity in these models (106).

Based on the premise that elimination of T_N from the graft could significantly reduce GVHD while maintaining pathogen- and tumor-specific immunity, Bleakley and colleagues developed a novel graft-engineering strategy using immunomagnetic beads coupled to a monoclonal Ab targeting CD45RA. The latter antigen is expressed on all T_N, but absent on Treg, T_{CM} and most T_M (107). This strategy was initially studied in patients with high risk hematologic malignancies undergoing MSD HCT, utilizing a 2-step selection procedure with a $CD34^+$ selection of stem cells (a minor subset of which expresses CD45RA) followed by depletion of $CD45RA^+$ cells from the $CD34^-$ fraction. This study demonstrated engraftment in all patients (n = 35), prompt immune recovery without excessive rates of infection or relapse and low chronic GVHD, but interestingly no reduction in acute GVHD although the latter was readily steroid-responsive (108).

Clinical results with CD45RA-depletion in the context of haplo-HCT are so far limited. A study of 17 pediatric patients with high risk hematologic malignancies using a RIC conditioning with total lymphoid irradiation (TLI) but without TBI or serotherapy, administered a $CD34^+$ selected PBSC product on day 0, followed by a CD45RA-depleted PBSC product which had been collected the

following day, and ultimately a donor NK cell product administered on day +6 with the use of Sirolimus or MMF post-transplant. Rapid neutrophil engraftment and memory T-cell reconstitution was observed, without any infectious deaths and with 76.5% of patients alive at a median of 225 days after HCT. Grade III-IV acute GVHD and chronic GVHD were seen in 3 and 6 of 17 patients, respectively (109). In a second small study, 5 children with combined immunodeficiency and chronic viral infections received a combination of a $CD34^+$ selected product and the CD45RA-depleted fraction of the CD34-negative product with post-HCT prophylaxis consisting of Cyclosporine and MMF. One patient died with graft failure. In the 4 engrafted patients, viral infections cleared within 2 months after HCT and an early T cell response against viral pathogens was documented in 2 patients (110). Further studies will be needed to further define the role of this approach in haplo-HCT (**Figure 4A**, bottom panel).

Ex vivo Induction of T Cell Anergy With CTLA-4Ig

An early strategy to minimize T-cell alloreactivity by interfering with the priming of alloreactive T cells in haplo-HCT was explored in a pediatric trial. This involved collection of patients' peripheral blood mononuclear cells (PBMC) prior to the start of myeloablation and a 36-h *in vitro* incubation of the recipient cells with non-mobilized donor bone marrow in a mixed lymphocyte reaction (MLR) setting in the presence of CTLA- 4Ig, a fusion protein which inhibits priming of alloreactive T cells by inhibiting costimulatory signaling between the B7 protein family (CD80/CD86) on APCs and CD28 on T cells (111). This reduced the frequency of T cells recognizing alloantigens of the

recipient while preserving responsiveness to alloantigens of other persons. In this trial of 11 evaluable patients most of which had persistent disease at the time of HCT, 5 were alive and in CR at 4.5–29 months after transplant with 3 patients developing steroid-responsive acute GVHD of the gut only. There were no deaths attributable to GVHD (112). However, this approach has not been explored further.

Photodynamic Purging of Adoptive T Cell Therapy Following TCD Haplo-HCT

A different approach to augment the TCD graft with an adoptive T cell therapy product devoid of alloreactive T cells is a process termed photoallodepletion. Prior to G-CSF mobilization of the PBSC graft, donors undergo non-mobilized leukapheresis to obtain T cells. Donor T cells are then incubated with recipient PBMC in an MLR in the presence of TH9402, a photosensitizer similar to rhodamine. T cell activation in the MLR, which occurs selectively in the alloreactive T cells but spares Tregs and pathogen-specific T cells, is associated with P-glycoprotein pump inhibition leading to mitochondrial accumulation of TH9402 in alloreactive T cells (113, 114). Subsequent activation of TH9402 with visible light leads is then selectively toxic to and eliminates alloreactive T cells via an oxidative damage mechanism (115). Early results from a clinical trial in which patients received the photodynamically allodepleted T-cell product subsequent to a $CD34^{+}$ selected graft appear promising (116).

ROLE OF INNATE IMMUNITY IN HAPLO-HCT

NK-cells are an important component of the innate immune system providing protection against infectious pathogens and cancer. Recent studies have elucidated that human NK cell diversity is much broader than the traditional distinction via $CD56^{bright}$ and $CD56^{dim}$ subsets reflective of differentiation stage and cytotoxic potential. The ability of NK cells to differentiate into long-lived cells with memory capacity (117) and the discovery of non-NK innate lymphoid cells has highlighted the complexity and potential roles of innate immune cells after HCT (118, 119). NK cells have potent anti-leukemia effector capacity, respond to viral infections via release of toxic granules, and facilitate engraftment without mediating GVHD. This is particularly important in the setting of heavily T cell-depleted grafts or T-cell directed post-transplant immunosuppression and has inspired a rich field of investigation to augment NK cell immunity in the context of HCT to develop leukemia-directed NK-cell based cellular therapies.

NK-cell activity is governed by the balance of a system of activating and inhibitory NK cell receptors (120). Activating signals are provided by receptors such as NKG2D, CD94/NKG2C and Natural Cytotoxicity Receptor (NCRs) including NKp30, 44, and 46 and by activating killer-cell Ig-like receptors (KIR). NKG2D recognizes MHC-class I related stress-ligands that can be upregulated by tissues in response to infection, inflammation, DNA-damage, and malignant transformation (121), while CD94/NKG2C binds to the non-classical HLA- E molecules and senses overall HLA-Class I expression on cells (**Figure 5A**). NK cells utilize a unique process to balance tolerance to self under steady state conditions with the ability to mediate an immune response to pathogens or malignant cells. This is referred to as NK-cell

education or licensing (122), is in large part regulated by inhibitory KIR receptors and impacts NK-cell alloreactivity in the setting of haplo-HCT and allogeneic NK-cell therapies (123).

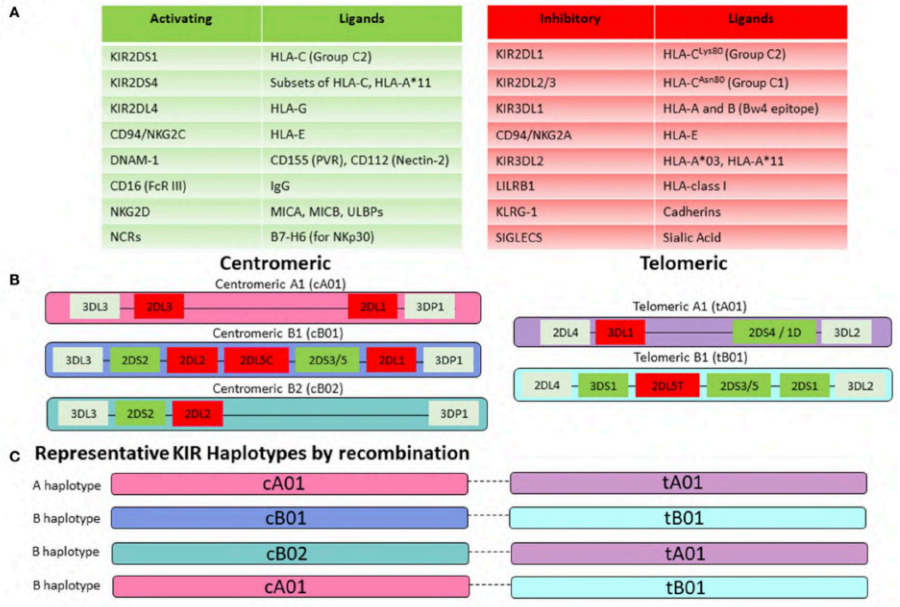

Figure 5. NK-cell receptor repertoire. (A) NK-cell activity is mediated by a balance of activating and inhibitory signaling. Key activating receptors and their corresponding ligands are listed in the green table, while inhibitory receptors are displayed in the red table. (B) KIR genes are highly polymorphic and organized in centromeric and telomeric motifs with structural variation that creates multiple gene content haplotypes. Group A haplotype motifs are characterized by fewer genes and predominantly those encoding for inhibitory KIRs. In contrast, Group B haplotype motifs are enriched for activating KIRs. (C) Centromeric and telomeric motifs are paired together to generate either a KIR A haplotype (composed of centromeric and telomeric A motifs) or a KIR B haplotype (containing at least one centromeric or telomeric B motif). Representative KIR haplotypes by recombination are shown here. Prominent linkage disequilibrium has been noted within the centromeric and telomeric motifs but not between them, suggesting that pairing occurs by recombination between the centromeric and telomeric regions.

KIRs are either activating or inhibitory based on their structure. The KIR nomenclature incorporates the number of extracellular Ig-like domains (two in KIR2D vs. three in KIR3D) and whether the KIR contains a long or short tail (KIR2DL vs. KIR2DS). KIRs are further numbered in order of their discovery within their structural group (KIR2DL1 vs. KIR2DL2). KIRs with long tails are generally inhibitory (with exception of KIR2DL4) and KIRs with short tails function as activating receptors according to presence or absence of immunoreceptor tyrosine-based inhibitory motifs (ITIMs) (124). There is tremendous variability within the KIR repertoire owing to a high degree of polymorphism among individual KIR genes as well as their organization and recombination within haplotypes (**Figures 5B, C**) (125). An individual's genetic KIR repertoire is determined by the inherited composition of centromeric and telomeric A and B haplotypes (**Figure 5B**). Group A haplotypes contain fewer genes and predominantly those encoding for inhibitory KIRs. Additionally, the activating KIR2DS4 gene exist as an inactive deletion variant, termed KIR1D in the majority of Caucasians, leaving the framework gene KIR2DL4 as the sole receptor on this haplotype with any activating function (126, 127). In contrast, Group B haplotypes are enriched for activating KIRs. Two groups of KIR haplotype can be assigned based on the combination of the centromeric and telomeric motifs. Presence of a centromeric or telomeric B-haplotype constitutes a KIR B haplotype whereas the combination of a centromeric and a telomeric A-haplotype results in a KIR A haplotype (**Figure5C**). Although more than 50 different haplotypes have been described, there are 11 common haplotypes derived by reciprocal recombination, which collectively

account for 94% of Caucasian haplotypes examined by Jiang et al. (128). Distribution of a KIR gene in the centromeric or telomeric region of chromosome 19q13.4 is further thought to impact KIR-mediated regulation of NK-cell activity (129). Additionally, KIR-cell surface expression at the protein level may vary substantially from the inherited KIR gene profile. This is attributable to the fact that KIRs are stochastically expressed on NK cells and each NK cell may therefore display a different cell-surface profile of inhibitory or activating KIRs (130). For the most accurate prediction of NK-cell alloreactivity between haploidentical donor and recipient, KIR-genotyping alone is insufficient and determination of the KIR phenotype (by flow cytometry) should also be pursued.

The majority of inhibitory KIRs recognize classical (HLA- A, B, and C) or non-classical HLA-class I molecules (HLA-G) as their cognate ligands (**Figure 5A**) (131). KIR genes are located on chromosome 19 whereas HLA-genes are located on chromosome 6. KIR and HLA genes therefore segregate independently, and an individual may or may not express the cognate HLA-ligand for any given KIR. This forms the basis for the concept of "education" or "licensing" of NK-cells, which allows NK-cells to maintain self-tolerance under physiologic conditions, while retaining the ability to mount an immune response (132). When NK cells encounter the matching HLA-class I ligand for their inhibitory KIR (based on the requisite germline inheritance of the appropriate HLA and KIR genes and their expression patterns on individual NK cells), they are considered "educated" or "licensed" and refrain from an attack on healthy tissues under steady state. However, when NK cells are

accustomed to this inhibitory signal and subsequently encounter a cell that does not express the appropriate KIR-ligand ("missing ligand"), this situation renders them functional to mount an effector response, if the target also expresses stress-ligands that trigger activating NK-cell receptors (133). A missing ligand may be encountered on malignant cells due to HLA-class I downregulation, or HLA-mismatched allogeneic transplantation such as haplo-HCT, when the recipient does not express the corresponding HLA-ligand (**Figure 6**). NK-cells are considered "unlicensed" when they do not encounter the matching HLA-class I ligand for their given inhibitory KIR. Due to the lack of exposure to their corresponding ligand, unlicensed NK-cells are "un-educated" and hyporesponsive at steady state rather than being triggered by self-tissues lacking the ligand (134). Unlicensed NK cells require a higher threshold for activation. However, in the absence of KIR inhibition, they can mediate higher levels of effector function when they receive strong stimulatory signals under inflammatory conditions (such as CMV infection or in the posttransplant setting) or when triggered for antibody-dependent cellular cytotoxicity (ADCC) (135, 136). Given that NK cells may surface-express variable combinations and densities of inhibitory KIRs, NK-cell education occurs on a continuum along which individual NK cells display graded levels of responsiveness based on their KIR profile and engagement of cognate HLA-class I ligands (122, 137, 138).

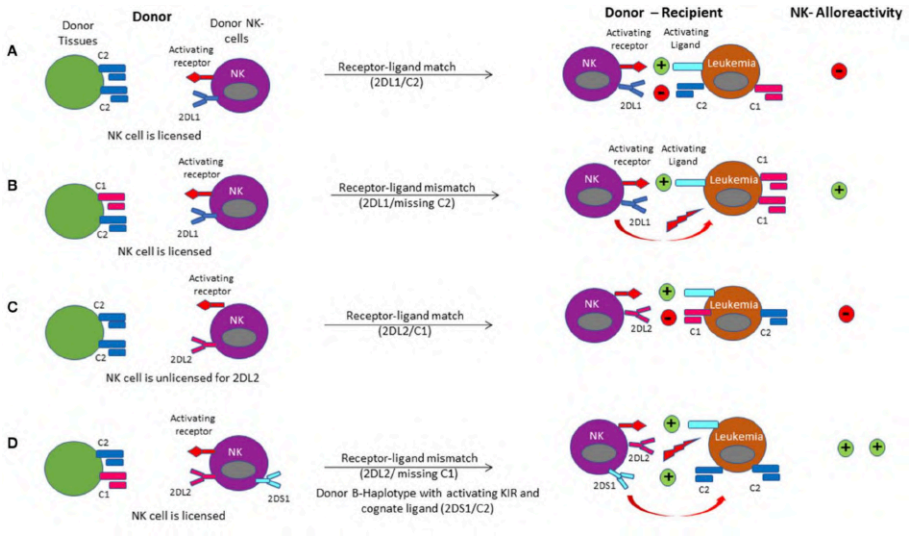

Figure 6. NK cell alloreactivity in haplo-HCT is demonstrated via the different models of receptor-ligand mismatch. (A) The donor-derived NK cell is licensed when its KIR2DL1 receptor had been engaged by expression of its cognate C2 ligand in the donor environment. Upon infusion of the licensed NK cell into the recipient, a leukemia cell expressing the C2 ligand will not activate the NK cell due to a receptor-ligand match. (B) A receptor-ligand mismatch occurs when the donor-derived NK cell is licensed, but the recipient does not express the C2 ligand (missing ligand). Provided that it is further driven by stimulation through activating receptors, this results in activation of the licensed donor NK cell upon infusion into the recipient, leading to a graft-vs.-leukemia effect. (C) If the donor does not express the appropriate class I ligand for its KIR receptor (HLA and KIR segregate independently), the donor NK cell is unlicensed. In this case, donor NK cells are accustomed to a missing ligand. They may be activated when encountering strong activating signals (like activating cytokines) or be further inhibited when encountering the inhibitory ligand in the recipient. (D) Licensing of the NK cell for the C1 ligand occurs in the donor. Upon transplant into the host, the missing C1 ligand coupled with binding of the activating ligand with the activating receptor on the NK cell results in alloreactivity. Binding of the activating KIR receptor KIR2DS1 to the C2 ligand on the target leukemia cell enhances NK cell alloreactivity.

Since the model of NK-cell alloreactivity in the context of mismatched HCT was first proposed, a number of studies have

evaluated its clinical impact (139). For the interpretation of HCT studies evaluating the role of NK-cell alloreactivity it is critical to consider the definition of the KIR-mismatch model employed in each study (131, 140) (**Figure 6**). The "KIR ligand-ligand mismatch model" is based on the hypothesis that the presence of the corresponding HLA-ligand prevents NK-cell alloreactivity, whereas a missing ligand in the HCT recipient triggers NK cell alloreactivity. However, while this model accounts for HLA-class I mismatches, it does not consider KIR-genotype or phenotype. In contrast, the "KIR receptor-ligand mismatch model" accounts for the fact that a missing ligand is irrelevant if NK cells do not express the corresponding KIR for a mismatched HLA-class I ligand. Therefore, this model incorporates the HLA-ligand repertoire in the recipient as well as the donor KIR genotype and ideally phenotype. Other groups have employed the "KIR- haplotype model" which takes into consideration the presence or absence of a B-KIR haplotype in the donor, as a measure of enrichment for activating vs. inhibitory KIRs. Use of this model demonstrated a reduced risk of leukemia relapse when patients were transplanted from donors with centromeric B-haplotypes (141–143). Similarly, more recent approaches have focused on the predicted overall degree of inhibitory and activating KIR-KIR ligand interactions between the recipient and potential donors with a highly variable KIR repertoire. This allows for selection of an optimal donor, even when the transplant recipient's HLA- class I repertoire is such that all KIR ligands are expressed and a missing-ligand scenario is unachievable.

Ruggeri et al. first established that a NK-cell alloreactivity of the donor toward recipient (based on KIR receptor-ligand mismatch in

the GVL direction and presence of alloreactive clones against recipient targets) lowered the AML relapse risk in the context of *ex vivo* depleted haplo-HCT (72). These results were subsequently consolidated in a larger cohort of 112 AML patients, where transplantation from a NK-cell alloreactive donor was associated with a significantly lower relapse rate (3% compared to 47%) when transplanted in complete remission and better EFS when transplanted in relapse (34% compared to 6%) or CR (67% compared to 18%) (144). Subsequent studies of sibling donor, unrelated donor (URD), and umbilical cord blood (UCB) donor sources have yielded variable results (14). Some studies showed no benefit or even inferior survival resulting from a mismatch in the KIR/KIR-ligand system. This may be partly related to the variable definition of KIR-mismatch models and transplant regimens used. In contrast, a large analysis in AML patients undergoing 9/10 or 10/10 URD employed an algorithm to predict the strength of inhibition between the ubiquitous KIR3DL1 and its ligand HLA-B and found that combinations with absent of weak inhibition were associated with significantly lower rates of relapse and overall mortality (145). The extent of T-cell depletion may also play an important role, since the presence of T cells in the graft affects NK cell reconstitution leading to lower KIR-receptor expression (146). Lastly, given that a KIR ligand-ligand mismatch implies an absence of a KIR ligand in the host that is present in the donor, it equates with the presence of a major HLA-class I mismatch. It is therefore not unexpected that such mismatch leads to significant T-cell alloreactivity and poor survival unless T-cell reactivity is minimized with methods such as TCD.

A retrospective analysis of 161 patients receiving TCD haploidentical allografts confirmed a beneficial role of NK cell alloreactivity. In the presence of KIR-receptor-ligand mismatches in the GVL direction, expression of activating KIR2DS1 or KIR3DS1 was associated with a significant reduction in NRM, largely owing to 50% reduction in infection rates (147). While much of the benefits of NK cell alloreactivity are reported for myeloid indications, a pediatric study of 85 patients undergoing TCD haplo-HCT showed that patients transplanted for ALL from a KIR B-haplotype donor had a significantly better EFS than those with KIR haplotype A donors. Additionally, a higher KIR B- content score (based on the number of centromeric and telomeric KIR B motifs) was associated with a significant reduction in relapse risk (148). Although limited by use of a KIR ligand- ligand model, a study of haplo-HCT with PTCy for various hematologic malignancies found that KIR-ligand mismatch was associated with a lower incidence of relapse and better PFS for patients transplanted in relapse but had no significant impact on those transplanted in CR (149). A growing ability to navigate the complexities of the KIR-system, such as recognition of varied strengths of inhibition among subtypes of inhibitory KIRs and its ligands resulting in discrete hierarchies of anti-leukemic cytotoxicity will aid in further revealing how donor selection based on KIR-compatibility may improve outcomes (145). While the beneficial effects of NK-cell alloreactivity are mostly documented in the context of *ex vivo* T cell-depleted haplo-HCT, the growing adaptation of T-cell replete haplo-HCT affords the opportunity to carefully study the role of NK-cell alloreactivity in these platforms.

IMMUNE RECONSTITUTION AFTER HAPLO-HCT

Transplant outcomes are directly related to the achievement of an acceptable restoration of the immune system. Several cell subsets play a key role in the protection toward infections and disease recurrence. In general, innate immunity recovers early after transplant and represents the first line of defense against pathogens. Specifically, monocytes followed by neutrophils and NK cells arise in the first month after transplant. Adaptive immunity mediated by T and B cell lymphocytes recovers later and is crucial for both immune tolerance maintenance and long-term protection against infections and disease relapse. T cell reconstitution can occur through two different mechanisms: thymus-independent T cell peripheral expansion of infused donor memory T cells and thymus-dependent *de novo* generation of donor T cells from donor hematopoietic progenitors (150).

While the kinetics of immune reconstitution and its correlation with HCT outcomes are well-established in the setting of matched donor transplant, more studies are needed in the setting of haplo-HCT. Different donor sources do not represent the only cause of possible differences in immune reconstitution kinetics. Specific haplo-HCT platforms and GVHD prophylaxis approaches are also crucial factors to consider (151). As detailed above, two major haplo-platforms are currently used: T-cell replete haplo-HCT that use an *in vivo* T-cell depletion with ATG or PTCY, and TCD haplo-HCT in which the graft is *ex vivo* manipulated with a CD34-positive selection or a T-cell negative selection. Here, we review the immune reconstitution of

different blood cell subsets after different types of haplo- HCT (**Figure 7**).

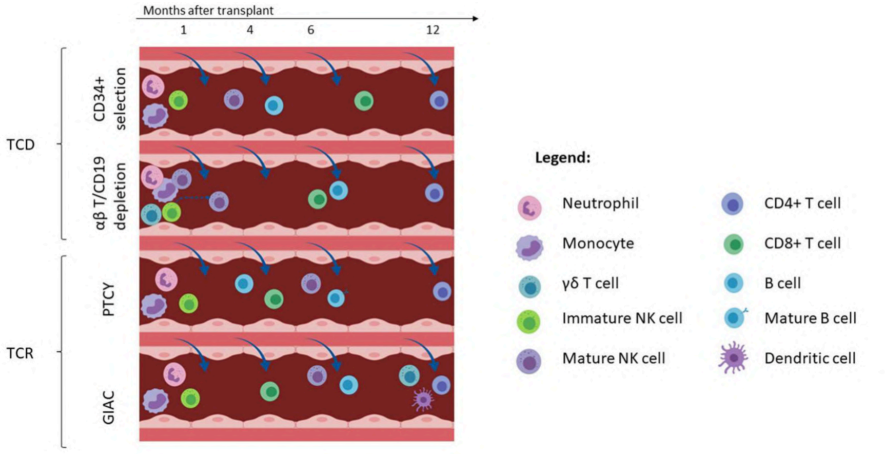

Figure 7. Immune reconstitution with different haploidentical transplant platforms. Only subsets which have been characterized by published primary data for each platform are included in this figure (e.g., data on dendritic cell reconstitution has only been described for the GIAC approach). Cells are depicted at the approximate time-point of reaching the lower range of normal. T-cell depleted (TCD) haploidentical transplant is associated with early recovery of neutrophils, monocytes, immature NK cells and rapid NK cell maturation which takes 6–8 weeks (top panel). Additionally, αβ-T cell/CD19 depletion is associated with early detection of γδT cells and mature NK cells that are infused with the graft infusion (2nd panel from the top). B cell recovery is delayed with CD19 depletion relative to CD34+ selection. T-cell replete (TCR) haploidentical transplant performed with post-transplant cyclophosphamide (PTCy) and GIAC protocols is associated with early reconstitution of immature NK cells (3rd panel from the top). It is also associated with earlier reconstitution of CD8+ T-cells than TCD protocols. The GIAC protocol is associated with delayed dendritic cell recovery (bottom panel). *This figure was created using BioRender.com.*

Monocytes

Monocytes are the first immune subset to recover after HCT. Rapid and robust monocyte $CD14^{+}$ cell reconstitution has been

correlated with the improvement of transplant outcomes in the setting of MSD (152) and UCB-HCT (153). Recently, a study by Turcotte and colleagues showed that higher absolute monocyte count (AMC) and higher classic monocyte subsets ($CD14^{bright}$ $CD16^{-}$) at day +28 were associated with a reduced risk of relapse and TRM, better 2-yr OS, and improved 2-yr PFS in a cohort of patients transplanted for different hematological malignancies using both RIC or MAC regimens and different stem cell sources (154). AMC was influenced by the graft origin, with a higher AMC found in UCB but no differences between BM and PBSC. However, no haplo- HCTs were included in this study. In a separate cohort of 144 patients treated with MAC conditioning for hematological malignancies, receiving a T-cell replete graft consisting of G-CSF- mobilized BM and PBSC from HLA-haploidentical or MSDs, the monocytes recovered rapidly, and the AMC was above the normal range starting from the first month to the first year after transplant. Both patient groups received GVHD prophylaxis with Methotrexate, Tacrolimus, MMF, and Cyclosporine with the addition of ATG in the haploidentical group (GIAC protocol). Monocyte reconstitution was comparable between recipients after HLA-matched and haplo-HCT on days +30, 90, and 180 after transplantation. None of the patient transplant characteristics impacted monocyte recovery in the multivariable analysis (155). Finally, in a pediatric cohort of 40 patients receiving TCD haplo-HCT using CD34 positive selection or CD3/CD19 cell depletion, monocyte expansion was rapid, reaching normal values for age within 30 days of transplant. Moreover, no differences in monocyte recovery were seen between different graft purification and conditioning intensity regimens (156).

Neutrophils

Depending on the study, neutrophil engraftment is defined by the presence of more than 500 or 1,000 neutrophils/μL of blood and represents a crucial step in the early phase after transplant. Prolonged neutropenia is associated with severe infection and increased TRM (157). In the setting of a T-cell replete transplant, neutrophil recovery occurs quickly. With GIAC protocols, the median neutrophil engraftment was achieved at 14 days (range 9–25) (158, 159), whereas with the RIC PTCY platform using BM grafts and Tacrolimus and MMF GVHD-based prophylaxis, the median time to neutrophil recovery was 15 days (range 11–42) (11). For both protocols, patients received recombinant human granulocyte colony-stimulating factor (rhG-CSF) from day +6 or +4 to engraftment, respectively.

In the context of TCD HCT using the Perugia protocol with $CD34^+$ selected megadose grafts, the median time to neutrophil recovery was 11 days (range 9–30) without G- CSF support (27). Studies using CD3/CD19 cell depletion in adult patients also showed rapid neutrophil recovery, with a median time of 12 days (range 9–50) without the addition of G-CSF (79, 80). Similar results were seen in a cohort of pediatric patients with acute leukemia undergoing MAC transplant. Specifically, patients in the αβ-T cell-depleted haplo- HCT had a faster neutrophil recovery compared to MUD, mismatch unrelated donors (mMUD), and those treated with Methotrexate and Calcineurin-inhibitors, with median time to neutrophil engraftment of 13 (range 6–23), 19 (range 9–46), and 20 days (range 10–120), respectively (97). All three groups received ATG during the conditioning for prevention of graft failure and GVHD, and none of the patients received G-CSF to

accelerate neutrophil recovery. Taken together, these data show that haplo-HCT provides a comparable or even expedited neutrophil recovery compared to standard matched donor-HCT.

Dendritic Cells

Dendritic cells (DCs) represent a rare population in the peripheral blood, accounting for 0.15–0.7% of mononuclear cells (160). In the context of T-cell replete haplo-HCT using the GIAC protocol, Wang and colleagues measured the frequencies of DCs and their subsets among white blood cells (WBCs) after haplo-HCT, including $CD123^+$ plasmacytoid DCs (pDCs) and $CD11c^+$ myeloid DCs (mDCs). Recipients had strikingly decreased proportions of DCs (0.49% vs. 0.27%, $P = 0.025$), mDCs (0.27% vs. 0.14%, $P < 0.001$), and pDCs (0.04% vs. 0.02%, $P = 0.008$) in the WBC compartment at ∼180 days post-haplo- HCT compared to healthy subjects. Since, it was reported that primary human DCs were the most potent expander of the γδ T cell subset $V\delta2^+$ (161), the authors also investigated whether the recovery levels of $V\delta2^+$ T cells were associated with the DC content following transplantation. Bivariate correlation analysis showed that the proportion of mDCs, but not DCs and pDCs, in WBCs was significantly correlated with the recovery of $V\delta2^+$ T cells after haplo-HCT. Specifically, slow recovery of mDCs was associated with a slow recovery of $V\delta2^+$ T cells in this haplo-HCT setting (162).

Chang and colleagues also described a slower DCs recovery at +15 and 30 days after HCT compared to those in the HLA- matched recipients in another study (158). In their protocol, ATG was

administrated only in the haplo-group. Indeed, it was described that ATG not only induced a tolerogenic phenotype in human DCs (163), but was also able to mediate a complement-mediated lysis of DCs (164). In summary, these findings may explain the delay in DC recovery in the setting of the haplo-HCT using the GIAC protocol. The kinetics of DC reconstitution in other haplo-HCT settings, remain to be fully characterized.

Natural Killer (NK) Cells

Due to the need to perform an extensive T cell depletion in haplo-HCT, anti-tumor efficacy is largely dependent on the graft-vs.-leukemia effect exerted by NK cells that eradicate residual leukemic blasts surviving the preparative regimen (72, 165–167). In the haplo-HCT setting performed through the infusion of positively selected $CD34^+$ cells, the first emergence of fully functioning, KIR alloreactive NK cells from hematopoietic progenitors may require at least 6–8 weeks, and therefore the benefit offered by their anti-leukemia effect is delayed (168–171). In the setting of αβ-T-cell/CD19 depletion, generation of NK cells from donor HSC takes ∼8 weeks but circulating NK cells can be detected earlier after transplant due to infusion with the graft (172). Moreover, CMV reactivation in this setting was associated with an expansion of memory-like NK cells ($NKG2C^+$, $CD57^+$, KIR^+) as early as 3 months after HCT (173). Surprisingly, in a pediatric comparison between TCD haplo-HCT performed with CD34 positive selection or CD3/19 negative selection, NK-cell recovery was faster in patients receiving PBSC from $CD34^+$ positive selection in the first 4 months after transplant (156).

In the T-cell replete haplo-HCT setting using PTCY, Russo and colleagues described that donor alloreactive NK cells infused with the graft were killed by cyclophosphamide (174). This translated into a delay of NK recovery and maturation resulting from a profound reduction after cyclophosphamide administration following a robust proliferation of donor-NK cells in the early phase after graft infusion. The absence of aldehyde dehydrogenase (ALDH)-positive NK cells suggested that they were susceptible to cyclophosphamide cytotoxicity, and this was then confirmed using an *in vitro* assay of mafosfamide-induced cell death (174). On the other hand, Russo et al. reported an IL-15 peak in patient sera at day +15 after transplant that was associated with a progressive increase of NK cells expressing an immature phenotype ($CD62L^{+}$, $NKG2A^{+}$, KIR^{-}) between day +15 and day +30 (174). The normal distribution of NK phenotypes was achieved only between 9 and 12 months after transplant, with a decrease of $CD56^{bright}$, NKG2A, and CD62L expression and an increase of maturation markers (CD16, CD57, and KIR). KIR expression returned to normal levels around day +60, but NKG2A expression decreased only after 6 months. Interestingly, in this cohort of patients, there was no difference in PFS between patients with or without a predicted KIR alloreactivity, suggesting that the protective anti-tumor activity of NK cells is dampened after T-cell replete haplo-HCT using the PTCY platform (174).

Another group described the transient and predominant expansion of an unconventional subset of NK cells characterized by a specific phenotype: $NKp46^{neg/low}$, $CD56^{dim}$, $CD16^{neg}$, $CD94/NKG2A^{high}$ starting from the second week after transplant and

maintained until the 7th week (175). This unconventional population retained its proliferative capacity and the ability to differentiate into the $CD56^{bright}$ subsets ($NKp46^{+}$, $CD56^{bright}$, $CD16^{-}$ cells) in response to IL-15 and IL-18. Despite the unconventional NK cells expressing a high level of activating receptors (NKG2D and NKp30), Granzyme-B and Perforin, they displayed a defective *in vitro* cytotoxicity highlighting again the need to improve NK reconstitution after PTCy haplo-HCT (175). Similar results were reported in the GIAC protocol in which early and higher expression of CD94/NKG2A was inversely correlated with KIR expression, and was associated with worse survival (176). The same group showed that NK cells from patients who developed GVHD had a lower expression of NKG2A, lower proliferative capacity and an increased rate of apoptosis, but retained their cytotoxicity after *in vitro* co-culture with the K562 cell line (177).

Finally, in contrast to TCD haplo-HCT, KIR-mismatch analysis between donor-recipient pairs when using only HLA and KIR genotyping without consideration of the KIR phenotype, was unable to predict post-transplantation outcomes in multivariate analyses in the setting of haplo-HCT using the GIAC protocol (178). However, it has been reported that KIR-driven NK cell alloreactivity is better predicted if donor KIR genotype is considered in conjunction with KIR cell surface expression (130). Moreover, in haplo-HCT using the GIAC protocol, the higher number of T-cells infused in the graft contributed to the high incidence of acute GVHD (178). This resulted in a need for increased immune suppression, thereby affecting NK alloreactivity.

T Cells

Achievement of an acceptable T cell reconstitution after HCT represents a crucial goal and correlates with better transplant outcomes. Impairment of T cell reconstitution is more pronounced after T cell depletion (152). In the context of T-cell replete haplo-HCT using the GIAC protocol, $CD3^+$ T cell counts were 125, 883, 1,163, and 1,308 cells/μL at 30, 90, 180, and 360 days after HCT, respectively (158). A lower median $CD3^+$ T cell count was reported after NMA haplo-HCT using a BM graft with PTCy, Tacrolimus and MMF based GVHD prophylaxis, with 206 cells/μL at day 40 and 219 cells/μL at day 100 (179). On the other hand, $CD3^+$ T-cell recovery was more rapid with 338 cells/uL at day +30 after MAC haplo-HCT using PBSC grafts with PTCy, MMF, and sirolimus GVHD-based prophylaxis (180).

In the setting of T-cell replete haplo-HCT with both GIAC and PTCy-based protocols, $CD8^+$ T cells recovered earlier than $CD4^+$ T cells (158, 181–183). Faster $CD8^+$ T cell recovery at day +90 correlated with higher $CD3^+$ cells in the graft but was not associated with a higher incidence of GVHD (184). The same studies highlighted that the recovery of $CD4^+$ T cells was impaired for the whole first year after transplant, but failed to demonstrate a correlation between delay in $CD4^+$ T cell reconstitution and NRM as was shown in the HLA-matched donor setting (185). Notably, in the GIAC experience the delay of $CD4^+$ T-cell reconstitution was compensated by the proportional increase of the $CD8^+$ T cell- and monocyte fractions, and the NRM was relatively low (19.5% in the haplo group vs. 17.4% for the matched-sibling donor cohort). This was likely due to patient care improvements, especially the management of CMV reactivation (158).

A retrospective EBMT registry study including both adult and pediatric patients undergoing haplo-HCT found an association between higher $CD3^+$, $CD4^+$, and $CD8^+$ T-cell counts and better OS with less NRM (186). However, in the multivariable analysis only higher $CD3^+$ and $CD8^+$ T-cell counts correlated with lower NRM. No association was found between any of the T-cell, B-cell, or NK-cell subset counts with relapse-related mortality. In this study, the majority of patients were treated with TCD haplo-HCT using both $CD34^+$ selection and CD3/19 depletion (186).

In the context of αβ T-cell depleted haplo-HCT, $CD3^+$, and $CD3^+/CD8^+$ T-cell recovery was slower compared to MUD or MMUD-HCT until 6 months after transplant (97). Recovery of $CD4^+$ T cells was delayed only in the first 3 months and became even better at 1 year after haplo-HCT compared to MUD and MMUD. In this pediatric experience, haplo-HCT patients did not receive any additional pharmacological GVHD prophylaxis, whereas MUD and MUD HCT were performed using standard calcineurin-based GVHD prophylaxis and short- term methotrexate (97).

T memory stem cells (T_{SCM}) represent a subset of early-differentiated human memory T cells with stem cell-like properties. T_{SCM} and naïve T cells (T_N) both express naïve markers such as CD45RA, CCR7, and CD62L, but in distinction to T_N and similar to other memory subsets, T_{SCM} are characterized by CD95 expression. In the context of haplo-HCT using PTCy, two different groups elegantly showed that donor-derived T_{SCM} reconstitute early after transplant, representing the majority of both CD4 and CD8 T cells at

day +8. At the polyclonal, antigen-specific, and clonal level, TSCM lymphocytes were preferentially derived from differentiation of TN infused within the graft, whereas most memory infused lymphocytes are purged by PTCy (182, 187).

Regulatory T (Treg) Cells

Treg cells play a key role in the modulation of immune tolerance after HCT. Higher Treg content in the graft has been associated with better OS and lower aGVHD (188), whereas a reduced frequency of Tregs contributed to cGVHD incidence after matched-donor transplant (189). In the matched donor setting, Kanakry and colleagues showed that Treg, especially memory CD45RA-Treg, were preserved and recovered rapidly while conventional T (Tcon) naïve cells were reduced when PTCy was used as the sole method of GVHD prophylaxis (48). This was ascribed to the high levels of aldehyde dehydrogenase (ALDH), as the major *in vivo* mechanism of Cyclophosphamide resistance in the Treg population. In addition, murine studies demonstrated the importance of Tregs for GVHD reduction in the context of the PTCy-based GVHD prophylaxis (49).

In the T-cell replete haplo-HCT setting using PTCy, naïve Tregs increased after cyclophosphamide administration. This was attributed to the lower Ki67 levels compared to the memory subsets at day +3. In addition, Tregs exhibited a lower proliferation profile compared to Tcons, suggesting a lower susceptibility to PTCy in the haploidentical setting (182). This effect seems to be enhanced when PTCy is combined with sirolimus instead of a calcineurin inhibitor (180). Cieri et al. showed an expansion of $CD25^{+}$ $CD127^{-}$ $FoxP3^{+}$ Tregs early after

transplant, relative to the donor leukapheresis content and to the quantity in healthy subjects. Interestingly, patients who did not experience acute GVHD had a higher percentage of circulating Tregs at day +15 compared to patients who developed acute GVHD (180). Notably, the ability of Sirolimus to boost Treg reconstitution has also been reported outside of the PTCy platform. Indeed, Peccatori and colleagues reported an expansion of Treg after haplo-HCT using a combination of ATG, sirolimus and MMF as GVHD prophylaxis (190). Moreover, in the Baltimore experience with a cohort of patients undergoing MAC haplo-HCT using PTCy, MMF, and tacrolimus-based GVHD prophylaxis, Tregs achieved normal donor levels at all time-points examined (day +30, +90, +180, and +365) (181). Finally, in haplo-HCT using the GIAC protocol, patients with a higher day +30 percentage of naive Treg, defined as $CD4^+$ $CD25^+$ $CD45RA^+$, had a significantly lower incidence of grades II–IV acute GVHD (191). This highlights the importance of reaching a satisfactory Treg reconstitution for the achievement of immune tolerance after haplo-HCT.

γδ T Cells

γδ T cells combine conventional adaptive immunity features with innate-like MHC-independent tumor recognition (192). In healthy donors the majority of circulating γδ T cells expresses the Vδ2 chain, whereas the minority expresses the Vδ1 chain. The former subgroup is able to recognize non-peptide phosphoantigens and to perform direct killing of tumor cells (193). The Vδ1 γδ T-cell subgroup on the other hand is associated with control of CMV infection and also retains antitumor activity (194). Both subgroups play a key role in the setting

of haplo-HCT because they do not induce GVHD but can exert immunological surveillance. In patients undergoing αβ-TCD haplo-HCT, γδ-T cells were the predominant T-cell subset for the first 2–3 weeks after transplant (91.5% of $CD3^+$ lymphocytes), while αβ T cells became the most prevalent population at 1 month (93). Moreover, patients had a higher proportion of γδ-T cells, especially the $V\delta2^+$ subset for the first 3 months. However, CMV reactivation (but not infection with other viruses) was associated with an expansion of Vδ1 γδ-T cells (93). Interestingly, the authors showed that zolendronic acid was able to potentiate $V\delta2^+$ killing against leukemia blasts after *in vitro* culture, indicating that the cytotoxicity was dependent on phosphoantigen recognition and providing a rationale for the development of future clinical trials to boost the γδ T anti-tumor effect (93). The same group tested the *in vivo* ability of zolendronic acid (ZOL) to enhance γδ T-cell recovery and function, by administrating the drug to pediatric patients undergoing αβ-TCR/CD19 depleted haplo-HCT. An induction of Vδ2-cell differentiation paralleled by increased cytotoxicity of both Vδ1 and Vδ2 cells against primary leukemia blasts was associated with ZOL treatment. Patients given three or more ZOL infusions had a better probability of survival in comparison to those given one or two treatments (86% vs. 54%, respectively, $p = 0.008$), suggesting that ZOL infusion promotes γδ T-cell differentiation and cytotoxicity and may influence the outcome of patients in this transplant setting (94).

B Cells

B cell recovery occurs late after HCT. B cells are almost undetectable during the first and second months and normal values are only reached around 12 months after transplant (195). In the setting of NMA haplo-BMT using PTCy, MMF and Tacrolimus as GVHD prophylaxis, B cells were undetectable until day +28. Recovery of B cells started from week 5 with an immature $CD38^{bright}$ $CD10^{+}$ Ki-67 negative phenotype, suggesting that the increase in B-cell number was not due to the homeostatic proliferation of transferred B cells but to *de novo* generation (196). Maturation of B cells was characterized by different expression of both transitional (T) markers CD5 and CD21: T0 ($CD5^{-}$ $CD21^{-}$), T1 ($CD5^{+}$ $CD21^{-}$), T2 ($CD5^{+}$ $CD21^{+}$), and the $CD5^{-}$ $CD21^{+}$ subset. Starting at week 9, mature B cells ($CD38^{dim}$ $CD10^{-}$) began to increase with a naïve phenotype (IgD^{+} , IgM^{+}). Overall, B cell maturation took 6 months to complete in the setting of a T-cell replete PTCy-based haplo-HCT (196).

With haplo-HCT using the GIAC protocol, median B cell counts did not differ from HLA-matched HCT at any of the time points examined (158).

In an analysis comparing CD34 positive selection and CD3/CD19 cell depletion, B cells reconstituted more rapidly in the former group (156). Furthermore, recovery of B cells after αβ T cell-depleted haplo-HCT was delayed for the first 6 months compared to a cohort of patients transplanted with a MUD or MMUD using standard calcineurin-based GVHD prophylaxis. However, this is at least in part attributable to the fact that in the αβ T-cell depletion setting, patients received one dose of Rituximab as part of the conditioning regimen in order to prevent post-transplant lymphoproliferative disorders (97).

RELAPSE AND IMMUNE EVASION MECHANISMS AFTER HAPLO-HCT

Recent data has highlighted the critical role of the immune system in the control of myeloid leukemia after HCT and elucidated our understanding regarding the immunologic mechanisms underlying relapse after haplo-HCT. Work by Vago and colleagues revealed that a substantial proportion of AML and MDS relapses after haplo-HCT are attributable to acquired uniparental disomy of chromosome 6p (copy-neutral loss of heterozygosity eliminating the incompatible HLA alleles without decreasing the overall level of expression of HLA class I molecules). This was shown to result in loss of the mismatched HLA molecules on leukemia cells and immune escape from leukemia control exerted by haploidentical donor T cells via the major histocompatibility mismatch (197). The maintained overall expression of class I molecules in this study also evaded activation of NK-cell mediated anti-leukemic responses which could potentially be based on a newly missing ligand to an inhibitory KIR receptor (197). Clinical suspicion for an immune evasion phenomenon was first raised when patients relapsing after haplo-HCT had discrepant findings in host chimerism monitoring between short-tandem-repeat amplification but not HLA typing (198). Recognition of this leukemia escape mechanism has therapeutic importance for patients who are candidates for subsequent haplo-HCT in whom a different donor is available who is mismatched for the HLA haplotype retained in the relapsed leukemic cells and/or is predicted to mediate NK-cell alloreactivity based on the newly missing KIR-ligand. The development of routine diagnostic methods is expected to facilitate this (198). Importantly, ~30% of relapses after haplo-HCT are

attributable to this mechanism of the elimination of the incompatible HLA alleles irrespective of the GVHD prophylaxis or platform used to control T-cell alloreactivity (190, 199, 200).

To identify other drivers of post-HCT relapse Toffalori et al. analyzed transcriptional signatures specific for post-transplant AML relapses (201). This study demonstrated deregulation of the costimulatory interface between donor T cells and host leukemia cells, with loss of costimulatory interactions and enforcement of inhibitory ones (PD-1/PDL-1) as evidenced by both changes in leukemic cells and donor T cells (**Figure 8**). Additionally, the study documented downregulation of surface expression of HLA class II molecules on leukemia cells due to the downregulation of the HLA class II regulator CIITA (201). Patients with AML relapse after HCT were found to have a higher proportion of BM—infiltrating T cells expressing inhibitory receptors (IR) compared to patients remaining in CR. The exhausted BM-T cell phenotype was associated with a restricted TCR repertoire, impaired effector functions and leukemia-reactive specificities. Furthermore, early detection of severely exhausted BM-memory stem T cells predicted relapse (202). Interestingly, IR-positive T cells infiltrating the BM of AML patients at relapse displayed a greater ability to recognize matched leukemic blasts after *in vitro* expansion compared with their IR-negative counterparts. This suggest that IR expression marks lymphocytes enriched for tumor specificity whose activity could be unleashed with therapeutic check-point blockade, although innovative targeted strategies will be required to avoid exacerbation of GVHD in the HCT context (202).

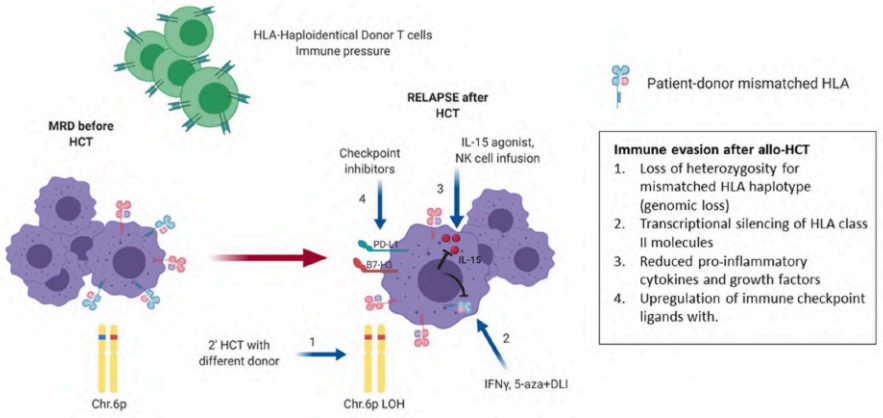

Figure 8. Mechanisms of relapse post haploidentical HCT. Late relapse after haploidentical allogeneic transplantation can be driven by a number of immunologic mechanisms as shown. Under the immune pressure of graft-vs.-leukemia (GVL) via HLA mismatch in a haploidentical environment, loss of heterozygosity for the mismatched HLA allele is a mechanism of escape from immune surveillance and relapse (1). Another mechanism involves transcriptional silencing of HLA class II molecule, thereby reducing T-cell mediated GVL. This effect can be partially reversed in the presence of immunomodulatory molecules such as IFN-y or the epigenetic regulator 5-azacitidine (5-aza) (2). Modification of the tumor microenvironment via suppression of release of mediators that promote GVL is another mechanism used by relapsing leukemia cells, which may be partially reversed via administration of IL-15 agonists and NK cell infusions that promote the secretion of proinflammatory cytokines (3). An additional common mechanism of relapse involves the emergence of T-cell exhaustion with associated upregulation of PD-L1 and other inhibitory receptors. The latter may be reversed through administration of checkpoint inhibitors (4). Blue arrows indicate possible therapeutic strategies to overcome the different mechanisms of immune evasion. MRD, minimal residual disease; LOH, loss of heterozygosity; Chr, chromosome; DLI, donor lymphocyte infusion. *This Figure was created using BioRender.com.*

HAPLO-HCT AS A PLATFORM FOR POST-TRANSPLANT IMMUNE THERAPIES

Numerous scientific advances have contributed to the resurgence of haplo-HCT as a viable transplant option for patients

requiring HCT and have achieved similar outcomes to those from other donor sources. The ability to perform haplo-HCT without costly *ex-vivo* T-cell depletion approaches, which require extensive cell manufacturing expertise frequently limited to large transplant centers, has been a major advance in transplant accessibility for patients in resource-limited countries that frequently do not perform unrelated donor transplantation (203). However, further efforts are required to improve immune reconstitution, control infectious complications and decrease relapse rates in patients after haplo-HCT. Fortunately, haplo-HCT provides an ideal platform characterized by unique immunologic properties and ready accessibility of the donor for additional cell products. This offers tremendous opportunities for the development and implementation of innovative adoptive immune cell therapies to augment infectious and antitumor immunity and further improve outcomes (**Figure 9**).

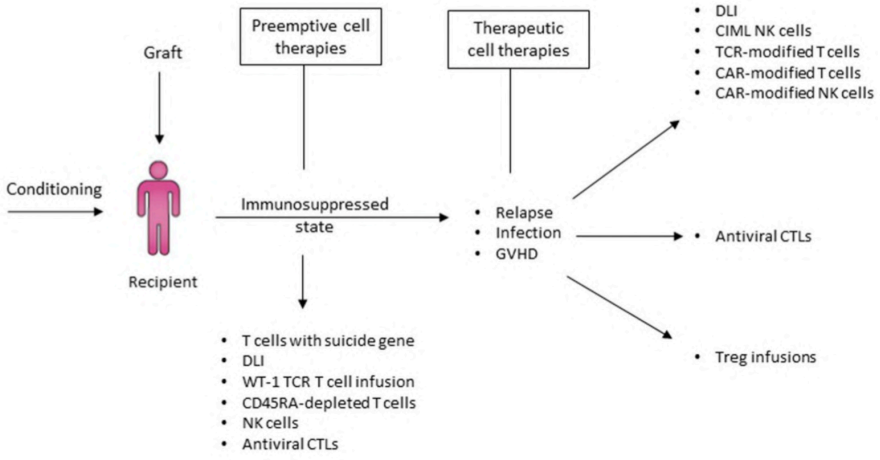

Figure 9. Haplo-HCT offers a platform for post-transplant immune therapies to prevent and treat relapse. In the context of a haploidentical transplant, there are several options to administer cellular therapies in order to

address relapse, infection and GVHD either pre-emptively or therapeutically. In the event of a relapse, enhancing GVL effect using cellular therapy that either relies on the haploidentical mismatch between donor and recipient or gene-modified donor immune effector cells T cells are potential options. Donors haploidentical to the recipient may also readily serve as a source of cells for the production of CAR-T or CAR-NK. In the event of significant viral infection post relapse, administration of antiviral cytotoxic T-cells may promote viral clearance without increasing the risk of GVHD. Finally, Treg infusions may be utilized to treat GVHD. DLI, Donor lymphocyte infusion; CIML NK cells, Cytokine-induced memory-like NK cells; TCR, T-cell receptor; CAR, Chimeric antigen receptor; CTLs, Cytotoxic T-lymphocytes.

Suicide Mechanisms for Defined T-Cell Content in the Graft and Post-transplant

Ex-vivo TCD haplo-HCT affords opportunities not only for the dose-titration but also the manipulation of the T cell product prior to infusion into the patient. Rather than *in-* or *ex-vivo* approaches to selectively deplete or attenuate T cells, a different approach is the infusion of polyclonal T cells that have been genetically engineered to include an inducible suicide gene. With this strategy, a defined dose of T cells can be administered to aid in engraftment and immune reconstitution, mediate a GVL effect, and provide infectious immunity while being selectively susceptible to an externally inducible suicide mechanism in the event of significant GVHD (204).

The first such approach was pioneered by Bonini and colleagues with the introduction of a herpes simplex virus thymidine kinase (HSV-TK) suicide gene into T cells using γ-retroviral transduction in which the transgene also contained the truncated selection marker ΔLNGFR. This allowed for the isolation and infusion of transduced cells bearing the suicide gene (205). With this strategy, administration of the drug

ganciclovir activated the suicide mechanism and successfully controlled GVHD in several patients after infusion (204). Interestingly, the first wave of circulating TK^+ cells after infusion facilitated thymic renewal and was followed by a second wave of long-term immune reconstitution with naïve lymphocytes. This was supported by an increase in TCR excision circles, $CD31^+$ recent thymic emigrants and expansion of thymic tissue on imaging and was further associated with an increase in serum IL-7 levels following each infusion (206).

Since then, other approaches have been developed, such as transduction of T-cells with the iCasp-9 suicide gene. This gene can be activated by an otherwise inert drug (207, 208). Novel approaches have also included the use of a different transduction marker such as truncated CD19 that allows for the confirmation of transduction and if desired positive isolation of transduced T cells prior to infusion. Brenner and colleagues first utilized this approach in children undergoing haplo-HCT and demonstrated impressively how iCasp-9 transduced T cells expressing the truncated CD19 aid in immune reconstitution and contribute to infectious immunity (207, 208). Activation of the suicide gene led to resolution of GVHD symptoms within hours (209, 210). Interestingly, while alloreactivity was rapidly abrogated, suicide gene transduced T cells were not permanently eliminated and able to reconstitute again without causing GVHD. Pediatric studies are underway to investigate suicide-gene equipped T-cell infusions after αβ-TCR/CD19 depleted haplo-HCT.

Haploidentical Donor Lymphocyte Infusions

A common approach to address relapse early after HCT is the infusion of donor lymphocyte infusions (DLI) to exert a GVL effect, but this is frequently accompanied by significant rates of GVHD. Zeidan and colleagues demonstrated the feasibility of this approach after haplo-HCT with PTCy in a retrospective analysis of a dose escalation approach at their center (211). Forty patients received 52 haplo-DLI doses initially at 1×10^5 $CD3^+$/kg and most commonly starting at 1×10^6 $CD3^+$/kg. Ten patients (25%) developed GVHD with Grade III-IV acute GVHD in 6 and chronic GVHD in 3 patients. Twelve patients (30%) achieved a CR with a median duration of 11.8 months (211).

Sun et al. reported on haplo-DLI following a number of different chemotherapy regimens (FLAG, Methotrexate and others) for relapse after haplo-HCT with the GIAC protocol. Of 86 patients, 20 developed Grade III-IV aGVHD and 41 developed cGHVD. NRM was 10.3%, and 62% of patients achieved a CR after chemo-DLI of which 50% experienced re-relapse at a median duration of 92 days (212). A modified GIAC backbone was also utilized to assess preemptive DLI at a median of 77 days post haplo-HCT in high risk patients to prevent relapse. With a sizeable median $CD3^+$ dose of 1.8×10^7/kg, the 100-day incidences of acute GVHD were 55.3% for Grade II–IV and 10.2% for Grade III–IV, respectively. Two-year incidence of chronic GVHD was 52%, among which 18.2% were severe. With this regimen, 2-year NRM was high at 33.1% with a 2-year relapse incidence of 32% (213).

Approaches to reduce GVHD while optimizing the GVL effect of preemptive or therapeutic DLI are likely to evolve over time and include the infusion of IL-10 anergized DLI (214), CD45-RA depleted

DLI (215) and adoptive transfer of gene modified cells as described in this section. Although experience in the haplo-HCT setting is limited to date, azacitidine or decitabine in conjunction with DLI have shown promising overall response rates on the order of 25– 33% for patients with AML or MDS relapsing after allogeneic HCT (216, 217).

CAR- T or CAR-NK-Cell Infusion

Chimeric antigen receptor (CAR) T cells targeting CD19 have revolutionized the treatment of relapsed/refractory B-cell acute lymphoblastic leukemias and aggressive B-cell lymphomas, with complete remission rates ranging from 70–90% in ALL (218, 219) and ~60% for refractory large B-cell lymphoma (220, 221). CAR-T cells have been successfully manufactured from donor T cells in patients with relapse after allogeneic HCT and infused without mediating GVHD. Autoimmune complications have not been observed after infusion of CAR-T cells derived from autologous T cells suggesting that the CAR-signal overrides TCR-based recognition. The use of third-party CAR-T cells has been explored with concurrent transcription activator-like effector nuclease (TALEN)-based gene editing of the endogenous TCR. These CAR-T cells did mediate GVHD in a limited study of three patients (222). The use of CAR-NK cells is also being explored in the relapse setting, and although long-term persistence may be more limited than that of CAR-T cells, this approach may be beneficial when there is a higher degree of HLA-mismatch such as after haplo-HCT (223). While the therapeutic success of CD19-targeting CAR-T cell therapy to date is limited to B-cell malignancies and multiple myeloma (224), studies are underway to investigate the safety,

feasibility, and preliminary efficacy of CAR-T cells directed against AML and MDS (225–227). Given this rapidly evolving field, the established efficacy potential of CAR-T cells and ability to utilize donor cells for CAR-T cell manufacture post-HCT, haploidentical HCT donors represent a readily available post-transplant cell source for donor-derived CAR-T cell or CAR-NK cell therapies for relapsed leukemia.

Antiviral Cytotoxic T Lymphocyte (CTL) Infusion

Infectious complications and particularly end-organ viral disease after HCT remain a challenge, particularly in haplo-HCT where *ex*- or *in*-vivo T-cell depletion is necessary. For example, the incidence of BK-virus hemorrhagic cystitis is higher in haplo-HCT (228). As demonstrated by Leen and Bollard the infusion of virus-specific CTL lines, generated by stimulating PBMC from adenovirus and EBV-seropositive donors, can safely be performed without inducing GVHD and can result in clearance of adenoviral disease and prevention of EBV-associated PTLD (229). The successful use of off-the-shelf multi-virus-specific T cells to treat viral infections after allogeneic HCT with minimal risk of GVHD has since been confirmed in a larger study and has the potential to mitigate serious viral disease after haplo-HCT either with third-party or haploidentical antiviral CTLs (230).

TCR-Edited T Cell Infusions

Whereas, CAR-transduced T cells recognize extracellular peptides on the surface of target cells in an MHC-independent manner, TCR-mediated T cell recognition mediates T cell immunity against

MHC-restricted, intracellular targets and minor histocompatibility antigens. With the advent of sophisticated strategies to optimize T cell transduction and prevent mis-coupling of transduced and endogenous TCR chains, TCR-edited T cells have successfully entered clinical trials for patients with an HLA-type required for the HLA-restricted expression of the antigen. Greenberg and colleagues cloned a high affinity TCR targeting the HLA-A2 restricted tumor antigen WT-1 from healthy donors and inserted this TCR into EBV-specific donor $CD8^+$ T cells (to minimize the GVHD risk and enhance persistence). The WT1-TCR modified donor T cells were then infused prophylactically into the HLA-A*0201+ recipients after they had received an allogeneic HCT from the same donor. This approach resulted in 100% relapse free survival in the WT-1 TCR-T cell group at 44 months as compared to a comparative group of similar risk AML patients with a 54% relapse-free survival after HCT (231). A separate approach is currently under investigation to target the HLA-A*0201-restricted minor histocompatibility antigen HA-1, which is exclusively expressed on hematopoietic cells (232). When the immunogenic single-nucleotide polymorphic variant of HA-1 is expressed on hematopoietic cells of the HLA-A2+HCT- recipient, donor T cells that have been transduced to encode a high-avidity TCR recognizing HA-1 can effectively eliminate leukemia and lymphoma cells *in vitro* (233). Given the facile availability of donor T cells, haplo-HCT can and should serve as a beneficial platform to explore new approaches to reduce relapse after HCT.

NK Cell Product Infusion to Augment Graft vs. Tumor Effect

As previously described, NK-cells can mediate GVL effects due to KIR-mediated alloreactivity in the haplo-HCT setting. In addition to selecting the donor based on predicted NK-cell alloreactivity, the availability of haploidentical donors for additional cell product collection affords the unique opportunity to utilize NK-cell infusions to provide for additional GVL or GVT effects after HCT prophylactically or in the face of relapse (234). Generation of adequate numbers of NK cells for post-transplant therapies can be challenging given the relatively low NK cell frequency in the blood but can be overcome by *in vitro* expansion such as with membrane-bound IL-21 expressing feeder cells (mbIL21). A Phase 1 study evaluated prophylactic NK cell infusions after haplo-HCT with PTCy on days −2, +7, and +28. Of 11 enrolled patients who received all 3 planned NK cell doses, 54% developed Grade I-II aGVHD, and none developed Grade III-IV aGVHD, chronic GVHD or dose-limiting toxicities. Only 1/11 patient relapsed. All others were alive and in remission at a median follow-up of 14.7 months (235). Administration of cytokines can facilitate NK cell expansion, but certain cytokines such as IL-2 also preferentially expand Tregs based on their constitutive expression of high-affinity IL-2R (CD25). These Tregs in turn inhibit NK cell proliferation (236). A study treating AML patients with haploidentical NK cell infusions after lymphodepletion with cyclophosphamide and fludarabine demonstrated that NK cell expansion was most pronounced and effective when IL-2-diphteria toxin fusion protein was administered to achieve host Treg depletion (237).

A recent trial administering haploidentical NK cells with rhIL15 for relapsed AML after lymphodepleting chemotherapy showed that

rhIL-15 achieved better rates of *in vivo* NK-cell expansion and remission compared to previous trials utilizing IL- 2, but also observed steroid- and tocilizumab-responsive cytokine release syndrome and neurologic toxicity which was associated with high levels of IL-6 (238).

Cytokine-induced memory-like (CIML) NK cells from haploidentical donors were able to induce complete remissions in relapsed/refractory AML patients outside of the transplant setting without any toxicities (239). This GVL effect may be even more durable when NK cells from the same haploidentical donor are infused after haplo-HCT because no immunologic rejection of the CIML NK cells from the same donor is expected. Studies to date have suggested that KIR- reactivity is less important when NK cells are cytokine-induced (240). Studies are now underway to evaluate the safety and efficacy of CIML NK cells for relapse after haplo-HCT.

Cytokine Support to Enhance NK-Cell Alloreactivity After Hct

An alternative strategy to address relapse after HCT is the administration of cytokines aimed at enhancing the anti- leukemic function of the existing post-transplant immune environment. One such approach employed ALT-803, an IL-15 superagonist complex designed to extend the *in vivo* half- life of IL-15 and mimic the physiologic *trans*-presentation of IL-15 (241). In contrast to IL-2 that can promote the survival, proliferation, and activation of lymphocytes, but that also stimulates Tregs, IL-15 preferentially expands $CD8^+$ T cells and NK cells via trans-presentation to the IL-2/15Rβγc- receptor while avoiding the stimulation of Tregs. In a recent Phase 1 trial ALT-803 was well-tolerated, particularly when administered subcutaneously, and induced

responses of 19% in patients relapsed after HCT (241), suggesting that such agents may also be explored in the haplo-HCT setting. Efforts are underway to test use of IL-15 or IL-15 superagonist complex alone or in combination with NK cell-based therapy to target relapse after haplo-HCT.

CONCLUSION

The initial immunologic barriers to haplo-HCT, namely GVHD and graft failure, have been overcome with different platforms that can be utilized to control T cell alloreactivity post-transplant. Comparable clinical outcomes have now been achieved relative to alternative donor sources and depending on the specific scenario, haplo-HCT can offer a lower risk of GVHD and/or improved control against relapse. The GVL effect in haplo- HCT is particularly intriguing given the concept of NK-cell alloreactivity based on the KIR/KIR-ligand system and ability to select donors accordingly. An emerging body of literature is elucidating immunologic mechanisms of GVHD and relapse that are potentially targetable and highlight the immune pressure exerted by donor immune cells after HCT. Given ready accessibility of the donor, haplo-HCT offers a unique platform for post-transplant cell-based immune therapies aimed at expediting immune reconstitution, improving thymic function, providing infectious immunity, and treating or protecting against relapse, while maintaining therapeutic control of those cell immunotherapies with methods such as suicide mechanisms. The rapid advancements in our understanding of the immunobiology of haplo-HCT are therefore poised to lead to increasingly sophisticated strategies

to fine-tune the transplant process and to further improve outcomes after haplo-HCT.

References

5. Copelan EA. Hematopoietic stem-cell transplantation. N Engl J Med. (2006) 354:1813–26. doi: 10.1056/NEJMra052638
6. Gragert L, Eapen M, Williams E, Freeman J, Spellman S, Baitty R, et al. HLA match likelihoods for hematopoietic stem-cell grafts in the U.S. registry. N Engl J Med. (2014) 371:339–48. doi: 10.1056/NEJMsa13 11707
7. Morishima Y, Kashiwase K, Matsuo K, Azuma F, Morishima S, Onizuka M, et al. Biological significance of HLA locus matching in unrelated donor bone marrow transplantation. Blood. (2015) 125:1189–97. doi: 10.1182/blood-2014-10-604785
8. Fuchs EJ. Haploidentical transplantation for hematologic malignancies: where do we stand? Hematology Am Soc Hematol Educ Program. (2012) 2012:230–6. doi: 10.1182/asheducation.V2012.1.230.3798312
9. Powles RL, Morgenstern GR, Kay HE, McElwain TJ, Clink HM, Dady PJ, et al. Mismatched family donors for bone-marrow transplantation as treatment for acute leukaemia. Lancet. (1983) 1:612–5. doi: 10.1016/S0140-6736(83)91793-2
10. Beatty PG, Clift RA, Mickelson EM, Nisperos BB, Flournoy N, Martin PJ, et al. Marrow transplantation from related donors other than HLA-identical siblings. N Engl J Med. (1985) 313:765–71. doi: 10.1056/NEJM198509263131301
11. Anasetti C, Beatty PG, Storb R, Martin PJ, Mori M, Sanders JE, et al. Effect of HLA incompatibility on graft-versus-host disease, relapse, and survival after marrow transplantation for patients with leukemia or lymphoma. Hum Immunol. (1990) 29:79–91. doi: 10.1016/0198-8859(90)90071-V
12. Reisner Y, Kapoor N, Kirkpatrick D, Pollack MS, Cunningham-Rundles S, Dupont B, et al. Transplantation for severe combined immunodeficiency with HLA-A,B,D,DR incompatible parental marrow cells fractionated by soybean agglutinin and sheep red blood cells. Blood. (1983) 61:341-8. doi: 10.1182/blood.V61.2.341.341

13. Bachar-Lustig E, Rachamim N, Li HW, Lan F, Reisner Y. Megadose of T cell depleted bone marrow overcomes MHC barriers in sublethally irradiated mice. Nat Med. (1995) 1:1268-73. doi: 10.1038/nm1295-1268
14. Reisner Y, Bachar-Lustig E, Li HW, Aversa F, Velardi A, Martelli MF. The role of megadose CD34+ progenitor cells in the treatment of leukemia patients without a matched donor and in tolerance induction for organ transplantation. Ann N Y Acad Sci. (1999) 872:336-48; discussion 48-50. doi: 10.1111/j.1749-6632.1999.tb08478.x
15. Luznik L, O'Donnell PV, Symons HJ, Chen AR, Leffell MS, Zahurak M, et al. HLA-haploidentical bone marrow transplantation for hematologic malignancies using nonmyeloablative conditioning and high-dose, posttransplantation cyclophosphamide. Biol Blood Marrow Transplant. (2008) 14:641-50. doi: 10.1016/j.bbmt.2008.03.005
16. Huang XJ, Liu DH, Liu KY, Xu LP, Chen H, Han W, et al. Haploidentical hematopoietic stem cell transplantation without in vitro T-cell depletion for the treatment of hematological malignancies. Bone Marrow Transplant. (2006) 38:291-7. doi: 10.1038/sj.bmt.1705445
17. Mavers M, Bertaina A. High-risk leukemia: past, present, and future role of NK cells. J Immunol Res. (2018) 2018:1586905. doi: 10.1155/2018/1586905
18. Gill S, Olson JA, Negrin RS. Natural killer cells in allogeneic transplantation: effect on engraftment, graft- versus-tumor, and graft-versus-host responses. Biol Blood Marrow Transplant. (2009) 15:765-76. doi: 10.1016/j.bbmt.2009.01.019
19. Lupo KB, Matosevic S. Natural killer cells as allogeneic effectors in adoptive cancer immunotherapy. Cancers. (2019) 11:769. doi: 10.3390/cancers11060769
20. Lee CJ, Savani BN, Mohty M, Labopin M, Ruggeri A, Schmid C, et al. Haploidentical hematopoietic cell transplantation for adult acute myeloid leukemia: a position statement from the Acute Leukemia Working Party of the European Society for Blood and Marrow Transplantation. Haematologica. (2017) 102:1810-22. doi: 10.3324/haematol.2017.176107
21. Zhang P, Tey SK. Adoptive T cell therapy following haploidentical hematopoietic stem cell transplantation. Front Immunol. (2019) 10:1854. doi: 10.3389/fimmu.2019.01854

22. Ottaviano G, Chiesa R, Feuchtinger T, Vickers MA, Dickinson A, Gennery AR, et al. Adoptive T cell therapy strategies for viral infections in patients receiving haematopoietic stem cell transplantation. Cells. (2019) 8:47. doi: 10.3390/cells8010047
23. Henslee PJ, Thompson JS, Romond EH, Doukas MA, Metcalfe M, Marshall ME, et al. T cell depletion of HLA and haploidentical marrow reduces graft-versus-host disease but it may impair a graft-versus-leukemia effect. Transplant Proc. (1987) 19(1 Pt 3):2701-6.
24. Szydlo R, Goldman JM, Klein JP, Gale RP, Ash RC, Bach FH, et al. Results of allogeneic bone marrow transplants for leukemia using donors other than HLA-identical siblings. J Clin Oncol. (1997) 15:1767-77. doi: 10.1200/JCO.1997.15.5.1767
25. Kernan NA, Collins NH, Juliano L, Cartagena T, Dupont B, O'Reilly RJ. Clonable T lymphocytes in T cell-depleted bone marrow transplants correlate with development of graft-v-host disease. Blood. (1986) 68:770-3. doi: 10.1182/blood.V68.3.770.770
26. Kernan NA, Flomenberg N, Dupont B, O'Reilly RJ. Graft rejection in recipients of T-cell-depleted HLA-nonidentical marrow transplants for leukemia. Identification of host-derived antidonor allocytotoxic T lymphocytes. Transplantation. (1987) 43:842-7. doi: 10.1097/00007890-198743060-00014
27. Reisner Y, Ben-Bassat I, Douer D, Kaploon A, Schwartz E, Ramot B. Demonstration of clonable alloreactive host T cells in a primate model for bone marrow transplantation. Proc Natl Acad Sci USA. (1986) 83:4012-5. doi: 10.1073/pnas.83.11.4012
28. Ash RC, Horowitz MM, Gale RP, van Bekkum DW, Casper JT, Gordon- Smith EC, et al. Bone marrow transplantation from related donors other than HLA-identical siblings: effect of T cell depletion. Bone Marrow Transplant. (1991) 7:443-52.
29. O'Reilly RJ, Keever C, Kernan NA, Brochstein J, Collins N, Flomenberg N, et al. HLA nonidentical T cell depleted marrow transplants: a comparison of results in patients treated for leukemia and severe combined immunodeficiency disease. Transplant Proc. (1987) 19 (6 Suppl 7):55–60.
30. Anasetti C, Amos D, Beatty PG, Appelbaum FR, Bensinger W, Buckner CD, et al. Effect of HLA compatibility on engraftment of bone marrow transplants in patients with leukemia or lymphoma. N Engl J Med. (1989) 320:197–204. doi: 10.1056/NEJM198901263200401

31. Aversa F, Terenzi A, Tabilio A, Falzetti F, Carotti A, Ballanti S, et al. Full haplotype-mismatched hematopoietic stem-cell transplantation: a phase II study in patients with acute leukemia at high risk of relapse. J Clin Oncol. (2005) 23:3447–54. doi: 10.1200/JCO.2005.09.117
32. Aversa F, Tabilio A, Velardi A, Cunningham I, Terenzi A, Falzetti F, et al. Treatment of high-risk acute leukemia with T-cell-depleted stem cells from related donors with one fully mismatched HLA haplotype. N Engl J Med. (1998) 339:1186–93. doi: 10.1056/NEJM199810223391702
33. Rachamim N, Gan J, Segall H, Krauthgamer R, Marcus H, Berrebi A, et al. Tolerance induction by "megadose" hematopoietic transplants: donor-type human CD34 stem cells induce potent specific reduction of host anti-donor cytotoxic T lymphocyte precursors in mixed lymphocyte culture. Transplantation. (1998) 65:1386–93. doi: 10.1097/00007890-199805270-00017
34. Gur H, Krauthgamer R, Bachar-Lustig E, Katchman H, Arbel-Goren R, Berrebi A, et al. Immune regulatory activity of CD34+ progenitor cells: evidence for a deletion-based mechanism mediated by TNF-alpha. Blood. (2005) 105:2585–93. doi: 10.1182/blood-2002-11-3463
35. Terenzi A, Aristei C, Aversa F, Perruccio K, Chionne F, Raymondi C, et al. Efficacy of fludarabine as an immunosuppressor for bone marrow transplantation conditioning: preliminary results. Transplant Proc. (1996) 28:3101.
36. Aversa F, Tabilio A, Terenzi A, Velardi A, Falzetti F, Giannoni C, et al. Successful engraftment of T-cell-depleted haploidentical "three-loci" incompatible transplants in leukemia patients by addition of recombinant human granulocyte colony-stimulating factor-mobilized peripheral blood progenitor cells to bone marrow inoculum. Blood. (1994) 84:3948–55. doi: 10.1182/blood.V84.11.3948.bloodjournal84113948
37. Berenbaum MC, Brown IN. Prolongation of homograft survival in mice with single doses of cyclophosphamide. Nature. (1963) 200:84. doi: 10.1038/200084a0
38. Colson YL, Li H, Boggs SS, Patrene KD, Johnson PC, Ildstad ST. Durable mixed allogeneic chimerism and tolerance by a nonlethal radiation-based cytoreductive approach. J Immunol. (1996) 157:2820–9.
39. Colson YL, Wren SM, Schuchert MJ, Patrene KD, Johnson PC, Boggs SS, et al. A nonlethal conditioning approach to achieve durable

multilineage mixed chimerism and tolerance across major, minor, and hematopoietic histocompatibility barriers. J Immunol. (1995) 155:4179–88.
40. Robinson TM, O'Donnell PV, Fuchs EJ, Luznik L. Haploidentical bone marrow and stem cell transplantation: experience with post-transplantation cyclophosphamide. Semin Hematol. (2016) 53:90–7. doi: 10.1053/j.seminhematol.2016.01.005
41. Nomoto K, Eto M, Yanaga K, Nishimura Y, Maeda T, Nomoto K. Interference with cyclophosphamide-induced skin allograft tolerance by cyclosporin A. J Immunol. (1992) 149:2668–74.
42. Dukor P, Dietrich FM. Prevention of cyclophosphamide-induced tolerance to erythrocytes by pretreatment with cortisone. Proc Soc Exp Biol Med. (1970) 133:280–5. doi: 10.3181/00379727-133-34456
43. Ross D, Jones M, Komanduri K, Levy RB. Antigen and lymphopenia-driven donor T cells are differentially diminished by post-transplantation administration of cyclophosphamide after hematopoietic cell transplantation. Biol Blood Marrow Transplant. (2013) 19:1430–8. doi: 10.1016/j.bbmt.2013.06.019
44. Eto M, Mayumi H, Tomita Y, Yoshikai Y, Nishimura Y, Maeda T, et al. Specific destruction of host-reactive mature T cells of donor origin prevents graft-versus-host disease in cyclophosphamide-induced tolerant mice. J Immunol. (1991) 146:1402–9.
45. Eto M, Mayumi H, Tomita Y, Yoshikai Y, Nishimura Y, Nomoto K. The requirement of intrathymic mixed chimerism and clonal deletion for a long- lasting skin allograft tolerance in cyclophosphamide-induced tolerance. Eur J Immunol. (1990) 20:2005–13. doi: 10.1002/eji.1830200919
46. Eto M, Mayumi H, Tomita Y, Yoshikai Y, Nishimura Y, Nomoto K. Sequential mechanisms of cyclophosphamide-induced skin allograft tolerance including the intrathymic clonal deletion followed by late breakdown of the clonal deletion. J Immunol. (1990) 145:1303–10.
47. Eto M, Mayumi H, Tomita Y, Yoshikai Y, Nomoto K. Intrathymic clonal deletion of V beta 6+ T cells in cyclophosphamide-induced tolerance to H-2-compatible, Mls-disparate antigens. J Exp Med. (1990) 171:97–113. doi: 10.1084/jem.171.1.97
48. McCurdy SR, Luznik L. Post-transplantation cyclophosphamide for chimerism-based tolerance. Bone Marrow Transplant. (2019) 54 (Suppl 2):769–74. doi: 10.1038/s41409-019-0615-0

49. Kong YY, Eto M, Omoto K, Umesue M, Hashimoto A, Nomoto K. Regulatory T cells in maintenance and reversal of peripheral tolerance in vivo. J Immunol. (1996) 157:5284–9.
50. Tomita Y, Mayumi H, Eto M, Nomoto K. Importance of suppressor T cells in cyclophosphamide-induced tolerance to the non-H-2-encoded alloantigens. Is mixed chimerism really required in maintaining a skin allograft tolerance? J Immunol. (1990) 144:463–73.
51. Wachsmuth LP, Patterson MT, Eckhaus MA, Venzon DJ, Gress RE, Kanakry CG. Post-transplantation cyclophosphamide prevents graft-versus- host disease by inducing alloreactive T cell dysfunction and suppression. J Clin Invest. (2019) 130:2357–73. doi: 10.1172/JCI124218
52. Kanakry CG, Ganguly S, Zahurak M, Bolaños-Meade J, Thoburn C, Perkins B, et al. Aldehyde dehydrogenase expression drives human regulatory T cell resistance to posttransplantation cyclophosphamide. Sci Transl Med. (2013) 5:211ra157. doi: 10.1126/scitranslmed.3006960
53. Ganguly S, Ross DB, Panoskaltsis-Mortari A, Kanakry CG, Blazar BR, Levy RB, et al. Donor CD4+ Foxp3+ regulatory T cells are necessary for posttransplantation cyclophosphamide-mediated protection against GVHD in mice. Blood. (2014) 124:2131–41. doi: 10.1182/blood-2013-10-5 25873
54. O'Donnell PV, Luznik L, Jones RJ, Vogelsang GB, Leffell MS, Phelps M, et al. Nonmyeloablative bone marrow transplantation from partially HLA-mismatched related donors using posttransplantation cyclophosphamide. Biol Blood Marrow Transplant. (2002) 8:377–86. doi: 10.1053/bbmt.2002.v8.pm12171484
55. Chang YJ, Huang XJ. Haploidentical stem cell transplantation: anti-thymocyte globulin-based experience. Semin Hematol. (2016) 53:82–9. doi: 10.1053/j.seminhematol.2016.01.004
56. Korbling M, Anderlini P. Peripheral blood stem cell versus bone marrow allotransplantation: does the source of hematopoietic stem cells matter? Blood. (2001) 98:2900–8. doi: 10.1182/blood.V98.10.2900
57. Anasetti C, Logan BR, Lee SJ, Waller EK, Weisdorf DJ, Wingard JR, et al. Peripheral-blood stem cells versus bone marrow from unrelated donors. N Engl J Med. (2012) 367:1487–96. doi: 10.1056/NEJMoa1203517

58. Arpinati M, Green CL, Heimfeld S, Heuser JE, Anasetti C. Granulocyte- colony stimulating factor mobilizes T helper 2-inducing dendritic cells. Blood. (2000) 95:2484–90. doi: 10.1182/blood.V95.8.2484
59. Pan L, Delmonte J Jr, Jalonen CK, Ferrara JL. Pretreatment of donor mice with granulocyte colony-stimulating factor polarizes donor T lymphocytes toward type-2 cytokine production and reduces severity of experimental graft-versus-host disease. Blood. (1995) 86:4422–9. doi: 10.1182/blood.V86.12.4422.bloodjournal86124422
60. Mielcarek M, Martin PJ, Torok-Storb B. Suppression of alloantigen-induced T-cell proliferation by CD14+ cells derived from granulocyte colony- stimulating factor-mobilized peripheral blood mononuclear cells. Blood. (1997) 89:1629–34. doi: 10.1182/blood.V89.5.1629
61. Tanaka J, Mielcarek M, Torok-Storb B. Impaired induction of the CD28- responsive complex in granulocyte colony-stimulating factor mobilized CD4 T cells. Blood. (1998) 91:347–52. doi: 10.1182/blood.V91.1.347
62. Mielcarek M, Graf L, Johnson G, Torok-Storb B. Production of interleukin- 10 by granulocyte colony-stimulating factor-mobilized blood products: a mechanism for monocyte-mediated suppression of T-cell proliferation. Blood. (1998) 92:215–22. doi: 10.1182/blood.V92.1.215.413k10_215_222
63. Morton J, Hutchins C, Durrant S. Granulocyte-colony-stimulating factor (G-CSF)-primed allogeneic bone marrow: significantly less graft-versus-host disease and comparable engraftment to G-CSF-mobilized peripheral blood stem cells. Blood. (2001) 98:3186–91. doi: 10.1182/blood.V98.12.3186
64. Huang B, Hirst AR, Smith DK, Castelletto V, Hamley IW. A direct comparison of one- and two-component dendritic self-assembled materials: elucidating molecular recognition pathways. J Am Chem Soc. (2005) 127:7130–9. doi: 10.1021/ja050412d
65. Chen SH, Li X, Huang XJ. Effect of recombinant human granulocyte colony- stimulating factor on T-lymphocyte function and the mechanism of this effect. Int J Hematol. (2004) 79:178–84. doi: 10.1532/IJH97.A10227
66. Zhao XY, Chang YJ, Huang XJ. Effects of rhG-CSF mobilization on immunological properties of grafts from peripheral blood and bone marrow. Zhongguo Shi Yan Xue Ye Xue Za Zhi. (2006) 14:787–90.

67. Wang Y, Liu QF, Xu LP, Liu KY, Zhang XH, Ma X, et al. Haploidentical vs identical-sibling transplant for AML in remission: a multicenter, prospective study. Blood. (2015) 125:3956–62. doi: 10.1182/blood-2015-02-627786
68. Arcese W, Picardi A, Santarone S, De Angelis G, Cerretti R, Cudillo L, et al. Haploidentical, G-CSF-primed, unmanipulated bone marrow transplantation for patients with high-risk hematological malignancies: an update. Bone Marrow Transplant. (2015)50 (Suppl 2):S24–30. doi: 10.1038/bmt.2015.91
69. Wang Y, Chang YJ, Xu LP, Liu KY, Liu DH, Zhang XH, et al. Who is the best donor for a related HLA haplotype-mismatched transplant? Blood. (2014) 124:843–50. doi: 10.1182/blood-2014-03-563130
70. Reisner Y, Kapoor N, O'Reilly RJ, Good RA. Allogeneic bone marrow transplantation using stem cells fractionated by lectins: VI, in vitro analysis of human and monkey bone marrow cells fractionated by sheep red blood cells and soybean agglutinin. Lancet. (1980) 2:1320–4. doi: 10.1016/S0140-6736(80)92394-6
71. Reisner Y, Itzicovitch L, Meshorer A, Sharon N. Hemopoietic stem cell transplantation using mouse bone marrow and spleen cells fractionated by lectins. Proc Natl Acad Sci USA. (1978) 75:2933–6. doi: 10.1073/pnas.75.6.2933
72. Reisner Y, Kapoor N, Kirkpatrick D, Pollack MS, Dupont B, Good RA, et al. Transplantation for acute leukaemia with HLA-A and B nonidentical parental marrow cells fractionated with soybean agglutinin and sheep red blood cells. Lancet. (1981) 2:327–31. doi: 10.1016/S0140-6736(81)90647-4
73. Civin CI, Strauss LC, Fackler MJ, Trischmann TM, Wiley JM, Loken MR. Positive stem cell selection–basic science. Prog Clin Biol Res. (1990) 333:387– 401; discussion 2.
74. Heimfeld S, Fogarty B, McGuire K, Williams S, Berenson RJ. Peripheral blood stem cell mobilization after stem cell factor or G-CSF treatment: rapid enrichment for stem and progenitor cells using the CEPRATE immunoaffinity separation system. Transplant Proc. (1992) 24:2818.
75. Handgretinger R, Dopfer R, Hammer S, Lang P, Daurer B, Kimmig A, et al. The efficiency of a new cell separation technique in bone marrow purging without damaging the purged tumor cells. Prog Clin Biol Res. (1990) 333:303–9.

76. Ruggeri L, Capanni M, Urbani E, Perruccio K, Shlomchik WD, Tosti A, et al. Effectiveness of donor natural killer cell alloreactivity in mismatched hematopoietic transplants. Science. (2002) 295:2097–100. doi: 10.1126/science.1068440
77. Handgretinger R, Klingebiel T, Lang P, Schumm M, Neu S, Geiselhart A, et al. Megadose transplantation of purified peripheral blood CD34(+) progenitor cells from HLA-mismatched parental donors in children. Bone Marrow Transplant. (2001) 27:777–83. doi: 10.1038/sj.bmt.1702996
78. Feuchtinger T, Richard C, Pfeiffer M, Neuhauser F, Lucke J, Handgretinger R, et al. Adenoviral infections after transplantation of positive selected stem cells from haploidentical donors in children: an update. Klin Padiatr. (2005) 217:339–44. doi: 10.1055/s-2005-872530
79. Lang P, Schumm M, Greil J, Bader P, Klingebiel T, Muller I, et al. A comparison between three graft manipulation methods for haploidentical stem cell transplantation in pediatric patients: preliminary results of a pilot study. Klin Padiatr. (2005) 217:334–8. doi: 10.1055/s-2005-872529
80. McManigle W, Youssef A, Sarantopoulos S. B cells in chronic graft-versus-host disease. Hum Immunol. (2019) 80:393–9. doi: 10.1016/j.humimm.2019.03.003
81. Liu L, Zhang X, Feng S. Epstein-barr virus-related post-transplantation lymphoproliferative disorders after allogeneic hematopoietic stem cell transplantation. Biol Blood Marrow Transplant. (2018) 24:1341–9. doi: 10.1016/j.bbmt.2018.02.026
82. Burns DM, Rana S, Martin E, Nagra S, Ward J, Osman H, et al. Greatly reduced risk of EBV reactivation in rituximab-experienced recipients of alemtuzumab-conditioned allogeneic HSCT. Bone Marrow Transplant. (2016) 51:825–32. doi: 10.1038/bmt.2016.19
83. Federmann B, Bornhauser M, Meisner C, Kordelas L, Beelen DW, Stuhler G, et al. Haploidentical allogeneic hematopoietic cell transplantation in adults using CD3/CD19 depletion and reduced intensity conditioning: a phase II study. Haematologica. (2012) 97:1523–31. doi: 10.3324/haematol.2011.059378
84. Bethge WA, Faul C, Bornhäuser M, Stuhler G, Beelen DW, Lang P, et al. Haploidentical allogeneic hematopoietic cell transplantation in adults using CD3/CD19 depletion and reduced intensity conditioning:

an update. Blood Cells Mol Dis. (2008) 40:13–9. doi: 10.1016/j.bcmd.2007.07.001
85. Handgretinger R, Schilbach K. The potential role of gammadelta T cells after allogeneic HCT for leukemia. Blood. (2018) 131:1063–72. doi: 10.1182/blood-2017-08-752162
86. Drobyski WR, Majewski D, Hanson G. Graft-facilitating doses of ex vivo activated gammadelta T cells do not cause lethal murine graft-vs.-host disease. Biol Blood Marrow Transplant. (1999) 5:222–30. doi: 10.1053/bbmt.1999.v5.pm10465102
87. Bendelac A, Bonneville M, Kearney JF. Autoreactivity by design: innate B and T lymphocytes. Nat Rev Immunol. (2001) 1:177–86. doi: 10.1038/35105052
88. Hayday AC. Gammadelta T cells and the lymphoid stress-surveillance response. Immunity. (2009) 31:184–96. doi: 10.1016/j.immuni.2009. 08.006
89. Viey E, Laplace C, Escudier B. Peripheral gammadelta T-lymphocytes as an innovative tool in immunotherapy for metastatic renal cell carcinoma. Expert Rev Anticancer Ther. (2005) 5:973–86. doi: 10.1586/14737140.5.6.973
90. Corvaisier M, Moreau-Aubry A, Diez E, Bennouna J, Mosnier JF, Scotet E, et al. V gamma 9V delta 2 T cell response to colon carcinoma cells. J Immunol. (2005) 175:5481–8. doi: 10.4049/jimmunol.175.8.5481
91. Bonneville M, Scotet E. Synergism and complementarity between human CD1 AND MHC-restricted T cells, two lymphoid subsets directed against distinct antigenic worlds. Front Biosci. (2005) 10:596–607. doi: 10.2741/1556
92. Dieli F, Troye-Blomberg M, Ivanyi J, Fournie JJ, Krensky AM, Bonneville M, et al. Granulysin-dependent killing of intracellular and extracellular Mycobacterium tuberculosis by Vgamma9/Vdelta2 T lymphocytes. J Infect Dis. (2001) 184:1082–5. doi: 10.1086/323600
93. Dudal S, Turriere C, Bessoles S, Fontes P, Sanchez F, Liautard J, et al. Release of LL-37 by activated human Vgamma9Vdelta2T cells: a microbicidal weapon against Brucella suis. J Immunol. (2006) 177:5533–9. doi: 10.4049/jimmunol.177.8.5533
94. Perko R, Kang G, Sunkara A, Leung W, Thomas PG, Dallas MH. Gamma delta T cell reconstitution is associated with fewer infections and improved event-free survival after hematopoietic stem cell

transplantation for pediatric leukemia. Biol Blood Marrow Transplant. (2015) 21:130–6. doi: 10.1016/j.bbmt.2014.09.027
95. Godder KT, Henslee-Downey PJ, Mehta J, Park BS, Chiang KY, Abhyankar S, et al. Long term disease-free survival in acute leukemia patients recovering with increased gammadelta T cells after partially mismatched related donor bone marrow transplantation. Bone Marrow Transplant. (2007) 39:751–7. doi: 10.1038/sj.bmt.1705650
96. Lamb LS Jr, Henslee-Downey PJ, Parrish RS, Godder K, Thompson J, Lee C, et al. Increased frequency of TCR gamma delta + T cells in disease- free survivors following T cell-depleted, partially mismatched, related donor bone marrow transplantation for leukemia. J Hematother. (1996) 5:503–9. doi: 10.1089/scd.1.1996.5.503
97. Airoldi I, Bertaina A, Prigione I, Zorzoli A, Pagliara D, Cocco C, et al. γδ T- cell reconstitution after HLA-haploidentical hematopoietic transplantation depleted of TCR-αβ+/CD19+ lymphocytes. Blood. (2015) 125:2349–58. doi: 10.1182/blood-2014-09-599423
98. Bertaina A, Zorzoli A, Petretto A, Barbarito G, Inglese E, Merli P, et al. Zoledronic acid boosts gammadelta T-cell activity in children receiving alphabeta(+) T and CD19(+) cell-depleted grafts from an HLA-haplo-identical donor. Oncoimmunology. (2017) 6:e1216291. doi: 10.1080/2162402X.2016.1216291
99. Locatelli F, Merli P, Pagliara D, Li Pira G, Falco M, Pende D, et al. Outcome of children with acute leukemia given HLA-haploidentical HSCT after alphabeta T-cell and B-cell depletion. Blood. (2017) 130:677–85. doi: 10.1182/blood-2017-04-779769
100. Bertaina A, Merli P, Rutella S, Pagliara D, Bernardo ME, Masetti R, et al. HLA-haploidentical stem cell transplantation after removal of alphabeta+ T and B cells in children with nonmalignant disorders. Blood. (2014) 124:822– 6. doi: 10.1182/blood-2014-03-563817
101. Bertaina A, Zecca M, Buldini B, Sacchi N, Algeri M, Saglio F, et al. Unrelated donor vs HLA-haploidentical alpha/beta T-cell- and B-cell- depleted HSCT in children with acute leukemia. Blood. (2018) 132:2594–607. doi: 10.1182/blood-2018-07-861575
102. Lang P, Handgretinger R, Meisel R, Mielke S, Niederwieser D, Schlegel PG, et al. Results of a prospective, multicenter, phase I/II clinical study in pediatric and adult patients using TCR alpha/beta and CD19 depleted haploidentical hematopoietic stem cell grafts

following reduced-intensity conditioning. Blood. (2018) 132 (Suppl 1):604. doi: 10.1182/blood-2018-99-110124

103. Restifo NP, Gattinoni L. Lineage relationship of effector and memory T cells. Curr Opin Immunol. (2013) 25:556–63. doi: 10.1016/j.coi.2013.09.003

104. Lanzavecchia A, Sallusto F. Dynamics of T lymphocyte responses: intermediates, effectors, and memory cells. Science. (2000) 290:92–7. doi: 10.1126/science.290.5489.92

105. Anderson BE, McNiff J, Yan J, Doyle H, Mamula M, Shlomchik MJ, et al. Memory CD4+ T cells do not induce graft-versus-host disease. J Clin Invest. (2003) 112:101–8. doi: 10.1172/JCI17601

106. Zheng H, Matte-Martone C, Li H, Anderson BE, Venketesan S, Sheng Tan H, et al. Effector memory CD4+ T cells mediate graft-versus-leukemia without inducing graft-versus-host disease. Blood. (2008) 111:2476–84. doi: 10.1182/blood-2007-08-109678

107. Zheng H, Matte-Martone C, Jain D, McNiff J, Shlomchik WD. Central memory CD8+ T cells induce graft-versus-host disease and mediate graft-versus-leukemia. J Immunol. (2009) 182:5938–48. doi: 10.4049/jimmunol.0802212

108. Dutt S, Tseng D, Ermann J, George TI, Liu YP, Davis CR, et al. Naive and memory T cells induce different types of graft-versus-host disease. J Immunol. (2007) 179:6547–54. doi: 10.4049/jimmunol.179.10.6547

109. Chen BJ, Cui X, Sempowski GD, Liu C, Chao NJ. Transfer of allogeneic CD62L- memory T cells without graft-versus-host disease. Blood. (2004) 103:1534–41. doi: 10.1182/blood-2003-08-2987

110. Li N, Matte-Martone C, Zheng H, Cui W, Venkatesan S, Tan HS, et al. Memory T cells from minor histocompatibility antigen-vaccinated and virus-immune donors improve GVL and immune reconstitution. Blood. (2011) 118:5965–76. doi: 10.1182/blood-2011-07-367011

111. Bleakley M, Heimfeld S, Jones LA, Turtle C, Krause D, Riddell SR, et al. Engineering human peripheral blood stem cell grafts that are depleted of naive T cells and retain functional pathogen-specific memory T cells. Biol Blood Marrow Transplant. (2014) 20:705–16. doi: 10.1016/j.bbmt.2014.01.032

112. Bleakley M, Heimfeld S, Loeb KR, Jones LA, Chaney C, Seropian S, et al. Outcomes of acute leukemia patients transplanted with naive T cell-depleted stem cell grafts. J Clin Invest. (2015) 125:2677–89. doi: 10.1172/JCI81229
113. Triplett BM, Shook DR, Eldridge P, Li Y, Kang G, Dallas M, et al. Rapid memory T-cell reconstitution recapitulating CD45RA-depleted haploidentical transplant graft content in patients with hematologic malignancies. Bone Marrow Transplant. (2015) 50:1012. doi: 10.1038/bmt.2015.139
114. Touzot F, Neven B, Dal-Cortivo L, Gabrion A, Moshous D, Cros G, et al. CD45RA depletion in HLA-mismatched allogeneic hematopoietic stem cell transplantation for primary combined immunodeficiency: a preliminary study. J Allergy Clin Immunol. (2015) 135:1303–9.e1–3. doi: 10.1016/j.jaci.2014.08.019
115. Gribben JG, Guinan EC, Boussiotis VA, Ke XY, Linsley L, Sieff C, et al. Complete blockade of B7 family-mediated costimulation is necessary to induce human alloantigen-specific anergy: a method to ameliorate graft- versus-host disease and extend the donor pool. Blood. (1996) 87:4887–93. doi: 10.1182/blood.V87.11.4887.bloodjournal87114887
116. Guinan EC, Boussiotis VA, Neuberg D, Brennan LL, Hirano N, Nadler LM, et al. Transplantation of anergic histoincompatible bone marrow allografts. N Engl J Med. (1999) 340:1704–14. doi: 10.1056/NEJM199906033402202
117. Bastien JP, Krosl G, Therien C, Rashkovan M, Scotto C, Cohen S, et al. Photodepletion differentially affects CD4+ Tregs versus CD4+ effector T cells from patients with chronic graft-versus-host disease. Blood. (2010) 116:4859–69. doi: 10.1182/blood-2010-03-273193
118. Perruccio K, Topini F, Tosti A, Carotti A, Burchielli E, Ruggeri L, et al. Optimizing a photoallodepletion protocol for adoptive immunotherapy after haploidentical SCT. Bone Marrow Transplant. (2012) 47:1196–200. doi: 10.1038/bmt.2011.237
119. Perruccio K, Topini F, Tosti A, Carotti A, Aloisi T, Aversa F, et al. Photodynamic purging of alloreactive T cells for adoptive immunotherapy after haploidentical stem cell transplantation. Blood Cells Mol Dis. (2008) 40:76–83. doi: 10.1016/j.bcmd.2007.06.022
120. Roy DC, Lachance S, Cohen S, Delisle JS, Kiss T, Sauvageau G, et al. Allodepleted T-cell immunotherapy after haploidentical

haematopoietic stem cell transplantation without severe acute graft-versus-host disease (GVHD) in the absence of GVHD prophylaxis. Br J Haematol. (2019) 186:754–66. doi: 10.1111/bjh.15970

121. Sun JC, Beilke JN, Lanier LL. Adaptive immune features of natural killer cells. Nature. (2009) 457:557–61. doi: 10.1038/nature07665

122. Vacca P, Montaldo E, Croxatto D, Moretta F, Bertaina A, Vitale C, et al. NK cells and other innate lymphoid cells in hematopoietic stem cell transplantation. Front Immunol. (2016) 7:188. doi: 10.3389/fimmu.2016.00188

123. Freud AG, Mundy-Bosse BL, Yu J, Caligiuri MA. The broad spectrum of human natural killer cell diversity. Immunity. (2017) 47:820–33. doi: 10.1016/j.immuni.2017.10.008

124. Vivier E, Raulet DH, Moretta A, Caligiuri MA, Zitvogel L, Lanier LL, et al. Innate or adaptive immunity? The example of natural killer cells. Science. (2011) 331:44–9. doi: 10.1126/science.1198687

125. Lanier LL. NKG2D receptor and its ligands in host defense. Cancer Immunol Res. (2015) 3:575–82. doi: 10.1158/2326-6066.CIR-15-0098

126. Boudreau JE, Hsu KC. Natural killer cell education and the response to infection and cancer therapy: stay tuned. Trends Immunol. (2018) 39:222–39. doi: 10.1016/j.it.2017.12.001

127. Locatelli F, Pende D, Mingari MC, Bertaina A, Falco M, Moretta A, et al. Cellular and molecular basis of haploidentical hematopoietic stem cell transplantation in the successful treatment of high-risk leukemias: role of alloreactive NK cells. Front Immunol. (2013) 4:15. doi: 10.3389/fimmu.2013.00015

128. Joyce MG, Sun PD. The structural basis of ligand recognition by natural killer cell receptors. J Biomed Biotechnol. (2011) 2011:203628. doi: 10.1155/2011/203628

129. Misra MK, Augusto DG, Martin GM, Nemat-Gorgani N, Sauter J, Hofmann JA, et al. Report from the Killer-cell Immunoglobulin-like Receptors (KIR) component of the 17th International HLA and Immunogenetics Workshop. Hum Immunol. (2018) 79:825–33. doi: 10.1016/j.humimm.2018.10.003

130. Hsu KC, Liu XR, Selvakumar A, Mickelson E, O'Reilly RJ, Dupont B. Killer Ig-like receptor haplotype analysis by gene content: evidence for genomic diversity with a minimum of six basic

framework haplotypes, each with multiple subsets. J Immunol. (2002) 169:5118–29. doi: 10.4049/jimmunol.169.9.5118

131. Hsu KC, Chida S, Geraghty DE, Dupont B. The killer cell immunoglobulin-like receptor (KIR) genomic region: gene-order, haplotypes and allelic polymorphism. Immunol Rev. (2002) 190:40–52. doi: 10.1034/j.1600-065X.2002.19004.x

132. Jiang W, Johnson C, Jayaraman J, Simecek N, Noble J, Moffatt MF, et al. Copy number variation leads to considerable diversity for B but not A haplotypes of the human KIR genes encoding NK cell receptors. Genome Res. (2012) 22:1845–54. doi: 10.1101/gr.137976.112

133. Pyo CW, Guethlein LA, Vu Q, Wang R, Abi-Rached L, Norman PJ, et al. Different patterns of evolution in the centromeric and telomeric regions of group A and B haplotypes of the human killer cell Ig-like receptor locus. PLoS ONE. (2010) 5:e15115. doi: 10.1371/journal.pone.0015115

134. Leung W, Iyengar R, Triplett B, Turner V, Behm FG, Holladay MS, et al. Comparison of killer Ig-like receptor genotyping and phenotyping for selection of allogeneic blood stem cell donors. J Immunol. (2005) 174:6540–5. doi: 10.4049/jimmunol.174.10.6540

135. Leung W. Use of NK cell activity in cure by transplant. Br J Haematol. (2011) 155:14–29. doi: 10.1111/j.1365-2141.2011.08823.x

136. Elliott JM, Yokoyama WM. Unifying concepts of MHC-dependent natural killer cell education. Trends Immunol. (2011) 32:364–72. doi: 10.1016/j.it.2011.06.001

137. Raulet DH. Missing self recognition and self tolerance of natural killer (NK) cells. Semin Immunol. (2006) 18:145–50. doi: 10.1016/j.smim.2006.03.003

138. Anfossi N, Andre P, Guia S, Falk CS, Roetynck S, Stewart CA, et al. Human NK cell education by inhibitory receptors for MHC class I. Immunity. (2006) 25:331–42. doi: 10.1016/j.immuni.2006.06.013

139. Orr MT, Murphy WJ, Lanier LL. 'Unlicensed' natural killer cells dominate the response to cytomegalovirus infection. Nat Immunol. (2010) 11:321–7. doi: 10.1038/ni.1849

140. Tarek N, Le Luduec JB, Gallagher MM, Zheng J, Venstrom JM, Chamberlain E, et al. Unlicensed NK cells target neuroblastoma

following anti-GD2 antibody treatment. J Clin Invest. (2012) 122:3260–70. doi: 10.1172/JCI62749

141. Joncker NT, Fernandez NC, Treiner E, Vivier E, Raulet DH. NK cell responsiveness is tuned commensurate with the number of inhibitory receptors for self-MHC class I: the rheostat model. J Immunol. (2009) 182:4572–80. doi: 10.4049/jimmunol.0803900

142. Boudreau JE, Mulrooney TJ, Le Luduec JB, Barker E, Hsu KC. KIR3DL1 and HLA-B density and binding calibrate NK education and response to HIV. J Immunol. (2016) 196:3398–410. doi: 10.4049/jimmunol.1502469

143. Valiante NM, Parham P. Natural killer cells, HLA class I molecules, and marrow transplantation. Biol Blood Marrow Transplant. (1997) 3:229–35.

144. Leung W, Iyengar R, Turner V, Lang P, Bader P, Conn P, et al. Determinants of antileukemia effects of allogeneic NK cells. J Immunol. (2004) 172:644–50. doi: 10.4049/jimmunol.172.1.644

145. McQueen KL, Dorighi KM, Guethlein LA, Wong R, Sanjanwala B, Parham P. Donor-recipient combinations of group A and B KIR haplotypes and HLA class I ligand affect the outcome of HLA-matched, sibling donor hematopoietic cell transplantation. Hum Immunol. (2007) 68:309–23. doi: 10.1016/j.humimm.2007.01.019

146. Cooley S, Trachtenberg E, Bergemann TL, Saeteurn K, Klein J, Le CT, et al. Donors with group B KIR haplotypes improve relapse-free survival after unrelated hematopoietic cell transplantation for acute myelogenous leukemia. Blood. (2009) 113:726–32. doi: 10.1182/blood-2008-07-171926

147. Cooley S, Weisdorf DJ, Guethlein LA, Klein JP, Wang T, Le CT, et al. Donor selection for natural killer cell receptor genes leads to superior survival after unrelated transplantation for acute myelogenous leukemia. Blood. (2010) 116:2411–9. doi: 10.1182/blood-2010-05-283051

148. Ruggeri L, Mancusi A, Capanni M, Urbani E, Carotti A, Aloisi T, et al. Donor natural killer cell allorecognition of missing self in haploidentical hematopoietic transplantation for acute myeloid leukemia: challenging its predictive value. Blood. (2007) 110:433–40. doi: 10.1182/blood-2006-07-038687

149. Boudreau JE, Giglio F, Gooley TA, Stevenson PA, Le Luduec JB, Shaffer BC, et al. KIR3DL1/HLA-B subtypes govern acute myelogenous leukemia relapse after hematopoietic cell

transplantation. J Clin Oncol. (2017) 35:2268–78. doi: 10.1200/JCO.2016.70.7059

150. Cooley S, McCullar V, Wangen R, Bergemann TL, Spellman S, Weisdorf DJ, et al. KIR reconstitution is altered by T cells in the graft and correlates with clinical outcomes after unrelated donor transplantation. Blood. (2005) 106:4370–6. doi: 10.1182/blood-2005-04-1644

151. Mancusi A, Ruggeri L, Urbani E, Pierini A, Massei MS, Carotti A, et al. Haploidentical hematopoietic transplantation from KIR ligand-mismatched donors with activating KIRs reduces nonrelapse mortality. Blood. (2015) 125:3173–82. doi: 10.1182/blood-2014-09-599993

152. Oevermann L, Michaelis SU, Mezger M, Lang P, Toporski J, Bertaina A, et al. KIR B haplotype donors confer a reduced risk for relapse after haploidentical transplantation in children with ALL. Blood. (2014) 124:2744– 7. doi: 10.1182/blood-2014-03-565069

153. Wanquet A, Bramanti S, Harbi S, Furst S, Legrand F, Faucher C, et al. Killer cell immunoglobulin-like receptor-ligand mismatch in donor versus recipient direction provides better graft-versus-tumor effect in patients with hematologic malignancies undergoing allogeneic T cell-replete haploidentical transplantation followed by post-transplant cyclophosphamide. Biol Blood Marrow Transplant. (2018) 24:549–54. doi: 10.1016/j.bbmt.2017.11.042

154. van den Brink MR, Velardi E, Perales MA. Immune reconstitution following stem cell transplantation. Hematology Am Soc Hematol Educ Program. (2015) 2015:215–9. doi: 10.1182/asheducation-2015.1.215

155. Ogonek J, Kralj Juric M, Ghimire S, Varanasi PR, Holler E, Greinix H, et al. Immune reconstitution after allogeneic hematopoietic stem cell transplantation. Front Immunol. (2016) 7:507. doi: 10.3389/fimmu.2016.00507

156. DeCook LJ, Thoma M, Huneke T, Johnson ND, Wiegand RA, Patnaik MM, et al. Impact of lymphocyte and monocyte recovery on the outcomes of allogeneic hematopoietic SCT with fludarabine and melphalan conditioning. Bone Marrow Transplantation. (2012) 48:708. doi: 10.1038/bmt.2012.211

157. Le Bourgeois A, Peterlin P, Guillaume T, Delaunay J, Duquesne A, Le Gouill S, et al. Higher early monocyte and total lymphocyte counts are associated with better overall survival after

standard total body irradiation, cyclophosphamide, and fludarabine reduced-intensity conditioning double umbilical cord blood allogeneic stem cell transplantation in adults. Biol Blood Marrow Transplant. (2016) 22:1473–9. doi: 10.1016/j.bbmt.2016.04.015

158. Turcotte LM, Cao Q, Cooley SA, Curtsinger J, Holtan SG, Luo X, et al. Monocyte subpopulation recovery as predictors of hematopoietic cell transplantation outcomes. Biol Blood Marrow Transplant. (2019) 25:883–90. doi: 10.1016/j.bbmt.2019.01.003

159. Pei X, Zhao X, Wang Y, Xu L, Zhang X, Liu K, et al. Comparison of reference values for immune recovery between event-free patients receiving haploidentical allografts and those receiving human leukocyte antigen-matched sibling donor allografts. Front Med. (2018) 12:153–63. doi: 10.1007/s11684-017-0548-1

160. Salzmann-Manrique E, Bremm M, Huenecke S, Stech M, Orth A, Eyrich M, et al. Joint modeling of immune reconstitution post haploidentical stem cell transplantation in pediatric patients with acute leukemia comparing CD34+-selected to CD3/CD19-depleted grafts in a retrospective multicenter study. Front Immunol. (2018) 9:1841. doi: 10.3389/fimmu.2018.01841

161. Offner F, Schoch G, Fisher L, Torok-Storb B, Martin P. Mortality hazard functions as related to neutropenia at different times after marrow transplantation. Blood. (1996) 88:4058–62. doi: 10.1182/blood.V88.10.4058.bloodjournal88104058

162. Chang Y-J, Zhao X-Y, Huo M-R, Xu L-P, Liu D-H, Liu K-Y, et al. Immune reconstitution following unmanipulated HLA-mismatched/haploidentical transplantation compared with HLA-identical sibling transplantation. J Clin Immunol. (2012) 32:268–80. doi: 10.1007/s10875-011-9630-7

163. Lin X, Lu ZG, Song CY, Huang YX, Guo KY, Deng L, et al. Long-term outcome of HLA-haploidentical hematopoietic stem cell transplantation without in vitro T-cell depletion based on an FBCA conditioning regimen for hematologic malignancies. Bone Marrow Transplant. (2015) 50:1092. doi: 10.1038/bmt.2015.108

164. Fearnley DB, Whyte LF, Carnoutsos SA, Cook AH, Hart DNJ. Monitoring human blood dendritic cell numbers in normal individuals and in stem cell transplantation. Blood. (1999) 93:728–36. doi: 10.1182/blood.V93.2.728

165. Soriano-Sarabia N, Sandvold H, Jomaa H, Kubin T, Bein G, Hackstein H. Primary MHC-class II+ cells are necessary to promote

resting Vδ2 cell expansion in response to (E)-4-hydroxy-3-methyl-but-2-enyl- pyrophosphate and isopentenyl pyrophosphate. J Immunol. (2012) 189:5212–22. doi: 10.4049/jimmunol.1200093

166. Wang X, Liu J, Gao H, Mo X-D, Han T, Xu L-P, et al. Dendritic cells are critical for the activation and expansion of Vδ2+ T cells after allogeneic hematopoietic transplantation. Front Immunol. (2018) 9:2528. doi: 10.3389/fimmu.2018.02528

167. Roider T, Katzfuß M, Matos C, Singer K, Renner K, Oefner PJ, et al. Antithymocyte globulin induces a tolerogenic phenotype in human dendritic cells. Int J Mol Sci. (2016) 17:2081. doi: 10.3390/ijms17122081

168. Monti P, Allavena P, Di Carlo V, Piemonti L. Effects of anti-lymphocytes and anti-thymocytes globulin on human dendritic cells. Int Immunopharmacol. (2003) 3:189–96. doi: 10.1016/S1567-5769(02)00253-9

169. Bari R, Rujkijyanont P, Sullivan E, Kang G, Turner V, Gan K, et al. Effect of donor KIR2DL1 allelic polymorphism on the outcome of pediatric allogeneic hematopoietic stem-cell transplantation. J Clin Oncol. (2013) 31:3782–90. doi: 10.1200/JCO.2012.47.4007

170. Moretta L, Locatelli F, Pende D, Marcenaro E, Mingari MC, Moretta A. Killer Ig-like receptor-mediated control of natural killer cell alloreactivity in haploidentical hematopoietic stem cell transplantation. Blood. (2011) 117:764–71. doi: 10.1182/blood-2010-08-264085

171. Pfeiffer MM, Feuchtinger T, Teltschik HM, Schumm M, Muller I, Handgretinger R, et al. Reconstitution of natural killer cell receptors influences natural killer activity and relapse rate after haploidentical transplantation of T- and B-cell depleted grafts in children. Haematologica. (2010) 95:1381–8. doi: 10.3324/haematol.2009.021121

172. Locatelli F, Merli P, Rutella S. At the bedside: innate immunity as an immunotherapy tool for hematological malignancies. J Leukoc Biol. (2013) 94:1141–57. doi: 10.1189/jlb.0613343

173. Nguyen S, Dhedin N, Vernant J-P, Kuentz M, Jijakli AA, Rouas-Freiss N, et al. NK-cell reconstitution after haploidentical hematopoietic stem-cell transplantations: immaturity of NK cells and inhibitory effect of NKG2A override GvL effect. Blood. (2005) 105:4135–42. doi: 10.1182/blood-2004-10-4113

174. Pende D, Marcenaro S, Falco M, Martini S, Bernardo ME, Montagna D, et al. Anti-leukemia activity of alloreactive NK cells in KIR ligand-mismatched haploidentical HSCT for pediatric patients: evaluation of the functional role of activating KIR and redefinition of inhibitory KIR specificity. Blood. (2009) 113:3119–29. doi: 10.1182/blood-2008-06-164103

175. Vago L, Forno B, Sormani MP, Crocchiolo R, Zino E, Di Terlizzi S, et al. Temporal, quantitative, and functional characteristics of single-KIR–positive alloreactive natural killer cell recovery account for impaired graft-versus-leukemia activity after haploidentical hematopoietic stem cell transplantation. Blood. (2008) 112:3488–99. doi: 10.1182/blood-2007-07-103325

176. Locatelli F, Pende D, Falco M, Della Chiesa M, Moretta A, Moretta L. NK cells mediate a crucial graft-versus-leukemia effect in haploidentical- HSCT to cure high-risk acute leukemia. Trends Immunol. (2018) 39:577–90. doi: 10.1016/j.it.2018.04.009

177. Muccio L, Bertaina A, Falco M, Pende D, Meazza R, Lopez-Botet M, et al. Analysis of memory-like natural killer cells in human cytomegalovirus- infected children undergoing alphabeta+T and B cell-depleted hematopoietic stem cell transplantation for hematological malignancies. Haematologica. (2016) 101:371–81. doi: 10.3324/haematol.2015.134155

178. Russo A, Oliveira G, Berglund S, Greco R, Gambacorta V, Cieri N, et al. NK cell recovery after haploidentical HSCT with posttransplant cyclophosphamide: dynamics and clinical implications. Blood. (2018) 131:247–62. doi: 10.1182/blood-2017-05-780668

179. Roberto A, Di Vito C, Zaghi E, Mazza EMC, Capucetti A, Calvi M, et al. The early expansion of anergic NKG2Apos/CD56dim/CD16neg natural killer represents a therapeutic target in haploidentical hematopoietic stem cell transplantation. Haematologica. (2018) 103:1390–402. doi: 10.3324/haematol.2017.186619

180. Zhao X-Y, Huang X-J, Liu K-Y, Xu L-P, Liu D-H. Reconstitution of natural killer cell receptor repertoires after unmanipulated HLA- mismatched/haploidentical blood and marrow transplantation: analyses of CD94:NKG2A and killer immunoglobulin-like receptor expression and their associations with

clinical outcome. Biol. Blood Marrow Transplant. (2007) 13:734–44. doi: 10.1016/j.bbmt.2007.02.010

181. Hu L-J, Zhao X-Y, Yu X-X, Lv M, Han T-T, Han W, et al. Quantity and quality reconstitution of NKG2A+ natural killer cells are associated with graft- versus-host disease after allogeneic hematopoietic cell transplantation. Biol Blood Marrow Transplant. (2019) 25:1–11. doi: 10.1016/j.bbmt.2018.08.008

182. Zhao X-y, Huang X-j, Liu K-y, Xu L-p, Liu D-h. Prognosis after unmanipulated HLA-haploidentical blood and marrow transplantation is correlated to the numbers of KIR ligands in recipients. Eur J Haematol. (2007) 78:338–46. doi: 10.1111/j.1600-0609.2007.00822.x

183. Raiola A, Dominietto A, Varaldo R, Ghiso A, Galaverna F, Bramanti S, et al. Unmanipulated haploidentical BMT following non-myeloablative conditioning and post-transplantation CY for advanced Hodgkin's lymphoma. Bone Marrow Transplant. (2013) 49:190. doi: 10.1016/j.bbmt.2012.08.014

184. Cieri N, Greco R, Crucitti L, Morelli M, Giglio F, Levati G, et al. Post- transplantation cyclophosphamide and sirolimus after haploidentical hematopoietic stem cell transplantation using a treosulfan-based myeloablative conditioning and peripheral blood stem cells. Biol Blood Marrow Transplant. (2015) 21:1506–14. doi: 10.1016/j.bbmt.2015.04.025

185. McCurdy SR, Vulic A, Symons HJ, Towlerton AM, Valdez BC, Jones RJ, et al. Comparable and robust immune reconstitution after HLA- haploidentical or HLA-matched allogeneic transplantation (BMT) utilizing posttransplantation cyclophosphamide. Biol Blood Marrow Transplant. (2015) 21:S71. doi: 10.1016/j.bbmt.2014.11.075

186. Roberto A, Castagna L, Zanon V, Bramanti S, Crocchiolo R, McLaren JE, et al. Role of naive-derived T memory stem cells in T-cell reconstitution following allogeneic transplantation. Blood. (2015) 125:2855– 64. doi: 10.1182/blood-2014-11-608406

187. McCurdy SR, Luznik L. Immune reconstitution after T-cell replete HLA-haploidentical transplantation. Semin Hematol. (2019) 56:221–6. doi: 10.1053/j.seminhematol.2019.03.005

188. Tian D-M, Wang Y, Zhang X-H, Liu K-Y, Huang X-J, Chang Y-J. Rapid recovery of CD3+CD8+ T cells on day 90 predicts superior survival after unmanipulated haploidentical blood and

Marrow transplantation. PLoS ONE. (2016) 11:e0156777. doi: 10.1371/journal.pone.0156777

189. Kim DH, Sohn SK, Won DI, Lee NY, Suh JS, Lee KB. Rapid helper T-cell recovery above 200 × 106/l at 3 months correlates to successful transplant outcomes after allogeneic stem cell transplantation. Bone Marrow Transplant. (2006) 37:1119–28. doi: 10.1038/sj.bmt.1705381

190. Bondanza A, Ruggeri L, Noviello M, Eikema D-J, Bonini C, Chabannon C, et al. Beneficial role of CD8+ T-cell reconstitution after HLA-haploidentical stem cell transplantation for high-risk acute leukaemias: results from a clinico-biological EBMT registry study mostly in the T-cell-depleted setting. Bone Marrow Transplant. (2019) 54:867–76. doi: 10.1038/s41409-018- 0351-x

191. Cieri N, Oliveira G, Greco R, Forcato M, Taccioli C, Cianciotti B, et al. Generation of human memory stem T cells after haploidentical T- replete hematopoietic stem cell transplantation. Blood. (2015) 125:2865–74. doi: 10.1182/blood-2014-11-608539

192. Fisher SA, Lamikanra A, Dorée C, Gration B, Tsang P, Danby RD, et al. Increased regulatory T cell graft content is associated with improved outcome in haematopoietic stem cell transplantation: a systematic review. Brit J Haematol. (2017) 176:448–63. doi: 10.1111/bjh.14433

193. Zorn E, Kim HT, Lee SJ, Floyd BH, Litsa D, Arumugarajah S, et al. Reduced frequency of FOXP3+ CD4+ CD25+ regulatory T cells in patients with chronic graft-versus-host disease. Blood. (2005) 106:2903–11. doi: 10.1182/blood-2005-03-1257

194. Peccatori J, Forcina A, Clerici D, Crocchiolo R, Vago L, Stanghellini MT, et al. Sirolimus-based graft-versus-host disease prophylaxis promotes the in vivo expansion of regulatory T cells and permits peripheral blood stem cell transplantation from haploidentical donors. Leukemia. (2015) 29:396–405. doi: 10.1038/leu.2014.180

195. Wang Y, Zhao XY, Xu LP, Zhang XH, Han W, Chen H, et al. Lower incidence of acute GVHD is associated with the rapid recovery of CD4(+)CD25(+)CD45RA(+) regulatory T cells in patients who received haploidentical allografts from NIMA-mismatched donors: a retrospective (development) and prospective (validation) cohort-based study. Oncoimmunology. (2016) 5:e1242546. doi: 10.1080/2162402X.2016.1242546

196. Vantourout P, Hayday A. Six-of-the-best: unique contributions of γδ T cells to immunology. Nat Rev Immunol. (2013) 13:88. doi: 10.1038/nri3384
197. Kabelitz D, Kalyan S, Oberg H-H, Wesch D. Human Vδ2 versus non Vδ2 γδ T cells in antitumor immunity. OncoImmunology. (2013) 2:e23304. doi: 10.4161/onci.23304
198. Knight A, Madrigal AJ, Grace S, Sivakumaran J, Kottaridis P, Mackinnon S, et al. The role of Vδ2-negative γδ T cells during cytomegalovirus reactivation in recipients of allogeneic stem cell transplantation. Blood. (2010) 116:2164– 72. doi: 10.1182/blood-2010-01-255166
199. Storek J, Geddes M, Khan F, Huard B, Helg C, Chalandon Y, et al. Reconstitution of the immune system after hematopoietic stem cell transplantation in humans. Semin Immunopathol. (2008) 30:425. doi: 10.1007/s00281-008-0132-5
200. Roberto A, Castagna L, Gandolfi S, Zanon V, Bramanti S, Sarina B, et al. B-cell reconstitution recapitulates B-cell lymphopoiesis following haploidentical BM transplantation and post-transplant CY. Bone Marrow Transplant. (2014) 50:317. doi: 10.1038/bmt.2014.266
201. Vago L, Perna SK, Zanussi M, Mazzi B, Barlassina C, Stanghellini MT, et al. Loss of mismatched HLA in leukemia after stem-cell transplantation. N Engl J Med. (2009) 361:478–88. doi: 10.1056/NEJMoa0811036
202. Ahci M, Stempelmann K, Buttkereit U, Crivello P, Trilling M, Heinold A, et al. Clinical utility of quantitative PCR for chimerism and engraftment monitoring after allogeneic stem cell transplantation for hematologic malignancies. Biol Blood Marrow Transplant. (2017) 23:1658– 68. doi: 10.1016/j.bbmt.2017.05.031
203. Crucitti L, Crocchiolo R, Toffalori C, Mazzi B, Greco R, Signori A, et al. Incidence, risk factors and clinical outcome of leukemia relapses with loss of the mismatched HLA after partially incompatible hematopoietic stem cell transplantation. Leukemia. (2015) 29:1143–52. doi: 10.1038/leu.2014.314
204. McCurdy SR, Iglehart BS, Batista DA, Gocke CD, Ning Y, Knaus HA, et al. Loss of the mismatched human leukocyte antigen haplotype in two acute myelogenous leukemia relapses after haploidentical bone marrow transplantation with post-transplantation

cyclophosphamide. Leukemia. (2016) 30:2102–6. doi: 10.1038/leu.2016.144

205. Toffalori C, Zito L, Gambacorta V, Riba M, Oliveira G, Bucci G, et al. Immune signature drives leukemia escape and relapse after hematopoietic cell transplantation. Nat Med. (2019) 25:603–11. doi: 10.1038/s41591-019-0400-z

206. Noviello M, Manfredi F, Ruggiero E, Perini T, Oliveira G, Cortesi F, et al. Bone marrow central memory and memory stem T-cell exhaustion in AML patients relapsing after HSCT. Nat Commun. (2019) 10:1065. doi: 10.1038/s41467-019-08871-1

207. Khan MA, Bashir Q, Chaudhry QU, Ahmed P, Satti TM, Mahmood SK. Review of haploidentical hematopoietic cell transplantation. J Glob Oncol. (2018) 4:1–13. doi: 10.1200/JGO.18.00130

208. Ciceri F, Bonini C, Stanghellini MT, Bondanza A, Traversari C, Salomoni M, et al. Infusion of suicide-gene-engineered donor lymphocytes after family haploidentical haemopoietic stem-cell transplantation for leukaemia (the TK007 trial): a non-randomised phase I-II study. Lancet Oncol. (2009) 10:489–500. doi: 10.1016/S1470-2045(09)70074-9

209. Bonini C, Ferrari G, Verzeletti S, Servida P, Zappone E, Ruggieri L, et al. HSV-TK gene transfer into donor lymphocytes for control of allogeneic graft-versus-leukemia. Science. (1997) 276:1719–24. doi: 10.1126/science.276.5319.1719

210. Vago L, Oliveira G, Bondanza A, Noviello M, Soldati C, Ghio D, et al. T-cell suicide gene therapy prompts thymic renewal in adults after hematopoietic stem cell transplantation. Blood. (2012) 120:1820–30. doi: 10.1182/blood-2012-01-405670

211. Straathof KC, Pule MA, Yotnda P, Dotti G, Vanin EF, Brenner MK, et al. An inducible caspase 9 safety switch for T-cell therapy. Blood. (2005) 105:4247– 54. doi: 10.1182/blood-2004-11-4564

212. Di Stasi A, Tey SK, Dotti G, Fujita Y, Kennedy-Nasser A, Martinez C, et al. Inducible apoptosis as a safety switch for adoptive cell therapy. N Engl J Med. (2011) 365:1673–83. doi: 10.1056/NEJMoa1106152

213. Zhou X, Dotti G, Krance RA, Martinez CA, Naik S, Kamble RT, et al. Inducible caspase-9 suicide gene controls adverse effects

from alloreplete T cells after haploidentical stem cell transplantation. Blood. (2015) 125:4103– 13. doi: 10.1182/blood-2015-02-628354

214. Zhou X, Di Stasi A, Tey SK, Krance RA, Martinez C, Leung KS, et al. Long-term outcome after haploidentical stem cell transplant and infusion of T cells expressing the inducible caspase 9 safety transgene. Blood. (2014) 123:3895–905. doi: 10.1182/blood-2014-01-551671

215. Zeidan AM, Forde PM, Symons H, Chen A, Smith BD, Pratz K, et al. HLA-haploidentical donor lymphocyte infusions for patients with relapsed hematologic malignancies after related HLA-haploidentical bone marrow transplantation. Biol Blood Marrow Transplant. (2014) 20:314–8. doi: 10.1016/j.bbmt.2013.11.020

216. Sun W, Mo XD, Zhang XH, Xu LP, Wang Y, Yan CH, et al. Chemotherapy plus DLI for relapse after haploidentical HSCT: the biological characteristics of relapse influences clinical outcomes of acute leukemia patients. Bone Marrow Transplant. (2018) 54:1198–207. doi: 10.1038/s41409-018-0406-z

217. Gao XN, Lin J, Wang SH, Huang WR, Li F, Li HH, et al. Donor lymphocyte infusion for prevention of relapse after unmanipulated haploidentical PBSCT for very high-risk hematologic malignancies. Ann Hematol. (2019) 98:185–93. doi: 10.1007/s00277-018-3482-7

218. Bacchetta R, Lucarelli B, Sartirana C, Gregori S, Lupo Stanghellini MT, Miqueu P, et al. Immunological outcome in haploidentical-HSC transplanted patients treated with IL-10-anergized donor T cells. Front Immunol. (2014) 5:16. doi: 10.3389/fimmu.2014.00016

219. Muller N, Landwehr K, Langeveld K, Stenzel J, Pouwels W, van der Hoorn M, et al. Generation of alloreactivity-reduced donor lymphocyte products retaining memory function by fully automatic depletion of CD45RA- positive cells. Cytotherapy. (2018) 20:532–42. doi: 10.1016/j.jcyt.2018 01.006

220. Schroeder T, Rachlis E, Bug G, Stelljes M, Klein S, Steckel NK, et al. Treatment of acute myeloid leukemia or myelodysplastic syndrome relapse after allogeneic stem cell transplantation with azacitidine and donor lymphocyte infusions–a retrospective multicenter analysis from the German Cooperative Transplant Study Group. Biol Blood Marrow Transplant. (2015) 21:653–60. doi: 10.1016/j.bbmt.2014.12.016

221. Schroeder T, Rautenberg C, Kruger W, Platzbecker U, Bug G, Steinmann J, et al. Treatment of relapsed AML and MDS after allogeneic stem cell transplantation with decitabine and DLI-a retrospective multicenter analysis on behalf of the German Cooperative Transplant Study Group. Ann Hematol. (2018) 97:335–42. doi: 10.1007/s00277-017-3185-5
222. Maude SL, Frey N, Shaw PA, Aplenc R, Barrett DM, Bunin NJ, et al. Chimeric antigen receptor T cells for sustained remissions in leukemia. N Engl J Med. (2014) 371:1507–17. doi: 10.1056/NEJMoa1407222
223. Gardner RA, Finney O, Annesley C, Brakke H, Summers C, Leger K, et al. Intent-to-treat leukemia remission by CD19 CAR T cells of defined formulation and dose in children and young adults. Blood. (2017) 129:3322– 31. doi: 10.1182/blood-2017-02-769208
224. Locke FL, Ghobadi A, Jacobson CA, Miklos DB, Lekakis LJ, Oluwole OO, et al. Long-term safety and activity of axicabtagene ciloleucel in refractory large B-cell lymphoma (ZUMA-1): a single-arm, multicentre, phase 1-2 trial. Lancet Oncol. (2019) 20:31–42. doi: 10.1016/S1470-2045(18) 30864-7
225. Locke FL, Neelapu SS, Bartlett NL, Siddiqi T, Chavez JC, Hosing CM, et al. Phase 1 results of ZUMA-1: a multicenter study of KTE-C19 anti-CD19 CAR T cell therapy in refractory aggressive lymphoma. Mol Ther. (2017) 25:285–95. doi: 10.1016/j.ymthe.2016.10.020
226. Qasim W, Zhan H, Samarasinghe S, Adams S, Amrolia P, Stafford S, et al. Molecular remission of infant B-ALL after infusion of universal TALEN gene-edited CAR T cells. Sci Transl Med. (2017) 9:eaaj2013. doi: 10.1126/scitranslmed.aaj2013
227. Tang X, Yang L, Li Z, Nalin AP, Dai H, Xu T, et al. First-in-man clinical trial of CAR NK-92 cells: safety test of CD33-CAR NK-92 cells in patients with relapsed and refractory acute myeloid leukemia. Am J Cancer Res. (2018) 8:1083–9.
228. Raje N, Berdeja J, Lin Y, Siegel D, Jagannath S, Madduri D, et al. Anti-BCMA CAR T-cell therapy bb2121 in relapsed or refractory multiple myeloma. N Engl J Med. (2019) 380:1726–37. doi: 10.1056/NEJMoa1817226
229. Baumeister SH, Murad J, Werner L, Daley H, Trebeden-Negre H, Gicobi JK, et al. Phase I trial of autologous CAR T cells targeting NKG2D ligands in patients with AML/MDS and multiple

myeloma. Cancer Immunol Res. (2019) 7:100–12. doi: 10.1158/2326-6066.CIR-18-0307

230. Kim MY, Yu KR, Kenderian SS, Ruella M, Chen S, Shin TH, et al. Genetic inactivation of CD33 in hematopoietic stem cells to enable CAR T cell immunotherapy for acute myeloid leukemia. Cell. (2018) 173:1439–53.e19. doi: 10.1016/j.cell.2018.05.013

231. Pizzitola I, Anjos-Afonso F, Rouault-Pierre K, Lassailly F, Tettamanti S, Spinelli O, et al. Chimeric antigen receptors against CD33/CD123 antigens efficiently target primary acute myeloid leukemia cells in vivo. Leukemia. (2014) 28:1596–605. doi: 10.1038/leu.2014.62

232. Copelan OR, Sanikommu SR, Trivedi JS, Butler C, Ai J, Ragon BK, et al. Higher incidence of hemorrhagic cystitis following haploidentical related donor transplantation compared with matched related donor transplantation. Biol Blood Marrow Transplant. (2019) 25:78590.10.1016/j.bbmt.2018.12.142

233. Leen AM, Christin A, Myers GD, Liu H, Cruz CR, Hanley PJ, et al. Cytotoxic T lymphocyte therapy with donor T cells prevents and treats adenovirus and Epstein-Barr virus infections after haploidentical and matched unrelated stem cell transplantation. Blood. (2009) 114:4283–92. doi: 10.1182/blood-2009-07-232454

234. Tzannou I, Papadopoulou A, Naik S, Leung K, Martinez CA, Ramos CA, et al. Off-the-shelf virus-specific T cells to treat BK virus, human herpesvirus 6, cytomegalovirus, epstein-barr virus, and adenovirus infections after allogeneic hematopoietic stem-cell transplantation. J Clin Oncol. (2017) 35:3547–57. doi: 10.1200/JCO.2017.73.0655

235. Chapuis AG, Egan DN, Bar M, Schmitt TM, McAfee MS, Paulson KG, et al. T cell receptor gene therapy targeting WT1 prevents acute myeloid leukemia relapse post-transplant. Nat Med. (2019) 25:1064–72. doi: 10.1038/s41591-019-0472-9

236. Marijt WA, Heemskerk MH, Kloosterboer FM, Goulmy E, Kester MG, van der Hoorn MA, et al. Hematopoiesis-restricted minor histocompatibility antigens HA-1- or HA-2-specific T cells can induce complete remissions of relapsed leukemia. Proc Natl Acad Sci USA. (2003) 100:2742–7. doi: 10.1073/pnas.0530192100

237. Dossa RG, Cunningham T, Sommermeyer D, Medina-Rodriguez I, Biernacki MA, Foster K, et al. Development of T-cell immunotherapy for hematopoietic stem cell transplantation recipients

at risk of leukemia relapse. Blood. (2018) 131:108–20. doi: 10.1182/blood-2017-07-791608

238. Cooley S, Parham P, Miller JS. Strategies to activate NK cells to prevent relapse and induce remission following hematopoietic stem cell transplantation. Blood. (2018) 131:1053–62. doi: 10.1182/blood-2017-08-752170

239. Ciurea SO, Schafer JR, Bassett R, Denman CJ, Cao K, Willis D, et al. Phase 1 clinical trial using mbIL21 ex vivo-expanded donor-derived NK cells after haploidentical transplantation. Blood. (2017) 130:1857–68. doi: 10.1182/blood-2017-05-785659

240. Moon BI, Kim TH, Seoh JY. Functional modulation of regulatory T cells by IL-2. PLoS ONE. (2015) 10:e0141864. doi: 10.1371/journal.pone.0141864

241. Bachanova V, Cooley S, Defor TE, Verneris MR, Zhang B, McKenna DH, et al. Clearance of acute myeloid leukemia by haploidentical natural killer cells is improved using IL-2 diphtheria toxin fusion protein. Blood. (2014) 123:3855–63. doi: 10.1182/blood-2013-10-532531

242. Cooley S, He F, Bachanova V, Vercellotti GM, DeFor TE, Curtsinger JM, et al. First-in-human trial of rhIL-15 and haploidentical natural killer cell therapy for advanced acute myeloid leukemia. Blood Adv. (2019) 3:1970–80. doi: 10.1182/bloodadvances.2018028332

243. Romee R, Rosario M, Berrien-Elliott MM, Wagner JA, Jewell BA, Schappe T, et al. Cytokine-induced memory-like natural killer cells exhibit enhanced responses against myeloid leukemia. Sci Transl Med. (2016) 8:357ra123. doi: 10.1126/scitranslmed.aaf2341

244. Romee R, Schneider SE, Leong JW, Chase JM, Keppel CR, Sullivan RP, et al. Cytokine activation induces human memory-like NK cells. Blood. (2012) 120:4751–60. doi: 10.1182/blood-2012-04-419283

245. Romee R, Cooley S, Berrien-Elliott MM, Westervelt P, Verneris MR, Wagner JE, et al. First-in-human phase 1 clinical study of the IL-15 superagonist complex ALT-803 to treat relapse after transplantation. Blood. (2018) 131:2515–27. doi: 10.1182/blood-2017-12-823757

Author Contributions: SB, BR, RS, and RR helped review the literature and wrote this manuscript.

Conflict of Interest: The authors declare that the research was conducted in the absence of any commercial or financial relationships that could be construed as a potential conflict of interest.

Chapter 3

Impaired T- and NK-cell reconstitution after haploidentical HCT with posttransplant cyclophosphamide

Benedetta Rambaldi,[1,2] Haesook T. Kim,[3] Carol Reynolds,[1] Sharmila Chamling Rai,[1] Yohei Arihara,[1] Tomohiro Kubo,[1] Leutz Buon,[4] Mahasweta Gooptu,[1] John Koreth,[1] Corey Cutler,[1] Sarah Nikiforow,[1] Vincent T. Ho,[1] Edwin P. Alyea,[1] Joseph H. Antin,[1] Catherine J. Wu,[1] Robert J. Soiffer,[1] Jerome Ritz,[1] and Rizwan Romee[1]

[1]Department of Medical Oncology, Dana-Farber Cancer Institute and Harvard Medical School, Boston, MA; [2]Clinical and Experimental Sciences Department, Bone Marrow Transplant Unit, ASST Spedali Civili, University of Pavia, Brescia, Italy; [3]Department of Data Sciences, Dana-Farber Cancer Institute, Harvard T.H. Chan School of Public Health, Boston, MA; and [4]Department of BioInformatics and Data Science, Dana-Farber Cancer Institute, Harvard Medical School, Boston, MA

Blood Advances 2021 Jan 26;5(2):352-364

doi: 10.1182/bloodadvances.2020003005. PMID: 33496734

Abstract

Administration of post-transplant cyclophosphamide (PTCy) has significantly expanded the number of patients undergoing HLA-haploidentical hematopoietic cell transplantation (haplo-HCT). To examine immune reconstitution in these patients, we monitored T- and natural killer (NK)-cell recovery in 60 patients receiving bone marrow or peripheral blood stem cell (PBSC) grafts after haplo-HCT with PTCy and 35 patients receiving HLA-matched donor PBSC grafts with standard graft-versus-host disease (GVHD) prophylaxis. Compared with HLA-matched recipients, early T-cell recovery was delayed in haplo-HCT patients and skewed toward effector memory T cells with markedly reduced naive T cells. We found higher regulatory T (Treg)-cell/conventional T (Tcon)-cell ratios early after HCT and increased PD-1 expression on memory T cells. Within the haplo-HCT, patients who did not develop chronic GVHD (cGVHD) had higher PD-1 expression on central and effector memory $CD4^+$ Treg cells at 1 month after transplant. These findings suggest an immunologic milieu that promotes immune tolerance in haplo-HCT patients. NK cells were decreased early after haplo-HCT with preferential expansion of immature $CD56^{bright}CD16^-$ NK cells compared with matched donor transplants. One month after transplant, mass cytometry revealed enrichment of immature NK-cell metaclusters with high NKG2A, low CD57, and low killer- cell immunoglobulin-like receptor expression after haplo-HCT, which partially recovered 3 months post-HCT. At 2 months, immature NK cells from both groups were functionally impaired, but interleukin-15 priming corrected these defects *in vitro*. Increased immature/ mature NK-cell ratios were associated with

cytomegalovirus reactivation and increased incidence of cGVHD after haplo-HCT. These homeostatic imbalances in T- and NK-cell reconstitution after haplo-HCT reveal opportunities for early immune-based interventions to optimize clinical outcomes.

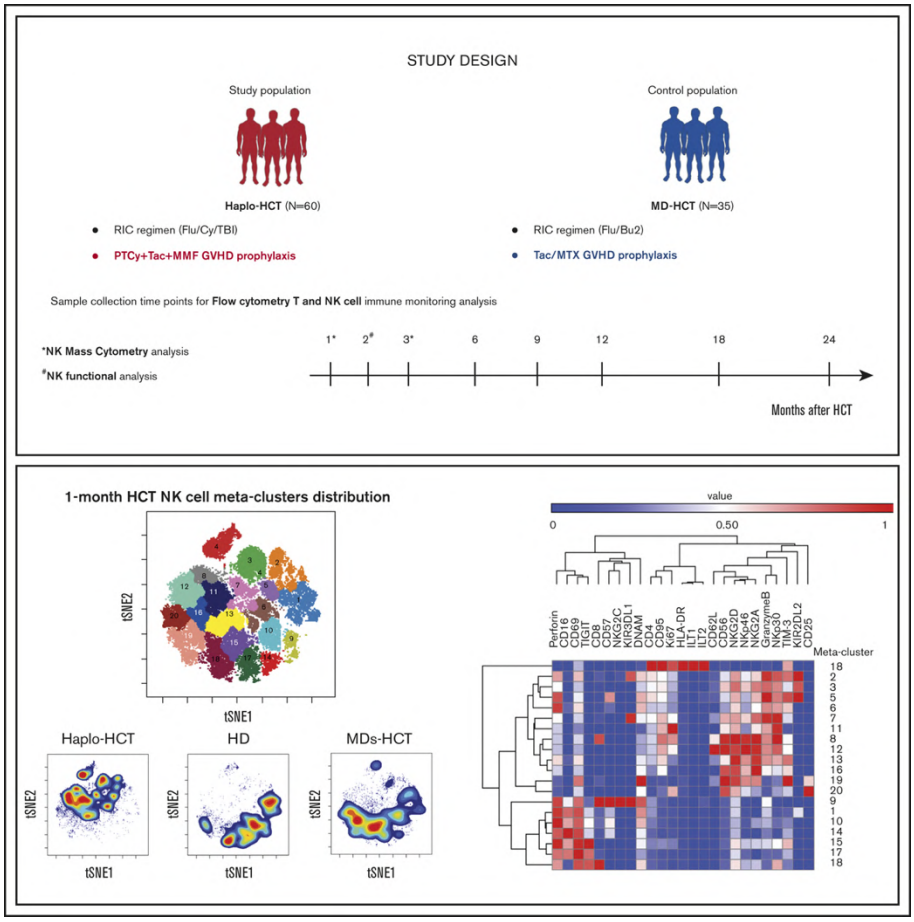

Introduction

HLA-haploidentical hematopoietic cell transplantation (haplo-HCT) has become a preferred transplant modality in patients who lack a readily available HLA-matched donor (1,2). This has been made possible by the development of novel strategies that markedly reduce the incidence of graft failure and severe graft- versus-host disease

(GVHD), the major complications associated with HLA-mismatched transplants (3-6).

Although different platforms for haplo-HCT have been developed, the administration of posttransplant cyclophosphamide (PTCy) on days +3 and +4 has become the most frequent approach since it is relatively easy to implement and does not require ex vivo graft manipulation (6). Multiple registry and single center studies have shown that outcomes after haplo-HCT with PTCy are comparable with HLA-matched related and unrelated donor HCT (7-11).

Recovery of innate and adaptive immune systems is needed to provide effective graft versus leukemia (GVL) and prevent posttransplant infections (12-14). While the kinetics of immune reconstitution and its correlation with post-HCT outcomes are well established in the setting of HLA-matched transplants, there are relatively little data in patients receiving PTCy after haplo-HCT (15,16). This is particularly relevant in the context of recent reports showing an increased incidence of viral infections, including cytomegalovirus (CMV) reactivation, after haplo-HCT with PTCy, suggesting T- and natural killer (NK)-cell immune impairment (17-21). Killer-cell immunoglobulin-like receptor (KIR) ligand or KIR haplotype mismatch also do not appear to impact outcomes after haplo-HCT with PTCy, suggesting abrogation of the NK-cell-mediated GVL effect after PTCy (22,23).

To examine the dynamics of immune reconstitution after haplo-HCT with PTCy, we prospectively monitored immune recovery in a cohort of 60 adult patients who underwent haplo-HCT with PTCy and a contemporaneous cohort of 35 adult patients receiving related or unrelated HLA-matched donor transplant (MD-HCT) with standard

GVHD prophylaxis. Using flow and mass cytometry to monitor recovery of innate and adaptive immunity and NK-cell functional assays, we found significant impairment of both T- and NK-cell reconstitution early after haplo-HCT. These studies suggest that novel strategies to enhance early immune reconstitution in patients receiving PTCy-based haplo-HCT may further enhance transplant outcomes in these patients.

Methods

Patients and sample collection

This study included 95 patients who underwent allogeneic HCT at the Dana-Farber Cancer Institute and Brigham and Woman's Hospital (Boston, MA) between November 2011 and November 2018. Sixty patients received stem cells from HLA-haploidentical donors (haplo-HCT group), and 35 had HLA-matched (8/8) related (11/35) or unrelated (24/35) donors (MD-HCT group). Both cohorts received reduced-intensity conditioning. GVHD prophylaxis consisted of PTCy (50 mg/kg) on days 13 and 14 and tacrolimus (TAC) plus mycophenolate mofetil for haplo-HCT patients and TAC plus methotrexate (MTX) for MD-HCT patients. Blood samples were obtained at 1, 2, 3, 6, 9, 12, 18, and 24 months after transplant for analysis of immune reconstitution (**supplemental Table 1**). Samples obtained after relapse were excluded from analysis. For mass cytometry and NK functional assays, samples were also collected from healthy donors (HDs; 6 females and 6 males) with a median age of 48.5 years (range, 23-68 years). Written informed consent was obtained from all

patients prior to sample collection, in accordance with the Declaration of Helsinki. Protocol approval was obtained from the Human Subjects Protection Committee of the Dana-Farber/Harvard Cancer Center. Detailed descriptions of transplant procedures and sample processing are provided in **supplemental Methods**.

Monitoring immune reconstitution

A panel of directly conjugated monoclonal antibodies (**supplemental Table 2**) was used to define functionally distinct immune cell subsets and homeostatic characteristics of each subset. After staining, cells were acquired on a Fortessa LSR flow cytometer (BD) and analyzed using FACSDiva software (BD). The cell gating strategy and markers used for cell subset definition are described in **supplemental Figures 1 and 2**.

NK-cell characterization

To examine NK-cell phenotype early after transplant, cryopreserved samples obtained 1 month after HCT were analyzed using mass cytometry with a panel of 35 metal-tagged antibodies (**supplemental Table 3**) (24). Samples were collected on a Helios-2 mass cytometer (Fluidigm) and data analyzed using Cytobank (25). The methods used to analyze high-dimensional single-cell mass cytometry data are described in **supplemental Methods**.

NK-cell function after coculture with or without 5 ng/mL interleukin-15 (IL-15) and target cells was evaluated by measuring CD107a as a marker of degranulation and by cytokine (interferon-γ [IFN-γ] and tumor necrosis factor α [TNF-α]) release. A detailed description of

sample preparation is provided in **supplemental Methods** and **supplemental Table 4**, and an example of the gating strategy is shown in **supplemental Figure 4.**

Statistical analysis

A detailed description of statistical analyses performed to com- pare experimental data and patient outcome is provided in the **supplemental Methods**.

Results

Patient characteristics

Clinical characteristics of patients in the study are summarized in **Table 1**. Median patient age at the time of transplant was 56 years (range, 20-75 years) for haplo-HCT and 63 years (range, 19-73 years) for MD-HCT (P = 0.07). Both cohorts were similar in terms of patient/donor sex, CMV patient/donor serostatus, hematologic disease, and disease status at the time of transplant. Median follow-up was 32.8 months (range, 12-92.9 months) for haplo-HCT and 16.8 months (range, 3.6-70.4 months) for MD-HCT patients (P = 0.07). The 2 groups differed markedly in stem cell source (P < 0.0001).

Patient Characteristics	Haplo-HCT N (%)	MD-HCT N (%)	P-value
Total	60 (100)	35 (100)	

Age at HCT, Median (Range), Years	56 (20-75)	63 (19-73)	0.07
Patient Sex, Male	32 (53.3)	25 (71.4)	0.13
Donor Sex, Male	40 (66.7)	25 (71.4)	0.66
Donor type			-
Matched Related Donor	-	11 (31.4)	
Matched Unrelated Donor	-	24 (68.6)	
Haploidentical Related Donor	60 (100)	-	
Female Donor for Male Recipient	5 (8.3)	5 (14.3)	0.49
Patient or Donor CMV Serostatus, Positive	36 (60)	20 (62.5)	1
Disease			0.37
ALL	2 (3.3)	3 (8.5)	
AML	12 (20)	10 (28.6)	
MDS	14 (23.3)	10 (28.6)	
NHL	16 (26.7)	8 (22.9)	
HL	6 (10)	1 (2.9)	
Others†	10 (16.7)	3 (8.5)	
Disease Status			0.09
CR	26 (43.3)	19 (54.3)	
PR	18 (30)	4 (11.4)	
Rel/IF/Untreated	16 (26.7)	12 (34.3)	
Cell Source			**<0.0001**
BM	47 (78.3)	0 (0)	

PBSC	13 (21.7)	35 (100)	
Follow-up Time (Months), Median (Range)	32.8 (12-92.9)	16.8 (3.6-70.4)	0.07

Table 1. Patient characteristics. Statistically significant P value is shown in bold. ALL, acute lymphoid leukemia; AML, acute myeloid leukemia; BM, bone marrow; CR, complete remission; HL, Hodgkin lymphoma; IF, induction failure; MDS, myelodysplastic syndrome; NHL, non-Hodgkin lymphoma; PR, partial remission; Rel, relapsed. *Chronic myeloid leukemia (n 5 3), chronic lymphocytic leukemia (n 5 3), chronic myelomonocytic leukemia (n 5 1), myeloproliferative neoplasm (n 5 2), mixed myelodys-plastic/myeloproliferative neoplasm (n 5 2), and red cell disorder (n 5 2).

Clinical outcomes

Haplo-HCT was associated with delayed neutrophil and platelet engraftment compared with MD recipients, with a median time to neutrophil engraftment of 16 days (range, 13-31) after haplo-HCT compared with 14 days (range, 6-26 days) after MD-HCT ($P < 0.01$). Median time to platelet engraftment was 26 days (range, 15-63 days) in haplo-HCT *vs* 19 days (range, 11-24 days) in MD-HCT ($P < 0.01$) (**supplemental Figure 5**). Late graft failure occurred in 1 patient in the haplo-HCT cohort. There was no difference in overall survival ($P = 0.71$), progression-free survival ($P = 0.95$), cumulative incidence of relapse ($P = 0.28$), nonrelapse mortality ($P = 0.7$), and grade II to IV (acute GVHD) ($P = 0.28$) between the 2 cohorts (**supplemental Figure 6**). The incidence of chronic GVHD (cGVHD) was significantly lower after haplo-HCT (22% at 2 years) compared with MD-HCT (53% at 2 years, $P = 0.019$).

Delayed lymphocyte reconstitution after haplo-HCT

The absolute lymphocyte count was significantly lower in the haplo-HCT group at 1 month but was similar to MD recipients at subsequent time points (**Figure 1A**). At 1 month, there were also significant differences in the distribution of major lymphocyte subsets in the 2 groups. NK cells were the predominant lymphocyte subset in haplo-HCT patients (median, 35.1% [range, 17.4%- 51.2%] vs 17.7% [range, 13.5%-28.6%] in the MD-HCT cohort; P = 0.015). All other lymphocyte subsets (T, B, and NKT) were significantly lower in the haplo-HCT group at this time point (**Figure 1B**). Although haplo-HCT patients had a higher proportion of NK cells at 1 month, the absolute number of NK cells was lower in these patients (P = 0.04; **Figure 1C**). Haplo-HCT recipients had lower T-cell numbers in the first 3 months and lower B-cell numbers for the first 2 months. In contrast, NKT cells remained lower for all time points up to 2 years in haplo-HCT recipients (**Figure 1C**).

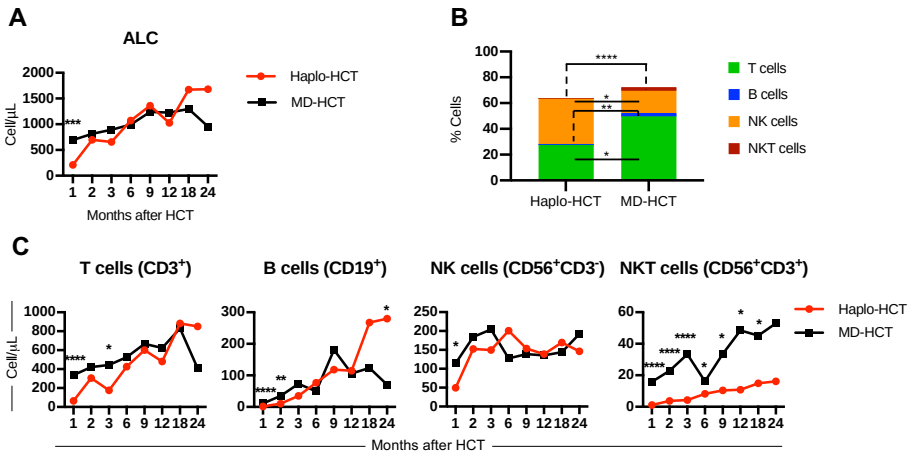

Figure 1. Reconstitution of major lymphocyte populations after haplo-HCT and MD-HCT. (A) Recovery of absolute lymphocyte counts (ALC) after haplo-HCT and MD-HCT. (B) Distribution of major lymphocyte populations in peripheral blood 1 month after haplo-HCT and MD-HCT. (C)

Reconstitution of $CD3^+$ T cells, $CD19^+$ B cells, $CD3^-CD56^+$ NK cells, and $CD3^+CD56^+$ NKT cells after haplo-HCT and MD-HCT. Haplo-HCT, n = 60; MD-HCT, n = 35. Median cell counts per microliter are represented at each time point. Statistically significant differences are noted in each figure (****P < 0.0001; ***P < 0.001; **P < 0.01; *P < 0.05; Wilcoxon rank-sum test). **See supplemental Table 7** for the median absolute values along with the corresponding interquartile values and P values for panels A and C.

Delayed $CD4^+$ Tcon-cell reconstitution after haplo-HCT

Delayed T-cell recovery after haplo-HCT was primarily due to slower $CD4^+$ conventional T (Tcon)-cell reconstitution (**Figure 2**). Compared with MD-HCT patients, the number of $CD4^+$ Tcon cells was lower for the first 3 months, while the number of $CD4^+$ Treg cells was lower only at 1 month in haplo-HCT patients. However, in both cohorts, $CD4^+$ T cells did not reach normal levels for the entire course of this analysis (**Figure 2A**). Similarly, the number of $CD8^+$ T cells was also lower in haplo-HCT patients at 1 and 3 months compared with MD-HCT patients, although differences were less marked compared with $CD4^+$ Tcon cells. In both groups, $CD8^+$ T cells reached normal levels by 6 months after transplant (**Figure 2A**). Delayed $CD4^+$ T-cell recovery after haplo-HCT resulted in a lower CD4/CD8 ratio, especially at 1 month after transplant (P < 0.0001; **Figure 2B**). The regulatory T (Treg)-cell/ Tcon-cell ratio was higher in the haplo-HCT group compared with MD-HCT group for the first 3 months after transplant, indicating slower recovery of $CD4^+$ Tcon cells compared with $CD4^+$ Treg cells early after haplo-HCT (**Figure 2B**).

Unbalanced recovery of naive and memory T cells after haplo-HCT

To characterize T-cell maturation, we monitored reconstitution of naive, central memory (CM), effector memory (EM), and terminal EM (TEMRA) subsets within each major T-cell population (**Figure 2C**). There was a profound reduction of naive subsets in $CD4^+$ Tcon, $CD4^+$ Treg, and $CD8^+$ T cells after haplo-HCT, lasting 12 months in the $CD4^+$ compartment and 3 months in the $CD8^+$ compartment. Reconstitution of CM cells was most delayed in $CD4^+$ Tcon cells with reduced absolute counts for 6 months after haplo-HCT. The number of CM $CD4^+$ Treg cells was reduced for 2 months after haplo-HCT. CM $CD8^+$ T cells reconstituted similarly in both groups but reached higher numbers in the haplo-HCT cohort at the 1-year mark. TEMRA subsets were significantly reduced for 3 months within $CD4^+$ Tcon and $CD8^+$ T cells. Finally, EM T cells were only decreased at 1 month in the $CD4^+$ group. After this time point EM T-cell reconstitution was similar or higher in the haplo-HCT group.

Increased PD-1 expression on T cells early after haplo-HCT

Programmed cell death 1 (PD-1) is a coinhibitory receptor and its expression in $CD4^+$ Tcon and $CD8^+$ T cells attenuates T-cell activation and plays an important role in peripheral tolerance (26). We observed increased expression of PD-1 on $CD4^+$ Tcon-cell, Treg- cell, and $CD8^+$ T-cell subsets after haplo-HCT (**Figure 2D-E**). These differences were evident in all memory subsets in the first 3 months after haplo-HCT with PTCy.

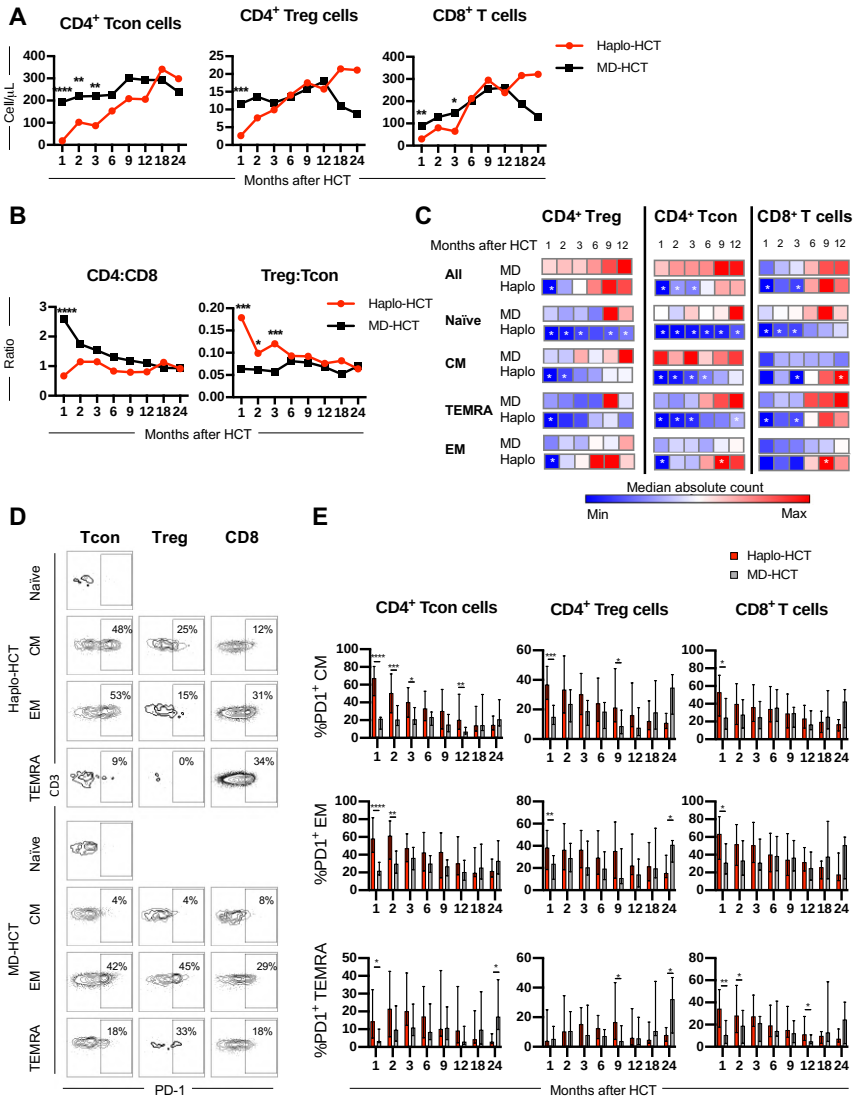

Figure 2. T-cell reconstitution after haplo-HCT and MD-HCT. (A) Peripheral blood reconstitution of CD4$^+$ Tcon, CD4$^+$ Treg, and CD8$^+$ T cells after transplant; the median cell counts per microliter are represented at each time point. (B) Median CD4/CD8 and Treg/Tcon ratio after HCT. (C) Heat map summarizes T-cell reconstitution during the first year after HCT.

Absolute median counts were scaled for the lowest and highest values in each group. Red denotes the highest value and blue denotes the smallest value in each group. (D) Flow cytometry plots from 2 representative patients (haplo-HCT and MD-HCT) showing PD-1 expression on T-cell subsets; $CD4^+$ Tcon naive cells were used as internal negative control. (E) Expression of PD-1 on $CD4^+$ Tcon, $CD4^+$ Treg, and $CD8^+$ T cells after haplo-HCT and MD-HCT. Values are expressed as median and range. Treg cells were defined as $CD4^+CD25^+CD127^-$ T cells and Tcon cells as $CD4^+$ conventional (non-T regulatory) T cells. Naïve T cells are $CD45RO^-CD62L^+$ lymphocytes; CM T cells are $CD45RO^+CD62L^+$ lymphocytes; TEMRA T cells are defined as $CD45RO^-CD62L^-$ lymphocytes and EM T cells are $CD45RO^+CD62L^-$ lymphocytes. Haplo-HCT, n = 60; MD-HCT, n = 35. Asterisks denote statistically significant differences comparing haplo-HCT and MD-HCT cohorts at specific time points (****P < 0.0001; ***P < 0.001; **P < 0.01; *P < 0.05). White stars within the heat map (C) denote P < 0.05 (Wilcoxon rank-sum test). See **supplemental Table 8** for the median absolute values along with the corresponding interquartile values and P values for panels A-C.

Delayed NK-cell reconstitution with a high $CD56^{bright}$ $CD16^-$ /$CD56^{dim}CD16^+$ NK-cell ratio early after haplo-HCT

To characterize NK-cell reconstitution, we divided NK cells into 4 subsets based on the expression of CD56 and CD16 (27): $CD56^{bright}CD16^-$, $CD56^{dim}CD16^+$, $CD56^{dim}CD16^-$, and $CD56^{bright}CD16^+$ NK cells (**Figure 3A**). In HD, $CD56^{bright}CD16^-$ NK cells account for 5% to 15% of circulating NK cells and are relatively immature cells with weak cytolytic activity (28). $CD56^{dim}CD16^+$ cells are the predominant NK-cell subset in peripheral blood of HD, with a mature phenotype and strong cytolytic activity (28). $CD56^{dim}CD16^-$ NK cells exhibit an immature phenotype (27), while $CD56^{bright}CD16^+$ NK cells represent an intermediate stage of

NK-cell maturation with cytotoxicity against tumor cells closer to that of $CD56^{dim}CD16^{+}$ NK cells but expressing a phenotype similar to $CD56^{bright}CD16^{-}$ NK cells (29). After haplo-HCT, we observed an increase in $CD56^{bright}$ $CD16^{-}$ NK cells with fewer mature $CD56^{dim}CD16^{+}$ NK cells during the first 6 months compared with MD-HCT group (**Figure 3B**). Differences in the distribution of $CD56^{dim}CD16^{-}$ NK cells and $CD56^{bright}CD16^{+}$ NK cells between haplo-HCT and MD- HCT cohorts were less marked. Consistent with these differences, haplo-HCT patients had higher absolute numbers of $CD56^{bright}$ $CD16^{-}$ NK cells and markedly lower numbers of $CD56^{dim}CD16^{+}$ NK cells during the first 3 months after transplant (**Figure 3C**). As a result, $CD56^{bright}CD16^{-}/CD56^{dim}CD16^{+}$ NK-cell ratio was higher in the haplo-HCT group for the first 6 months after transplant, highlighting the imbalanced reconstitution of the 2 major NK subsets in this transplant setting (**Figure 3D**).

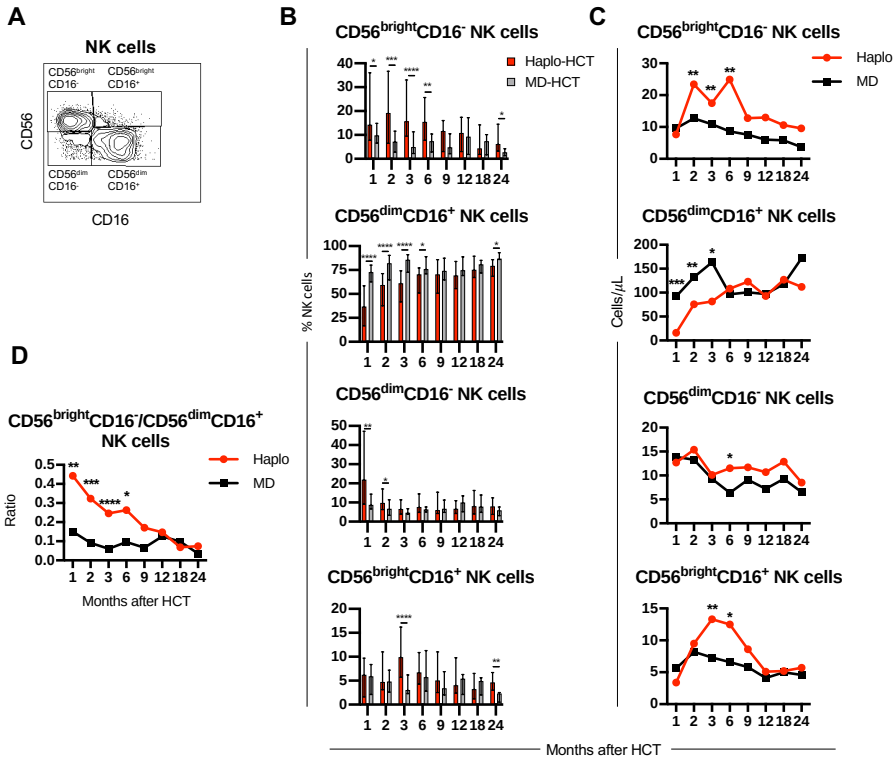

Figure 3. Reconstitution of NK-cell populations after haplo-HCT and MD-HCT. (A) Representative gating strategy used to define NK-cell subsets based on expression of CD56 and CD16. (B) Reconstitution of NK-cell subsets after haplo-HCT and MD-HCT. Values are expressed as median and range. (C) Absolute number of NK-cell subsets in peripheral blood after haplo-HCT and MD-HCT. Median cell counts per microliter are represented at each time point. (D) Median $CD56^{bright}CD16^{-}/CD56^{dim}CD16^{+}$ NK-cell ratio after haplo-HCT and MD-HCT. Statistically significant differences are noted (****P = 0.0001; ***P = 0.001; **P = 0.01; *P = 0.05; Wilcoxon rank-sum test). See **supplemental Table 9** for the median absolute values along with the corresponding interquartile values and P values for panels C and D.

NK cells reconstituting early after haplo-HCT have immature phenotypes

To further characterize the dynamics of NK-cell reconstitution, we analyzed samples from patients 1 month after transplant (6 patients after

haplo-HCT and 3 patients after MD-HCT) and HDs (n = 3) using a 35-marker mass cytometry panel (see **supplemental Table 5** for patient clinical characteristics). In this analysis, MD-HCT patients received sirolimus in addition to TAC and MTX for GVHD prophylaxis (MDs-HCT). At 1 month, the FlowSOM algorithm identified 20 different NK-cell metaclusters (**Figure 4A**) based on the levels of expression of different markers included in the panel (**Figure 4B**). These metaclusters naturally subdivided the 4 previously established NK-cell populations: $CD56^{bright}CD16^{-}$, $CD56^{dim}CD16^{+}$, $CD56^{dim}CD16^{-}$, and $CD56^{bright}CD16^{+}$ (**Figure 4A-B**).

$CD56^{bright}CD16^{-}$ NK-cell metaclusters (8, 11, 12, 16, 19, and 20) were characterized by a higher expression of inhibitory receptor NKG2A and activating receptors NKp30, NKp46, and NKG2D. Metaclusters 8 and 12 also expressed CD62L, reflecting a more immature phenotype, while metacluster 11 had the highest level of Ki67, a proliferation marker. Metaclusters 19 and 20 also represent the only subsets with CD25 expression and are the only $CD56^{bright}CD16^{-}$ NK-cell metaclusters also present in HDs (**Figure 4D**).

$CD56^{bright}CD16^{+}$ NK-cell metaclusters (2, 3, 5, 6, 7, and 13) share similar phenotype with $CD56^{bright}CD16^{-}$ NK-cell metaclusters for NKG2A, NKG2D, NKp30, and NKp46. However, several of these metaclusters showed high expression of KIR (metaclusters 2, 3, 5, and 7), CD57 (metacluster 5), granzyme B (metaclusters 2, 3, 5, 6, 7, and 13), and perforin (metacluster 2, 5, 6, and 13), suggesting an intermediate stage of NK-cell maturation.

$CD56^{dim}CD16^{+}$ NK-cell metaclusters (1, 9, 10, 14, 15, and 17) expressed higher levels of maturity markers (KIRs and CD57) and activation markers (CD69 and perforin) compared with $CD56^{bright}CD16^{-}$ NK-cell metaclusters. The viSNE map identified a maturation gradient for $CD56^{dim}CD16^{+}$ NK-cell metaclusters, where metaclusters 15 and 17 represented more immature cells expressing CD16, CD69, perforin, and TIGIT; metaclusters 10 and 14 represented an intermediated maturation stage, expressing also CD57; and metacluster 1 recapitulates the mature $CD56^{dim}CD16^{+}$ NK cells expressing both CD57 and KIR. Finally, metacluster 9 mirrored memory-like NK cells, with coexpression of CD57 and NKG2C in addition to KIRs. We were also able to identify one metacluster that recapitulated the $CD56^{dim}CD16^{-}$ NK cells (metacluster 18), which expressed low levels of NKp46 and NKG2A, intermediate levels of NKp30, NKG2D and DNAM, and high levels of perforin, TIGIT, CD69, and CD8. One month after haplo-HCT, this analysis showed an enrichment of immature $CD56^{bright}CD16^{-}$ and $CD56^{bright}CD16^{+}$ NK-cell metaclusters with a reduction of more mature $CD56^{dim}CD16^{+}$ NK-cell metaclusters compared with HD and MDs-HCT (**Figure 4C-D**).

We also used the same mass cytometry panel to examine NK cells 3 months after HCT. This comparison included 17 patients (8 after haplo-HCT, 3 after MDs-HCT, and 6 after MD-HCT with TAC/MTX only) and 4 HDs. At this time point, the FlowSOM algorithm identified 16 different NK-cell metaclusters (**Figure 4E, F**), with fewer immature metaclusters representing $CD56^{bright}CD16^{-}$ (metaclusters 1 and 6) and

$CD56^{bright}CD16^{+}$ NK cells (metacluster 2) and most representing more mature $CD56^{dim}CD16^{+}$ NK cells (metaclusters 3, 4, 5, 7, 9, 11, 12, 14, and 15). Haplo-HCT samples continued to display a proportional reduction of $CD56^{dim}CD16^{+}$ NK-cell metaclusters (12, 14, and 15), compared with HD and MD-HCT (**Figure 4G and H**). However, no differences were observed when compared with the MDs-HCT group. Interestingly, haplo-HCT patients who had experienced CMV reactivation had higher representation of mature $CD56^{dim}CD16^{+}KIR^{+}$ NK-cell metaclusters (3, 5, and 11) compared with haplo-HCT patients without CMV reactivation, where immature metaclusters were enriched (metaclusters 2, 4, and 6; see **supplemental Figure 7**).

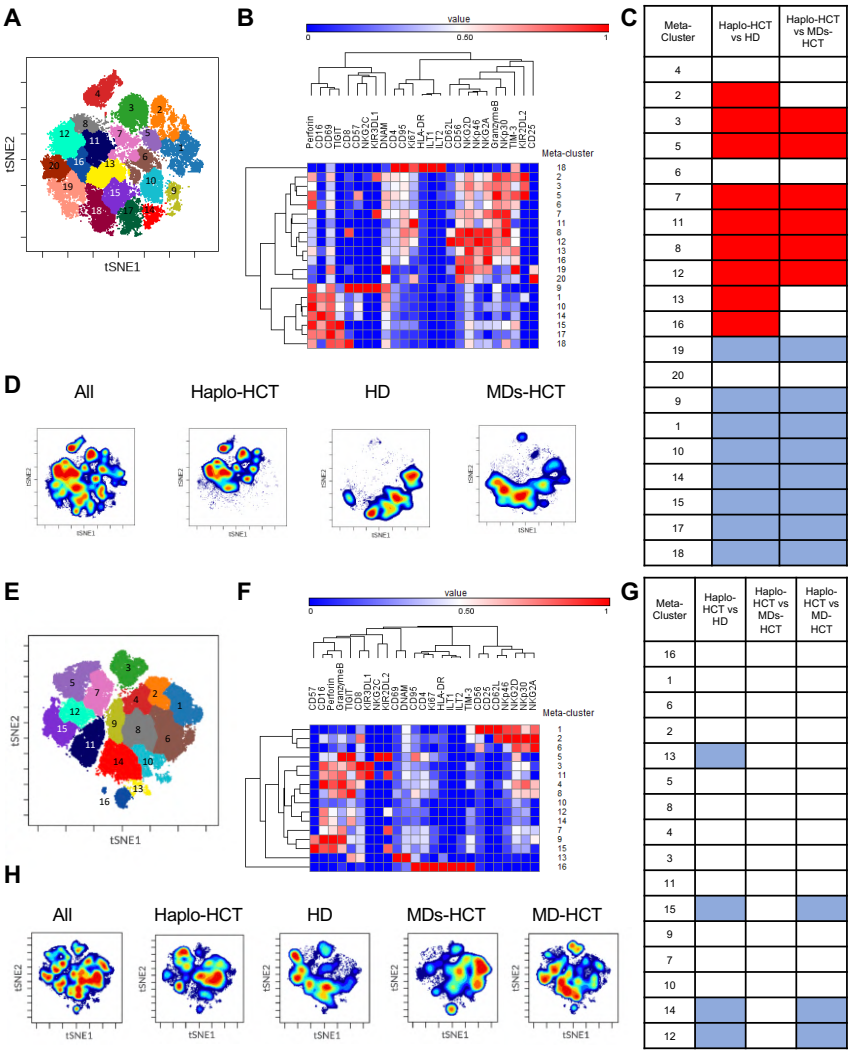

Figure 4. Mass cytometry analysis of NK-cell maturation after haplo-HCT. Mass cytometry analysis was performed using cryopreserved PBMCs obtained 1 and 3 months after transplant (haplo-HCT n = 10, MD-HCT n = 6, MDs-HCT n = 4) and from HDs (n = 7). (A) FlowSOM analysis of all 1-month samples overlaid on viSNE map identified 20 distinct NK-cell metaclusters.

(B) Heat map summarizes the expression of different markers in each NK-cell metacluster 1 month after HCT. (C) Relative representation of each NK-cell metacluster in haplo-HCT, MDs-HCT, and HD samples 1 month after HCT. Indicated columns compare representation of each meta-cluster in haplo- HCT vs HD and haplo-HCT vs MD-HCT samples. (D) One-month density viSNE map representation of all NK-cell metaclusters depicting data for all samples (n = 12), haplo- HCT (n = 6), HD (n = 3), and MD-HCT (n = 3). The location of each NK-cell metacluster is the same as in panel A. (E) FlowSOM analysis of all 3-month samples overlaid on viSNE map identified 16 distinct NK-cell metaclusters. (F) Heat map summarizes the expression of different markers in each NK metacluster 3 months after HCT. (G) Relative representation of each NK metacluster in haplo-HCT, MDs-HCT, MD-HCT, and HD samples. Indicated columns compare representation of each metacluster in haplo-HCT vs HD, haplo-HCT vs MDs-HCT, and haplo-HCT vs MD-HCT samples. (H) Three-month density viSNE map representation of all NK-cell metaclusters depicting data for all samples (n = 21), haplo-HCT (n = 8), HD (n = 4), MDs-HCT (n = 3), and MD-HCT (n = 6). For the heat maps median intensity was normalized for the highest value for each marker; red indicates the highest value, and blue represents the lowest value. For the tables shown in panels C and G, blue squares indicate a relative decrease, red squares represent a relative increase, and white squares indicate no change. Only statistically significant changes ($P < 0.05$) are reported. For comparison, the Wilcoxon rank-sum test for unpaired group was used. viSNE allows visualization of high-dimensional single-cell data and is based on the t-Distributed Stochastic Neighbor Embedding (t-SNE) algorithm.

IL-15 restores NK-cell function after haplo-HCT

To assess NK-cell function, we evaluated NK-cell degranulation and cytokine production after stimulation with K562 target cells. Experiments were carried out with peripheral blood mononuclear cells (PBMCs) obtained 2 months after transplant (haplo-HCT and MD-HCT) and from HD (**Figure 5A**; see **supplemental Table 6** for patient clinical characteristics). After K562 stimulation, NK cells from haplo-HCT and MD-HCT patients exhibited degranulation levels (CD107a) similar to HD NK cells (**Figure 5B**). However, NK cells from both

transplant cohorts had significant impairment of cytokine production, especially for IFN-γ (**Figure 5B**). IL-15 is critical for the generation and maintenance of NK cells in vivo, and incubation with IL-15 can enhance NK-cell function in vitro (30). To test if IL-15 can overcome defects in NK-cell function in the posttransplant setting, we incubated PBMCs from haplo-HCT, MD- HCT, and HDs for 12 to 15 hours in media containing recombinant human IL-15 (5 ng/mL) and subsequently assessed function after stimulation with K562. IL-15 priming effectively restored IFN-γ secretion from haplo-HCT NK cells to normal levels, with levels of CD107a degranulation and TNF-α secretion after haplo-HCT actually becoming higher than HDs and MD-HCT, respectively (**Figure 5B**). We also compared the NK-cell function in samples from relapsed vs nonrelapsed patients within the haplo-HCT and MD-HCT cohorts, and no statistical differences were observed (data not shown).

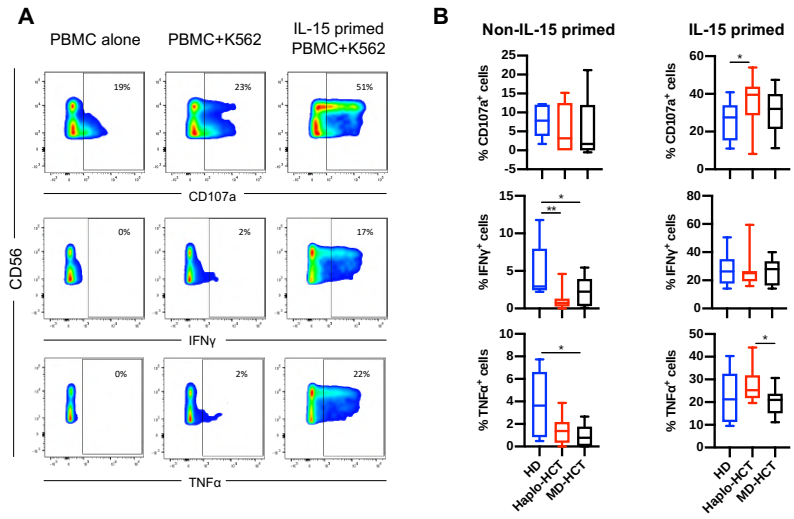

Figure 5. Functional analysis of NK cells after haplo-HCT. Assays were carried out using cryopreserved PBMCs collected 2 months after haplo-HCT (red boxes, n = 9), MD-HCT (black boxes, n = 9) and from HDs (blue boxes, n = 8). Thawed PBMCs were cultured overnight with media alone or media plus IL-15 (5 ng/mL) and then stimulated with K562 target cells (effector to target ratio = 5:1). (A) Flow cytometry plots from a representative haplo-HCT patient showing surface staining of CD107a and intracellular staining for IFN-γ and TNF-α at baseline (PBMC alone), with target cells (PBMC + K562), and with target cells after priming with IL-15 (IL-15-primed PBMC + K562). (B) Summary data for all samples showing percentage of $CD107a^+$, IFN-γ^+, and TNF-α^+ NK cells upon coculture with K562 cells in the absence or presence of IL-15 priming. The background staining for CD107a, IFN-γ, and TNF-α present at baseline was subtracted. Box and whisker plots show medians, along with minimum and maximum values. Data were compared using the Wilcoxon signed-rank test for paired comparison (**P < 0.01; *P < 0.05).

Delayed NK-cell reconstitution correlates with CMV reactivation after haplo-HCT

To assess the potential clinical impact of impaired NK-cell reconstitution, we compared CMV reactivation in both cohorts. Only 3 of 35 MD-HCT patients (8.6%) developed CMV reactivation, with a median of 110 days (range, 27-205 days) to CMV reactivation. In contrast, 18 of 60 haplo-HCT patients (30%) developed CMV reactivation at a median of 36 days (range, 11- 100 days; P = 0.015; **Figure 6A**). Despite letermovir prophylaxis given to 7 patients after haplo-HCT, this group still experienced more CMV reactivation. Since expression of CD16 distinguishes immature from mature NK cells, we correlated the ratio of $CD16^-/CD16^+$ NK cells with the occurrence of CMV reactivation. Patients who developed CMV reactivation had an increased $CD16^-/CD16^+$ NK-cell ratio at 1 and 2 months compared with haplo-HCT patients who did not develop CMV reactivation

(**Figure 6B**), suggesting a correlation between delayed NK-cell maturation and CMV reactivation. Analysis of absolute counts of $CD16^+$ and $CD16^-$ NK-cell and NK-cell subsets ($56^{bright}CD16^-$, $56^{dim}CD16^+$, $56^{bright}CD16^+$, and $56^{dim}CD16^-$) 1 and 2 months after haplo-HCT showed similar results (**supplemental Figure 8**). In this analysis, increased numbers of $CD16^+$ NK cells 1 and 2 months after haplo-HCT were significantly associated with a lower incidence of CMV reactivation.

NK- and T-cell reconstitution associated with cGVHD after haplo-HCT

Consistent with previous reports, haplo-HCT patients had a lower incidence of cGVHD than MD-HCT patients (**Figure 6C**). To examine whether NK-cell reconstitution influenced the development of cGVHD, we compared the ratio of $CD16^-/CD16^+$ NK cells in haplo-HCT patients with and without cGVHD. For this analysis, only cGVHD that occurred within 1 year after transplant was considered. We observed a higher $CD16^-/CD16^+$ NK-cell ratio at 1, 2, and 6 months after transplant ($P = 0.04$, $P = 0.001$, and $P = 0.04$, respectively) in patients who developed cGVHD after haplo-HCT (**Figure 6D**). Analysis of absolute NK-cell counts confirmed that increased numbers of $CD16^+$ NK cells 2 months after haplo-HCT were associated with a lower incidence of subsequent cGVHD (**supplemental Figure 8**). To determine whether early PD-1 expression influenced subsequent development of cGVHD, we examined the percentage of PD-1^+ cells in different T-cell subsets. Within the haplo-HCT cohort, PD-1 expression was higher in CM $CD4^+$ Treg cells and EM $CD4^+$ Treg cells

at 1 month in patients who did not develop cGVHD (P = 0.0023 and P = 0.0418, respectively; **Figure 6E**). No differences in PD-1 expression were observed in the $CD4^+$ Tcon-cell compartment regarding the subsequent development of cGVHD.

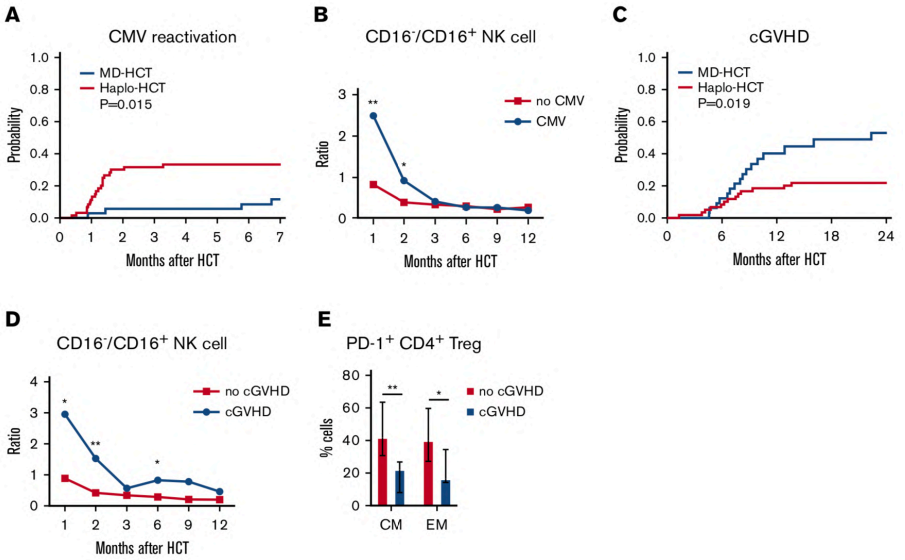

Figure 6. Correlation of immune reconstitution and clinical outcomes after haplo-HCT. (A) Probability of CMV reactivation after haplo-HCT and MD-HCT. (B) Comparison of $CD16^-/CD16^+$ NK-cell ratio in patients after haplo-HCT with and without CMV reactivation after transplant. The median values per microliter are represented at each time point (**P < 0.01; *P < 0.05). (C) Probability of cGVHD after haplo-HCT and MD-HCT. (D) Comparison of $CD16^-/CD16^+$ NK-cell ratio in patients after haplo-HCT with and without cGVHD after transplant; the median values per microliter are represented at each time point. (E) Distribution of PD-1^+ CM and EM $CD4^+$ Treg cells at 1 month after haplo-HCT according to cGVHD onset. Values are expressed as median and range. Statistically significant differences are noted (**P < 0.01; *P < 0.05; Wilcoxon rank-sum test). CM T cells are defined as $CD45RO^+CD62L^+$ and EM as $CD45RO^+CD62L^-$ T lymphocytes. See **supplemental Tables 10 and 11** for the median absolute values along with the corresponding interquartile values and P values for panels B and D.

Discussion

Prompt and successful reconstitution of both T- and NK-cell immunity after HCT is critical for the prevention of GVHD, infection, and relapse, which remain the leading causes of mortality in patients after allogeneic HCT (31). The use of PTCy has revolutionized haplo-HCT by decreasing GVHD and graft failure, but recent studies have reported increased rates of infections, including CMV and community respiratory viruses, highlighting potential immune defects in these patients. Using detailed immunophenotypic and functional assays, our study reveals significant delays in T- and NK-cell recovery in the first 3 months after haplo-HCT with PTCy compared with MD-HCT with conventional GVHD prophylaxis. Delayed recovery of naive T cells along with a significantly higher Treg-cell/Tcon-cell ratio and PD-1 expression on memory $CD4^+$ T cells likely contribute to the low incidence of cGVHD. Delayed NK-cell reconstitution, with the preferential expansion of immature $CD56^{bright}CD16^-NKG2A^+$ NK cells, may contribute to the higher rate of CMV reactivation after haplo-HCT.

Delayed T-cell reconstitution after haplo-HCT was primarily driven by a reduced number of $CD4^+$ Tcon cells, with a relative sparing of $CD4^+$ Treg cells, resulting in a higher Treg-cell/Tcon-cell ratio early after transplant. Relative sparing of $CD4^+$ Treg cells after PTCy has been found in previous studies and may be due to higher levels of aldehyde dehydrogenase expression in these cells (15, 32-35). We also observed a profound reduction of naive T cells and a predominance of EM cells in all major T-cell populations that persisted for 1 year after haplo-HCT. Increased sensitivity of naive T cells to cyclophosphamide or rapid

differentiation of naive into memory/effector T cells after transplant could potentially explain preferential recovery of memory T cells in patients receiving PTCy (33,36). T-cell recovery early after transplant is primarily driven by homeostatic proliferation in response to persistent lymphopenia rather than through generation of new T cells from hematopoietic precursors. However, the prolonged delay of naive T-cell recovery lasting 1 year after haplo- HCT suggests that de novo T-cell generation may also be impaired in this transplant setting.

Regulation of cell survival can also affect T-cell reconstitution after transplant. In $CD4^+$ Tcon cells and $CD8^+$ T cells, activation of PD-1 delivers inhibitory signals that regulate the balance between T-cell activation, tolerance, and terminal differentiation (26,37). Both murine models (38,39) and clinical studies (40-42) support the importance of PD- 1 in maintaining immune tolerance and preventing GVHD. In our analysis, we observed increased expression of PD-1 in all T-cell subsets at early time points after haplo-HCT. The common γ-chain cytokines IL-2, IL-17, IL-15, and IL-21 induce expression of PD-1, especially on memory T-cell subsets (43), and increased levels of these cytokines after transplant may explain the increased expression of PD-1 observed in our haplo-HCT cohort (23). In the haplo-HCT cohort, we also found that patients who did not develop cGVHD had higher PD-1 expression on CM and EM $CD4^+$ Treg cells at 1 month after transplant. We previously demonstrated that PD-1 promotes IL-2–induced $CD4^+$ Treg-cell proliferation and prolongs $CD4^+$ Treg-cell survival in a murine model and in patients receiving low-dose IL-2 therapy for cGVHD (37). These findings are also consistent with previous studies

in murine models where PTCy was found to efficiently ameliorate GVHD by preventing $CD4^+$ Treg-cell apoptosis and reducing $CD4^+$ Tcon-cell expansion (44).

We observed a profound and persistent reduction of NKT cells in haplo-HCT compared with MD-HCT recipients. In a previous report, NKT cells remained low for 1 to 3 months after haplo-HCT compared with conventional transplant. However, in this study, NKT cells were defined as $CD3^+CD161^+$ cells, and haplo-HCT patients received a different conditioning regimen and GVHD prophylaxis that included anti-thymocyte globulin (45).

NK cells contribute to GVL and also provide antiviral immunity after transplant (46,47). Consistent with previous studies (23,27), we found a significant delay in NK-cell reconstitution, with immature $CD56^{bright}NKG2A^+CD16^-KIR^-CD57^-$ NK cells predominating the early posttransplant period in haplo-HCT patients. We also found a higher $CD16^-/CD16^+$ NK-cell ratio in patients who developed CMV reactivation after haplo-HCT, suggesting a link between predominance of immature NK cells and viral reactivation. Although absolute count and subset distribution of immune cells represent an imperfect surrogate marker for protection against infection, we observed a significantly higher risk of CMV reactivation after haplo-HCT where both T- and NK-cell reconstitution was delayed compared with MD-HCT. Interestingly, patients who experienced CMV reactivation showed a more mature NK-cell profile at mass cytometry analysis performed at 3 months, suggesting that CMV reactivation may promote NK-cell maturation (48-50). We also observed a higher $CD16^-/CD16^+$

NK-cell ratio in patients who subsequently developed cGVHD. The mechanism whereby delayed recovery of $CD16^+$ NK cells may contribute to the development of cGVHD is not known, but this may be related to reduced NK-cell-mediated killing of antigen presenting cells and T cells, which has been reported to prevent GVHD in murine models (51).

IL-15 is important for normal NK-cell homeostasis (52) and has been used to enhance antitumor and antiviral immunity (53-57). We hypothesized that the NK-cell functional defects in our haplo-HCT patients were primarily due to the predominance of immature subsets and demonstrated that this impairment can be rescued by IL-15 priming. Although functional studies and mass cytometry studies were done with a small number of representative samples, these results suggest that haplo-HCT with PTCy represents a suitable setting to test the ability of IL-15 or IL-15 analogs to boost NK-cell function and improve clinical outcomes. Adoptive transfer of NK cells early after transplant is another potential strategy (58,59). Our group recently described cytokine-induced memory-like NK cells with enhanced antitumor activity and increased proliferation capacity (60,61). Adoptive transfer of cytokine-induced memory-like NK cells after haplo-HCT with PTCy may be another approach to overcome delayed NK-cell reconstitution without increasing GVHD.

It is also important to acknowledge key limitations in our comparison of haplo-HCT with MD-HCT. First, GVHD prophylaxis differed between the 2 transplant cohorts and might contribute to differences in immune recovery after HCT. In addition to PTCy, haplo-HCT patients received mycophenolate mofetil and TAC after transplant, while MD-

HCT patients received MTX and TAC. However, the preferential recovery of EM and TEMRA T cells observed in our haplo-HCT cohort was also reported after MD-HCT treated with PTCy as a single agent for GVHD prophylaxis (62), suggesting that this effect could be driven specifically by PTCy. Second, stem cell sources differed, with haplo-HCT patients receiving primarily bone marrow compared with MD-HCT patients who received peripheral blood stem cells (PBSCs). PBSC grafts contain higher numbers of donor T cells, and this may contribute to faster T-cell recovery in this cohort. Previous studies have not suggested that NK-cell reconstitution is affected by graft source (14,23). However, a recent study reported a positive correlation between graft NK-cell dose and early NK-cell reconstitution, suggesting that graft composition may have contributed to the different patterns of NK-cell recovery observed in our study (63). Third, profound HLA mismatch in haplo-HCT patients may also affect recovery of thymic function and delay the generation of naive T cells. Thus, all of the differences we observed in our comparison may not be entirely attributed to the administration of high-dose cyclophosphamide in the early posttransplant period. We cannot exclude the possibility that additional variables, including the initiation of TAC (day -3 vs day +5), the start of granulocyte colony- stimulating factor (day +11 vs day +5), or the intensity and type of conditioning might have played a role in the different patterns of immune reconstitution we observed.

In conclusion, our comparison of haplo-HCT with conventional MD-HCT revealed several significant differences in T- and NK-cell reconstitution. These findings are consistent with an immune milieu promoting tolerance, leading to a lower rate of cGVHD. Interventions

that selectively promote the generation, expansion, and persistence of functional NK cells to reduce viral reactivation and enhance GVL, without increasing the risk of GVHD, may further improve outcomes in patients undergoing haplo-HCT with PTCy.

References

1. Passweg JR, Baldomero H, Bader P, et al. Use of haploidentical stem cell transplantation continues to increase: the 2015 European Society for Blood and Marrow Transplant activity survey report. Bone Marrow Transplant. 2017;52(6):811-817.
2. D'Souza A, Lee S, Zhu X, Pasquini M. Current use and trends in hematopoietic cell transplantation in the united states. Biol Blood Marrow Transplant. 2017;23(9):1417-1421.
3. Aversa F, Terenzi A, Tabilio A, et al. Full haplotype-mismatched hematopoietic stem-cell transplantation: a phase II study in patients with acute leukemia at high risk of relapse. J Clin Oncol. 2005;23(15):3447-3454.
4. Bertaina A, Zecca M, Buldini B, et al. Unrelated donor vs HLA-haploidentical a/b T-cell- and B-cell-depleted HSCT in children with acute leukemia. Blood. 2018;132(24):2594-2607.
5. Chang Y-J, Huang X-J. Haploidentical stem cell transplantation: anti-thymocyte globulin-based experience. Semin Hematol. 2016;53(2):82-89.
6. Luznik L, O'Donnell PV, Symons HJ, et al. HLA-haploidentical bone marrow transplantation for hematologic malignancies using nonmyeloablative conditioning and high-dose, posttransplantation cyclophosphamide. Biol Blood Marrow Transplant. 2008;14(6):641-650.
7. Ciurea SO, Zhang M-J, Bacigalupo AA, et al. Haploidentical transplant with posttransplant cyclophosphamide vs matched unrelated donor transplant for acute myeloid leukemia. Blood. 2015;126(8):1033-1040.
8. Rashidi A, Hamadani M, Zhang M-J, et al. Outcomes of haploidentical vs matched sibling transplantation for acute myeloid leukemia in first complete remission. Blood Adv. 2019;3(12):1826-1836.
9. Lorentino F, Labopin M, Bernardi M, et al; Acute Leukemia Working Party of the European Society for Blood and Marrow Transplantation. Comparable outcomes of haploidentical, 10/10 and 9/10 unrelated donor

transplantation in adverse karyotype AML in first complete remission. Am J Hematol. 2018; 93(10):1236-1244.
10. Dreger P, Sureda A, Ahn KW, et al. PTCy-based haploidentical vs matched related or unrelated donor reduced-intensity conditioning transplant for DLBCL. Blood Adv. 2019;3(3):360-369.
11. Mart´ınez C, Gayoso J, Canals C, et al; Lymphoma Working Party of the European Group for Blood and Marrow Transplantation. Post-transplantation cyclophosphamide-based haploidentical transplantation as alternative to matched sibling or unrelated donor transplantation for hodgkin lymphoma:
a registry study of the Lymphoma Working Party of the European Society for Blood and Marrow Transplantation. J Clin Oncol. 2017;35(30):3425-3432.
12. van den Brink MRM, Velardi E, Perales M-A. Immune reconstitution following stem cell transplantation. Hematology Am Soc Hematol Educ Program. 2015; 2015:215-219.
13. Ogonek J, Kralj Juric M, Ghimire S, et al. Immune reconstitution after allogeneic hematopoietic stem cell transplantation. Front Immunol. 2016;7:507.
14. Abrahamsen IW, Sømme S, Heldal D, Egeland T, Kvale D, Tjønnfjord GE. Immune reconstitution after allogeneic stem cell transplantation: the impact of stem cell source and graft-versus-host disease. Haematologica. 2005;90(1):86-93.
15. McCurdy SR, Luznik L. Immune reconstitution after T-cell replete HLA-haploidentical transplantation. Semin Hematol. 2019;56(3):221-226.
16. Nakamae H, Fujii K, Nanno S, et al. A prospective observational study of immune reconstitution following transplantation with post-transplant reduced-dose cyclophosphamide from HLA-haploidentical donors. Transpl Int. 2019;32(12):1322-1332.
17. Crocchiolo R, Bramanti S, Vai A, et al. Infections after T-replete haploidentical transplantation and high-dose cyclophosphamide as graft-versus-host disease prophylaxis. Transpl Infect Dis. 2015;17(2):242-249.
18. Mohty R, Brissot E, Battipaglia G, et al. Infectious complications after post-transplantation cyclophosphamide and anti-thymocyte globulin-based haploidentical stem cell transplantation. Br J Haematol. 2019;187(3):e64-e68.
19. Slade M, Goldsmith S, Romee R, et al. Epidemiology of infections following haploidentical peripheral blood hematopoietic cell transplantation. Transpl Infect Dis. 2017;19(1):e12629.

20. Goldsmith SR, Slade M, DiPersio JF, et al. Cytomegalovirus viremia, disease, and impact on relapse in T-cell replete peripheral blood haploidentical hematopoietic cell transplantation with post-transplant cyclophosphamide. Haematologica. 2016;101(11):e465 LP-e468.
21. Goldsmith SR, Fuchs EJ, Bashey A, et al. Incidence and impact of cytomegalovirus infection in haploidentical and matched-related donors receiving post-transplant cyclophosphamide (PTCy): a CIBMTR analysis. Biol Blood Marrow Transplant. 2020;26(3):S69-S70.
22. Shimoni A, Labopin M, Lorentino F, et al. Killer cell immunoglobulin-like receptor ligand mismatching and outcome after haploidentical transplantation with post-transplant cyclophosphamide. Leukemia. 2019;33(1):230-239.
23. Russo A, Oliveira G, Berglund S, et al. NK cell recovery after haploidentical HSCT with posttransplant cyclophosphamide: dynamics and clinical implications. Blood. 2018;131(2):247-262.
24. Hirakawa M, Matos TR, Liu H, et al. Low-dose IL-2 selectively activates subsets of CD41 Tregs and NK cells. JCI Insight. 2016;1(18):e89278.
25. Kotecha N, Krutzik PO, Irish JM. Web-based analysis and publication of flow cytometry experiments. Curr Protoc Cytom. 2010;53(1):10.17.1-10.17.24.
26. Keir ME, Butte MJ, Freeman GJ, Sharpe AH. PD-1 and its ligands in tolerance and immunity. Annu Rev Immunol. 2008;26(1):677-704.
27. Roberto A, Di Vito C, Zaghi E, et al. The early expansion of anergic NKG2Apos/CD56dim/CD16neg natural killer represents a therapeutic target in haploidentical hematopoietic stem cell transplantation. Haematologica. 2018;103(8):1390-1402.
28. Cooper MA, Fehniger TA, Caligiuri MA. The biology of human natural killer-cell subsets. Trends Immunol. 2001;22(11):633-640.
29. Béziat V, Duffy D, Quoc SN, et al. CD56bright/CD161NKcells: a functional intermediate stage of NK cell differentiation. J Immunol. 2011;186(12): 6753-6761.
30. Wagner JA, Rosario M, Romee R, et al. CD56bright NK cells exhibit potent antitumor responses following IL-15 priming. J Clin Invest. 2017;127(11): 4042-4058.
31. Alho AC, Kim HT, Chammas MJ, et al. Unbalanced recovery of regulatory and effector T cells after allogeneic stem cell transplantation contributes to chronic GVHD. Blood. 2016;127(5):646-657.
32. Wachsmuth LP, Patterson MT, Eckhaus MA, Venzon DJ, Gress RE, Kanakry CG. Post-transplantation cyclophosphamide prevents graft-

versus-host disease by inducing alloreactive T cell dysfunction and suppression. J Clin Invest. 2019;129(6):2357-2373.
33. Roberto A, Castagna L, Zanon V, et al. Role of naive-derived T memory stem cells in T-cell reconstitution following allogeneic transplantation. Blood. 2015; 125(18):2855-2864.
34. Cieri N, Greco R, Crucitti L, et al. Post-transplantation cyclophosphamide and sirolimus after haploidentical hematopoietic stem cell transplantation using a treosulfan-based myeloablative conditioning and peripheral blood stem cells. Biol Blood Marrow Transplant. 2015;21(8):1506-1514.
35. Kanakry CG, Ganguly S, Zahurak M, et al. Aldehyde dehydrogenase expression drives human regulatory t cell resistance to posttransplantation cyclophosphamide. Sci Transl Med. 2013;5(211):211ra157.
36. Cieri N, Oliveira G, Greco R, et al. Generation of human memory stem T cells after haploidentical T-replete hematopoietic stem cell transplantation. Blood. 2015;125(18):2865-2874.
37. Asano T, Meguri Y, Yoshioka T, et al. PD-1 modulates regulatory T-cell homeostasis during low-dose interleukin-2 therapy. Blood. 2017;129(15): 2186-2197.
38. Blazar BR, Carreno BM, Panoskaltsis-Mortari A, et al. Blockade of programmed death-1 engagement accelerates graft-versus-host disease lethality by an IFN-N-dependent mechanism. J Immunol. 2003;171(3):1272-1277.
39. Saha A, Aoyama K, Taylor PA, et al. Host programmed death ligand 1 is dominant over programmed death ligand 2 expression in regulating graft-versus-host disease lethality [published correction appears in Blood. 2014;123(21):3364]. Blood. 2013;122(17):3062-3073.
40. Merryman RW, Kim HT, Zinzani PL, et al. Safety and efficacy of allogeneic hematopoietic stem cell transplant after PD-1 blockade in relapsed/refractory lymphoma. Blood. 2017;129(10):1380-1388.
41. Herbaux C, Merryman R, Devine S, et al. Recommendations for managing PD-1 blockade in the context of allogeneic HCT in Hodgkin lymphoma: taming a necessary evil. Blood. 2018;132(1):9-16.
42. Ijaz A, Khan AY, Malik SU, et al. Significant risk of graft-versus-host disease with exposure to checkpoint inhibitors before and after allogeneic transplantation. Biol Blood Marrow Transplant. 2019;25(1):94-99.
43. Kinter AL, Godbout EJ, McNally JP, et al. The common N-chain cytokines IL-2, IL-7, IL-15, and IL-21 induce the expression of programmed death-1 and its ligands. J Immunol. 2008;181(10):6738-6746.

44. Ikegawa S, Meguri Y, Kondo T, et al. PTCy ameliorates GVHD by restoring regulatory and effector T-cell homeostasis in recipients with PD-1 blockade. Blood Adv. 2019;3(23):4081-4094.
45. Park BG, Park C-J, Jang S, et al. Reconstitution of lymphocyte subpopulations after hematopoietic stem cell transplantation: comparison of hematologic malignancies and donor types in event-free patients. Leuk Res. 2015;39(12):1334-1341.
46. Locatelli F, Pende D, Falco M, Della Chiesa M, Moretta A, Moretta L. NK cells mediate a crucial graft-versus-leukemia effect in haploidentical-HSCT to cure high-risk acute leukemia. Trends Immunol. 2018;39(7):577-590.
47. Vacca P, Montaldo E, Croxatto D, et al. NK cells and other innate lymphoid cells in hematopoietic stem cell transplantation. Front Immunol. 2016;7:188.
48. Béziat V, Liu LL, Malmberg J-A, et al. NK cell responses to cytomegalovirus infection lead to stable imprints in the human KIR repertoire and involve activating KIRs. Blood. 2013;121(14):2678-2688.
49. Della Chiesa M, Falco M, Podesta` M, et al. Phenotypic and functional heterogeneity of human NK cells developing after umbilical cord blood transplantation: a role for human cytomegalovirus? Blood. 2012;119(2):399-410.
50. Foley B, Cooley S, Verneris MR, et al. Cytomegalovirus reactivation after allogeneic transplantation promotes a lasting increase in educated NKG2C1 natural killer cells with potent function. Blood. 2012;119(11):2665-2674.
51. Simonetta F, Alvarez M, Negrin RS. Natural killer cells in graft-versus-host-disease after allogeneic hematopoietic cell transplantation. Front Immunol. 2017; 8:465.
52. Rautela J, Huntington ND. IL-15 signaling in NK cell cancer immunotherapy. Curr Opin Immunol. 2017;44:1-6.
53. Tang F, Zhao LT, Jiang Y, Ba N, Cui LX, He W. Activity of recombinant human interleukin-15 against tumor recurrence and metastasis in mice. Cell Mol Immunol. 2008;5(3):189-196.
54. Rhode PR, Egan JO, Xu W, et al. Comparison of the superagonist complex, ALT-803, to IL15 as cancer immunotherapeutics in animal models. Cancer Immunol Res. 2016;4(1):49-60.
55. Stoklasek TA, Schluns KS, Lefrançois L. Combined IL-15/IL-15Ra immunotherapy maximizes IL-15 activity in vivo. J Immunol. 2006;177(9):6072-6080.

56. Romee R, Cooley S, Berrien-Elliott MM, et al. First-in-human phase 1 clinical study of the IL-15 superagonist complex ALT-803 to treat relapse after transplantation. Blood. 2018;131(23):2515-2527.
57. Webb GM, Molden J, Busman-Sahay K, et al. The human IL-15 superagonist N-803 promotes migration of virus-specific CD81 T and NK cells to B cell follicles but does not reverse latency in ART-suppressed, SHIV-infected macaques. PLoS Pathog. 2020;16(3):e1008339.
58. Jaiswal SR, Zaman S, Nedunchezhian M, et al. CD56-enriched donor cell infusion after post-transplantation cyclophosphamide for haploidentical transplantation of advanced myeloid malignancies is associated with prompt reconstitution of mature natural killer cells and regulatory T cells with reduced incidence of acute graft versus host disease: a pilot study. Cytotherapy. 2017;19(4):531-542.
59. Ciurea SO, Schafer JR, Bassett R, et al. Phase 1 clinical trial using mbIL21 ex vivo-expanded donor-derived NK cells after haploidentical transplantation [published correction appears in Blood. 2018;132(26):2782]. Blood. 2017;130(16):1857-1868.
60. Romee R, Schneider SE, Leong JW, et al. Cytokine activation induces human memory-like NK cells. Blood. 2012;120(24):4751-4760.
61. Romee R, Rosario M, Berrien-Elliott MM, et al. Cytokine-induced memory-like natural killer cells exhibit enhanced responses against myeloid leukemia. Sci Transl Med. 2016;8(357):357ra123.
62. Kanakry CG, Coffey DG, Towlerton AMH, et al. Origin and evolution of the T cell repertoire after posttransplantation cyclophosphamide. JCI Insight. 2016; 1(5):e86252.
63. Minculescu L, Fischer-Nielsen A, Haastrup E, et al. Improved relapse-free survival in patients with high natural killer cell doses in grafts and during early immune reconstitution after allogeneic stem cell transplantation. Front Immunol. 2020;11:1068.

Acknowledgments

The authors are grateful to all patients and HDs who kindly volunteered to participate in this study. The authors thank the Pasquarello Hematologic Malignancies Tissue Bank and Doreen Hearsey for prospective collection and processing of serial blood samples. The authors thank Susan Lazo for excellent assistance with flow cytometry analysis and Eric R. Haas for excellent technical support for mass cytometry analysis. This work was supported by the National Cancer Institute, National Institutes of Health (P01CA229092).

Authorship

Contribution: B.R. designed research studies, conducted experiments, acquired and analyzed data, and wrote the manuscript; H.T.K. analyzed data, performed statistical analysis, and wrote the manuscript; C.R., S.C.R., and Y.A. acquired and analyzed data; T.K. designed the mass cytometry panel; L.B. provided informatic sup- port; M.G., J.K., C.C., S.N., V.T.H., E.P.A., J.H.A., C.J.W., and R.J.S. analyzed data and edited the manuscript; and J.R. and R.R. designed research studies, analyzed data, and wrote the manuscript.

Conflict-of-interest disclosure: J.K. reports research support from Amgen, Equillium, BMS, Miltenyi Biotec, Regeneron, and Clinigen and consulting income from Amgen, Equillium, and Moderna Therapeutics, and is a scientific advisory board member for Cugene and Therakos. S.N. reports ad hoc advisory boards for Novartis, Kite/Gilead and Nkarta. C.J.W. is a founder of Neon Therapeutics and a member of its scientific advisory board and receives research funding from Pharmacyclics. R.J.S. serves on the board of directors for Kiadis and Be The Match/National Marrow Donor Program; provided consulting for Gilead, Rheos Therapeu- tics, Cugene, Jazz, Mana Therapeutics, VOR Biopharma, and Novartis; and is on the data safety monitoring board for Juno/Cel- gene. J.R. reports research funding from Amgen, Equillium, and Kite Pharma and consulting income from Avrobio, Falcon Therapeutics, Infinity Pharmaceuticals, LifeVault Bio, Rheos Medicines, Talaris Therapeutics, and TScan Therapeutics. The remaining authors declare no competing financial interests.

The current affiliation for T.K. is Department of Medical Oncology and Hematology, Sapporo Medical University School of Medicine, Sapporo, Japan.

The current affiliation for E.P.A. is Duke Cancer Institute, Department of Medicine, Duke University, Durham, NC.

ORCID profiles: C.C., 0000-0001-8728-4314; J.R., 0000- 0001-5526-4669.

Correspondence: Jerome Ritz, Department of Medical Oncology, Dana-Farber Cancer Institute and Harvard Medical School, 450 Brookline Ave, Boston, MA 02215; e-mail: jerome_ritz@ dfci.harvard.edu; and Rizwan Romee, Department of Medical Oncology, Dana-Farber Cancer Institute and Harvard Medical School, 450 Brookline Ave, Boston, MA 02215; e-mail: rizwan_romee@ dfci.harvard.edu.

Supplemental Materials

Patients, Transplantation Procedures and sample collection

This study included 95 patients who underwent allogeneic HCT at the Dana-Farber Cancer Institute and Brigham and Woman's Hospital (Boston, MA) between November 2011 and November 2018. Of these, 60 patients received a haploidentical T cell replete haplo-HCT with PTCy (haplo-HCT group) and 35 underwent a matched (8/8) related (11/35) or unrelated (24/35) donor transplant (MD-HCT group). Both cohorts received reduced intensity conditioning (RIC): cyclophosphamide (29 mg/kg) and fludarabine (120 mg/m2) and low dose of total body irradiation (TBI, 200 cGy) for haplo-HCT group and intravenous low dose busulfan (260 mg/m2 or 3.2 mg/Kg) and fludarabine (120 mg/m2) for MD-HCT group. GVHD prophylaxis for haplo-HCT patients consisted of PTCy (50 mg/kg on days +3 and +4) and tacrolimus (TAC) and mycophenolate mofetil (MMF) starting from day +5. MMF was discontinued at day +28. No systemic corticosteroids were allowed until 24 hours after completion of day +4 cyclophosphamide. GVHD prophylaxis for MD-HCT patients consisted of methotrexate (MTX, 5 mg/m2) on days +1, +3, +6, +11 and TAC beginning from day –3. Patients received G-CSF (Tbo-Filgrastim) starting from day +5 in the haplo-HCT group and after the last dose of MTX in the MD-HCT group, until ANC was >500 for 2 consecutive days. Patients in both cohorts received acyclovir for viral prophylaxis, with the exception of seven patients in the haplo-HCT group that also received letermovir per institutional policy, after it was approved for cytomegalovirus (CMV) prophylaxis. Any CMV DNA

detectable by PCR above the sensitivity threshold after transplant was considered as viral reactivation. Flow cytometry staining for immune reconstitution analysis was performed on fresh whole blood samples. For analysis, both percentages and absolute numbers of the parental cells were considered. Absolute numbers were calculated from the complete blood cell count (CBC) performed on the same day as flow cytometry analysis. For mass cytometry by time of flight (CyTOF) and NK functional assays, PBMC were isolated from freshly drawn blood samples by density gradient centrifugation (Ficoll-Paque PLUS; GE Healthcare) and cryopreserved in RPMI 10% DMSO before being utilized.

Analysis of single cell mass cytometry data for NK cell characterization

NK cells were identified by 2-dimensional gating for the expression of CD45+CD3-CD19-CD14-CD56+ markers (supplemental Figure 3). Dimensionality reduction was performed on a concatenated dataset after downsampling NK cells to 5000 events from each sample (approx. 60000 total events for analysis performed at 1 month and 100000 events at 3 months). To interpret high dimensional single-cell data that were produced by mass cytometry, we used a tool based on the viSNE algorithm,1 which allows visualization of high-dimensional cytometry data on a 2-dimensional map at single-cell resolution and preserve the nonlinearity.2 In the viSNE map, cell position reflects their proximity in high dimensional space based on the similarity of marker expression. A FlowSOM analysis3 was then run to identify distinct NK cell meta-clusters. A self-organized map (SOM) is an unsupervised technique for

clustering and dimensionality reduction, in which a discretized representation of the input space is trained.4

Flow cytometry-based NK functional assay

NK activation after co-culture with target cells was evaluated by measuring the expression of CD107a as a marker of degranulation and by cytokine (IFNγ and TNFα) release. PBMC from patients and HD were thawed using CTL Anti-Aggregate (CTL-AA-001, Cellular Technology Limited) solution (1:20 dilution with RPMI) and then resuspended in RPMI medium with 10% FBS. After thawing, PBMC were left at 37°C overnight in the presence or absence of IL-15 (5 ng/ml) (Miltenyi Biotec) for NK priming. PBMC were then washed 2 times and cultured for 6 hours at 37 with K562 cells (effector:target ratio 5:1) previously stained with Cell Trace Violet (CTV, Invitrogen C34557) according to the manufacturer's recommended protocol. To detect cytokine release, Golgi Stop (Protein transport inhibitor Monensin BD 554724) and Golgi Plug (Protein transport inhibitor Brefeldin A BD 51-2301KZ) were added after 1 h of co-culture. After co-culture, cells were collected and stained using a panel of surface and intracellular mAbs shown in supplemental Table 4. Zombie Red staining (Biolegend 423109) was used to distinguish live and dead cells. Samples were then resuspended in PBS 2% FBS and acquired on Fortessa LSR flow cytometer (BD). FCS files were analyzed using FlowJo Version 10 software. An example of the gating strategy is shown in supplemental Figure 4.

Statistical analysis

Patient baseline characteristics and immunophenotype data were analyzed primarily descriptively. Overall survival (OS) was defined as the time from stem cell transplant to death from any cause. Progression-free survival (PFS) was defined as the time from stem cell infusion to disease relapse, progression or death from any cause, whichever occurred first. Patients who were alive without disease relapse or progression were censored at the time of the last visit. The Kaplan-Meier method was used to estimate PFS and OS whereas cumulative incidence of non-relapse mortality (NRM), relapse, and GVHD was estimated in the context of a competing risks framework considering relapse for NRM, NRM for relapse, and death or relapse without developing GVHD for GVHD as a competing event. The log-rank and Gray tests5 were used for comparing estimates of PFS and OS and estimates of cumulative incidence of NRM and relapse, respectively. Immunophenotype data, CyTOF data and NK functional data were compared using the Wilcoxon rank-sum test for unpaired group comparison and the Wilcoxon signed-rank test for paired comparison. All tests were 2-sided at the significance level of 0.05 and multiple comparisons were not considered. Statistical analyses for immune reconstitution analysis were performed using SAS version 9.2 (SAS Institute, Inc., Cary, NC) and R version 3.3.2 (the CRAN project), while functional and CyTOF data were analyze using Prism software (GraphPad). All graphs were made using Prism software (GraphPad). Heatmaps were generated using GENE-E (http://www.broadinstitute.org/ cancer/software/GENE-E).

Supplemental References

1. van der Maaten L, Hinton G. Visualizing Data using t-SNE. J. Mach. Learn. Res. 2008;9:2579–2605.

2. Amir ED, Davis KL, Tadmor MD, et al. viSNE enables visualization of high dimensional single-cell data and reveals phenotypic heterogeneity of leukemia. Nat. Biotechnol. 2013;31(6):545–552.

3. Van Gassen S, Callebaut B, Van Helden MJ, et al. FlowSOM: Using self-organizing maps for visualization and interpretation of cytometry data. Cytom. Part A. 2015;87(7):636–645.

4. Kohonen T. Improved versions of learning vector quantization. 1990 IJCNN Int. Jt. Conf. Neural Networks. 1990;545–550 vol.1.

5. Gray RJ. A Class of K-Sample Tests for Comparing the Cumulative Incidence of a Competing Risk. Ann. Stat. 1988;16(3):1141–1154.

6. Chen Y-B, McDonough S, Hasserjian R, et al. Expression of CD30 in patients with acute graft-versus-host disease. Blood. 2012;120(3):691–696.

7. Tinago W, Coghlan E, Macken A, et al. Clinical, Immunological and Treatment-Related Factors Associated with Normalised $CD4^+/CD8^+$ T-Cell Ratio: Effect of Naïve and Memory T-Cell Subsets. PLoS One. 2014;9(5):e97011.

Supplemental Tables

Months after HCT	***1***	***2***	***3***	***6***	***9***	***12***	***18***	***24***
Haplo-HCT, n	37	51	46	36	24	25	18	17
MD-HCT, n	21	26	20	14	14	12	10	7

Table S1. Number of samples tested by flow cytometry at each time point after transplant were used for graphs displayed in Figures 1, 2, 3 and 6. Missing data 1 month after HCT was due to technical difficulties drawing samples on inpatient hospital units. This trend was proportionally similar between the two cohorts: 37/60 (62%) and 51/60 (85%) haplo-HCT display a

1 and 2 months sample respectively, versus 21/35 (60%) and 26/35 (74%) for MD-HCT.

TUBE	TARGET	FLUOROCHROME	CLONE	COMPANY	PRODUCT
T cells	CD45RO	FITC	UCHL1	BD	555492
	CD279 PD-1	PE	eBioJ105	eBio	12-2799-42
	CD127	PE-Cy5	eBioRDR5	eBio	15-1278-42
	CD25	PE-Cy7	M-A251	BD	557741
	CD62L	APC	DREG-56	BD	559772
	CD4	APC-H7	RPA-T4	BD	560158
	CD3	Pac Blue (V450)	UCHT1	BD	560365
	CD8	BV510	RPA-T8	BioLegend	301047
B cells	BAFF-R	FITC	8A7	eBio	11-9117-42
	IgD	PE	IA6-2	BD	555779
	CD27	PE-Cy5	O323	eBio	15-0279-42
	CD38	PE-Cy7	HIT2	BD	560677
	CD19	APC	HIB19	BD	555415
	CD20	APC-H7	2H7	BD	560734
	CD5	Pac Blue (V450)	UCHT2	BD	561154
	CD45	BV510	HI30	BD	563204
NK cells	CD16	FITC	3G8	BD	555406
	CD56	PE	B159	BD	555516
	CD8	PE-Cy7	RPA-T8	BD	557746
	NKG2D	APC	1D11	BD	558071
	CD45	APC-H7	2D1	BD	560178
	CD3	Pac Blue (V450)	UCHT1	BD	560365
	CD4	BV510	SK3	BD	562970

Table S2. Conjugated monoclonal antibodies in the flow cytometry immune monitoring panel.

	TARGET	SPECIES	CLONE	ISOTOPE	COMPANY
Surface					
1	CD45	Human	HI30	89Y	Fluidigm
2	HLA-DR	Cross	L243	141Pr	Biolegend
3	CD95	Human	DX2	164Dy	Fluidigm
4	CD3	Human	UCHT1	170Er	Fluidigm
5	CD4	Human	SK3	174Yb	Fluidigm
6	CD8	Human	SK1	168Er	Fluidigm
7	CD25	Human	2A3	149Sm	Fluidigm
8	CD14	Human	M5E2	160Gd	Fluidigm
9	CD19	Human	HIB19	142Nd	Fluidigm
10	CD56	Human	HCD56	145Nd	Biolegend
11	CD16	Human	3G8	209Bi	Fluidigm
12	CD57	Human	HCD57	165Ho	BioLegend
13	CCR7	Human	G043H7	148Nd	BioLegend
14	CD62L	Human	DREG-56	153Eu	Fluidigm
15	CD69	Human	FN50	163Dy	Biolegend
16	TIM-3	Human	F38-2E2	144Nd	BioLegend
17	ICOS(CD278)	Human	DX29	151Eu	Fluidigm
18	ILT1 (CD85h)	Human	24	115In	Biolegend
19	NKp30 (CD337)	Human	Z25	159Tb	Fluidigm
20	NKp44 (CD336)	Human	P44-8	147Sm	Biolegend
21	NKp46 (CD335)	Human	BAB281	162Dy	Fluidigm
22	NKG2D (CD314)	Human	1D11	161Dy	BD Bioscience
23	NKG2C(CD195c)	Human	134591	166Er	R&D
24	DNAM1(CD226)	Human	DX11	152Sm	BD Bioscience
25	NKG2A (CD94a)	Human	Z199	169Tm	Fluidigm
26	ILT2 (CD85j)	Human	GHI/75	156Gd	Fluidigm
27	KIR2DL1/DS1(CD158a,h)	Human	EB6B	158Gd	Milteni
28	KIR2DL2/2DS3(CD158b)	Human	CH-L	172Yb	BD Bioscience
29	KIR3DL1	Human	DX9	167Er	Fluidigm
30	TIGIT	Human	MBSA43	154Sm	Fluidigm
31	TRAIL	Human	RIK-2	150Sm	Biolegend
Intracellular					
32	Ki67	Cross	B56	176Yb	BD Bioscience
33	CTLA-4(CD152)	Human	14D3	146Nd	eBioscience
34	Perforin	Human	B-D48	175Lu	Fluidigm
35	GranzymeB	Human	GB11	173Tb	Fluidigm

Table S3. Antibody-metal conjugate panel used for mass cytometry.

TARGET	FLUOROCHROME	CLONE	COMPANY	PRODUCT
Extracellular				
CD3	AF 700	UCHT1	BD Pharmingen	557943
CD56	BV 510	HCD56 NCAM	Biolegend	318340
CD16	APC/Cy7	3G8	Biolegend	302018
CD107a LAMP-1	APC	H4A3	Biolegend	328620
Isotype mouse IgG1 k	APC	MOPC-21	Biolegend	400122
Intracellular				
IFNγ	PE-Cy7	B27	BD Pharmingen	557643
Isotype mouse IgG1 k	PE-Cy7	MOPC-21	BD Pharmingen	557872
TNFα	FITC	MAb11	BD Pharmingen	552889
Isotype mouse IgG1 k	FITC	MOPC-21	BD Pharmingen	555748

Table S4. Conjugated monoclonal antibodies used in the flow cytometry NK functional assay panel.

UPN	Disease	Sample 1 Mo	Sample 3 Mo	AGE at HCT	SEX	CMV	DAY from HCT to CMV	aGVHD	DAY from HCT to aGVHD	cGVHD	DAY from HCT to cGVHD	Relapse	DAY from HCT to relapse
Haplo_1	NHL	Yes	No	64	F	Yes	31	Yes	31	No		No	
Haplo_2	NHL	Yes	Yes	68	M	Yes	41	No		Yes	202	Yes	614
Haplo_3	MDS	Yes	Yes	68	M	No		Yes	68	Yes	817	No	
Haplo_4	MDS	Yes	Yes	75	M	Yes	35	Yes	163	No		No	
Haplo_5	NHL	Yes	No	49	F	No		No		No		Yes	63
Haplo_6	NHL	Yes	Yes	52	M	Yes	41	Yes	41	No		No	
Haplo_7	NHL	No	Yes	53	M	Yes	41	No		Yes	246	No	
Haplo_8	NHL	No	Yes	56	M	No		Yes	40	No		No	
Haplo_9	CML	No	Yes	20	M	No		No		No		No	
Haplo_10	MDS	No	Yes	73	M	Yes	49	Yes	114	No		No	
MDs_1	HD	Yes	Yes	24	M	No		No		No		Yes	111
MDs_2	ALL	Yes	No	68	F	No		No		Yes	223	Yes	130
MDs_3	HD	Yes	Yes	45	M	Yes	237	Yes	211	No		No	
MDs_4	NHL	Yes	Yes	64	M	No		Yes	27	Yes	197	No	
MD_1	MDS	No	Yes	68	M	No		Yes	55	Yes	302	No	
MD_2	AML	No	Yes	64	M	No		No		Yes	165	No	
MD_3	AML	No	Yes	73	M	No		Yes	42	Yes	488	No	
MD_4	MDS	No	Yes	68	F	No		No		Yes	264	No	
MD_5	HD	No	Yes	19	F	No		No		No		No	
MD_6	PMF	No	Yes	65	M	No		No		Yes	202	No	

Table S5. Clinical characteristics of patients tested in CyTOF assay at 1 and 3 months after HCT. Samples were selected based on the availability of an adequate number of frozen cells. Haploidentical cell transplantation (HAPLO), matched donor cell transplantation with sirolimus/TAC/MTX GVHD prophylaxis (MDs) and matched donor cell transplantation with TAC/MTX GVHD prophylaxis (MD).

UPN	Disease	Age	Sex	CMV	DAY from HCT to CMV	aGVHD	cGVHD	DAY from HCT to cGVHD	Relapse	DAY from HCT to relapse
Haplo_2	NHL	68	M	Yes	41	No	Yes	202	Yes	614
Haplo_5	NHL	49	F	No		No	No		Yes	63
Haplo_11	AML	63	F	No		No	No		Yes	132
Haplo_12	HD	38	F	No		No	No		No	
Haplo_13	ALL	55	F	Yes	26	No	No		Yes	72
Haplo_14	NHL	39	F	Yes	40	No	No		Yes	980
Haplo_15	NHL	69	M	No		No	No		No	
Haplo_16	MDS	73	M	No		No	No		No	
Haplo_17	MDS	47	M	No		No	Yes	145	No	
MD_2	AML	64	M	No		No	Yes	165	No	
MD_4	MDS	68	F	No		No	Yes	264	No	
MD_5	HD	19	F	No		No	No		No	
MD_7	MDS	70	F	No		No	No		No	
MD_8	ALL	74	M	Yes	176	No	Yes	225	No	
MD_9	CMML	67	M	No		No	No		Yes	61
MD_10	AML	62	M	No		No	No		Yes	91
MD_11	AML	66	M	No		No	Yes	120	No	
MD_12	AML	61	F	Yes	51	No	No		Yes	58

Table S6. Clinical characteristics of patients tested in NK functional assays 2 months after HCT. Samples were selected based on the availability of an adequate number of cryopreserved cells.

		MD-HCT				Haplo-HCT				
	Months	N	Med	Q1	Q3	N	Med	Q1	Q3	p-value
ALC	1	21	693	495.9	1084.6	37	210	120	514.08	**0.0002**
	2	26	814.59	700.05	1397	51	699.3	375	1216.8	0.10
	3	20	893.4	645	1378.2	46	658.3	384.2	882	0.07
	6	14	993.3	522.0	1114.1	36	1071.1	531.6	1511.7	0.66
	9	14	1240.7	1039.5	1472.2	24	1360.7	625.4	2368.2	0.80
	12	12	1228.7	840.5	2368.4	25	1026.8	750.0	2494.4	0.66

	18	10	1296.2	851.4	1793.0	18	1674.2	821.3	2723.2	0.28
	24	7	956.8	863.3	1828.3	17	1679.9	871.7	2651.0	0.31
$CD3^+$	1	21	337.5	263.6	458.6	37	65.4	25.4	147.1	**<.0001**
	2	26	420.5	255.8	695.7	51	305.0	113.4	616.9	0.11
	3	20	443.2	257.4	803.8	46	176.4	113.8	404.5	**0.013**
	6	14	526.2	374.3	746.2	36	426.2	184.1	891.9	0.87
	9	14	667.5	501.2	934.9	24	600.7	260.6	1514.5	0.92
	12	12	624.2	465.1	1289.7	25	481.4	318.3	1514.1	0.62
	18	10	829.7	272.6	1228.2	18	881.9	504.7	1607.6	0.40
	24	7	408.3	163.4	1170.1	17	851.7	329.2	1895.5	0.20
$CD19^+$	1	21	11.3	5.4	18.3	37	1.8	0.6	4.0	**<.0001**
	2	26	35.3	17.6	97.3	51	10.4	4.2	47.6	**0.0065**
	3	20	73.0	21.1	120.2	46	35.0	6.5	158.9	0.28
	6	14	49.4	5.7	135.3	36	76.4	21.3	206.4	0.44
	9	14	181.3	69.6	243.0	24	118.4	76.1	211.6	0.58
	12	12	105.7	26.0	160.8	25	114.8	74.3	270.8	0.51
	18	10	123.8	40.4	362.4	18	267.6	167.0	408.0	0.22
	24	7	70.3	54.4	144.6	17	280.0	183.3	323.2	**0.049**
$CD56^+3^-$	1	21	115.3	77.1	221.8	37	52.7	23.9	130.1	**0.03**
	2	26	163.2	95.2	271.9	51	153.1	103.4	272.8	0.70
	3	20	178.8	122.6	226.7	46	156.6	72.9	248.2	0.66
	6	13	109.0	76.6	136.5	36	184.8	102.7	264.4	0.10
	9	14	126.9	80.7	237.0	24	119.9	71.5	416.0	0.75
	12	12	164.6	72.7	205.3	25	113.1	87.8	198.6	0.99
	18	10	172.9	95.3	220.8	18	176.9	110.7	330.9	0.55
	24	7	192.5	65.8	268.3	17	182.8	93.0	238.2	0.95
$CD56^+3^+$	1	20	15.9	8.7	42.9	36	1.1	0.4	3.1	**<.0001**
	2	26	22.8	11.4	61.7	52	3.7	1.6	8	**<.0001**
	3	20	33.4	11.2	90	49	4.3	1.5	9.7	**<.0001**
	6	13	16.1	8.4	71.3	41	8.2	2.7	14.9	**0.04**
	9	14	33.6	6.7	87.4	28	10.4	3.1	24.2	**0.0217**
	12	11	48.5	4.9	77.6	26	10.8	3.3	23.6	**0.0249**
	18	10	45.2	13.3	65.4	20	14.9	6	26.8	**0.0408**
	24	7	53	18.2	86.7	20	16.2	7	27.3	0.0563

Table S7. The median absolute values (cells/μL) along with corresponding inter-quartile values and p-values referring to Figures 1A and 1C.

		MD-HCT			Haplo-HCT					
	Months	**N**	**Med**	**Q1**	**Q3**	**N**	**Med**	**Q1**	**Q3**	**p-value**
Treg ($CD4^+25^+127^-$)	1	21	11.6	4.9	14.8	37	2.6	1.2	7.7	**0.0002**
	2	26	12.3	6.9	18.3	51	7.7	4.0	15.4	0.09
	3	20	11.9	5.4	20.7	45	10.4	5.7	16.0	0.59
	6	14	13.5	5.6	30.6	36	14.1	8.1	19.1	0.91
	9	14	15.8	10.2	56.6	24	17.5	10.1	31.9	0.75
	12	12	17.9	10.3	39.9	25	15.8	8.6	23.5	0.47
	18	10	10.9	4.5	25.2	18	21.4	16.7	31.2	0.06
	24	7	8.8	3.5	27.6	17	21.1	16.1	36.5	0.31
Treg EM ($CD25^+127^-45RO^+62L^-$)	1	21	2.4	1.2	5.8	37	0.9	0.4	2.6	**0.01**
	2	26	3.2	2.3	4.8	51	3.2	1.5	7.6	0.68
	3	20	2.9	1.2	5.3	45	3.8	1.3	8.6	0.19
	6	14	3.7	0.5	9.2	36	6.3	3.1	9.7	0.16
	9	14	3.5	1.1	9.9	24	6.4	3.4	17.2	0.20
	12	12	4.6	2.1	9.0	25	4.2	1.4	9.7	0.64
	18	10	3.7	2.7	4.9	18	6.6	3.5	13.1	0.09
	24	7	2.5	1.5	7.1	17	8.6	6.1	10.8	0.09
Treg CM ($CD25^+127^-45RO^+62L^+$)	1	21	5.5	2.6	7.8	37	1.2	0.2	2.9	**0.0003**
	2	26	5.3	2.4	9.5	51	2.6	1.1	5.2	**0.023**
	3	20	8.1	1.5	10.9	45	4.0	1.6	7.3	0.19
	6	14	6.1	4.0	15.5	36	4.5	1.6	7.3	0.16
	9	14	7.5	2.6	22.1	24	6.2	2.8	8.7	0.30
	12	12	11.6	5.0	17.1	25	6.3	2.0	15.0	0.31
	18	10	4.7	1.6	13.3	18	7.6	3.9	16.0	0.46
	24	7	2.1	0.8	6.0	17	11.8	3.0	17.1	0.11
Treg TEMRA ($CD25^+127^-45RO^-62L^-$)	1	21	0.57	0.36	0.80	37	0.05	0.02	0.26	**<.0001**
	2	26	0.49	0.14	1.30	51	0.21	0.09	0.64	0.07
	3	20	0.37	0.06	0.94	45	0.31	0.12	0.72	0.94
	6	14	0.38	0.00	2.07	36	0.69	0.25	1.85	0.31
	9	14	1.77	0.38	3.09	24	0.82	0.22	2.55	0.47
	12	12	0.82	0.33	2.97	25	0.46	0.16	2.13	0.29
	18	10	0.87	0.14	2.59	18	1.55	0.30	3.06	0.72
	24	7	0.71	0.34	4.34	17	1.56	0.67	3.28	0.41
	1	21	0.74	0.28	1.39	37	0.03	0.00	0.22	**<.0001**

Treg naïve ($CD25^{+}127^{-}45RO^{-}62L^{+}$)	2	26	0.60	0.14	2.40	51	0.10	0.02	0.23	**0.0002**
	3	20	0.69	0.18	2.59	45	0.26	0.08	0.56	**0.03**
	6	14	0.48	0.22	3.32	36	0.30	0.08	0.69	0.06
	9	14	1.80	0.49	6.11	24	0.34	0.09	0.57	**0.0027**
	12	12	1.20	0.70	2.79	25	0.45	0.11	1.34	**0.05**
	18	10	0.56	0.21	3.53	18	0.47	0.13	0.92	0.61
	24	7	0.33	0.15	5.75	17	0.80	0.10	1.57	1.00
Tcon	1	21	193.5	119.5	248.7	37	18.7	6.8	35.7	**<.0001**
	2	26	219.0	124.4	298.3	51	102.3	39.7	192.0	**0.0041**
	3	20	220.2	110.6	408.6	45	90.1	51.7	136.6	**0.0038**
	6	14	225.7	141.3	404.5	36	153.0	108.3	226.2	0.11
	9	14	300.4	161.2	348.6	24	208.3	129.1	304.5	0.20
	12	12	293.6	213.9	351.7	25	206.0	119.0	396.8	0.36
	18	10	292.0	133.5	613.9	18	341.1	236.6	448.4	0.79
	24	7	238.5	66.6	432.3	17	298.5	188.4	458.3	0.48
Tcon EM (Tcon $45RO^{+}62L^{-}$)	1	21	51.0	37.0	82.3	37	8.7	2.7	18.5	**<.0001**
	2	26	64.0	25.3	103.9	51	60.8	25.7	123.4	0.80
	3	20	62.1	37.2	87.9	45	57.5	29.8	91.3	0.76
	6	14	52.0	39.3	129.9	36	99.3	58.4	158.4	0.16
	9	14	70.5	33.9	105.1	24	139.6	86.1	196.0	**0.019**
	12	12	76.8	57.4	101.5	25	126.7	53.2	181.6	0.57
	18	10	102.2	61.5	269.3	18	143.0	76.0	264.2	0.38
	24	7	87.1	24.4	218.1	17	134.5	100.3	274.3	0.20
Tcon CM (Tcon $45RO^{+}62L^{+}$)	1	21	60.6	28.4	82.9	37	7.1	0.9	15.6	**<.0001**
	2	26	44.7	9.9	125.9	51	9.6	4.4	33.8	**0.0032**
	3	20	62.7	15.8	115.9	45	14.9	7.9	35.8	0.01
	6	14	40.6	19.1	100.5	36	20.9	10.2	37.3	0.04
	9	14	49.9	15.7	80.9	24	25.9	12.3	46.2	0.30
	12	12	56.7	30.0	121.4	25	32.8	18.2	80.6	0.29
	18	10	38.8	4.7	162.7	18	59.6	18.6	122.8	0.58
	24	7	29.9	4.7	95.4	17	72.9	23.9	104.5	0.18
Tcon TEMRA (Tcon $45RO^{-}62L^{-}$)	1	21	20.5	8.2	39.0	37	0.3	0.1	1.3	**<.0001**
	2	26	17.4	7.6	57.7	51	3.1	1.2	9.1	**0.0001**
	3	20	22.9	7.0	38.7	45	5.3	2.6	9.3	**0.0033**

	6	14	42.0	1.9	97.4	36	14.4	6.7	27.5	0.54
	9	14	52.2	11.2	79.8	24	15.8	7.7	32.2	0.06
	12	12	60.8	20.0	73.9	25	22.1	5.2	44.1	**0.05**
	18	10	56.5	34.4	127.8	18	27.8	13.8	60.8	0.14
	24	7	50.2	18.2	87.3	17	49.4	16.1	80.0	0.90
Tcon naïve (Tcon 45RO$^-$ 62L$^+$)	1	21	31.8	16.0	63.4	37	0.3	0.1	0.8	**<.0001**
	2	26	26.0	3.0	54.6	51	0.9	0.3	2.7	**<.0001**
	3	20	38.0	6.1	90.0	45	2.3	0.7	6.3	**<.0001**
	6	14	31.8	8.5	84.9	36	4.2	1.3	8.3	**0.0008**
	9	14	34.3	17.4	170.8	24	4.2	1.3	9.3	**<.0001**
	12	12	62.7	15.0	106.3	25	11.1	1.5	18.4	**0.0099**
	18	10	41.6	5.1	83.1	18	8.1	2.8	31.4	0.35
	24	7	18.6	4.8	41.5	17	17.0	5.1	34.9	0.75
CD8$^+$	1	21	88.7	45.3	163.9	37	30.2	8.6	78.5	**0.0066**
	2	26	128.7	59.1	242.8	51	80.3	24.3	334.9	0.26
	3	20	147.8	80.9	289.4	46	64.9	16.2	198.6	0.03
	6	14	202.0	116.7	266.7	36	212.6	69.8	600.5	0.69
	9	14	255.0	141.7	435.0	24	295.0	113.8	1098.4	0.58
	12	12	261.1	156.0	558.4	25	238.3	94.0	1043.3	0.86
	18	10	187.0	108.0	747.7	18	316.0	173.9	982.1	0.30
	24	7	130.7	75.8	631.9	17	321.6	111.3	867.6	0.25
CD8 EM (CD8$^+$45RO$^+$ 62L$^-$)	1	21	23.1	9.7	39.4	37	11.0	4.0	43.3	0.32
	2	26	31.3	14.0	52.4	51	26.7	6.5	151.7	0.90
	3	20	32.3	16.6	72.9	46	14.8	4.7	96.1	0.17
	6	14	42.1	24.3	76.3	36	63.0	30.5	266.8	0.23
	9	14	45.7	12.2	102.8	24	97.2	40.3	427.2	**0.04**
	12	12	55.4	14.2	89.8	25	73.2	32.0	285.4	0.21
	18	10	37.3	25.4	213.9	18	117.5	31.5	467.5	0.13
	24	7	23.0	15.2	410.7	17	104.1	57.2	265.7	0.10
CD8 CM (CD8$^+$45RO$^+$ 62L$^+$)	1	21	5.4	3.6	8.3	37	3.7	0.9	9.3	0.15
	2	26	8.7	2.9	35.2	51	8.6	0.7	17.8	0.26
	3	20	8.9	4.9	24.5	46	3.7	0.7	9.0	**0.0089**
	6	14	8.6	4.0	24.0	36	11.0	3.4	31.3	0.84
	9	14	8.6	4.1	12.7	24	15.7	7.2	28.4	0.06
	12	12	7.3	4.9	11.7	25	18.2	6.9	49.4	**0.03**

	18	10	8.7	3.0	23.8	18	19.4	14.4	51.3	0.12
	24	7	3.0	0.6	14.7	17	20.3	9.7	62.2	**0.02**
CD8 TEMRA ($CD8^+45RO^-62L^-$)	1	21	39.2	17.4	68.0	37	4.6	1.2	17.0	**<.0001**
	2	26	55.1	24.7	81.1	51	28.3	7.7	95.2	0.06
	3	20	51.4	19.9	151.6	46	23.8	7.9	58.8	**0.05**
	6	14	117.2	21.6	156.0	36	72.8	25.7	282.2	0.80
	9	14	119.7	85.6	256.6	24	120.9	31.3	439.2	0.99
	12	12	136.2	69.0	295.5	25	100.2	31.5	566.3	0.78
	18	10	103.2	64.9	403.7	18	146.6	37.1	418.5	0.90
	24	7	79.7	53.7	258.2	17	193.9	58.2	495.4	0.45
CD8 naïve ($CD8^+45RO^-62L^+$)	1	21	18.2	6.3	26.8	37	1.2	0.3	2.9	**<.0001**
	2	26	21.2	5.8	39.3	51	6.9	0.8	15.5	**0.0017**
	3	20	22.2	6.1	62.2	46	6.8	0.8	15.2	**0.0033**
	6	14	27.6	9.4	59.6	36	12.6	3.1	32.4	0.09
	9	14	41.6	15.7	55.6	24	15.3	6.1	52.7	0.09
	12	12	25.3	8.4	97.9	25	18.6	9.1	40.7	0.53
	18	10	24.8	14.7	75.3	18	25.5	6.8	105.2	0.90
	24	7	10.7	2.8	19.7	17	26.2	8.4	71.1	0.16
Treg:Tcon ratio	1	21	0.064	0.043	0.088	37	0.179	0.089	0.342	**0.0001**
	2	26	0.059	0.043	0.087	51	0.099	0.056	0.155	**0.03**
	3	20	0.058	0.052	0.091	45	0.12	0.083	0.178	**0.0005**
	6	14	0.081	0.035	0.125	36	0.093	0.067	0.135	0.42
	9	14	0.078	0.038	0.134	24	0.092	0.062	0.14	0.52
	12	12	0.068	0.035	0.134	25	0.076	0.055	0.096	0.60
	18	10	0.052	0.031	0.076	18	0.082	0.056	0.105	0.12
	24	7	0.07	0.022	0.1	17	0.064	0.05	0.098	0.66
CD4:CD8 ratio	1	21	2.579	1.687	2.863	37	0.671	0.362	1.549	**<.0001**
	2	26	1.741	0.6	2.335	51	1.148	0.351	2.901	0.51
	3	20	1.532	0.893	1.988	46	1.148	0.644	2.984	0.99
	6	14	1.3	0.845	1.66	36	0.837	0.36	2.027	0.16
	9	14	1.191	0.634	2.391	24	0.792	0.334	1.823	0.17
	12	12	1.094	0.635	2.338	25	0.806	0.392	1.806	0.25
	18	10	0.941	0.465	1.331	18	1.127	0.506	1.444	0.90
	24	7	0.931	0.698	2.95	17	0.92	0.57	1.485	0.37

Table S8. The median absolute values along with the corresponding inter-quartile values and p-values referring to Figures 2A, 2B, 2C.

Supplemental Figures

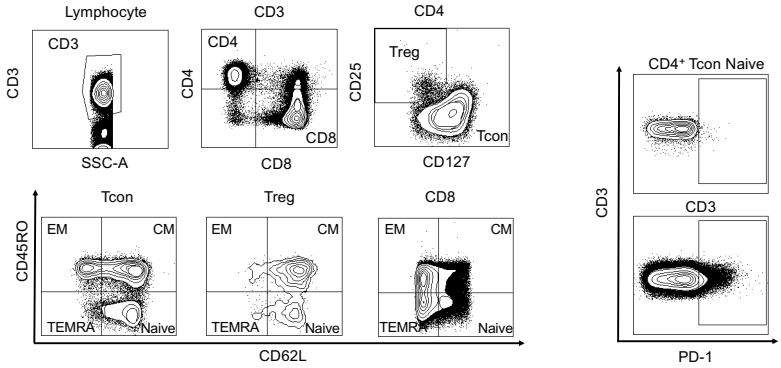

Figure S1. Gating strategy for T cell subset analysis. Three major T cell populations, CD4Treg, CD4Tcon, and CD8 T cells, were defined as $CD3^+CD4^+CD8^-CD25^+CD127^-$, $CD3^+CD4^+CD8^-$ non-Treg cells and $CD3^+CD4^-CD8^+$, respectively. Within each T cell population, subsets were defined as follows: naïve ($CD45RO^-CD62L^+$), central memory (CM, $CD45RO^+CD62L^+$), effector memory (EM, $CD45RO^+CD62L^-$), and terminally differentiated effector memory (TEMRA, $CD45RO^-CD62L^-$) T cells. PD-1 expression was monitored on each T cell subset (6,7).

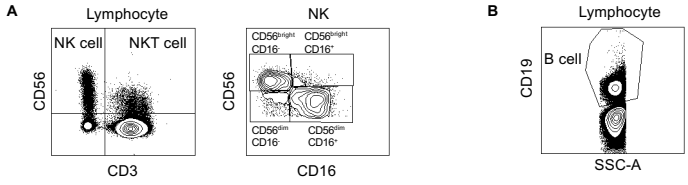

Figure S2. Gating strategy for analyzing NK and B cells. A) NK cells were defined as $CD45^+CD3^-CD56^+$ lymphocytes and divided in 4 subsets based on the expression of CD56 and CD16: $CD56^{bright}CD16^-$, $CD56^{dim}CD16^+$,

$CD56^{dim}CD16^{-}$ and $CD56^{bright}CD16^{+}$ NK cells. NKT cells were defined as $CD45^{+}CD3^{+}CD56^{+}$ lymphocytes. B) B cells were defined as $CD45^{+}CD19^{+}$ lymphocytes.

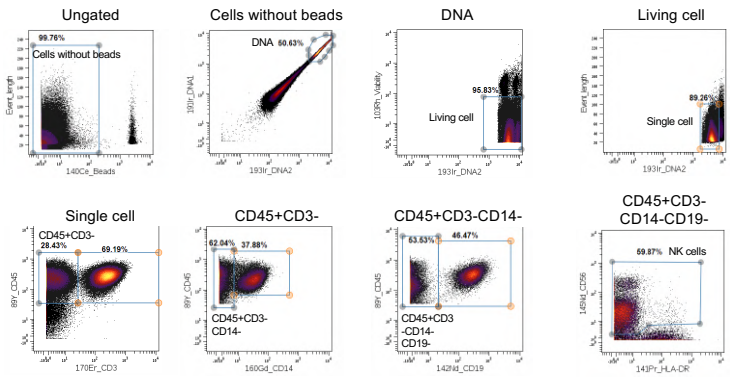

Figure S3. Mass cytometry NK cell gating strategy.

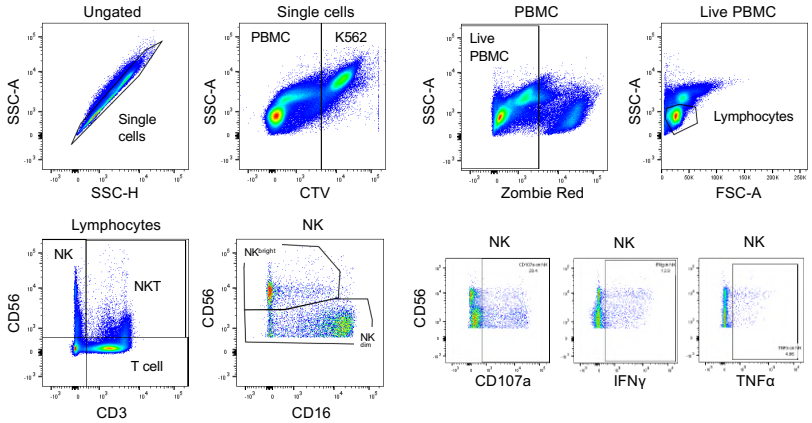

Figure S4. Flow cytometry NK cell gating strategy for functional assays.

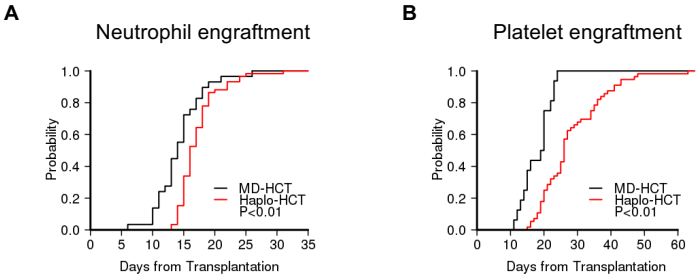

Figure S5. Engraftment after HCT. A) Probability of neutrophil engraftment. B) Probability platelet engraftment. Values are plotted for haploidentical cohort (haplo-HCT n=60, red line) and matched donor cohort (MD-HCT n=35, black line).

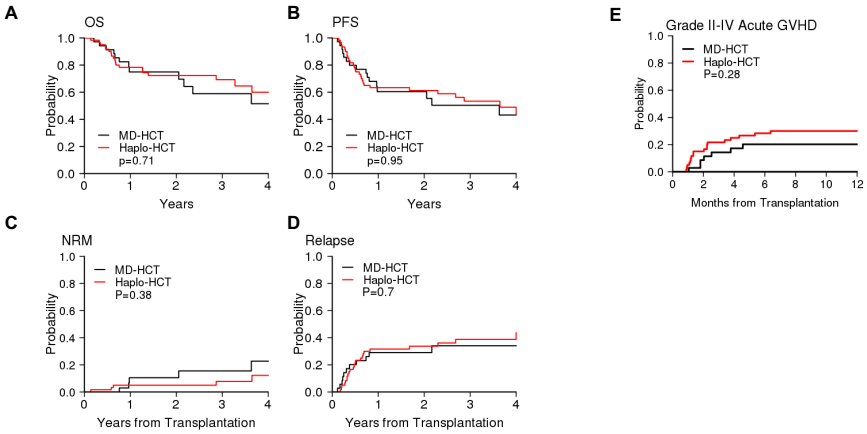

Figure S6. Clinical outcomes in haplo-HCT and MD-HCT cohorts. A) Probability of overall survival (OS). B) Probability of progression free survival (PFS). C) Probability of non-relapse mortality (NRM). D) Probability of relapse. E) Probability of acute graft versus host disease (aGVHD). Values are plotted for haploidentical cohort (haplo-HCT n=60, red line) and matched donor cohort (MD-HCT n=35, black line).

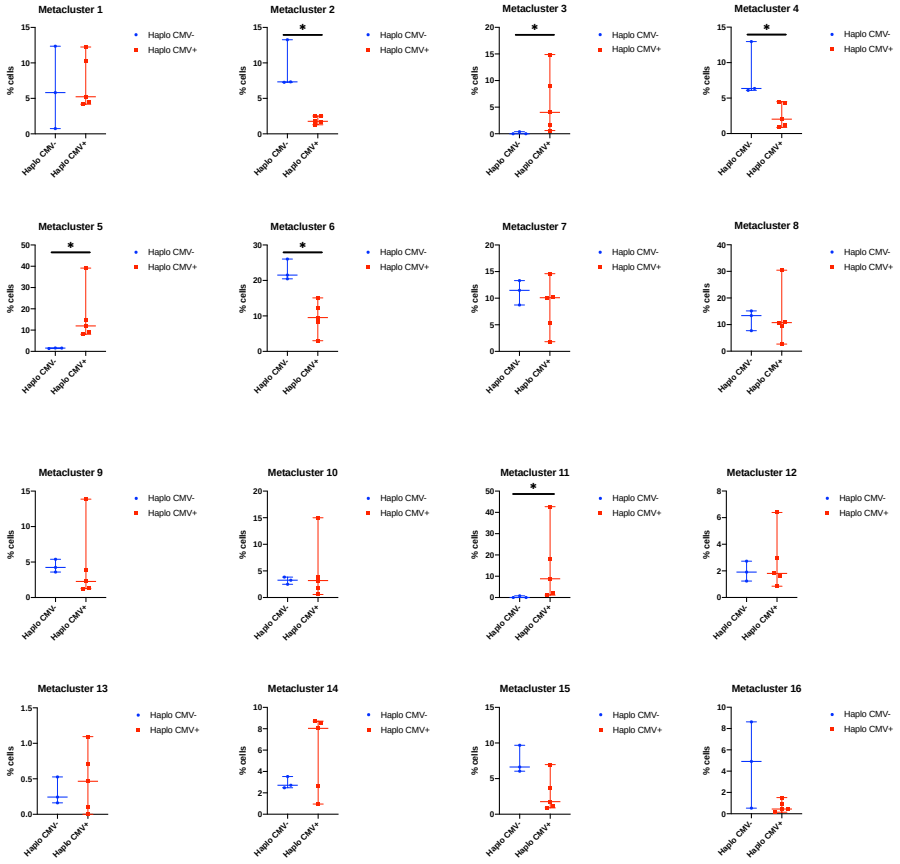

Figure S7. NK cell meta-cluster distribution 3 months after haplo-HCT in patients with and without CMV reactivation. A) Representation of FlowSOM meta-clusters in 8 haplo-HCT samples. B) viSNE density map of haplo-HCT patients with CMV reactivation (n=5) and without (n=3). C) Percentage distribution of FlowSOM NK cell meta-clusters in patients with CMV reactivation (n=5) compared to patients without (n=3). Data are expressed as median and range and compared using Wilcoxon signed-rank test for comparison, * P< 0.05.

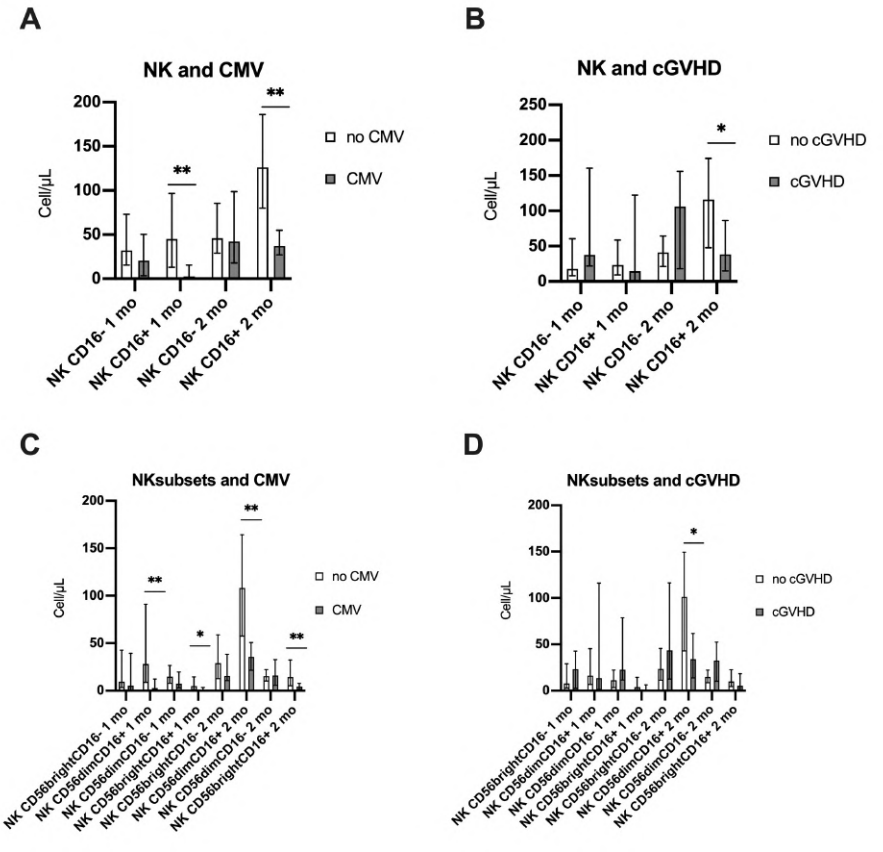

Figure S8. Absolute numbers of peripheral blood CD16+ and CD16- NK cells and NK cell subsets ($CD56^{bright}CD16^{-}$, $CD56^{dim}CD16^{+}$, $CD56^{bright}CD16^{+}$ and $CD56^{dim}CD16^{-}$) 1 and 2 months after haplo-HCT. A and C: Comparison of patients with and without CMV reactivation. B and D: Comparison of patients who later developed or did not develop cGVHD. Box and whisker plots show medians, along with minimum and maximum values. Groups were compared using Wilcoxon signed-rank test for paired comparison, * $P< 0.05$ and ** $P< 0.01$.

Chapter 4

Expansion, persistence, and efficacy of donor memory- like NK cells infused for posttransplant relapse

Roman M. Shapiro,[1] Grace C. Birch,[1] Guangan Hu,[2] Juliana Vergara Cadavid,[1] Sarah Nikiforow,[1] Joanna Baginska,[3] Alaa K. Ali,[1] Mubin Tarannum,[1] Michal Sheffer,[1] Yasmin Z. Abdulhamid,[1] **Benedetta Rambaldi,**[1,4] Yohei Arihara,[1] Carol Reynolds,[1] Max S. Halpern,[1] Scott J. Rodig,[5] Nicole Cullen,[5] Jacquelyn O. Wolff,[5] Kathleen L. Pfaff,[5] Andrew A. Lane,[6] R. Coleman Lindsley,[6] Corey S. Cutler,[1] Joseph H. Antin,[1] Vincent T. Ho,[1] John Koreth,[1] Mahasweta Gooptu,[1] Haesook T. Kim,[7] Karl-Johan Malmberg,[8,9,10] Catherine J. Wu,[1] Jianzhu Chen,[2] Robert J. Soiffer,[1] Jerome Ritz,[1] and Rizwan Romee[1]

[1]Division of Transplantation and Cellular Therapies, Dana-Farber Cancer Institute, Harvard Medical School, Boston, Massachusetts, USA. [2]Koch Institute for Integrative Cancer Research and Department of Biology, Massachusetts Institute of Technology, Cambridge, Massachusetts, USA. [3]Center for Immuno-oncology, Dana-Farber Cancer Institute, Harvard Medical School, Boston, Massachusetts, USA. [4]University of Milano-Bicocca, Monza, Italy. [5]Department of Pathology and [6]Department of Medical Oncology, Dana-Farber Cancer Institute, Harvard Medical School, Boston, Massachusetts, USA. [7]Department of Data Science, Dana-Farber Cancer Institute/Harvard T.H. Chan School of Public Health, Boston,

Massachusetts, USA. [8]Department of Cancer Immunology, Institute for Cancer Research, Oslo University Hospital, Oslo, Norway. [9]Institute for Clinical Medicine, The University of Oslo, Oslo, Norway. [10]Center for Infectious Medicine, Department of Medicine, Karolinska Institutet, Solna, Sweden.

Journal of Clinical Investigation. 2022 Jun 1;132(11):e154334. doi: 10.1172/JCI154334.

PMID: 35349491

Abstract

BACKGROUND. Responses to conventional donor lymphocyte infusion for postallogeneic hematopoietic cell transplantation (HCT) relapse are typically poor. Natural killer (NK) cell–based therapy is a promising modality to treat post-HCT relapse.

METHODS. We initiated this ongoing phase I trial of adoptively transferred cytokine-induced memory-like (CIML) NK cells in patients with myeloid malignancies who relapsed after haploidentical HCT. All patients received a donor-derived NK cell dose of 5 to 10 million cells/kg after lymphodepleting chemotherapy, followed by systemic IL-2 for 7 doses. High-resolution profiling with mass cytometry and single-cell RNA sequencing characterized the expanding and persistent NK cell subpopulations in a longitudinal manner after infusion.

RESULTS. In the first 6 enrolled patients on the trial, infusion of CIML NK cells led to a rapid 10- to 50-fold *in vivo* expansion that was sustained over months. The infusion was well tolerated, with fever and pancytopenia as the most common adverse events. Expansion of NK cells was distinct from IL-2 effects on endogenous post-HCT NK cells, and not dependent on CMV viremia. Immunophenotypic and transcriptional profiling revealed a dynamic evolution of the activated CIML NK cell phenotype, superimposed on the natural variation in donor NK cell repertoires.

CONCLUSION. Given their rapid expansion and long-term persistence in an immune-compatible environment, CIML NK cells serve as a promising platform for the treatment of posttransplant relapse of myeloid disease. Further characterization of their unique *in vivo*

biology and interaction with both T cells and tumor targets will lead to improvements in cell-based immunotherapies.

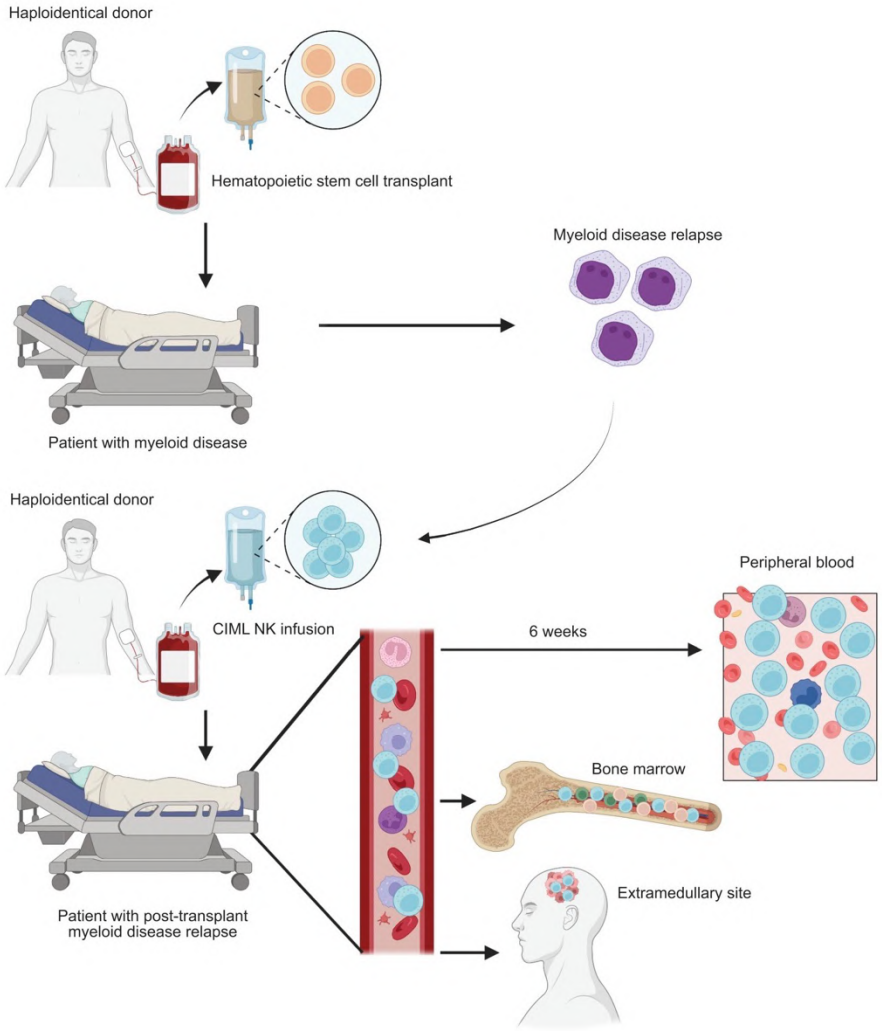

Introduction

Relapse of acute myeloid leukemia (AML) occurs in up to 50% of patients after allogeneic hematopoietic stem cell transplant (HCT) and

heralds an extremely poor prognosis (1). In several series of patients with AML who relapsed following HCT, the median overall survival was less than 6 months (2–3). Traditional approaches for the treatment of post-HCT relapse include the use of donor lymphocyte infusions (DLIs) or additional chemotherapy followed by a second HCT (1). While DLI is associated with remission rates of 10% to 25%, it is also associated with a high risk of moderate to severe graft-versus-host disease (GvHD), and long-term survival with this approach remains poor (4). With the recent increase in haploidentical HCT (haplo-HCT), whereby it is less clear whether the risk of GvHD due to DLI is outweighed by its efficacy (5–8), the treatment of posttransplant relapse must be improved.

The development of approaches for the management of post-HCT relapse of myeloid disease remains a high-priority area of research. Early post-HCT reconstitution of natural killer (NK) cells has been associated with a reduced risk of relapse in a number of retrospective studies, including in the T cell–depleted setting (9–11). NK cells are an attractive platform for the management of post-HCT relapse because they can mediate a graft-versus-leukemia effect without causing GvHD (11–15). The heterogeneity in clinical efficacy of predicted NK cell alloreactivity has been attributed in part to non-persistence of NK cells following infusion, inhibition from Treg or myeloid suppressor cells, and tumor-induced NK cell anergy (16, 17). Strategies to overcome these barriers have focused on generating sufficient NK cell numbers that persist *in vivo* and retain their efficacy against potential target cells (18–20).

The incubation of donor-derived NK cells with interleukin-12 (IL-12), IL-15, and IL-18 generates a phenotype known as cytokine-induced memory-like (CIML) NK cells, which are capable of enhanced survival, expansion, and avoidance of anergy *in vivo* (21, 22). In preclinical studies, CIML NK cells exhibited a lower threshold of activation in response to cytokine restimulation as well as enhanced cytotoxicity against target leukemia cells (22). In a phase I trial of adoptively transferred CIML NK cells from a haploidentical donor in patients whose AML was relapsed/refractory and who never received a stem cell transplant, complete remission or complete remission with insufficient hematological recovery (CR/CRi) was attained in greater than 50% of subjects (21, 23). While exhibiting enhanced cytotoxicity against leukemia, the CIML NK cells were only detectable for 2 to 4 weeks in these treated patients due to HLA incompatibility. In contrast, adoptive transfer of CIML NK cells in the context of a syngeneic mouse model (24) resulted in persistence of functional cells for several months, arguing that their transfer into an immune-compatible environment can prolong their survival (25).

The prolonged persistence of functional CIML NK cells in an immune-compatible syngeneic mouse model supports their use in the post-HCT setting, a setting in which immune compatibility results from a common donor for both stem cells and subsequent adoptive transfer of NK cells (24). We therefore initiated a phase I trial of CIML NK cells to treat patients with relapsed myeloid malignancies after haplo-HCT. Here we describe the detailed characterization of the CIML NK cells *in vivo* in the first 6 patients treated on this trial, including transcriptome and proteome analysis at single-cell resolution.

Methods

Study design.

Patients with relapsed myeloid disease, including AML, MDS, myeloproliferative neoplasm (MPN), or BPDCN following haplo-HCT were eligible to be treated in an ongoing single-center phase I dose de-escalation clinical trial of CIML NK cell therapy (NCT04024761). The primary endpoints are safety and identification of the maximum tolerated dose (MTD) of CIML NK cells administered following stem cell transplantation. The trial schema involves treatment of 5 patients at a starting dose of 5×10^6 to 10×10^6 cells/kg, a second dose level of 1×10^6 to 2×10^6 cells/kg in the event of at least 2 dose-limiting toxicities at the starting dose, and plan to treat 10 additional patients at the MTD in phase Ib. CIML NK cells were derived from the same donor who provided stem cells for the original transplant. Patients receiving therapy had relapsed disease that was confirmed by morphological evaluation, flow cytometry, next-generation sequencing, or PET-CT imaging, did not previously receive DLI, and had to have at least 20% donor T cell chimerism. NK cells were purified from nonmobilized apheresis products by a 2-step CD3 depletion followed by $CD56^+$ selection (CliniMACS device, Miltenyi Biotec), consistently achieving greater than 90% purity for $CD3^-CD56^+$ NK cells. The purified NK cells were subsequently activated overnight (12–16 hours) with IL-12 (10 ng/mL), IL-15 (50 ng/mL), and IL-18 (50 ng/mL) to generate the CIML NK cells under GMP conditions. The cells were washed and were subject to quality control assessment, including a requirement for a T cell dose of less than 3×10^5 cells/kg in the product. All patients

treated so far were infused as inpatients by their healthcare team at the starting NK cell dose of 5×10^6 to 10×10^6 cells/kg over at least 15–30 minutes after a course of lymphodepleting chemotherapy. Patients 1, 3, and 4 were treated with a combination of fludarabine (25 mg/m^2, days –6, –5, –4, –3, and –2), and cyclophosphamide (60 mg/kg, given on days –5 and –4). Patient 2 received a protocol deviation and was treated at a reduced dose of fludarabine (30 mg/m^2 i.v. over 1 hour on days –4, –3, and –2) and cyclophosphamide 60 mg/kg i.v. over 1 hour (on days –4 and –3) due to concern about tolerating potential chemotherapy-induced cytopenia. The lymphodepleting chemotherapy doses for patients 5 and 6 were adjusted to fludarabine (30 mg/m^2 i.v. over 1 hour on days –5, –4, and –3) and cyclophosphamide 500 mg/m^2 i.v. over 1 hour (on days –5 and –4) after a trial amendment. The first 5 patients were treated with a low dose of human recombinant IL-2 (1×10^6 IU/m^2) subcutaneously every other day for a total of 7 doses. Patient 6 received only 2 doses of IL-2 due to the development of transaminitis. Response evaluation included day +28 bone marrow biopsy and a PET-CT in patient with extramedullary disease (patient with BPDCN).

All patients were followed for up to 5 years or until disease relapse or mortality from the time of trial recruitment as per protocol.

Patient and healthy donor samples.

Patients with relapsed AML, MDS, MDS/MPN, or BPDCN provided written informed consent prior to participation under an IRB-approved protocol at the Dana-Farber Cancer Institute (DFCI) where all protocol

procedures were performed and data were collected. Correlative samples included peripheral blood collected at screening for the trial, on day –7 (before starting lymphodepletion), day 0, day +7, day +21–28, day +42, day +60, day +100, and relapse time points after infusion. Healthy donor PBMCs were isolated by Ficoll centrifugation, and NK cells were purified using RosetteSep (STEMCELL Technologies). All PBMCs were cryopreserved according to a standard internal laboratory protocol at the time of collection from patients.

Cryopreserved PBMC samples from 4 additional patients were retrieved and analyzed from a previously published clinical trial (30) involving subcutaneous administration of IL-2 (at the same dose as in the current CIML NK trial) in the post–stem cell transplant setting (NCT00529035). These samples included baseline (before IL-2), during (7 days after initiation of IL-2), and after (2–4 weeks after completion of IL-2). NK cells from these patients were analyzed using flow cytometry and mass cytometry and their phenotype compared to the NK cells from our CIML NK trial patients. These analyses were performed to potentially evaluate major phenotypic changes with the use of IL-2 on endogenous NK cells in the post-HCT setting versus CIML NK cells in the current study.

Flow cytometric analysis.

A custom NK and T cell panel of antibodies was used (**Supplemental Tables 7 and 8**). All cell staining for flow cytometry was performed as previously described (21), and data were acquired on a BD LSR Fortessa flow cytometer and analyzed using FlowJo (Tree Star) software. Gating strategies are described in **Supplemental Figure 3**.

The absolute lymphocyte count was measured using a clinical assay. For any lymphocyte population not measurable directly with the clinical assay, the absolute count of this population was determined by multiplying its percentage of total lymphocytes, as measured with flow cytometry, by the total lymphocyte count measured at the same time point using the clinical assay.

Mass cytometry (CYTOF).

Metal-tagged antibodies used for our mass cytometry panel are listed in **Supplemental Table 9**. In-house conjugations of antibodies were performed with a Maxpar labeling kit per the manufacturer's instructions (Fluidigm). All antibodies were used per the manufacturer's recommendation (Fluidigm).

Cryopreserved patient PBMC samples were thawed, counted using acridine orange and propidium iodide (AO/PI), and pelleted by centrifugation at 800*g* for 3 minutes. Cells were then incubated in 103Rh viability stain for 15 minutes, washed in CyFACS, and incubated with undiluted Human TruStain FcX for 10 minutes for Fc receptor blocking. Antibody master mix was applied to cell suspensions for 30 minutes, washed and fixed/permeabilized with FoxP3 Fixation/Permeabilization Concentrate and Diluent, prepared following the manufacturer's guidelines (eBioscience). A mix of intracellular antibodies prepared with 1× Perm Wash was added to each sample and incubated for 30 minutes. Next, cells were washed with 1× Perm Wash and incubated overnight at 4°C in FoxP3 Fixation/Permeabilization Concentrate and Diluent, containing 191/193Ir DNA intercalator (Fluidigm). Prior to acquisition, samples were transferred to 5 mL

round-bottom polystyrene tubes with cell strainer caps, washed and filtered with Cell Staining Buffer (CSB), Cell Acquisition Solution (CAS), and resuspended in CAS supplemented with EQ Four Element Calibration Beads (1:10) (Fluidigm). All mass cytometry data were collected on a Helios Mass Cytometer (Fluidigm). The instrument was tuned using CYTOF Tuning Solution according to the Helios User Guide (Fluidigm, pp. 60–68). A brief overview of tuning steps includes Pre-XY Optimization, Mass Calibration, XY Optimization, DV Calibration, Dual Calibration, Gases/Cur- rent Calibration, and QC report. EQ Four Element Calibration Beads (1:10 in CAS) were used according to the manufacturer protocol before and during acquisition. The data were normalized using the FCS Processing tab of Fluidigm CYTOF software v7.0.8493. Data analysis was manually performed using FlowJo 10.7.1. Initial data cleanup was based on a previously described gating strategy (40). Cell events were gated to remove dead cells and debris through biaxial plots of time versus event length, beads (for removal of the EQ Calibration Beads), and Gaussian-derived parameters (residual, width, offset). The viability stain 103Rh was used to gate out dead cells on PBMC populations. All viable cells were back-gated on both DNA parameters (191Ir and 193Ir) to ensure no doublets were included. Clustering of NK cell populations was performed both with R-Phenograph and FlowSOM methods in R (41–44).

Luminex cytokine assays.

Patient plasma samples were thawed and prepared for soluble analyte assay according to previously published methods (45, 46). Analytes were measured on a Luminex FLEX- MAP3D per the manufacturer's

protocol. Soluble eotaxin, GM-CSF, GROα, IFN-α, IFN-γ, IL-1β, IL-1α, IL-1RA, IL-2, IL-4, IL-5, IL-6, IL-7, IL-8, IL-9, IL-10, IL-12 p70, IL-13, IL-15, IL-17A, IL-18, IL-21, IL-22, IL-23, IL-27, IL-31, IP-10, MCP-1, MIP-1α, MIP-1β, RANTES, SDF1α, TNF-α, and TNF-β were tested. Of all soluble markers measured, 33 were within detectable range and could be quantified by extrapolation of mean fluorescence intensities to the respective standard curve between lower limit of quantitation and upper limit of quantitation. Analyte concentration for each patient was calculated using standard curves. Fold changes were calculated as a ratio relative to the patient's baseline (C0D1) (47–49).

Functional and flow-based cytotoxicity assays.

Frozen PBMCs were thawed and cultured overnight in RP-10 medium (RPMI 1640 supplemented with 10% FBS, 1× penicillin/streptomycin, 2 mM L-glutamine, and 7.5 mM HEPES) with 1 ng/mL IL-15. K562 cells (ATCC CCL-243) were cultured in RP-10 medium and labeled with 5 μM CellTrace Violet (Thermo Fisher Scientific) in PBS for 20 minutes at 37°C. PBMCs and K562 cells were washed twice with RP-10 and cocultured at the indicated effector/target (E:T) ratios. To measure NK cell cytotoxicity, PBMCs and K562 cells were cocultured for 4 hours, and then stained with PE–annexin V and 7-AAD (BD Biosciences) for 15 minutes at room temperature. To measure intracellular IFN-γ and degranulation, PBMCs and K562 cells were cocultured for 1 hour, followed by the addition of 0.2 μL GolgiPlug (BD Biosciences), 0.13 μL GolgiStop (BD Biosciences), and 1 μL of APC-CD107a (BioLegend). After an additional 5 hours of coculture, cells were stained for intracellular IFN-γ using Cytofix/Cytoperm (BD

Biosciences). Cells were acquired using BD LSR Fortessa and analyzed using FlowJo.

scRNA-seq and analysis.

Cryopreserved PBMC samples from patients were thawed and diluted with prewarmed complete RPMI 1640, and cells were centrifuged at 200*g* for 10 minutes to remove dead cells. Cell pellets were resuspended in 25% Percoll solution in PBS and centrifuged at 300*g* for 10 minutes to further remove dead cells. Live cells were resuspended in 2% FBS/PBS for single-cell isolation and cDNA library construction. The relapse samples were depleted of $CD34^+$ cells using a $CD34^+$ positive selection kit (STEMCELL Technolo- gies), with the $CD34^+$ cells resuspended as independent tumor samples. Single-cell libraries were prepared using the 10× Chromium Next GEM Single Cell 3′ Kit (10× Genomics), according to the manufacturer's instructions. The single-cell cDNA libraries were sequenced by NovaSeq S4 flowcell (Illumina), with data deposited in the NCBI Gene Expression Omnibus database (GEO GSE198141). Raw sequences were demultiplexed, aligned, and filtered. Barcode counting and unique molecular identifier (UMI) counting was done with Cell Ranger software v3.1 (10× Genomics) to digitalize the expression of each gene for each cell. Analysis was performed using the Seurat 3.0 package (50). Data from individual samples were analyzed separately prior to combining the data from multiple samples. The outlier cells with very low number of gene features (<500) or low total UMI (<1000), or high number of gene features (>5000) or high total UMI as doublets (>20,000) were removed. Cells with high mitochondrial ratio (>15%) from each data

set were also removed. Subsequently, samples were combined based on the identified anchors for the following integrated analysis. Principal component analysis (PCA) was performed and the first 15 principal components (PCs) were used to cluster cells using the Louvain algorithm in Seurat. These PCs were then used to run UMAP clustering. Well-defined marker genes for each cluster were used to identify potential cell populations, such as T cells (*CD3E*, *CD4*, *CD8A*), naive T cells (*IL7R*, *CCR7*), B cells (*CD19*, *CD20*, *SDC1*, *MS4A1*), $CD14^{+}$ monocytes (*CD14*, *LYZ*), NK cells (*NKG7*, *GNLY*), and platelets (*PPBP*). Differential gene expression analysis was performed in Seurat using the nonparametric Wilcoxon's rank-sum test [Find markers () function] and the MAST test. Volcano plots were used to visualize data and were generated in the ggplot2 package in R (https://cran.r-project.org/package=ggplot2). For gene sets representing specific cellular functions or pathways, we performed functional enrichment analysis with the online tool Reactome GSA (https://www.biorxiv.org/content/early/2020/04/18/2020.04.16.044958) (51).

Statistics.

All flow cytometry data were tested for normal distribution (Shapiro-Wilk test), and if the data were not normally distributed, the appropriate nonparametric tests were used (GraphPad Prism v5.0). *P* values corresponding to the differential expression using mass cytometry data were acquired using the diffcyt package in R (52). Differential expression of scRNA-seq data was performed using Wilcoxon's rank-sum test as part of the Seurat package (50). All statistical comparisons are indicated in the figure legends. All comparisons used a 2-sided α of

0.05 for significance testing, with adjustment for multiple comparisons where required.

Study approval.

This study was reviewed and approved by the institutional review board of the DFCI, Boston, Massachusetts, USA (ClinicalTrials.gov NCT04024761). The study was performed in compliance with the provisions of the Declaration of Helsinki and Good Clinical Practice guidelines. Written informed consent was obtained from participants before inclusion in the study.

Results

Adoptive transfer of donor-derived CIML NK cells is safe and associated with clinical responses.

Six patients whose myeloid disease relapsed after haplo-HCT were treated with a donor-derived CIML NK cell product as part of a phase I clinical trial (**Figure 1, A and B**). These included 3 with AML, 1 with myelodysplastic syndrome (MDS), 1 with blastic plasmacytoid dendritic cell neoplasm (BPDCN), and 1 with CML in blast crisis (patient characteristics are reported in **Supplemental Table 1**; supplemental material available online with this article; https://doi.org/10.1172/JCI154334DS1). As per trial inclusion criteria, none of the patients received any prior DLI, nor any other therapy concurrent with the CIML NK cell infusion. Patients tolerated the CIML NK cell infusion and expansion well, with fever as the most common side effect (temperature ranging from 38.1°C to 39.3°C)

during the 12 days of IL-2 administration. One patient developed grade 2 cytokine release syndrome (CRS) 7 days after CIML NK cell infusion and was treated with tocilizumab. Four of 6 patients developed pancytopenia after CIML NK infusion. In 2 cases the pancytopenia was prolonged, and these patients received $CD34^+$ cell–selected stem cell boosts from their original donors 5 and 6 weeks after CIML NK therapy, respectively. Both patients responded to the stem cell boosts, with neutrophil recovery evident within 9 to 14 days after boost (Supplemental Figure 1). No patient developed any evidence of acute or chronic GvHD. One patient (patient 6) experienced a transient increase in alanine aminotransferase and aspartate aminotransferase while on IL-2, resulting in premature discontinuation of IL-2 (the patient received a total of 2 doses).

All patients were evaluable at the day +28 response assessments following infusion of CIML NK cells, and 4 of 6 patients attained a response to therapy. Three of 6 patients met European Leukemia Net (ELN) 2017 criteria for CR in AML or International Working Group criteria for marrow CR in MDS (26, 27). These included patients 4 (BPDCN patient with entirely extramedullary disease relapse) who achieved a PET-negative CR (confirmed by tumor site biopsy) (**Figure 1C**), while patient 2 (with MDS and multiple pathogenic mutations) and patient 3 (with AML and pathogenic *TP53* mutation) had no detectable residual disease by next-generation sequencing after CIML NK cell therapy (**Figure 1D**). Patient 1, with FMS-like tyrosine kinase 3 internal tandem duplication–positive (*FLT3*-ITD^+) AML, attained a morphologic leukemia-free state with clearance of some of the pathogenic mutations present at the time of post–haplo-HCT relapse but

had a persistent *FLT3*-ITD mutation on day +28 bone marrow assessment. Patients 5 and 6 exhibited disease refractoriness on the day +28 response assessment.

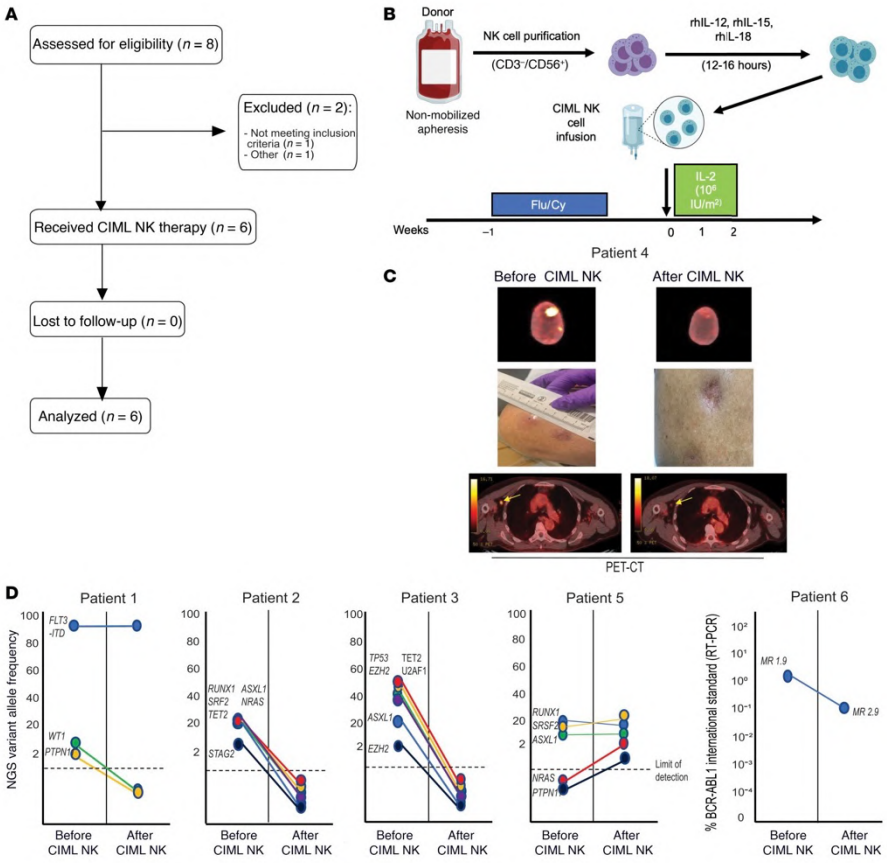

Figure 1. Phase I trial schema and clinical responses. (A) CONSORT flow diagram for the patients evaluated for the phase I trial. (B) Schema describing the generation of CIML NK infusion product and trial therapy. For each patient, the same donor who had previously given stem cells underwent nonmobilized apheresis of peripheral blood followed by CD3 depletion and CD56-positive selection. The resulting product was incubated with a cytokine cocktail for 12–16 hours, washed, and infused into the lymphodepleted patient. Following NK cell infusion, low-dose IL-2 was administered subcutaneously every other day for 7 doses. (C) Disease response of the BPDCN patient who had entirely extramedullary disease. Shown is the PET-

CT imaging of the 2 identified lesions in the scalp with the corresponding visual evaluation of these lesions, and the active axillary lymph node. (D) Next-generation sequencing (NGS) or RT-PCR was used to track individual mutations or transcripts before and after treatment with the CIML NK cells. Patients 2 and 3 exhibited marrow CR (for MDS) and CR without minimal residual disease (for AML) on the day +28 assessment, respectively, while patient 1 exhibited a morphologic leukemia-free state with persistently detectable FLT3-ITD. Patient 5 had progressive disease as per ELN 2017 criteria for AML. Patient 6 exhibited a reduction in BCR-ABL1 transcripts after CIML NK infusion as measured with quantitative RT-PCR, but had persistent disease suggesting refractoriness to therapy.

CIML NK cell infusion is associated with rapid and prolonged expansion in the peripheral blood NK cell compartment without changes in Treg numbers.

Following CIML NK cell infusion, NK cell numbers dramatically expanded to a median peak of 10-fold (range 10- to 50-fold; **Figure 2A**). NK cells constituted the dominant lymphocyte subset, with increased NK cell numbers persisting for up to several months beyond the last dose of IL-2 (day +12) in these patients (**Figure 2B**). T cells constituted a minority of peripheral blood mononuclear cells (PBMCs) in the peripheral blood compartment after NK cell expansion. There was no significant increase in the Treg numbers (**Figure 2B**); $CD8^+$ T cells were the major subset of T cells present in the first weeks after CIML NK infusion (**Supplemental Figure 2**). During their expansion, NK cells were predominantly $CD56^{dim}$ cells (**Supplemental Figure 3**) and displayed classical NK cell maturity markers, including KIR and CD57 (**Figure 2C and Supplemental Figure 3**). Expansion of the NK cell population on day +28 following infusion of CIML NK cells was associated with reduced expression of several markers, including CD2,

TIGIT, CD161, CD226, granzyme B, and perforin when compared with NK cells in the infusion product (Wilcoxon's rank-sum test $P < 0.05$; **Figure 2D**).

Functional evaluation of infused NK cells on day +28 and day +60 after infusion was performed by cytokine (IL-12 plus IL- 18) stimulation or coculture with K562 cells and comparing with NK cells from the screening time point before any therapy. On day +28 following infusion, IFN-γ expression was increased in response to cytokine stimulation (**Figure 2E**). CD107a expression was upregulated after coculture with K562 on day +28 compared with the time of screening in patients 1, 2, and 4, but not in other patients.

Evaluation of the expression of a panel of endogenous cytokines potentially associated with NK cell proliferation revealed the lack of increase in IL-15 or IL-21 at the time of exogenous IL-2 administration, although IL-15 appeared to increase in patient 4 after day +7 (**Figure 2F**). Patient 3, who developed CRS after NK cell infusion, had a corresponding increase in IL-6 and TNF-α, supporting the diagnosis (**Supplemental Figure 4**).

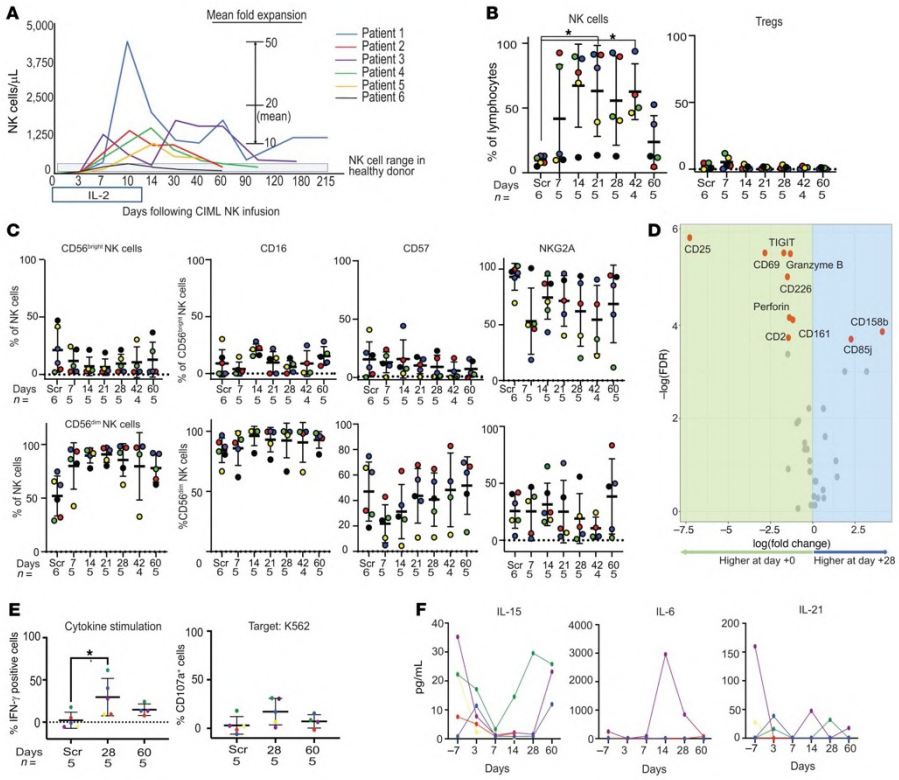

Figure 2. Rapid expansion of NK cells follows infusion of CIML NK product into the patients. (A) Mean NK cell counts/μL of peripheral blood deter- mined from the lymphocyte count. (B) Flow cytometry was used to evaluate NK cells in the peripheral blood as a proportion of total lymphocytes. Data presented are $CD56^{+}CD3^{-}$ cells as a percentage of total lymphocytes, mean ± SD. Right: Tregs ($CD3^{+}CD4^{+}CD25^{+}CD127^{-}$) cells as a percentage of total lymphocytes, mean ± SD. The value for each patient is shown with a colored dot, and the coloring scheme corresponds to that in panel A. *$P < 0.05$ by Mann-Whitney U test, with significance adjusted by Holm's method for multiple comparisons. (C) Flow cytometry–based evaluation of key markers distinguishing the $CD56^{dim}$ NK cell population from the $CD56^{bright}$ NK cell population. There was no significant difference in expression of markers between time points as determined by the Mann-Whitney U test. (D) Differential expression analysis of mass cytometry markers in the predominant $CD56^{dim}$ clusters between day 0 (infusion product) and day +28 after infusion. Markers labeled in red are differentially expressed (Wilcoxon's signed-rank test, $P < 0.05$). (E) Functional characterization of the expanded NK cell compartment using both cytokine stimulation and coculture with

K562 target cells at an E:T ratio of 5:1. The y axis shows percentage expression of the indicated marker relative to the corresponding unstimulated control, and the dashed line represents the same functional assays applied to healthy donor control PBMCs. In B, C, and E, the screening time point (Scr) refers to endogenous patient NK cells prior to infusion. *$P < 0.05$ by Mann-Whitney U test. (F) Measurement of plasma cytokines following CIML NK cell infusion. The x axis of each plot shows days relative to CIML NK cell infusion (day 0).

Longitudinal evaluation of the NK cell compartment after CIML NK cell infusion reveals expansion and persistence of both adaptive and nonadaptive NK cell subpopulations.

To be able to longitudinally evaluate the NK cell compartment in all 6 patients after CIML NK infusion, we defined the NK cell populations present in the infusion products using flow cytometry, a 39-marker mass cytometry panel, and single-cell RNA sequencing (scRNA-seq). All infusion products met product release criteria (≥70% $CD3^{-}CD56^{+}$ and $<3 \times 10^{5}$/kg $CD3^{+}$ cells) and had a high purity of NK cells. On mass cytometric analyses, the NK cell subpopulations that could be identified included adaptive $CD56^{dim}$ NK cells, those that expressed NKG2A, both $CD16^{+}$ and $CD16^{-}$ fractions, and those that expressed CD8 (**Supplemental Figure 5, A and B**). To deconvolute each patient's contribution to these clusters (patient 6 was excluded from this specific analysis as they received only 2 out of planned 7 IL-2 doses), we used the following set of markers: CD56, CD3, NKG2A, IL-7Ra, KIR2DL1, NKG2C, NKp46, NKp30, and Ki67. The resulting clusters delineated several identifiable NK cell populations in the infusion product, including adaptive NK cells ($NKG2C^{+}KIR^{+}$), $CD56^{bright}$ NK cells ($CD56^{hi}NKG2A^{hi}KIR2DL1^{-}$), and $CD56^{dim}NKG2A^{lo}$ NK

cells (**Supplemental Figure 5C**). The infusion products in patients 1 and 2 had a large subpopulation of adaptive NK cells expressing both NKG2C and KIR. Patients 3 and 4, on the other hand, had a subpopulation with a higher level of CD56 and NKG2A expression and a relatively low KIR and NKG2C expression, consistent with $CD56^{bright}$ NK cells that were largely absent in the other patients (**Supplemental Figure 5C**). Additional characterization of the CIML NK infusion products with scRNA-seq also identified several $CD56^{dim}$ and adaptive NK cell populations, as well as additional $CD56^{bright}$ NK cell subpopulations that were not detected by mass cytometry (**Supplemental Figure 6A**). The $CD56^{dim}$ subpopulations in the infusion product had a similar lev- el of expression of NK cell lineage markers, with the only noticeable differences being in the expression of *FCER1G* and *NCR3* genes (**Supplemental Figure 6B**).

To investigate the specific phenotypic imprint of the CIML NK cell preparation, we compared the CIML NK cell infusion product with the original resting donor-derived repertoire from screening samples using mass cytometry. The latter samples corresponded to the allogeneic donor-derived NK cell compartment within the recipient following HCT, but prior to receiving the infusion product. Compared with the resting donor NK cell repertoire, CIML NK cells exhibited a cytokine-stimulated signature, including a higher expression of CD25 and CD69, and a trend toward higher expression of CD161 that is thought to mark cytokine-responsive NK cells (Supplemental Figure 7 and ref. 28). Expression of NKG2D and TRAIL was lower on the infusion products from all patients compared with the screening time point. The immuno-

modulatory markers TIM3 and TIGIT were more highly expressed on the infusion product than at screening (**Supplemental Figure 7**).

Phenotypic evaluation over time of the NK cell subpopulations present in the infusion product showed their persistence on day +28 after CIML NK infusion (**Figure 3**). Patients 1, 3, and 4 exhibited the longest persistence of NK cell subpopulations phenotypically matching those that were infused (**Figure 3A**). We used scRNA-seq to compare major clusters present in the infusion product and at the day +28 time point. Distinct clusters of $CD56^{dim}$, adaptive $CD56^{dim}$, and $CD56^{bright}$ NK cells were identified, alongside several nonadaptive $CD56^{dim}$ NK cell clusters (**Figure 3B**). Characterization of the nonadaptive $CD56^{dim}$ clusters revealed distinct expression of the chemokine genes *CCL4* (Dim1) and *CCL3* (Dim2) in 2 of the clusters present on day +28. *IFNG* was shown to be more highly expressed in Dim2 and Dim4, while the cells in Dim3 expressed a higher level of *LAG3* (**Figure 3C**).

We then compared the gene expression in $CD56^{dim}$ clusters at infusion with those present on day +28 after CIML NK cell infusion. These genes included *KLRC2*, *CD52*, and *IFNG*, the expression of which is typically associated with adaptive NK cells (**Figure 3D**). Expression of the *IFNG* gene was increased in all NK cell subpopulations on day +28 when compared with the infusion time point (Figure 3E). Additional genes associated with NK cell activation, including *JUN*, *FOSB*, and *DUSP1*, as well as the chemokine *CCL3* had increased expression in each of the major NK cell subpopulations (**Figure 3E**). The top 50 differentially expressed genes in the $CD56^{dim}$ and $CD56^{bright}$ NK clusters at infusion compared with day +28 are summarized in **Supplemental Tables 2 and 3**.

We then longitudinally evaluated the transcriptionally defined NK cell populations using mass cytometry in all the trial patients on days +7, +28, and +60 (**Figure 3F**). The persistence of NK cell clusters identified in the infusion product was most notable in patients 1, 2, and 5. Patients 3 and 4 both exhibited a dominance of NK clusters on day +28 and day +60 that constituted a minor portion of the infusion product. Patient 6 had a poor expansion of infused CIML NK cells. The majority of $CD25^{+}$ NK cell subsets were absent after day +7 in all patients. Furthermore, the majority of infused CIML NK cells that expanded by day +28 and persisted to day +60 were $Ki67^{-}$.

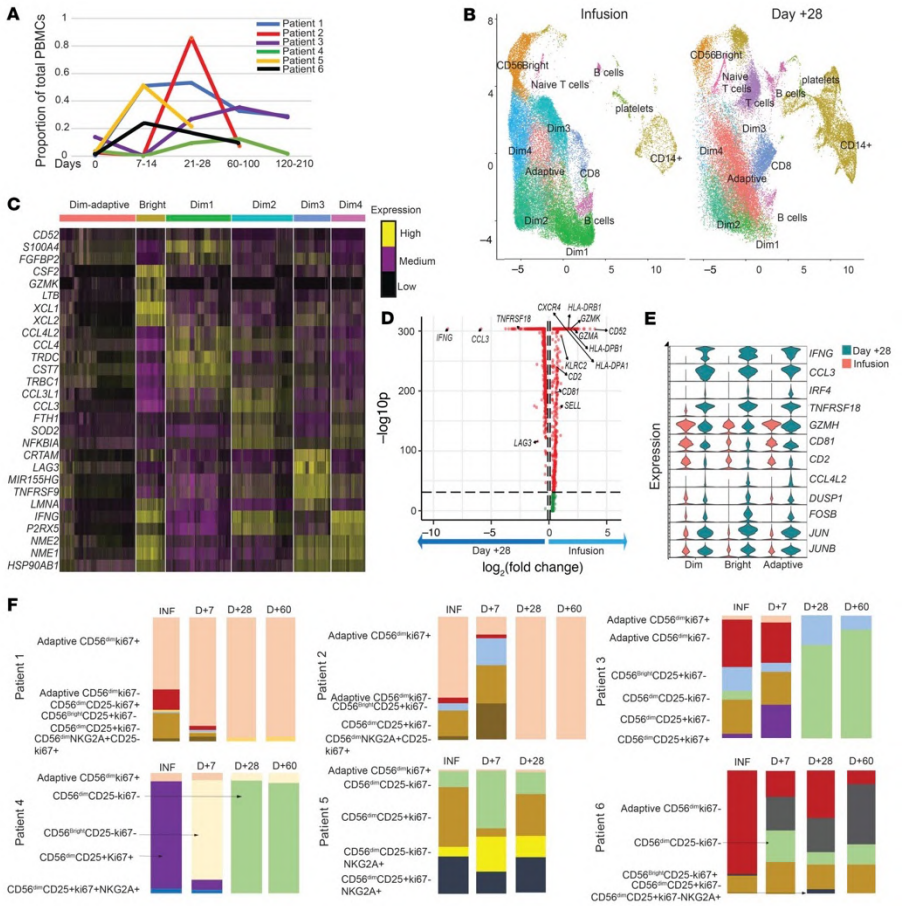

Figure 3. Evaluation of subpopulations of NK cells present in the infusion product over time. (A) Median proportion of total PBMCs that were $CD56^{+}CD3^{-}$ at the indicated time points. Days after infusion of the CIML NK product are indicated above the time point labels. (B) UMAP of NK cell clusters defined with single-cell RNA sequencing at day +28 compared to the infusion product for all patients whose CIML NK cells expanded. The $CD56^{dim}$ NK cell subpopulations that persist include Dim1, Dim2, $CD56^{bright}$, and adaptive NK cells. (C) Identification of defined NK cell subpopulations based on transcriptional profiling reveals the expansion of several CD56dim subpopulations and adaptive $CD56^{dim}$ NK cell populations. The heatmap shows the top 5 differentially expressed genes in each NK cell cluster when compared with other clusters using Wilcoxon's rank-sum test (log[fold change] threshold = 0.25). (D) Volcano plot showing the top differentially expressed genes in all $CD56^{dim}$ clusters between infusion and day +28; fold change cutoff = 0.5, P-value cutoff = 10 × 10–32. Differential gene expression

was determined using the nonparametric Wilcoxon's rank-sum test. (E) Violin plot to show the expression of select genes within the $CD56^{dim}$, $CD56^{bright}$, and adaptive $CD56^{dim}$ NK populations at infusion (red) and day +28 (green) time points. Shown are the most differentially expressed markers as well as genes associated with NK cell activation. (F) Evaluation of NK cell subpopulations over time as a proportion of total NK cells in each of the clinical trial patients treated with CIML NK cell therapy. Key subpopulations include adaptive NK cells ($CD56^{+}CD3^{-}CD57^{+}KIR^{+}NKG2C^{+}Fc\varepsilon RI^{-}$), $CD56^{bright}$ NK cells ($CD56^{hi}CD3^{-}NKG2A^{+}IL\text{-}7R^{+}$), $CD56^{dim}NKG2A^{+}$ NK cells, and $CD56^{dim}Ki67^{+}$ NK cells, among others. The sample time points for each patient are labeled. INF, at time of infusion.

CMV reactivation drives the expansion of adaptive NK cells, but not other NK cell subsets.

Three of the patients had a low-titer CMV viremia during this trial, although none of these patients developed CMV disease and/or needed treatment. To address the potential impact of CMV reactivation on the expanding NK cell compartment, we correlated absolute NK cell numbers with CMV reactivation (**Supplemental Figure 8, A and B**) and compared the expansion of NK cells between patients 1, 2, and 3 who had CMV reactivation (CMV+ group), and patients 4 and 5 who had no CMV reactivation (CMV– group). Patient 6 was excluded from this analysis because the patient was positive for CMV serology but did not reactivate CMV. By day +7 after CIML NK infusion, the CMV+ group had an identifiable adaptive NK cell population (although nonadaptive NK cells still constituted the major subset), which was largely absent in the CMV– group (**Figure 4A**). Both the adaptive and nonadaptive NK cell clusters persisted to day +28 after CIML NK cell infusion, but nonadaptive NK cells remained the dominant subset in both the patient groups (**Figure 4B**). There were minimal differences

in the expression of measured markers within the nonadaptive CD56^{dim} NK cell population when com- paring CMV+ and CMV– patients on day +28 after CIML NK cell infusion (**Figure 4C**). Comparison of the CMV+ and CMV– groups with scRNA-seq also showed adaptive NK cell clusters in the infusion product (**Supplemental Figure 8, C and E**) that expanded on day +28 in the CMV+ patients (**Figure 4D and Supplemental Table 4**) and persisted to day +60 (**Supplemental Figure 8, D and F**). Among the CMV+ patients, the adaptive NK cell clusters on day +28 expressed more genes associated with mitochondrial ATP synthase when compared with the CMV– group (**Figure 4E**). Distinct clusters of nonadaptive CD56^{bright} and CD56^{dim} NK cells were also present in both the CMV+ and CMV– groups (**Figure 4, D and F**). The expression of genes used to characterize functionally mature CD56^{dim} NK cells such as *GZMB*, *PRF1*, and *ZEB2* (29) did not differ between the CMV+ and CMV– groups (**Figure 4F and Supplemental Figure 8, E and F**). Therefore, mature CD56^{dim} NK adaptive and nonadaptive NK cells expanded in both CMV+ and CMV– patients.

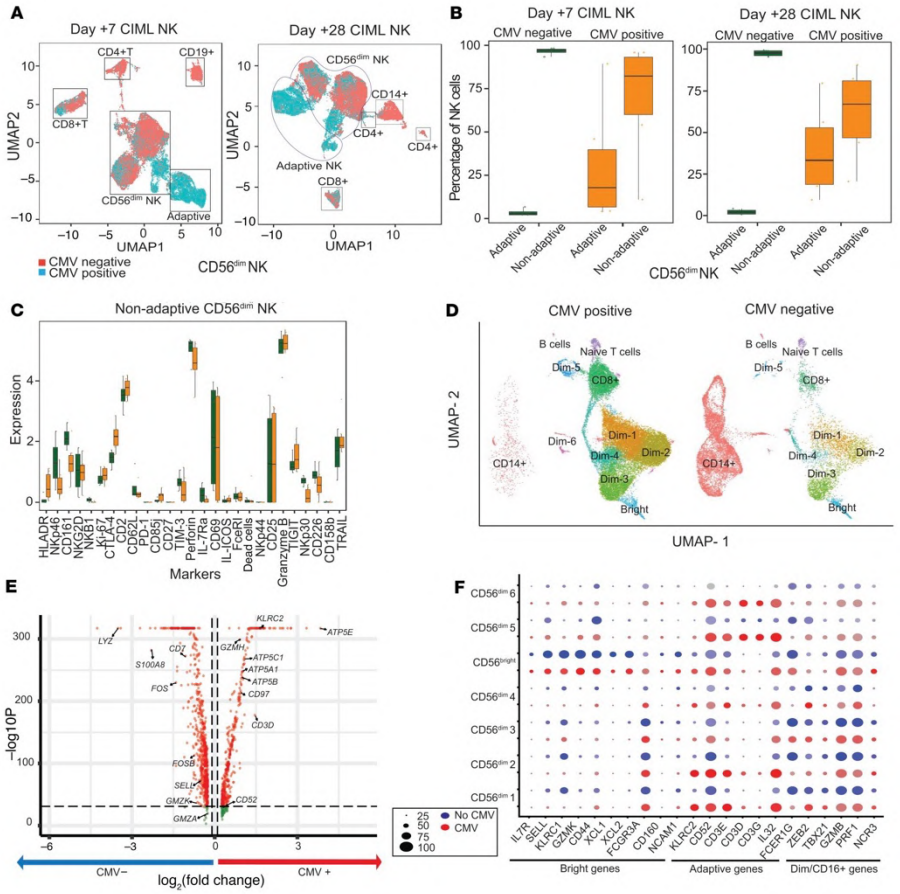

Figure 4. Distribution of adaptive and nonadaptive CD56dim NK cell populations and markers in the CMV+ (n = 3) and CMV– (n = 2) groups. (A) UMAP of PBMC subpopulations identified by mass cytometric analysis showing both CMV+ (light green) and CMV– (red) cells on both day +7 and day +28. (B) Distribution of adaptive and nonadaptive CD56^{dim} NK cells in the CMV– (green) and CMV+ group (orange) on day +7 and day +28 after CIML NK cell infusion. (C) Differential expression of markers on the nonadaptive CD56^{dim} NK cell subpopulations on day +28 after CIML NK cell infusion shows no differ- ences in this subpopulation between CMV+ and CMV– groups. *P < 0.05 by Wilcoxon's rank-sum test, with significance adjusted for multiple comparisons (43). (D) UMAP of PBMC subpopulations in CMV+ and CMV– patients evaluated with scRNA-seq on day +28 after CIML NK cell infusion. The adaptive Dim1, Dim2, Dim5, and Dim6 subpopulations are expanded predominantly in the CMV+ group, while the Dim3 and Dim4 subpopulations are comparable between groups. (E) Volcano

plot to show the most differentially expressed genes in the adaptive $CD56^{dim}$ NK cell clusters between CMV+ and CMV– groups (P-value cutoff = 10 × 10–32, fold change cutoff = 0.1). The MAST test was used to determine differentially expressed markers between the 2 groups (log[fold change] threshold = 0.25). (F) Dot plot showing genes defining the individual clusters identified in the CMV+ and CMV– patient groups on day +28 after infusion. Subsets of genes corresponding to $CD56^{bright}$, adaptive $CD56^{dim}$, and nonadaptive $CD56^{dim}CD16^{+}$ NK cells are indicated.

Expansion of the NK cell compartment after CIML NK cell infusion is distinct from endogenous NK cells in HCT patients receiving IL-2.

In the absence of a trackable marker on the CIML NK cells and to dissect how much expansion of the NK cell compartment was driven by IL-2 effects on endogenous post-HCT NK cells, we compared the NK cell compartment following CIML NK infusion to the corresponding NK cell compartment from 4 patients who received IL-2 after transplant on a previously published clinical trial (NCT00529035; ref. 30). On flow cytometry, $CD56^{dim}$ and $CD56^{bright}$ NK cell population proportions were similarly distributed in the CIML NK and IL-2 trial patients both during and 2 to 4 weeks after IL-2 therapy (**Supplemental Figure 9**). However, on mass cytometry, there were major differences in both NK cell subpopulation distribution and global marker expression on NK cells from the CIML NK cell and IL-2 trial samples. NK cell populations at baseline in both the CIML NK patients and in the post-HCT patients on the IL-2 trial included $CD56^{dim}$ NK cells that were $CD57^{+}CD16^{+}$, $CD57^{+}CD16^{-}$, and $CD57^{-}CD16^{-}$ in clusters I and III and adaptive NK cells ($NKG2C^{+}CD57^{+}$) in cluster II (**Figure 5A**). However, clusters I and II

in CIML NK cells were predominantly absent from the IL-2 trial patients at all evaluated time points (**Figure 5B**). Globally CIML NK cells had a higher expression of the markers CD2, TRAIL, and TIM3 on day +7 after onset of the therapy (**Figure 5C**). A similar comparison between the 2 patient cohorts 2 to 4 weeks after completion of their IL-2 treatment showed higher expression of CD2, TRAIL, TIGIT, and granzyme B in the CIML NK cell trial samples, suggestive of continued enhanced effector function in these patients weeks after stopping IL-2 treatment (**Figure 5D**).

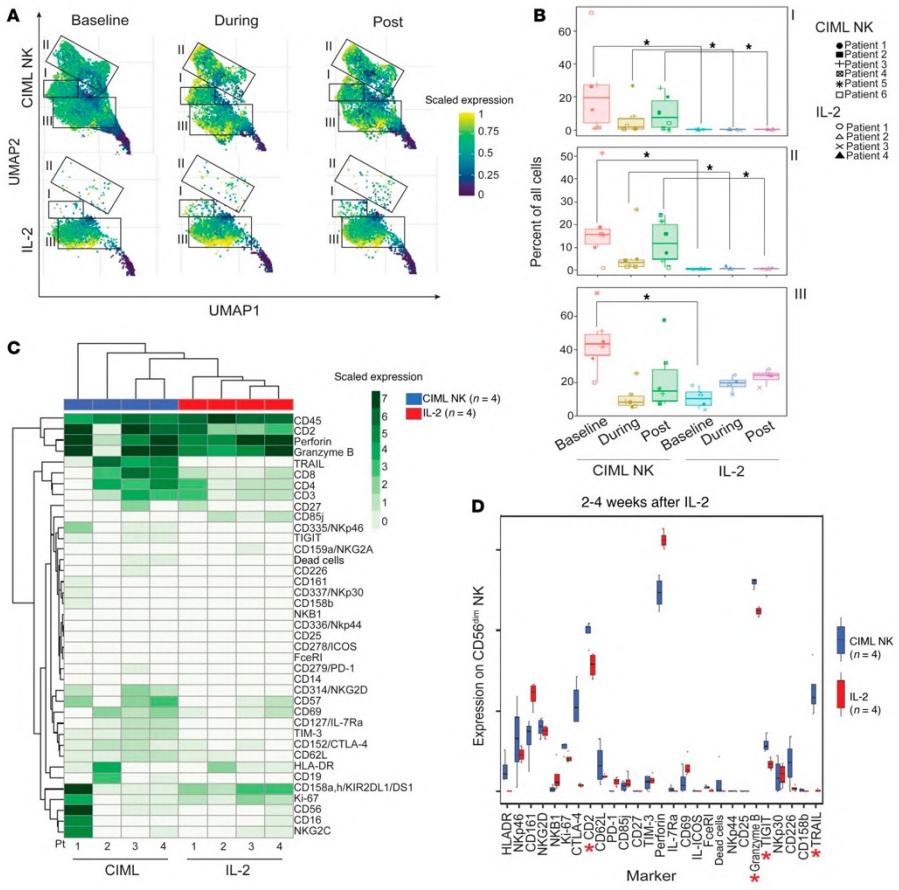

Figure 5. Immunophenotype of CIML NK–treated patients compared to the posttransplant IL-2–treated patients. Peripheral blood samples from 3 time points from CIML NK cell trial (n = 4) and IL-2 trial (n = 4) were evaluated using mass cytometry. The time points included at baseline prior to IL-2 start, during IL-2 treatment 1 week after starting it, and 2 to 4 weeks after completion of IL-2 therapy. (A) UMAP of $CD3^{-}CD56^{+}$ clusters in patients treated with IL-2 (lower insets) compared to patients on the CIML NK trial who also received IL-2 as part of the trial protocol. (B) Distribution of clusters of $CD3^{-}CD56^{+}$ cell subpopulations in both the CIML NK– and IL-2–treated patients. *P < 0.05 by Mann-Whitney U test, with significance adjusted by Holm's method for multiple comparisons. (C) Distribution of marker expression on PBMCs between CIML NK– and IL-2–treated patients during therapy. (D) A comparison of marker expression between CIML NK trial (blue) and IL-2 trial (red) patients 2 to 4 weeks after completion of IL-2. CIML NK–treated patients exhibited a higher expression of CD2, granzyme B, TIGIT, and TRAIL compared with IL-2–treated patients. *P < 0.05 by Wilcoxon's rank-sum test, with significance adjusted for multiple comparisons (43).

The NK cell compartment undergoes a phenotypic shift with expansion, but reverts back to the screening phenotype after day +60 after CIML NK infusion.

$CD56^{dim}$ NK cells accounted for approximately 35% of all lymphocytes in the peripheral blood at the day +60 time point, in contrast to a median of 7% at the screening time point (**Figure 6A**). $CD56^{dim}$ NK cells by day +60 phenotypically resembled the corresponding NK cells at screening (**Figure 6B**). There were no significant differences in mass cytometry marker expression between the 2 time points (**Figure 6C**). We sought to identify the subpopulation of NK cells that might sustain this greater abundance by identifying a cluster among the NK cells that was highly positive for Ki67. The relative abundance of this subpopulation on day +60 was significantly

increased compared with the screening time point in all evaluable patients (0.32% vs. 0.075% of all PBMCs, P = 0.04 by Wilcoxon's rank-sum test), although the number of Ki67^{+} NK cells was less than 1% of PBMCs at both time points (**Figure 6D**). Similar to the predominant CD56^{dim} population, there were no mass cytometry markers that were significantly differentially expressed among the CD56^{bright} NK cells between the 2 time points (**Supplemental Figure 10**).

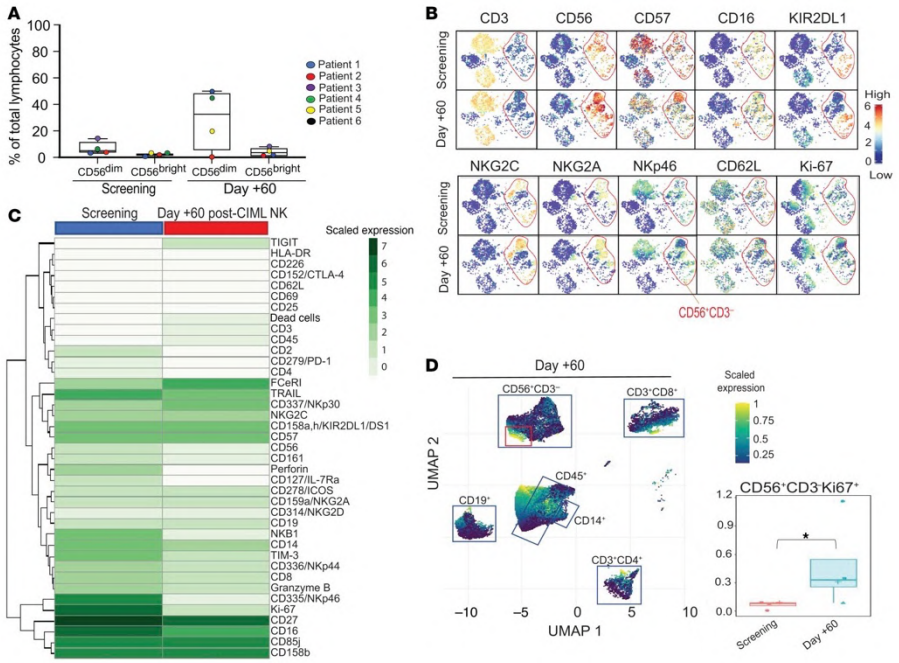

Figure 6. Phenotypic changes of the dominant NK cell subsets in the peripheral blood over time. NK cell phenotype was compared at screening and day +60 after CIML NK cell infusion using flow cytometry and mass cytometry. (A) Comparison of the CD56^{dim} and CD56^{bright} NK cell subset proportion of total lymphocyte count at screening and day +60. At screening, the median CD56^{dim} NK proportion of lymphocytes was 3.3% (min 1.3%, max 15.2%), while the median CD56^{bright} NK proportion of lymphocytes was 0.7% (min 0.1%, max 1%). On day +60, the median CD56^{dim} proportion of

lymphocytes was 32.6% (min 0%, max 50.9%), while the median $CD56^{bright}$ NK proportion of lymphocytes was 2.5% (min 0 %, max 8.4%). (B) tSNE plot comparison of PBMC populations at screening and day +60 time points in representative patient 3. NK cells are in the red circle. (C) Differential expression of mass cytometry markers in the $CD3^{-}CD56^{dim}$ cell subpopulations (Wilcoxon's rank-sum test, with significance adjusted for multiple comparisons). Screening (n = 6) and day +60 (n = 5). Patient 5 did not have a day +60 sample. (D) Clustering of PBMCs to identify the $Ki67^{+}$ subpopulation (red squares) of $CD3^{-}CD56^{+}$ NK cells. $CD3^{-}CD56^{+}Ki67^{+}$ cells as a proportion of total PBMCs at both screening and day +60. Individual patient values are shown superimposed on the box plots. The median percentage of $CD3^{-}CD56^{+}Ki67^{+}$ cells at screening and day +60 was 0.075% (min 0%, max 0.09%) and 0.32% (min 0.07%, max 1.15%), respectively. *Differential abundance, with $P < 0.05$ using Wilcoxon's rank-sum test.

NK cells traffic to sites of disease after CIML NK cell infusion.

We evaluated whether expansion of the NK cell populations after CIML NK cell infusion is associated with the presence of NK cells at sites of disease. Multiparameter immunofluorescence imaging (MIFI) was used to investigate the expression of multiple markers in the bone marrow and tissue biopsy samples before and after CIML NK cell infusion. Patient 1 had nearly no detectable NK cells in the bone marrow on day +100 after HCT, and yet had a definite NK cell infiltration on day +28 after CIML NK cell infusion despite the marrow being hypocellular (<10% cellularity) (**Figure 7A**). Patient 3, on the other hand, had NK cells present in the day +100 post-HCT bone marrow (50% cellularity) and in the day +28 post–CIML NK infusion bone marrow (**Figure 7A**). Further longitudinal evaluation of available bone marrow samples from patient 3 showed a paucity of NK cells on day +60 and at the time of relapse after CIML NK cell infusion. In patient 4 with extramedullary disease, CIML NK cell infusion was associated with an NK cell

infiltrate at the tumor site 7 days after infusion. This infiltrate was juxtaposed to the $CD123^{+}$ leukemia blasts, which were substantially reduced on day +7. The leukemia blasts and NK cells were undetectable by day +28 after CIML NK cell infusion (**Figure 7B**). The reduction in blast burden in this patient was also associated with an influx of T cells into the tumor site. Further characterization of the immune cell infiltrate in this patient on day +7 revealed that most NK cells were $CD16^{-}$, with some cells expressing granzyme B and only a minority expressing CD57 (**Figure 7C**). Similarly, the majority of the T cells were $CD8^{+}$. In all other patients with bone marrow involvement of their disease, NK cells were present in the marrow on day +28 after infusion (**Supplemental Figure 11**).

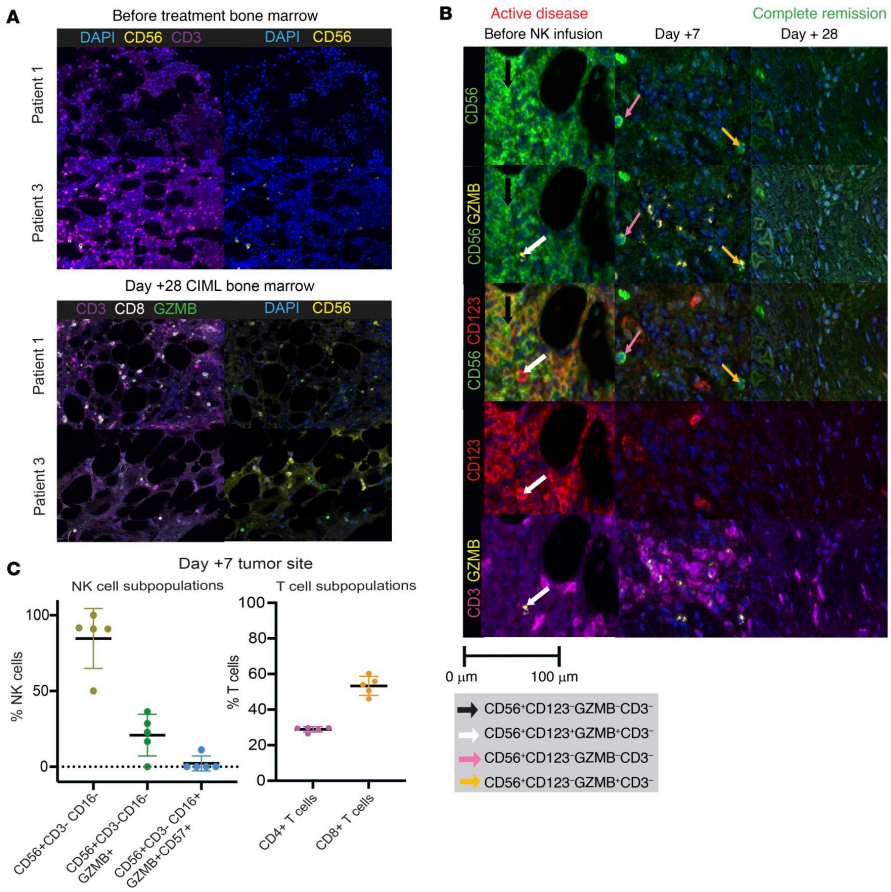

Figure 7. Immune effector cell infiltration at the site of disease. (A) Multiparameter immunofluorescence imaging (MIFI) was applied to the pretreatment bone marrow and day +28 after CIML NK therapy applied to 2 representative patients. NK cell infiltration was relatively sparse in patients 1 and 3 before therapy, as exemplified by the general lack of CD56 positivity relative to the predominance of CD3 positivity. In contrast, on day +28 after CIML NK infusion, the $CD3^{-}CD56^{+}$ staining was relatively enhanced. (B) Infiltration of immune effector cells in the patient with BPDCN in the context of active $CD123^{+}$ extramedullary disease. Prior to CIML NK cell infusion, diseased cells (white arrow) were juxtaposed to some NK cells (black arrow) and $CD3^{+}$ cells. On day +7 after CIML NK infusion, substantial reduction in the $CD123^{+}$ blasts, with residual NK cell subpopulations (pink and yellow arrows) and $CD3^{+}$ cell populations noted. By day +28 after CIML NK infusion, the extramedullary lesion was involuted and with no detectable blasts and NK or T cell cellular infiltrate. Original magnification, ×200 (A and

B). (C) Quantitation of NK cell and T cell subpopulations (individual dots represent quantitation within a specific field in the biopsy, 5 fields evaluated) from day +7 MIFI panel from extramedullary disease site in BPDCN patient.

AML blasts present at relapse after CIML NK therapy express inhibitory NK cell ligand genes.

Patients 1 and 3 both exhibited longterm persistence of NK cell populations that were present in their infusion products. At the time of AML relapse, they both had a coexistence of leukemia blasts with the NK cells in the peripheral blood, providing an opportunity to potentially understand NK and leukemia cell interactions (**Figure 8A**). Using scRNA-seq, we conducted a differential expression analysis comparing NK cell clusters between day +28 and relapse time points in both patients 1 and 3 to determine whether there was a change associated with relapse (**Figure 8B**). All NK cell clusters at the time of relapse expressed genes associated with NK cell activation (**Figure 8B**). The *FOS* gene had increased expression at the time of relapse in both these patients (**Figure 8C and Supplemental Tables 5 and 6**). All the NK clusters in patient 1 had a significant reduction in the expression of *CXCR4* at the time of relapse (**Figure 8C**). Patient 3, on the other hand, had an upregulation of genes associated with the $CD56^{bright}$ phenotype of NK cells at the time of relapse (**Supplemental Table 6**). We conducted gene set enrichment analysis on all differentially expressed genes in the $CD56^{dim}$ and $CD56^{bright}$ NK cell clusters that were present at relapse in patients 1 and 3 (**Figure 8D**). We identified genes in the *FGFR1c* pathway, thought to be involved in the differentiation of $CD56^{bright}$ NK cells to a $CD56^{dim}$ phenotype (31), as being differentially expressed at the time of AML relapse compared with day

+28 in both patients. Other pathways that exhibited differential expression included those involving polyamines and histamine receptors.

We next evaluated whether post–CIML NK relapse of AML was associated with the expression of ligands for activating and inhibitory receptors present on the persistent NK cells in the peripheral blood. Using scRNA-seq, we identified $CD34^+$-containing clusters enriched for AML blasts, and confirmed that these did not express typical NK cell markers (**Supplemental Figure 12**). *HLA-E*, an inhibitory ligand that binds NKG2A and CD94 (*KLRD1*), was highly expressed on the $CD34^+$ clusters in patient 1 but its expression was lower on the $CD34^+$ clusters in patient 3 (**Figure 8E**). The leukemia-containing clusters were found to have a low expression of *CD48* and *CD58*, the genes coding for activating ligands that bind CD2. Galectin-9 (*LGALS9*), a known inhibitory ligand for NK cells, was expressed predominantly on the $CD34^+$ clusters in both patients. TIM3 (*HAVCR2*), a receptor for galectin-9, was not expressed in the $CD34^-$ clusters at either the expansion or relapse time point, but its receptor, CD44, was expressed at relapse. The expression of most other NK activating and inhibitory ligands was either not present or not assessable with 3′ scRNA-seq (**Supplemental Figure 13**).

Since CD2 ligands were found to be downregulated in the context of AML relapse and CD2 was highly expressed on $CD56^{dim}$ CIML NK cells (**Figure 5D**), we evaluated the effect of blocking CD2 on CIML NK activation, cytokine secretion, or cytotoxicity *in vitro* using a blocking anti-CD2 monoclonal antibody. While blockade of CD2 led to reduced secretion of TNF-α in conventional NK cells, it did not have

any significant effect on CIML NK cell activation, cytokine secretion, or cytotoxicity (**Supplemental Figure 14**), suggesting that other activating NK cell receptors are able to compensate for lack of CD2 signaling for activation in CIML NK cells.

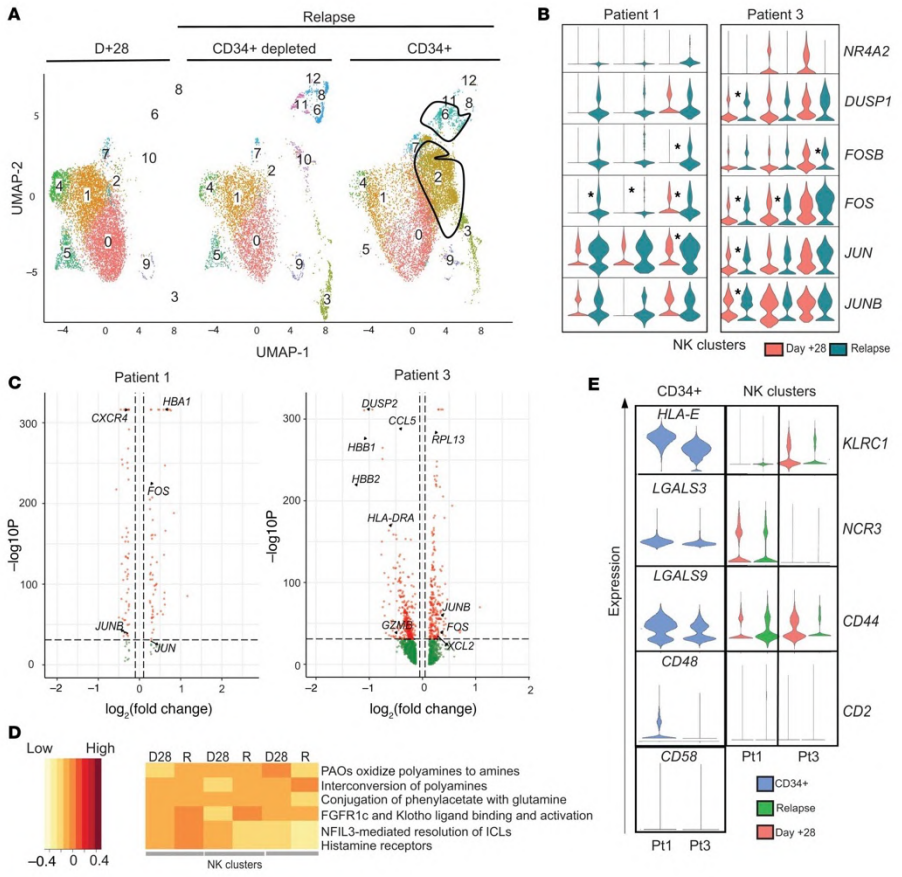

Figure 8. Transcriptomic evaluation of NK cells and AML blasts at the time of disease relapse by scRNA-seq. (A) Representative UMAP from scRNA-seq analysis in patient 1. The outlined populations are $CD34^+$ blasts that were identified at relapse. (B) Violin plots corresponding to the expression of activation markers in $CD3^-CD56^+$ NK cell clusters defined using scRNA-seq. *$P < 0.05$ by Wilcoxon's rank-sum test, with significance adjusted for multiple comparisons (50). (C) Volcano plots for patient 1 (left) and patient 3 (right) comparing gene expression in NK cell–containing scRNA-seq clusters at day +28 to relapse. Genes on the left of the violin plot are downregulated while those on the right are upregulated at the time of

relapse. (D) Gene set enrichment analysis corresponding to differentially expressed genes in NK cell clusters derived from scRNA-seq data in patient 1 as a representative example. Within every cluster, every pair of columns corresponds to day +28 (D28) and relapse (R) time points. The intensity of expression is represented by the color of the legend on the left. (E) Expression of specific NK cell receptors within the NK clusters on day +28 and relapse in patient 1 (P1) and patient 3 (P3) and their corresponding NK ligands on the relapsed leukemia blasts are indicated in blue ($CD34^+$ cells).

Discussion

We demonstrate that infusion of donor-derived CIML NK cells into an immune-compatible environment for the management of post–haplo-HCT relapse of myeloid disease is safe and results in rapid expansion and long-term persistence of NK cells. The expansion of the NK cell compartment following CIML NK cell infusion was distinct from IL-2 effects on endogenous posttransplant NK cells and was not dependent on CMV reactivation. In preliminary outcomes of this ongoing trial, infusion of CIML NK cells was associated with a reduction in measurable disease burden in 4 of 6 treated patients, including a patient with BPDCN. Response to therapy was sustained for several months. CIML NK cells were well tolerated, with the main adverse effect being the development of cytopenia in most patients. Importantly, infusion of these donor lymphocytes was not associated with severe CRS or neurotoxicity. Furthermore, in spite of the administration of low-dose IL-2 in the posttransplant setting, no patient developed any GvHD.

The lifespan of conventional NK cells is thought to be in the range of 12 to 14 days, but adoptive transfer of CIML NK cells in a syngeneic murine model was associated with significant prolongation of their expected lifespan (23). In a previous clinical trial using CIML NK cells to treat relapsed/refractory AML in a nontransplant HLA-mismatched

setting, the donor-derived NK cells could not be detected beyond day +28 after infusion (21). In the current clinical trial, expansion of donor CIML NK cells and subsequent persistence of these cells for several months was noted. We hypothesize that this was due in part to the immune-compatible posttransplant milieu since all treated patients had high T cell chimerism at the time of CIML NK infusion.

CMV reactivation likely contributed to the expansion and persistence of immunophenotypically and transcriptionally identified adaptive $CD56^{dim}$ NK cell subsets. However, nonadaptive $CD56^{dim}$ NK cells were the dominant subset and expanded in both the CMV+ and CMV– patients. Furthermore, the presence of CMV did not significantly affect the surface marker or gene expression of nonadaptive $CD56^{dim}$ NK cells. This suggests that CMV reactivation was not the sole driver of NK cell expansion. Additional work will be required to determine whether there is any difference in antitumor activity between the adaptive NK cells expanded in response to CMV and the nonadaptive NK cells.

The expanded NK cell compartment following infusion of CIML NK cells was associated with presence of NK cells at disease sites and reduction of disease burden. This was most dramatic in patient 4 with BPDCN whose disease burden visibly shrank and became undetectable on PET-CT. MIFI demonstrated the presence of NK cell and $CD8^+$ T cell infiltrates in the extramedullary mass in this patient, suggesting a possible interaction between these 2 cell populations in mediating disease reduction and pre- venting disease relapse. The infiltration of $CD8^+$ T cells into the site of disease was also seen in patient 3. Further work is required to explore the possible interaction between $CD8^+$ T

cells that appear to infiltrate disease sites following CIML NK infusion and the infused NK cell subsets.

While the use of CIML NK cells was safe and not associated with severe CRS, neurotoxicity, or GvHD, it is of note that all patients with bone marrow involvement of myeloid disease exhibit- ed pancytopenia. In 2 of these patients, a $CD34^{+}$-selected stem cell boost was required to promote peripheral blood cell recovery, while in the others the peripheral blood counts recovered on their own. Prolonged pancytopenia after adoptive cell transfer was observed in prior CAR-T trials and may be related to the lymphodepleting chemotherapy (32). One patient exhibited clinical and laboratory features of grade 2 CRS, requiring treatment with tocilizumab that resolved the syndrome. CRS was reported in a recently published haploidentical NK cell therapy trial, although the higher reported rate in that trial could have been due to the use of subcutaneous IL-15 to expand the NK cells (33). Consistent with this trial and other published NK cell trials, no patient developed any GvHD despite receiving a product that is mismatched to the recipient. The tolerability of the adoptively transferred CIML NK cell therapy in this trial is similar to what has been seen in other NK cell therapy trials, including those using IL-21–expanded NK cells (34, 35).

The deeper immunophenotypic evaluation of infused CIML NK cells using mass cytometry revealed interpatient heterogeneity, likely reflecting the diversity of the NK cell populations inherent in the donor (36). It was demonstrated that the mass cytometry–defined CIML phenotype persists long term as an imprint superimposed on the original NK cell repertoire. This imprint was not driven by IL-2 alone, as a

comparator group of patients who received the same dose of IL-2 at least 6 months after transplant did not yield expansion of the same $CD56^{dim}$ NK cell subpopulations. The NK cell compartment following CIML NK infusion expressed higher levels of CD2, TIGIT, TRAIL, and granzyme B that persisted several weeks after the last dose of IL-2, suggesting that this set of markers could perhaps distinguish the CIML NK–expanded NK cells from endogenous NK cells. We hope to build upon this finding in future studies with larger patient numbers, as lack of distinct marker(s) makes tracking CIML NK cells *in vivo* challenging particularly when using autologous products and in a post–allo-HCT setting. By day +60 after infusion, the NK cell compartment largely resembled that seen prior to infusion of CIML NK cells.

scRNA-seq analysis of the NK cell compartment at the time of AML relapse after CIML NK cell therapy demonstrated the persistence of both $CD56^{bright}$ and adaptive NK cell populations, among others. Gene set enrichment analysis suggested that in the patient with a sizeable expansion and persistence of $CD56^{bright}$ NK cells, there was downregulation of the *FGFR1c* pathway involved in NK cell maturation from $CD56^{bright}$ to $CD56^{dim}$, potentially explaining why the $CD56^{bright}$ NK cells were able to persist (31). The expression of HLA-E in the relapsed AML blasts in this patient with an expanded NKG2A-expressing $CD56^{bright}$ NK population suggests a potential evasion mechanism, in agreement with previous analysis of residual leukemic cells following allogeneic NK cell therapy (37). Since this patient also exhibited an infiltrate of $CD8^{+}$ T cells at the site of disease, possibly promoted by the cytokine secretion from the $CD56^{bright}$ NK

cells, evasion of $CD8^+$ T cells may have contributed significantly to the relapse mechanism. Additional mechanisms of AML relapse after CIML NK therapy may be associated with the absence of ligands for CD2, a receptor that is expressed on the NK cell populations after infusion, and that is involved in mediating tumor target cytotoxicity via interaction with CD16 (38). In patient 1, in whom most of the expanded and persistent NK cells exhibited a mature cytotoxic $CD56^{dim}CD16^+$ phenotype, the absence of expression of CD48 and CD58 on relapsed leukemia could suggest a resistance mechanism. Our in vitro analysis, however, suggests that CD2 blockade is not sufficient to reduce CIML NK cell activation, cytokine secretion, or cytotoxicity. This does not exclude CD2 as a relevant receptor for targeting of myeloid disease, as conventional NK cells were affected by the blocking antibody, but does suggest that the lower activation threshold of CIML NK cells leads to additional mechanisms being involved in mediating escape of AML from their effects. Such additional mechanisms of AML relapse may involve the inhibitory ligand galcetin-9, since its receptor, CD44 (39), was expressed on the $CD34^-$ PBMCs at the time of relapse. The expression of galectin-9 may have played an additional role in the survival of residual leukemia clones early after NK cell infusion when its receptor TIM3 was more highly expressed in the infused CIML NK cell product.

While this study consistently demonstrated the rapid expansion and persistence of donor-derived CIML NK cells without any GvHD or severe CRS complications, it has important limitations. First, the number of treated patients was relatively small. Furthermore, as the infused NK cells shared HLA expression with the NK cells already

present in the transplanted patient and there was no traceable marker in the infused CIML NK cells, it was not possible to use donor chimerism or other direct means to track the infused NK cells. The mass cytometry marker signature determined by comparison of the NK compartments from the CIML NK trial patients and IL-2–treated posttransplant patients must also be interpreted with caution, as the NK cells being compared came from patients who are not at identical times in their posttransplant course. Although these limitations prevent immediate generalizations of the findings, the deep high-throughput analyses of longitudinally collected samples do reveal a number of important hypothesis-generating observations with the potential for clinical translation in the near future. Additional work is necessary to elucidate the mechanism(s) of the prolonged alterations in the NK cell compartment after donor CIML NK cell infusion, as well as their interaction with other immune effector cells as a means to treat posttransplant relapse of myeloid disease.

Conclusion

In summary, we demonstrate that CIML NK cells infused into an immune-compatible milieu in the context of a haploidentical stem cell transplant are associated with marked NK expansion and long-term persistence. We show that CIML NK cell products comprise predominantly cytotoxic $CD56^{dim}$ NK cells but also exhibit donor-specific heterogeneity in both the presence of additional NK cell subsets as well as in the expression of NK cell markers associated with the memory-like phenotype. The NK cell subpopulations present at the time of NK cell infusion undergo significant phenotypic changes

associated with enhanced NK cell activity and the development of a memory-like phenotype by day +28, but by about day +60 after infusion phenotypically resemble the NK cells present prior to infusion in significantly increased numbers. We also show that expansion of the NK cell compartment following CIML NK cell infusion is distinct from IL-2 effects on endogenous posttransplant NK cells and is not dependent on CMV reactivation. Finally, we speculate that relapse of AML after CIML NK cell therapy is associated with expression of NK inhibitory ligands, and may occur in the context of evasion of CD2-mediated activation in addition to other mechanisms that remain to be determined. Because of their capacity for rapid expansion and long-term persistence, CIML NK cells offer an attractive platform for further improvement of NK cell therapies by combining them with immunomodulatory agents and/ or by arming them with CAR gene constructs.

References

1. Rautenberg C, et al. Relapse of acute myeloid leukemia after allogeneic stem cell transplantation: prevention, detection, and treatment. Int J Mol Sci. 2019;20(1):228.
2. McCurdy SR, et al. Comparable composite endpoints after HLA-matched and HLA-haploidentical transplantation with post-trans- plantation cyclophosphamide. Haematologica. 2017;102(2):391–400.
3. Brambilla CZ, et al. Relapse after allogeneic stem cell transplatation of acute myelogenous leukemia and myelodysplastic syndrome and the importance of second cellular therapy. Trans- plant Cell Ther. 2021;27(9):771.e1–771.e10.
4. Patriarca F, et al. Donor lymphocyte infusions after allogeneic stem cell transplantation in acute leukemia: A survey from the Gruppo Italiano Trapianto Midollo Osseo (GITMO). Front Oncol. 2020;10:572918.

5. Toffalori C, et al. Immune signature drives leukemia escape and relapse after hematopoietic cell transplantation. Nat Med. 2019;25(4):603–611.
6. Frey NV, Porter DL. Graft-versus-host disease after donor leukocyte infusions: presentation and management. Best Pract Res Clin Haematol. 2008;21(2):205–222.
7. Zeidan AM, et al. HLA-haploidentical donor lymphocyte infusions for patients with relapsed hematologic malignancies after related HLA-haploidentical bone marrow transplantation. Biol Blood Marrow Transplant. 2014;20(3):314–318.
8. Ghiso A, et al. DLI after haploidentical BMT with post-transplant CY. Bone Marrow Transplant. 2015;50(1):56–61.
9. Ruggeri L, et al. Effectiveness of donor natural killer cell alloreactivity in mis- matched hematopoietic transplants. Science. 2002;295(5562):2097–2100.
10. Chouaib S, et al. Improving the outcome of leukemia by natural killer cell-based immunotherapeutic strategies. Front Immunol. 2014;5:95.
11. Locatelli F, et al. NK cells mediate a crucial graft-versus-leukemia effect in haploidentical-HSCT to cure high-risk acute leukemia. Trends Immunol. 2018;39(7):577–590.
12. Gill S, et al. Natural killer cells in allogeneic trans- plantation: effect on engraftment, graft- versus-tumor, and graft-versus-host responses. Biol Blood Marrow Transplant. 2009;15(7):765–776.
13. Carlsten M, Järås M. Natural killer cells in myeloid malignancies: immune surveillance, NK cell dysfunction, and pharmacological opportunities to bolster the endogenous NK cells. Front Immunol. 2019;10:2357.
14. Lupo KB, Matosevic S. Natural killer cells as allogeneic effectors in adoptive cancer immunotherapy. Cancers (Basel). 2019;11(6):769.
15. McQueen KL, et al. Donor-recipient combi- nations of group A and B KIR haplotypes and HLA class I ligand affect the outcome of HLA- matched, sibling donor hematopoietic cell trans- plantation. Hum Immunol. 2007;68(5):309–323.
16. Shaffer BC, et al. Phase II study of haploidentical natural killer cell infusion for treatment of relapsed or persistent myeloid malignancies following allogeneic hematopoietic cell transplantation. Biol Blood Marrow Transplant. 2016;22(4):705–709.
17. Ardolino M, et al. Cytokine therapy reverses NK cell anergy in MHC-deficient tumors. J Clin Invest. 2014;124(11):4781–4794.

18. Bae DS, Lee JK. Development of NK cell expansion methods using feeder cells from human myelogenous leukemia cell line. Blood Res. 2014;49(3):154–161.
19. Oyer JL, et al. Generation of highly cytotoxic natural killer cells for treatment of acute myelogenous leukemia using a feeder-free, particle-based approach. Biol Blood Marrow Transplant. 2015; 21(4):632–639.
20. Ben-Shmuel A, et al. Unleashing natural killer cells in the tumor microenvironment-the next generation of immunotherapy? Front Immunol. 2020;11:275.
21. Romee R, et al. Cytokine-induced memory-like natural killer cells exhibit enhanced responses against myeloid leukemia. Sci Transl Med. 2016;8(357):357ra123.
22. Romee R, et al. Cytokine activation induces human memory-like NK cells. Blood. 2012;120(24):4751–4760.
23. Berrien-Elliott MM, et al. Multidimensional analyses of donor memory-like NK cells reveal new associations with response after adoptive immunotherapy for leukemia. Cancer Discov. 2020;10(12):1854–1871.
24. Keppel MP, et al. Murine NK cell intrinsic cytokine-induced memory-like responses are maintained following homeostatic proliferation. J Immunol. 2013;190(9):4754–4762.
25. Fehniger TA, Cooper MA. Harnessing NK cell memory for cancer immunotherapy. Trends Immunol. 2016;37(12):877–888.
26. Dohner H, et al. Diagnosis and management of AML in adults: 2017 ELN recommendations from an international expert panel. Blood. 2017;129(4):424–447.
27. Cheson BD, et al. Clinical application and propos- al for modification of the International Working Group (IWG) response criteria in myelodysplasia. Blood. 2006;108(2): 419–425.
28. Kurioka A, et al. CD161 defines a functionally distinct subset of pro-inflammatory natural killer cells. Front Immunol. 2018;9:486.
29. Yang C, et al. Heterogeneity of human bone marrow and blood natural killer cells defined by single-cell transcriptome. Nat Commun. 2019;1(1):3931.
30. Koreth J, et al. Interleukin-2 and regulatory T cells in graft-versus-host disease. N Engl J Med. 2011;365(22):2055–2066.
31. Cichocki F, et al. Human NK cell development: one road or many? Front Immunol. 2019;10:2078.
32. Fried S, et al. Early and late hematologic toxicity following CD19 CAR-T cells. Bone Marrow Transplant. 2019;54(10):1643–1650.

33. Cooley S, et al. First-in-human trial of rhIL-15 and haploidentical natural killer cell therapy for advanced acute myeloid leukemia. Blood Adv. 2019;3(13):1970–1980.
34. Ciurea SO, et al. Phase 1 clinical trial using mbIL21 ex vivo-expanded donor-derived NK cells after haploidentical transplantation. Blood. 2017;130(16):1857–1868.
35. Vasu S, et al. BMT CTN 1803: trial to investigate if haploidentical natural killer cells (CSTD002) prevent post-transplant relapse in AML and MDS (NK-REALM). Biol Blood Marrow Transplant. 2020;26(3):371–372.
36. Freud AG, et al. The broad spectrum of human natural killer cell diversity. Immunity. 2017;47(5):820–833.
37. Björklund AT, et al. Complete remission with reduction of high-risk clones following haploidentical NK-cell therapy against MDS and AML. Clin Cancer Res. 2018;24(8):1834–1844.
38. Binder C, et al. CD2 immunobiology. Front Immunol. 2020;11:1090.
39. Motamedi M, et al. Galectin-9 expression defines a subpopulation of NK cells with impaired cyto- toxic effector molecules but enhanced IFN-γ production, dichotomous to TIGIT, in HIV-1 infection. Immunohorizons. 2019;3(11):531–546.
40. Thrash EM, et al. High-throughput mass cytom- etry staining for immunophenotyping clinical samples. STAR Protoc. 2020;1(2):100055.
41. Levine JH, et al. Data-driven phenotypic dissec- tion of AML reveals progenitor-like cells that correlate with prognosis. Cell. 2015;1(1):184–197.
42. Van Gassen S, et al. FlowSOM: Using self- organizing maps for visualization and inter- pretation of cytometry data. Cytometry A. 2015;87(7):636–645.
43. Opzoomer JW, et al. ImmunoCluster provides a computational framework for the nonspecialist to profile high-dimensional cytometry data. Elife. 2021;30:10:e62915.
44. Nowicka M, et al. CyTOF workflow: differential discovery in high-throughput high-dimensional cytometry datasets. F1000Res. 2019;6:748.
45. Patel T, et al. Development of an 8-color antibody panel for functional phenotyping of human CD8+ cytotoxic T cells from peripheral blood mononuclear cells. Cytotechnology. 2018;70(1):1–11.
46. Cunningham RA, et al. Detection of clinically rel- evant immune checkpoint markers by multicolor flow cytometry. J Biol Methods. 2019;6(2):e114.

47. Holland M, et al. Separation, banking, and quality control of peripheral blood mononuclear cells from whole blood of melanoma patients. Cell Tissue Bank. 2018;19(4):783–790.
48. Sridharan V, et al. Effects of definitive chemoradiation on circulating immunologic angiogenic cytokines in head and neck cancer patients. J Immunother Cancer. 2016;4:32.
49. Schoenfeld JD, et al. Pneumonitis resulting from radiation and immune checkpoint blockade illustrates characteristic clinical, radiologic and circulating biomarker features. J Immunother Cancer. 2019;7(1):112.
50. Stuart T, et al. Comprehensive integration of single-cell data. Cell. 2019;177(7):1888–1902.
51. Griss J, et al. ReactomeGSA - efficient multi-om- ics comparative pathway analysis. Mol Cell Pro- teomics. 2020;19(12):2115–2125.
52. Weber LM, et al. difficyt: Differential discovery in high-dimensional cytometry via high-resolution clustering. Commun Biol. 2019;2:183.

Author contributions

RMS and GCB contributed equally to the study, with RMS listed first because he is the principal investigator on the trial. RMS, SN, RJS, JR, and RR designed the clinical study protocol. RMS, GCB, and RR designed the correlative studies. SN prepared CIML NK products under GMP guidelines and was responsible for quality control of the products. CR and MSH processed and prepared patient samples for correlative studies. JVC, AKA, MT, and GCB performed the NK cell functional assays. BR and YA performed flow cytometry. GH performed single-cell RNA-seq. JB performed mass cytometry. SJR and NC performed multiparameter immunofluorescence on bone marrow biopsies. MS and YZA assisted with the design and conduct of the CD2 blockade functional experiments. YA assisted with conducting and analyzing flow cytometry on patient samples. JOW and KLP conducted the MIFI experiment on tissue biopsies. AAL provided BPDCN patient samples. CSC, JHA, VTH, JK, and MG recruited clinical trial participants. RCL and HTK reviewed the data from correlative studies and statistical analyses, respectively, and provided critical feedback. RMS and GCB analyzed all the data and designed the figures. RMS, GCB, and RR interpreted the data and wrote the first draft of the manuscript. KJM, CJW, JC, RJS, and JR reviewed the manuscript, and provided critical feedback on the results of the correlative studies. All authors revised the manuscript critically and approved the final version.

Acknowledgments
We would like to thank M. Shipp (DFCI) for discussion and guidance, and D. Hearsey (DFCI) for assistance in processing and banking clinical samples. We are grateful for the patient volunteers who gave their time and provided the samples for all correlative studies. We are also grateful to the bone marrow transplant and research coordinators at the DFCI. This work was supported by grants awarded to RR, including the Dunkin' Donuts Breakthrough grant, the NIH/National Cancer Institute R21 CA245413 grant, and the Leukemia and Lymphoma Society Scholar and Translational Research Program awards. KJM is supported by the Research Council of Norway, The Norwegian Cancer Society, the Swedish Cancer Foundations, The Swedish Research Council, and Knut and Alice Wallenberg Foundation grant 2018.0106. Additional philanthropic support was provided by the Michelle D. and Douglas W. Bell Fund for Engineered Adoptive Immunotherapy, the Ted and Eileen Pasquarello Research Fund, and the McNamara Fund. RMS was supported by the Goldfarb Family Fellowship during the course of this work. The funding source had no role in the design of this study, its execution, analyses, interpretation of the data, or decision to submit the results.

TRIAL REGISTRATION. ClinicalTrials.gov NCT04024761.
FUNDING. Dunkin' Donuts, NIH/National Cancer Institute, and the Leukemia and Lymphoma Society.

Conflict of interest: SN is on the advisory boards of Kite, Novartis, and Nkarta. SR receives research funding from Bristol Myers Squibb (BMS) and KITE/Gilead and is on the scientific advisory board for Immunitas Pharmaceuticals. AAL consults for Qiagen and receives research funding from AbbVie and Stemline Therapeutics. CSC consults, is on the advisory board, or has an educational role with CareDx, Mallinckrodt, Pfizer, Editas, Deciphera, Sanofi, Janssen, BMS, CTI Biopharma, Equillium, Incyte, Kadmon, Jazz, Medsenic, Generon, and Mesoblast. JK is on the advisory boards of Therakos and Cugene, and receives research funding from Miltenyi Biotec, BMS, and Regeneron. CJW is an equity holder in BioNTech and receives funding from Pharmacyclics. KJM is a consultant at Fate Therapeutics and Vycellix and receives research funding from Fate Therapeutics and Merck. RJS consults or is on the advisory board of Kiadis, Juno Therapeutics, Gilead, Jasper, Jazz Pharmaceuticals, Precision Biosciences, Rheo Therapeutics, Takeda, and NMDP – Be the Match. JR receives research funding from Amgen, Equillium, Kite/ Gilead, and Novartis,

and consults or is on advisory boards for AvroBio, Akron Bio- tech, Clade Therapeutics, Garuda Therapeutics, Immunitas Therapeutics, LifeVault Bio, Novartis, Rheos Medicines, Talaris Therapeutics, and TScan Therapeutics. RR receives funding from CRISPR Therapeutics, Skyline Therapeutics, and is on the advisory board of Glycostem.

Supplemental Materials

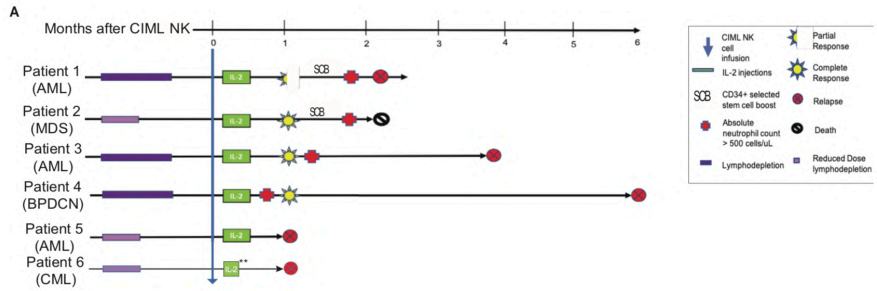

Figure S1. Clinical course and responses of patients treated with CIML NK cell therapy. A The clinical outcomes of patients treated with CIML NK cells are shown. All patients had measurable disease post haplo-HCT and prior to receiving CIML NK cells. Complete response and morphologic leukemia-free state are defined per the ELN 2017 criteria for AML, and marrow CR is defined as per the IWG criteria for MDS. **Patient 6 only received 2/7 IL2 doses due to the development of hepatotoxicity.

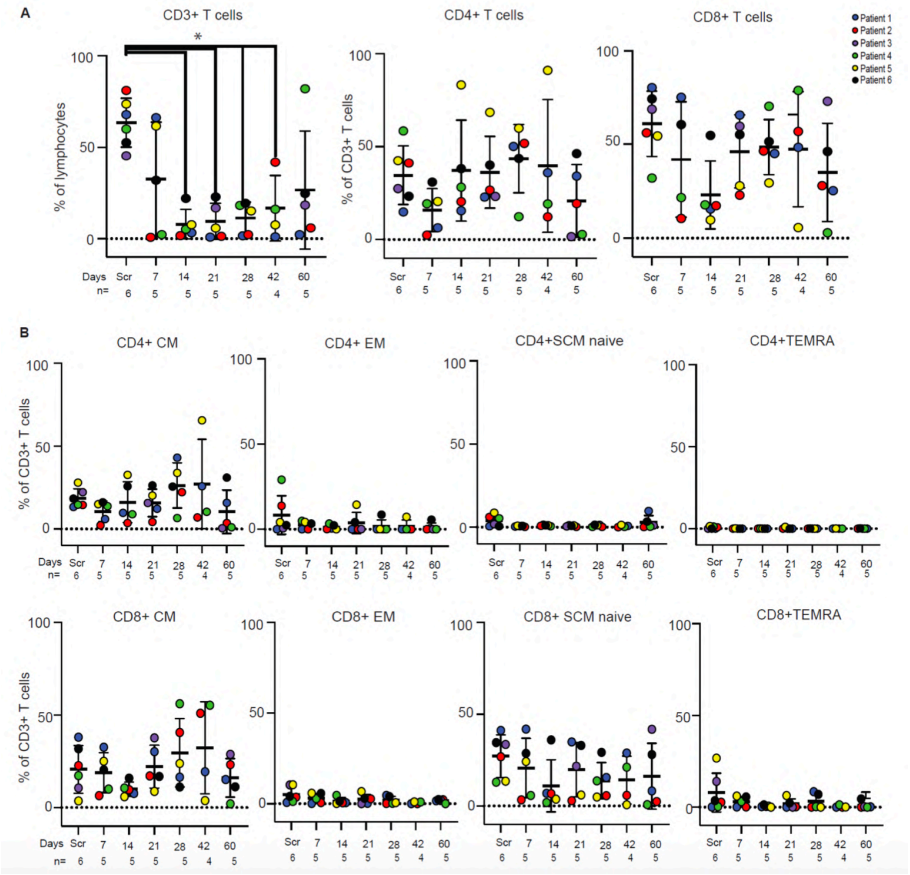

Figure S2. T-cell subpopulations following CIML NK cell infusion. A Longitudinal evaluation of $CD3^+$, $CD4^+$, and $CD8^+$ T-cell subpopulations in all patients using a customized flow cytometry panel. Comparison of abundance of $CD3^+$ T-cell subpopulations at the different time points is shown. *$p<0.05$ Mann-Whitney U test, with significance adjusted by Holm's method for multiple comparisons. B Longitudinal evaluation of $CD4^+$ and $CD8^+$ subpopulations, including central memory (CM), effector memory (EM), stem cell memory naive (SCM naive), and effector memory T-cells expressing CD45RA (TEMRA). The abundance of $CD4^+$ and $CD8^+$ T-cell subpopulations at the different time points is shown.

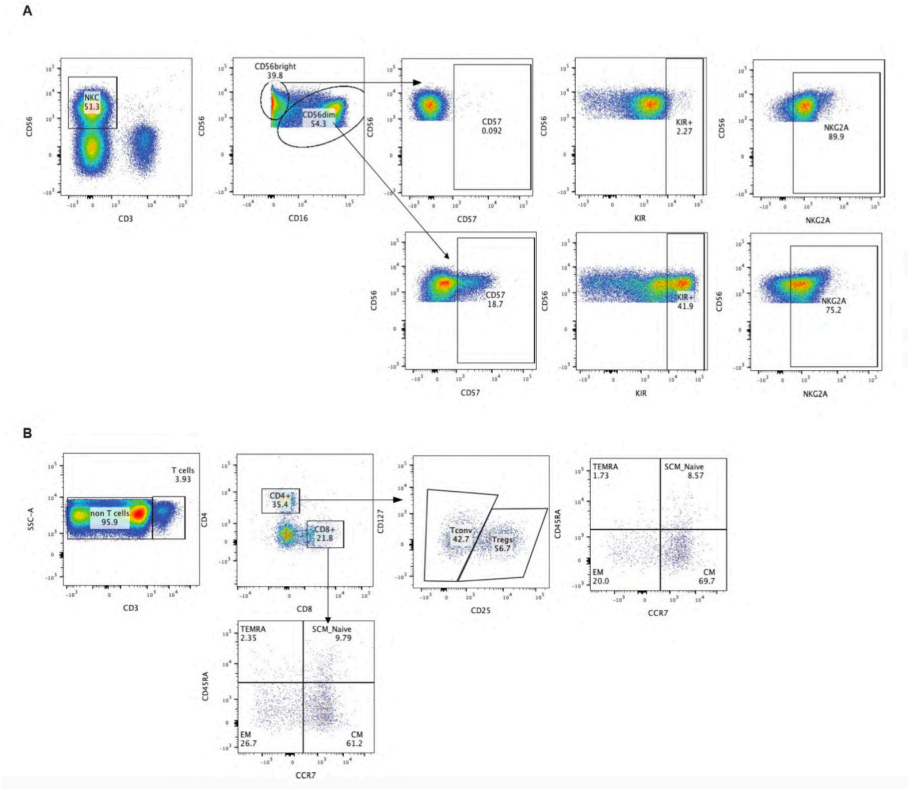

Figure S3. Gating strategies for characterization of NK and T cell subsets by flow cytometry. A NK cells are $CD56^{+}CD3^{-}$. Bright and dim NK cells are characterized by the expression of CD56 and CD16. The expression of CD57, KIR and NKG2A is determined in bright and dim populations. B T cells are $CD3^{+}$. $CD8^{+}$ and $CD4^{+}$ subsets are characterized by the expression of CD4 and CD8. Conventional $CD4^{+}$ T cells are $CD127^{+}CD25^{-}$, where $CD127^{-}CD25^{+}$ cells are Tregs. Conventional $CD4^{+}$ and $CD8^{+}$ T cell subsets are characterized by the expression of CD45RA and CCR7 where effector memory (EM) T cells are $CD45RA^{-}CCR7^{-}$, central memory (CM) T cells are $CCR7^{+}CD45RA^{-}$, terminally differentiated effector memory T cells (TEMRA) are defined by $CD45RA^{+}CCR7^{-}$ and stem cell memory T cells (SCM naive) are characterized as $CD45RA^{+}CCR7^{+}$. Representative flow plots are patient 5 day +42 and patient 4 day+14, respectively.

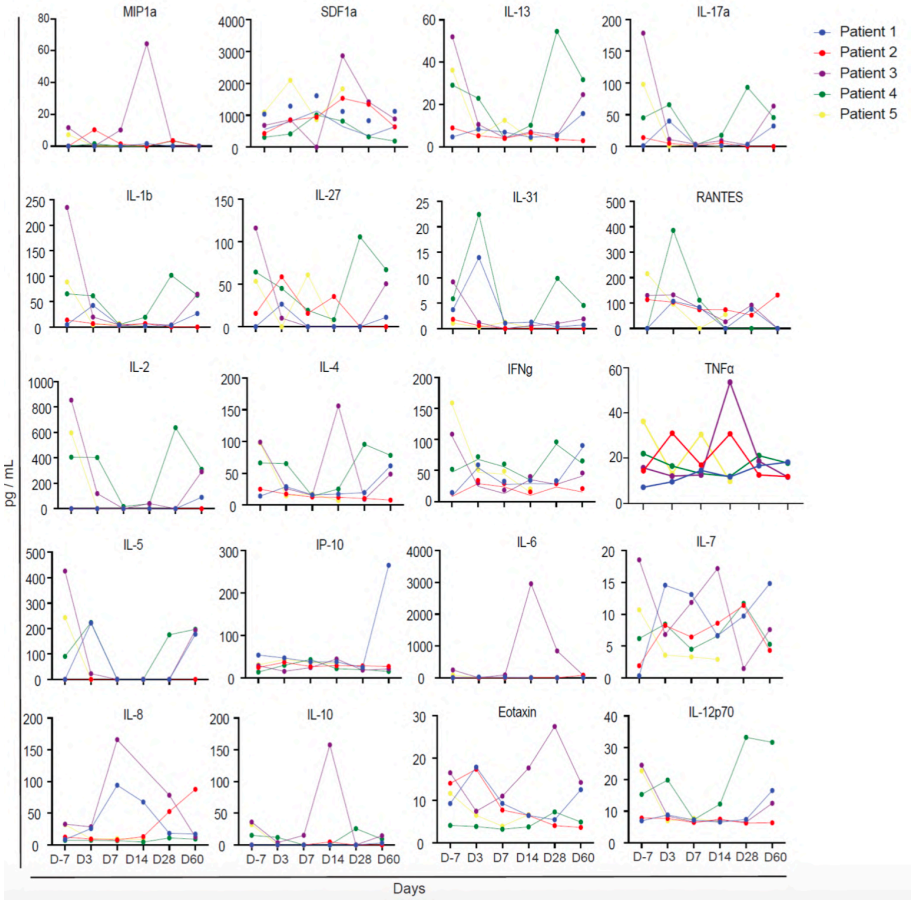

Figure S4. Evaluation of endogenous cytokines in longitudinal serum samples from patients on the CIML NK trial. Each measured serum cytokine is indicated above each graph. Longitudinal time points include day -7 (D-7), day +3 (D3), day +7 (D7), day +14 (D14), day +28 (D28), and day +60 (D60) following CIML NK infusion.

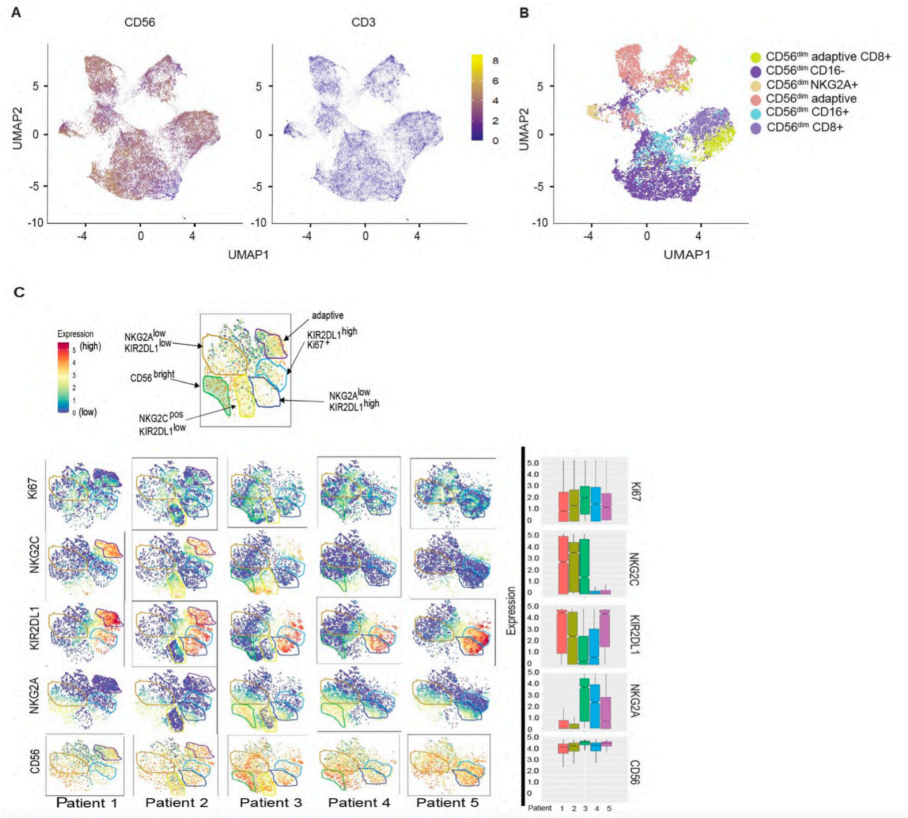

Figure S5. The infusion product contains distinct subpopulations with natural variation in donor NK cell repertoires. A The infusion product in all patients is enriched with $CD56^{+}CD3^{-}$ NK cell populations. Shown is the UMAP of immune cell clusters expressing $CD56^{+}$ and $CD3^{-}$ derived from the infusion products of all 6 patients treated with CIML NK cell therapy. B Distribution of NK cell clusters among all patient infusion products within the CYTOF marker UMAP space, showing a number of existing CIML NK subpopulations. C The NK cell subpopulations in the infusion products are compared against each other in tSNE plots derived from the first 5 patients on the trial, with distinct NK cell subpopulations identified using PhenoGraph clustering. The scale of expression on the tSNE plots is indicated in the top left corner. The scaled expression of the indicated markers is shown as boxplots on the right, with each boxplot corresponding to an individual patient.

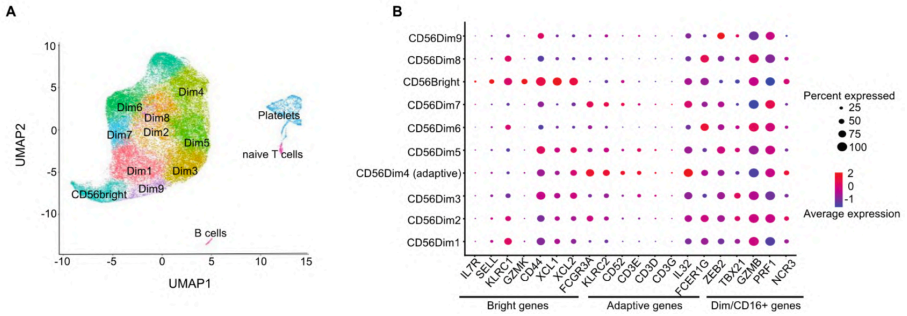

Figure S6. Single cell RNA sequencing characterization of donor infusion products yields distinct NK cell subpopulations. A Distribution of NK cell clusters among all patient infusion products within the gene expression UMAP space identifies a number of CD56^{dim} populations among the CIML NK cells. A CD56^{bright} NK cluster is identified that could not be well-characterized with mass cytometry. B Dot plot of genes characterizing the individual CD56^{dim} and CD56^{bright} NK subpopulations among all CIML NK infusion products.

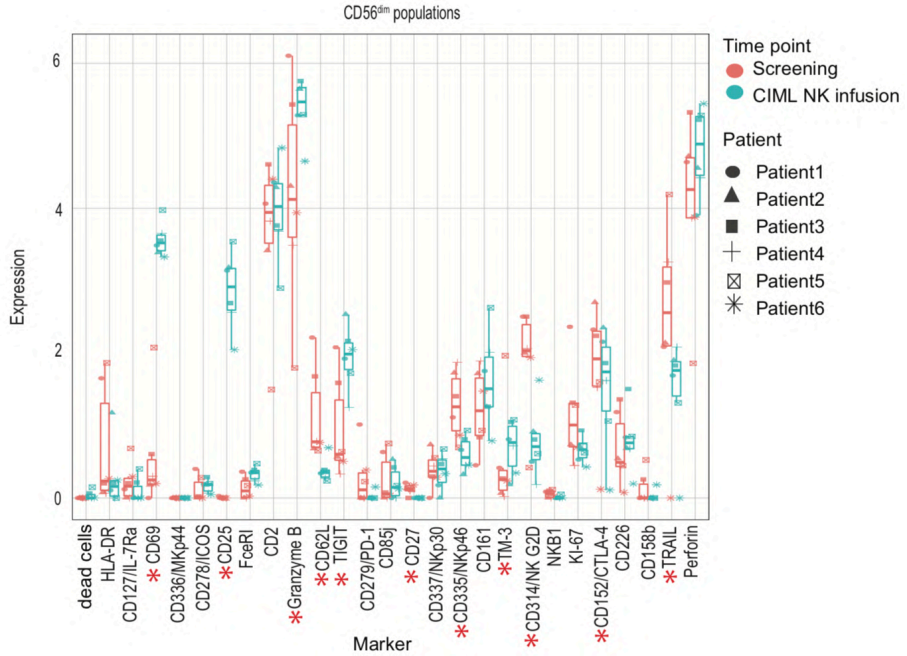

Figure S7. Differential expression analysis of marker expression on CD56^{dim} populations in the infusion product compared to the screening time point. CD56^{dim} NK cells from the screening time point before CIML NK infusion (red) from all patients treated on the trial are compared to the CD56^{dim}

NK cells in the infusion product (green). * p<0.05 by Wilcoxon rank sum test, with significance adjusted for multiple comparisons (43).

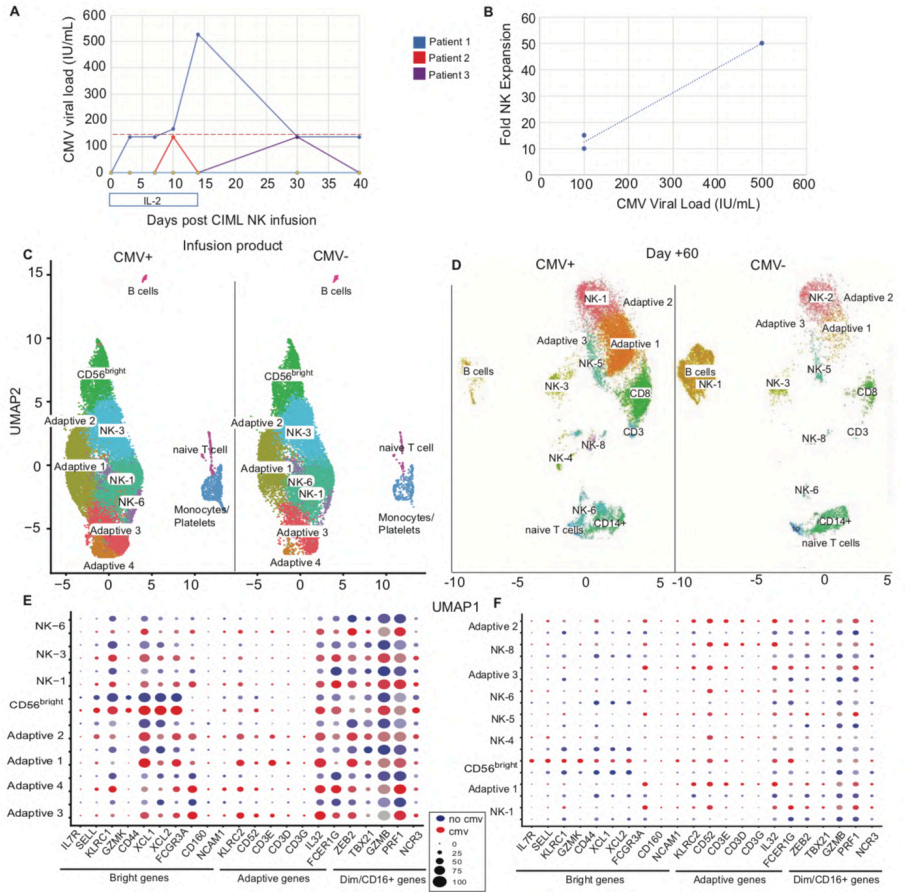

Figure S8. CMV reactivation is associated with expansion of an adaptive NK cell population, while non-adaptive NK cell subpopulations expand independently of CMV. A CMV reactivation occurred in 3/6 treated patients, with viral load measured using a clinical grade assay. B Correlation between CMV viral load after reactivation and fold NK expansion in the 3 patients in whom CMV reactivated. C Gene expression UMAP of CIML NK infusion products in patients who reactivated CMV (CMV+) compared to those who did not (CMV-), showing a similar distribution of NK cell subpopulations. D Gene expression UMAP of NK cell subpopulations at the day +60 time point after CIML NK cell infusion. E Dot plot of NK cell subpopulations in the infusion product, showing genes associated with the adaptive NK cell phenotype, the CD56^{bright} NK cell phenotype, and with the CD56^{dim}/CD16^{+}

mature NK cell phenotype. Samples from both CMV- (blue dots) and CMV+ (red dots) are shown. F Dot plot of NK cell subpopulations at day +60 after CIML NK cell infusion, showing persistence of both adaptive and non-adaptive NK cells in both CMV+ and CMV- groups.

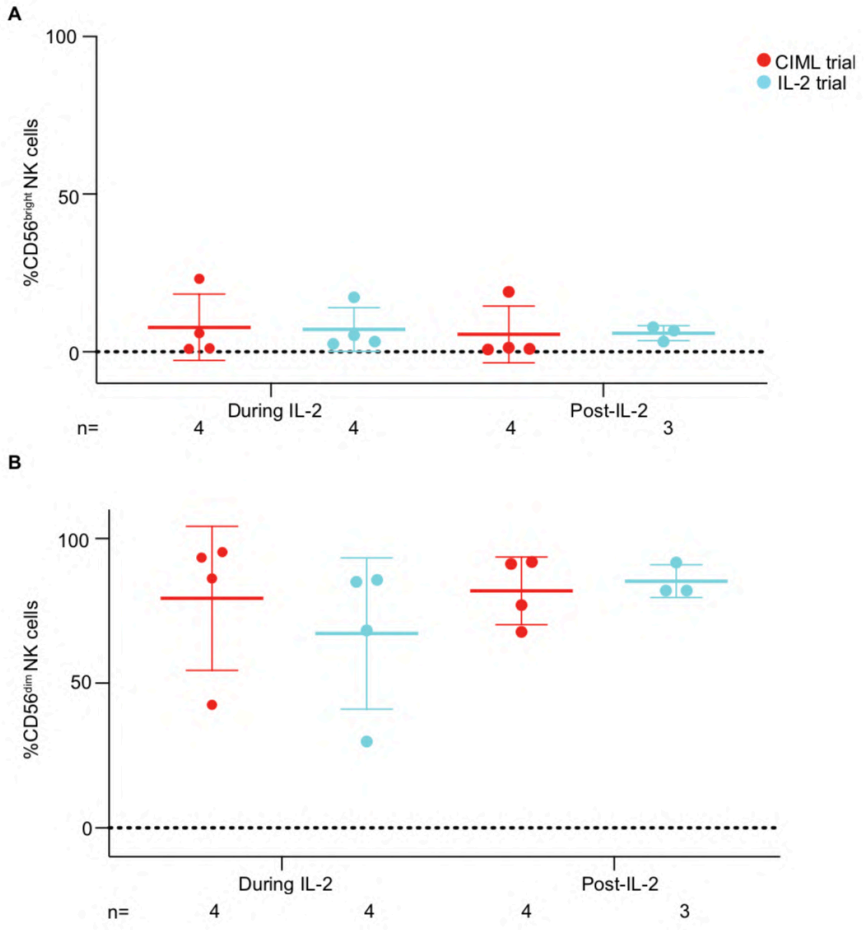

Figure S9. There is no difference in the percentage of peripheral blood NK cells that are CD56^{bright} or CD56^{dim} between post-HCT patients receiving IL-2 and CIML NK infusion patients receiving IL-2. A CD56^{bright} and B CD56^{dim} NK cells in the peripheral blood of patients treated with CIML NK cell infusion and post-transplant IL-2 treated patients. Data presented is CD56^{dim} and CD56^{bright} populations as a percentage of total CD56^{+}CD3^{-} lymphocytes as determined by flow cytometry. Mean + SD. $p > 0.05$ by Wilcoxon rank sum test, comparing CIML trial and IL-2 trial samples at each of the indicated time points.

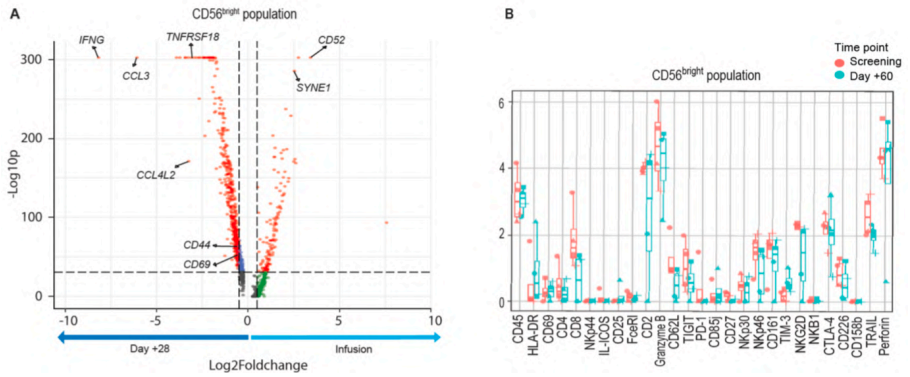

Figure S10. Evaluation of the CD56^{bright} NK cell population following CIML NK infusion. A Volcano plot showing most differentially expressed genes between the CIML NK infusion product to the day+28 time point after infusion of CIML NK cells (p cut off = 10e-32, fold change cut off = 0.5). The Wilcoxon rank sum test was used to determine differentially expressed markers between the two groups, with significance adjusted for multiple comparisons (50). B Differential expression analysis of mass cytometry markers comparing the screening time point prior to CIML NK infusion to the day+60 time point after infusion ($p > 0.05$ by Wilcoxon rank sum test).

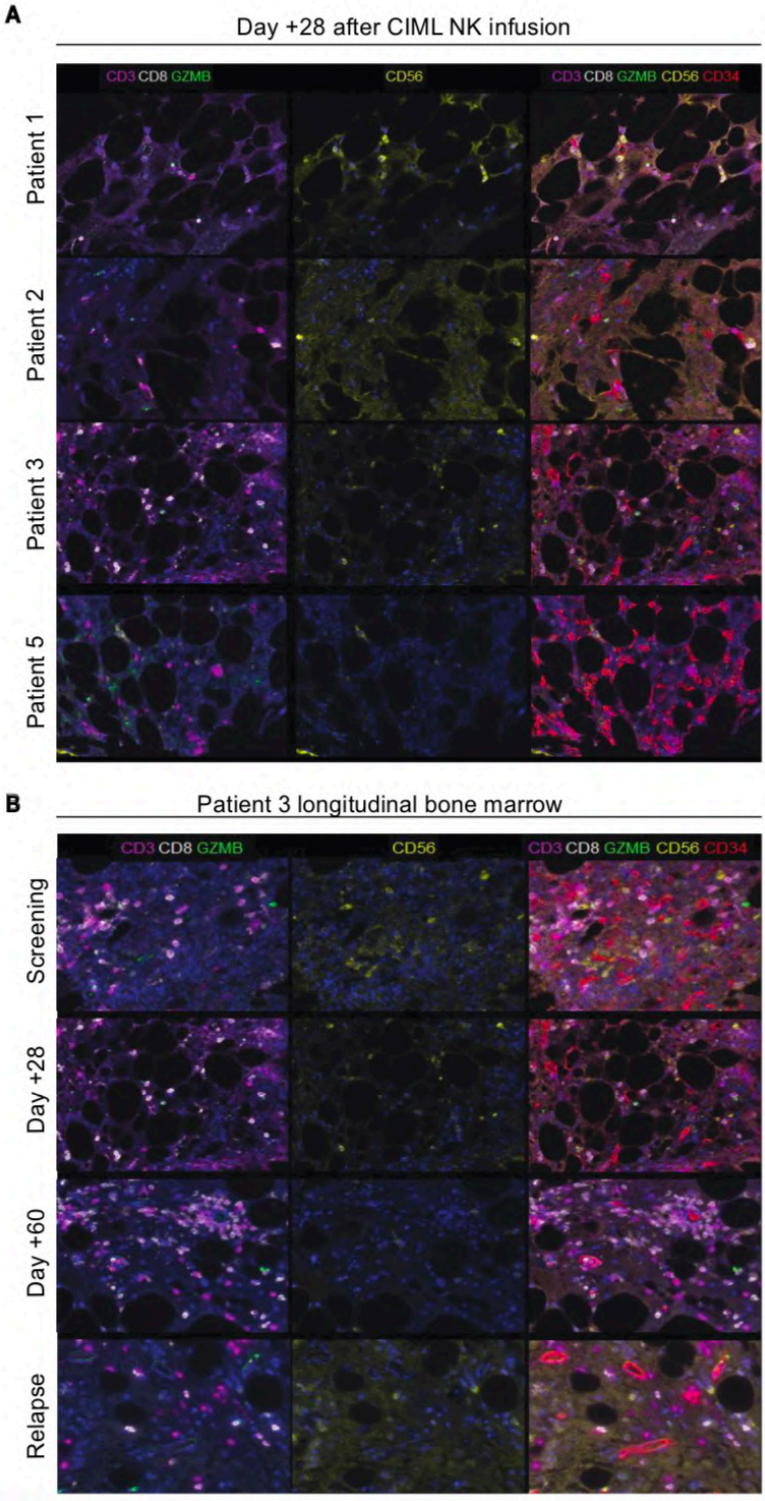
A
Day +28 after CIML NK infusion
CD3 CD8 GZMB
CD56
CD3 CD8 GZMB CD56 CD34
Patient 1
Patient 2
Patient 3
Patient 5
B
Patient 3 longitudinal bone marrow
CD3 CD8 GZMB
CD56
CD3 CD8 GZMB CD56 CD34
Screening
Day +28
Day +60
Relapse

Figure S11. NK cell infiltration into the bone marrow following CIML NK infusion. A Distribution of markers in bone marrow core biopsies from each patient taken at day +28 following CIML NK infusion in patients with bone marrow disease. Shown are $CD3^+$ cells (purple), $CD8^+$ cells (white), $CD56^+$ cells (yellow), and juxtaposition of these cells next to $CD34^+$ cells (blasts). B Longitudinal bone marrow core samples in representative patient 3. The time points correspond to screening (prior to CIML NK infusion), day +28 following CIML NK, day +60 following CIML NK infusion, and relapse (day +120 following CIML NK infusion).

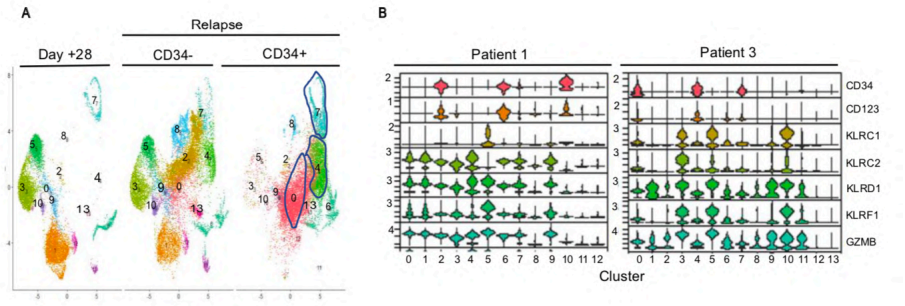

Figure S12. Identification of $CD34^+$ blasts relapsed following CIML NK therapy in patient. A Representative UMAP plot of scRNAseq data applied to both $CD34^-$ and $CD34^+$ fractions of post-CIML NK relapse sample from patient 3. The clusters at relapsed are compared to the clusters at day +28 following CIML NK cell infusion. Clusters 0, 4, and 7 represent relapsed leukemia blasts. B Violin plots corresponding to relapse clusters in both patient 1 and patient 3, both of whom had $CD34^+CD123^+$ blasts in the peripheral blood. The remaining clusters express NK cell genes.

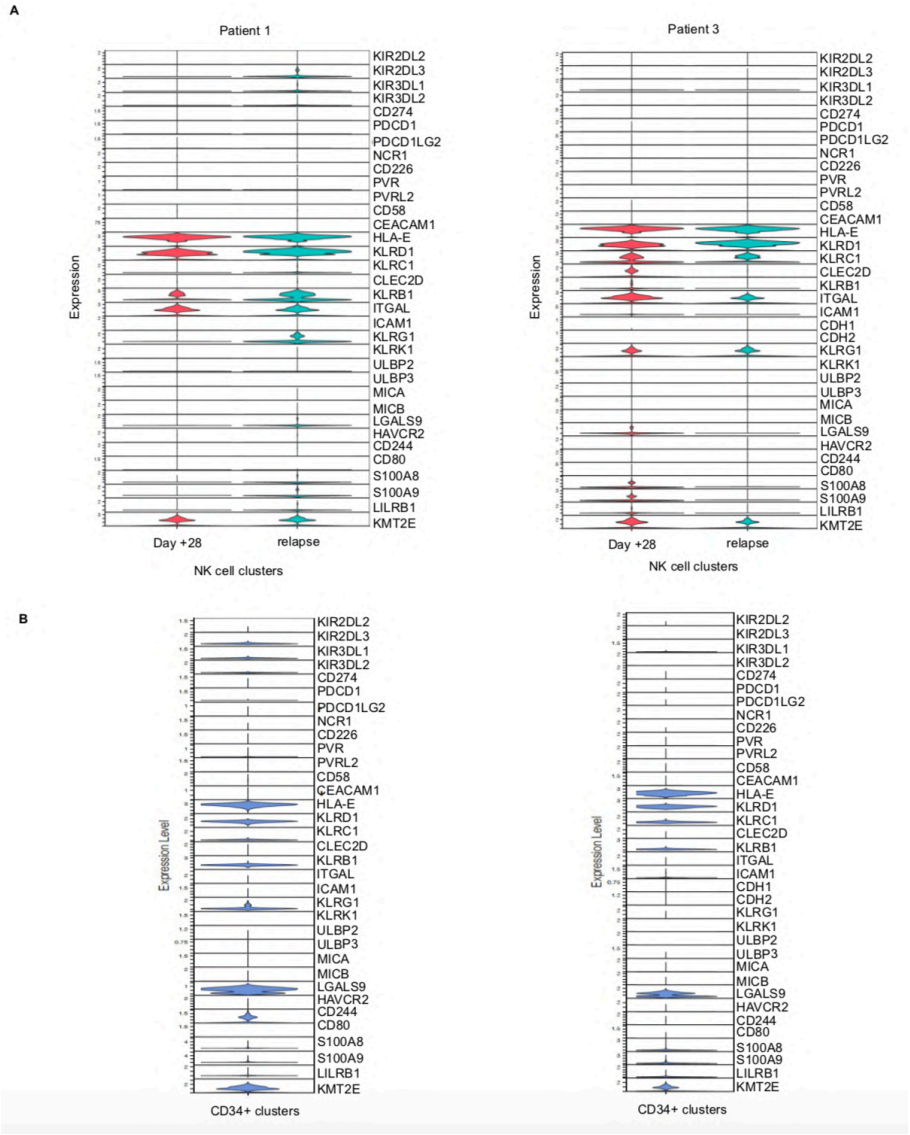

Figure S13. Single-cell RNA sequencing of peripheral blood mononuclear cells from Patient 1 (left) and Patient 3 (right) at the day +28 and relapse time points, with the cells from the latter fraction separated into CD34-depleted ($CD34^-$) fractions (A) and CD34-enriched ($CD34^+$) fractions (B). A Within the CD34-depleted fraction, NK cell clusters were identified based on the expression of the markers NCAM1, KLRD1, KLRF1, NCR1, NKG7, GNLY, CD3D, CD3E, and CD3G. Violin plots show gene expression of known NK receptors on the NK cell clusters in both patients. B Within the CD34-enriched fraction, clusters corresponding to leukemia blasts were

identified based on the expression of CD34 and CD123, and absence of the aforementioned NK cell markers. Violin plots show the expression of known NK activating and inhibitory ligands on leukemia blasts in Patient 1 (left) and Patient 3 (right).

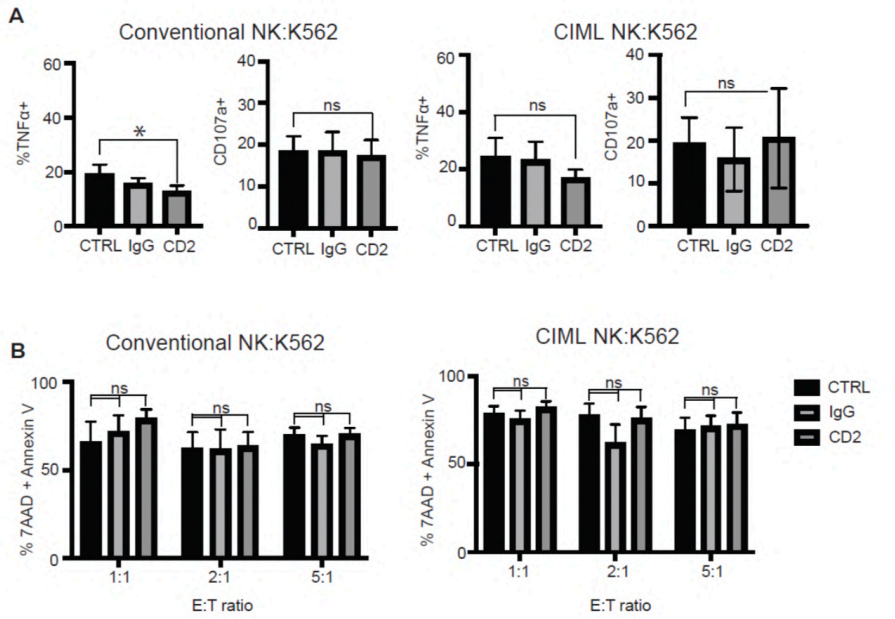

Figure S14. CD2 blockade is not sufficient to alter the function of CIML NK cells *in vitro*. A Conventional and CIML NK cells from healthy donors were preincubated with an anti-human mAb against CD2 or an IgG1 isotype control for 30 minutes before coculture with K562 for 6 hours at an E:T ratio of 5:1. Data presented show the mean percentage ± SEM of NK cells that were positive for TNFα and CD107a. n= 6 healthy donors in 2 independent experiments. B Following preincubation for 30 minutes with mAb against CD2 or an IgG1 isotype control, CIML and conventional NK cells were co-cultured with K562 at 3 E:T ratios for 4 hours. Data presented is the mean percentage ± SEM of 7AAD and Annexin V positive K562 target cells. N=6 healthy donors in 2 independent experiments. * $p<0.05$ with Wilcoxon matched pairs signed rank test.

Patient	Diagnosis[A]	Treatment prior to CIML NK (#months relative to HCT)[B]	CMV serostatus and reactivation[C]	Response at Day +28[D]	Adverse Events
Patient 1	Secondary AML with FLT3-ITD	(-3m) 3+7 + Midostaurin (0m) RIC PBSC HCT (8m) Relapse (9m) Gilteritinib (11m) added Decitabine (12m) added Venetoclax (14m) CIML NK	Donor: **seropositive** Recipient: **seronegative** Day of reactivation post-CIML NK: **day +4[D]**	Morphologic leukemia-free state	Fever Prolonged pancytopenia requiring stem cell boost
Patient 2	MDS with excess blasts II, multiple pathogenic mutations	(-8m) AZA x 2 (-5m) AZA + Venetoclax x 2 (0m) RIC PBSC HCT (7m) Relapse (8m) CIML NK	Donor: **seropositive** Recipient: **seropositive** Day of reactivation post-CIML NK: **day +10**	Complete Remission	Fever Prolonged pancytopenia requiring stem cell boost Fungal infection
Patient 3	Secondary AML with TP53 mutation, multiple other pathogenic mutations	(-4m) 3+7 (0m) RIC PBSC HCT (14m) Relapse (15m) CIML NK	Donor: **seropositive** Recipient: **seropositive** Day of reactivation post-CIML NK: **day +20**	Complete Remission	Cytokine Release Syndrome Pancytopenia
Patient 4	BPDCN	(-2m) Tagraxofusp (0m) RIC PBSC HCT (10m) Relapse (11m) CIML NK	Donor: **seronegative** Recipient: **seronegative** Day of reactivation post-CIML NK: **no reactivation**	Complete Remission	Fever
Patient 5	Secondary AML with multiple pathogenic mutations	(-34m) clinical trial #1[E] (-28m) RIC DUCBT (-11m) Relapse (-11m) clinical trial #2 (-9m) clinical trial #3 (-6m) Decitabine + Venetoclax (0m) RIC PBSC HCT (18m) Relapse (20m) CIML NK	Donor: **seronegative** Recipient: **seronegative** Day of reactivation post-CIML NK: **no reactivation**	Refractory to therapy	Fever
Patient 6	CML with blast crisis	(-30m) Dasatinib (-6m) 3+7 + imatinib (0m) MAC PBSC HCT (4m) Relapse (5m) Ponatinib (7m) CIML NK	Donor: **seropositive** Recipient: **seropositive** Day of reactivation post-CIML NK: **no reactivation**	Refractory to therapy	Elevations in ALT and AST during IL-2 injections

Table S1. Clinical characteristics and outcomes of patients treated with CIML NK cells.

[A] AML: acute myeloid leukemia, MDS: myelodysplastic syndrome, BPDCN: blastic plasmacytic dendritic cell neoplasm, 3+7: induction chemotherapy with daunorubicin and cytarabine, AZA: azacytidine, RIC: reduced intensity conditioning, PBSC: peripheral blood stem cell graft, DUCBT: double-umbilical cord blood transplant

[B] Refers to sequence of therapy and disease status prior to CIML NK cell therapy. The date of treatment or disease status is indicated as relative to the date of haploidentical stem cell transplant (HCT), and is reported in the number of months. Dates prior to HCT are reported with a negative number of months.

[C] Refers to CMV reactivation as measured with a clinical grade viral load PCR assay, with the time indicated relative to Day 0, the day of CIML NK cell infusion

[D] Refers to number of days from the date of CIML NK infusion, which is day 0

[E] The therapy administered in all prior clinical trials did not meet any exclusion criteria for the CIML NK phase I trial

	p_val	avg_log2FC	pct.1	pct.2	p_val_adj
SH3BGRL3	0	1.65331181	0.974	0.888	0
CD52	0	3.97972095	0.948	0.172	0
TXNIP	0	3.0052993	0.983	0.623	0
S100A6	0	1.66046365	0.884	0.613	0
S100A4	0	2.61905797	0.953	0.415	0
ZFP36L2	0	1.83817706	0.772	0.387	0
CXCR4	0	1.55517544	0.44	0.075	0
SPON2	0	1.92245792	0.486	0.066	0
FGFBP2	0	2.44657005	0.797	0.31	0
PLAC8	0	1.9099973	0.688	0.205	0
GZMK	0	1.89216035	0.282	0.082	0
GZMA	0	2.11772155	0.934	0.596	0
HLA-DRB1	0	1.74417085	0.702	0.276	0
HLA-DPA1	0	1.55767892	0.716	0.383	0
HLA-DPB1	0	1.83412091	0.75	0.264	0
SYNE1	0	1.80584775	0.611	0.106	0
ANXA1	0	1.93570063	0.836	0.322	0
CLIC3	0	2.27539824	0.664	0.113	0
IFITM2	0	2.37491916	0.946	0.511	0
LSP1	0	1.59845272	0.732	0.274	0
HBB	0	2.01463116	0.268	0.006	0
AHNAK	0	1.90097637	0.722	0.19	0
CTSW	0	1.59840065	0.918	0.618	0
PTPRCAP	0	2.49806396	0.511	0.001	0
CD3E	0	1.78442371	0.614	0.177	0
KLRF1	0	1.54904867	0.566	0.218	0
C12orf75	0	1.54173437	0.693	0.27	0
CYBA	0	1.64655632	0.987	0.832	0
CCL5	0	1.91953293	0.934	0.769	0
GZMM	0	1.82067048	0.731	0.293	0
MYO1F	0	1.54492026	0.611	0.128	0
KLF2	0	1.81982876	0.876	0.401	0
HCST	0	2.16144266	0.947	0.699	0
TYROBP	0	2.26032535	0.899	0.531	0
NKG7	0	1.71676172	0.98	0.975	0
ITGB2	0	1.54818858	0.814	0.432	0
C1orf63	0	1.68819122	0.382	0	0
ATPIF1	0	1.77427207	0.42	0	0
ATP5I	0	1.58326068	0.375	0	0
GNB2L1	0	3.06501041	0.556	0	0
SEPT7	0	2.24526951	0.487	0	0
RARRES3	0	2.15968985	0.466	0	0
ATP5L	0	2.39470426	0.508	0	0
ATP5G2	0	1.88736811	0.425	0	0
TCEB2	0	2.1870572	0.492	0	0
ATP5E	0	3.55722961	0.573	0	0
ATP5D	0	1.54817761	0.372	0	0
UQCR11.1	0	1.98973427	0.452	0	0
AES	0	2.44035938	0.514	0	0
GLTSCR2	0	1.55772267	0.363	0	0

Table S2: Top 50 differentially expressed genes in CD56^{dim} NK cell clusters between infusion and day + 28

	p_val	avg_log2FC	pct.1	pct.2	p_val_adj
CD52	0	3.41543025	0.716	0.064	0
TXNIP	0	2.75710844	0.893	0.432	0
SYNE1	1.46E-290	2.53441101	0.703	0.142	4.07E-286
AHNAK	2.43E-242	2.06382346	0.721	0.238	6.80E-238
FGFBP2	7.89E-234	2.34423541	0.66	0.175	2.21E-229
FLNA	3.55E-193	1.47454092	0.817	0.546	9.92E-189
CD3E	1.64E-191	2.11837858	0.55	0.11	4.58E-187
MYO1F	2.23E-190	1.93276621	0.598	0.154	6.23E-186
ZFP36L2	9.08E-187	1.81076321	0.719	0.369	2.54E-182
SYNE2	1.05E-181	1.4538044	0.807	0.512	2.93E-177
LSP1	1.22E-179	1.86455679	0.617	0.214	3.43E-175
GNB2L1	6.42E-179	2.56115414	0.412	0	1.80E-174
AES	7.02E-176	2.50267211	0.406	0	1.97E-171
ATP5E	6.33E-174	2.60946411	0.403	0	1.77E-169
PPP2R5C	1.48E-165	1.42645973	0.764	0.478	4.14E-161
CEP78	5.14E-163	2.01447744	0.532	0.138	1.44E-158
ITGAL	2.92E-162	1.65468092	0.646	0.277	8.18E-158
S100A4	6.60E-156	1.93165464	0.617	0.249	1.85E-151
CXCR4	8.46E-155	2.2292528	0.428	0.046	2.37E-150
C1orf63	1.64E-150	2.19578669	0.359	0	4.60E-146
PIK3R1	2.20E-148	1.79271327	0.631	0.312	6.17E-144
SPON2	1.73E-144	2.01129084	0.416	0.05	4.85E-140
EVL	1.01E-142	1.54721041	0.633	0.294	2.82E-138
GZMM	9.99E-139	1.74313164	0.529	0.186	2.80E-134
SEPT7	1.36E-135	1.97662615	0.33	0	3.81E-131
PTPRCAP	1.14E-133	1.9471082	0.326	0	3.19E-129
CLIC3	6.07E-133	1.87405125	0.418	0.068	1.70E-128
RNF166	1.18E-125	1.87182167	0.4	0.066	3.31E-121
IFITM2	1.55E-119	1.7243972	0.534	0.233	4.35E-115
SIGIRR	5.46E-118	1.75242777	0.396	0.079	1.53E-113
ADD3	7.17E-118	1.6197146	0.472	0.144	2.01E-113
TMEM2	1.72E-116	1.79550939	0.291	0	4.81E-112
MIR142	3.02E-112	1.73403551	0.282	0	8.44E-108
MATR3	1.09E-110	1.63500419	0.28	0.001	3.04E-106
GLTSCR2	1.68E-108	1.64528312	0.274	0	4.71E-104
ATP5L	2.02E-106	1.58086705	0.269	0	5.66E-102
TRAF3IP3	1.01E-104	1.52752185	0.408	0.109	2.83E-100
FYB	3.32E-104	1.62696743	0.265	0	9.29E-100
TCEB2	5.27E-102	1.50250187	0.26	0	1.48E-97
RARRES3	1.17E-98	1.48095953	0.252	0	3.28E-94
HBB	1.50E-98	7.57984421	0.259	0.004	4.20E-94
ANXA1	1.61E-97	1.52293179	0.452	0.169	4.52E-93
TSPAN32	7.88E-97	1.46555292	0.26	0.007	2.21E-92
RASGRP2	1.67E-96	1.54118622	0.281	0.02	4.67E-92
SAMD3	7.50E-95	1.42581733	0.419	0.136	2.10E-90
RNF125	8.22E-90	1.53670272	0.345	0.078	2.30E-85
RBL2	3.85E-88	1.55776093	0.368	0.106	1.08E-83
CNOT6L	5.38E-77	1.52702371	0.431	0.194	1.51E-72
ATG2A	1.76E-75	1.46246015	0.292	0.061	4.92E-71
GZMA	7.85E-6	1.47955672	0.556	0.359	2.20E-63

Table S3: Top 50 differentially expressed genes in CD56^{bright} NK cell clusters between infusion and day +28

	p_val	avg_log2FC	pct.1	pct.2	p_val_adj
AC092580.4	0	1.4779754	0.359	0	0
AES	0	2.76725441	0.648	0	0
ATP5D	0	1.7596341	0.452	0	0
ATP5E	0	3.83398683	0.717	0	0
ATP5G2	0	2.12903297	0.522	0	0
ATP5G3	0	1.62384338	0.414	0	0
ATP5I	0	1.78379868	0.453	0	0
ATP5J	0	1.53747166	0.398	0	0
ATP5J2	0	1.63283646	0.425	0	0
ATP5L	0	2.64266367	0.621	0	0
ATPIF1	0	1.97915341	0.496	0	0
C14orf2	0	1.63054298	0.421	0	0
C19orf43	0	1.76281172	0.448	0	0
C1orf63	0	2.0174922	0.487	0	0
C9orf142	0	1.64491835	0.413	0	0
CD3E	0	1.29820465	0.757	0.325	0
FAM65B	0	1.49932932	0.364	0	0
FYB	0	1.65372855	0.397	0	0
GLTSCR2	0	1.82301591	0.46	0	0
GNB2L1	0	3.33028553	0.7	0	0
GPR56	0	1.44789096	0.341	0	0
IL32	0	1.32768016	0.954	0.562	0
KIAA1551	0	1.42232532	0.339	0	0
KLRC2	0	1.62574862	0.663	0.242	0
MATR3	0	1.66987422	0.414	0	0
MINOS1	0	1.35789976	0.35	0	0
MIR142	0	1.69421205	0.403	0	0
MYEOV2	0	1.5530903	0.409	0	0
NDUFB8.1	0	1.66278626	0.434	0	0
PTPRCAP	0	2.75664284	0.634	0.001	0
RARRES3	0	2.36319521	0.569	0	0
SEPT7	0	2.48928405	0.6	0	0
SEPW1	0	1.38196054	0.353	0	0
SF3B14	0	1.26828252	0.332	0	0
TCEB2	0	2.43125446	0.6	0	0
TMEM2	0	1.53594732	0.355	0	0
TMEM66	0	1.58271183	0.401	0	0
UQCR11.1	0	2.19370078	0.55	0	0
USMG5	0	1.66462395	0.431	0	0
TMBIM4.1	2.070E-321	1.21335159	0.31	0	5.42382E-317
SELK	2.500E-321	1.22242695	0.31	0	6.5527010E-317
WHSC1L1	9.097E-320	1.25582106	0.308	0	2.38920571E-315
LSMD1	1.8320168783E-313	1.18548997	0.303	0	0.00E+00
ALDOA	0.00E+00	1.35181772	0.441	0.126	1.02E-304
U2AF1	4.19E-308	1.33559683	0.381	0.039	1.10E-303
NHP2L1	2.78E-307	1.16647545	0.298	0	7.29E-303
C20orf24	1.05E-301	1.19194305	0.294	0	2.75E-297
MGEA5	2.45E-300	1.24916678	0.292	0	6.43E-296
SEPT9	9.86E-291	1.19018818	0.284	0	2.59E-286
CD3D	7.70E-183	1.45615361	0.315	0.053	2.02E-178

Table S4: Top 50 differentially expressed genes in adaptive NK cell clusters between CMV^+ and CMV^- groups

	p_val	avg_log2FC	pct.1	pct.2	p_val_adj
HBA1	0	0.6608472	0.686	0.041	0
HBA2	0	0.73567322	0.682	0.007	0
HBB	0	0.68960964	0.644	0.001	0
HBG1	0	0.45516876	0.331	0	0
HBG2	0	0.69251925	0.417	0	0
FOS	4.28E-229	0.30346976	0.614	0.289	8.55E-226
SNORD3B-2	2.23E-115	0.32173532	0.333	0.116	4.46E-112
HBA11*	0	0.64873468	0.707	0.038	0
HBA21	0	0.58470732	0.674	0.007	0
HBB1	0	0.4813301	0.677	0.002	0
HBG21	2.9881E-319	0.76336277	0.386	0	5.97621810E-316
HBG11	4.59E-251	0.61967926	0.312	0	9.19E-248
AKR1C3	1.84E-211	0.31075672	0.479	0.132	3.69E-208
SNORD3A1	3.86E-97	0.38469356	0.39	0.148	7.72E-94
WDR74	2.58E-91	0.33721122	0.497	0.26	5.17E-88
SNORD3B-21	7.40E-63	0.3035759	0.227	0.066	1.48E-59
HBB2	5.02E-215	0.63773936	0.785	0.005	1.00E-211
HBA22	4.52E-192	0.83533409	0.73	0.004	9.05E-189
YWHAH	1.68E-183	0.32109328	0.752	0.056	3.36E-180
HBA12	3.78E-170	0.63136327	0.693	0.02	7.56E-167
LGALS3	4.31E-165	0.31754888	0.804	0.141	8.63E-162
IGFBP7	7.42E-165	0.38121629	0.739	0.074	1.48E-161
RANBP1	2.31E-160	0.30437346	0.718	0.073	4.63E-157
C1orf561	2.14E-137	0.31171922	0.856	0.265	4.29E-134
CCL3	2.80E-104	0.41372658	0.549	0.063	5.60E-101
RNU12	5.93E-102	0.36551292	0.46	0.011	1.19E-98
HBG22	2.90E-89	1.16468274	0.38	0	5.80E-86
FOSB	5.94E-86	0.59769954	0.567	0.101	1.19E-82
TNFRSF18	3.10E-76	0.30856559	0.669	0.247	6.19E-73
HIST1H2AC	3.06E-72	0.32513061	0.417	0.048	6.11E-69
HBG12	1.42E-70	0.51878803	0.307	0	2.83E-67
FOS1	4.17E-67	0.4331315	0.497	0.117	8.33E-64
IER2	3.53E-63	0.33575119	0.712	0.308	7.06E-60
SLAMF7	8.63E-48	0.34283179	0.448	0.133	1.73E-44
TRIP11	8.26E-44	0.31395986	0.371	0.092	1.65E-40
PYCARD	7.87E-29	0.57527888	0.31	0.069	1.57E-25
SNORD3B-22	1.48E-26	0.41087487	0.261	0.055	2.95E-23
CCL4	2.71E-25	0.84084499	0.574	0.287	5.41E-22
HSPA1A	2.02E-23	0.52299782	0.175	0.028	4.04E-20
HBB3	2.24E-140	0.59562776	0.687	0.002	4.48E-137
HBA23	3.31E-131	0.42161268	0.649	0.006	6.62E-128
HBA13	7.55E-110	0.31291468	0.632	0.037	1.51E-106
IFNG	5.32E-103	0.39581654	0.675	0.085	1.06E-99
PTGDS	1.62E-93	0.6093024	0.57	0.051	3.23E-90
HBG23	1.12E-78	0.61712815	0.427	0	2.24E-75
FCRL3	6.74E-70	0.32678229	0.512	0.064	1.35E-66
PPP1R12A	1.59E-66	0.31396117	0.874	0.423	3.18E-63
HBG13	1.62E-66	0.56972567	0.368	0	3.24E-63
SNORD3B-23	2.60E-26	0.50264403	0.427	0.131	5.21E-23
PPP1R101	6.38E-25	0.35182414	0.594	0.3	1.28E-21

* Genes that are differentially expressed in more than one NK cell cluster have a numerical digit appended at the end of their name corresponding to the order of their appearance

Table S5: Top 50 differentially expressed genes in NK cell clusters between day + 28 and relapse Patient 1

	p_val	avg_log2FC	pct.1	pct.2	p_val_adj
RPS18	0	0.700509	1	1	0
RPS6	0	0.76173785	0.999	0.997	0
EEF1B2	2.65E-210	0.77566438	0.982	0.943	5.06E-206
GIMAP7	5.59E-199	1.11587312	0.76	0.466	1.07E-194
TXNIP	3.77E-184	0.82871694	0.964	0.898	7.20E-180
PIM1	1.06E-70	0.70949004	0.31	0.115	2.02E-66
CD63	1.17E-67	0.67785939	0.614	0.434	2.24E-63
JUN	6.02E-61	0.86009722	0.635	0.461	1.15E-56
IL7R	5.40E-54	0.87082682	0.437	0.322	1.03E-49
FOS	4.56E-44	0.73085073	0.52	0.357	8.70E-40
GNLY	1.79E-30	0.93158689	0.474	0.339	3.43E-26
KLRD11*	7.49E-121	0.66830854	0.923	0.827	1.43E-116
GIMAP71	8.22E-70	0.67472664	0.696	0.484	1.57E-65
CCL4	1.11E-66	0.80084414	0.815	0.673	2.13E-62
JUNB	9.06E-65	0.74750387	0.644	0.476	1.73E-60
TSC22D31	3.29E-60	0.69771497	0.582	0.39	6.29E-56
FOS1	6.89E-53	0.79958494	0.454	0.254	1.32E-48
JUN1	2.77E-48	0.80594125	0.509	0.33	5.28E-44
GIMAP72	3.12E-57	0.79535422	0.661	0.406	5.96E-53
CCL41	6.91E-52	1.00953839	0.884	0.772	1.32E-47
GIMAP12	2.33E-43	0.71288445	0.294	0.1	4.45E-39
CCL31	8.79E-33	1.00561965	0.381	0.223	1.68E-28
JUN2	6.01E-29	0.75015941	0.527	0.341	1.15E-24
FOS2	1.10E-24	0.66940254	0.537	0.375	2.10E-20
PTGDS	1.59E-14	1.19419469	0.158	0.093	3.03E-10
RPS183	6.93E-125	0.75125554	1	1	1.32E-120
RPL133	4.01E-119	0.71053855	1	1	7.66E-115
TPT13	3.73E-103	0.85552981	1	1	7.12E-99
RPS63	3.19E-91	0.75093638	1	1	6.08E-87
EEF1B23	3.55E-84	0.93643545	0.991	0.983	6.78E-80
RPL83	2.24E-80	0.751967	0.999	0.994	4.28E-76
IL7R1	1.04E-74	2.15841253	0.735	0.251	1.99E-70
RPS53	3.00E-60	0.68805089	0.996	0.992	5.73E-56
XCL1	1.85E-46	1.42752161	0.613	0.179	3.53E-42
XCL22	3.45E-46	1.36426031	0.797	0.452	6.58E-42
FOS3	1.00E-43	1.41131223	0.763	0.581	1.91E-39
KLRD13	3.83E-41	0.77951748	0.938	0.915	7.31E-37
GIMAP73	1.07E-39	0.86547934	0.72	0.642	2.04E-35
TSC22D33	3.80E-28	0.87787925	0.745	0.609	7.26E-24
CMC11	1.02E-27	0.87037086	0.854	0.705	1.95E-23
SPTSSB	2.44E-27	0.98625473	0.32	0.047	4.67E-23
HIST1H4C3	2.36E-25	0.69646004	0.642	0.545	4.51E-21
JUN3	4.95E-24	1.00508101	0.695	0.559	9.44E-20
DUSP13	1.07E-23	0.85891481	0.588	0.479	2.04E-19
TNFRSF18	1.74E-23	0.91695844	0.445	0.163	3.32E-19
MAL	5.15E-23	0.9940858	0.231	0.025	9.82E-19
LTB2	2.86E-22	1.18456058	0.604	0.366	5.46E-18
XBP13	2.91E-19	0.69847236	0.636	0.488	5.56E-15
C1orf1623	1.70E-16	0.71063648	0.527	0.298	3.24E-12
EVA1B	3.57E-14	0.78676492	0.299	0.14	6.82E-10

* Genes that are differentially expressed in more than one NK cell cluster have a numerical digit appended at the end of their name corresponding to the order of their appearance

Table S6: Top 50 differentially expressed genes in NK cell clusters between day + 28 and relapse patient 3

Antibody	Fluorochrome	Clone	Amount (uL)	Vendor	Catalog #
CD16	FITC	3G8	2.0	BD	555406
PD-1	PE	J105	2.0	Invitrogen	12-2799-42
CD95	PeCF594	DX2	1.0	BioLegend	305633
NKG2D	APC	1D11	10.0	BD	558071
CD8	Alexa 700	RPA-T8	1.0	BioLegend	301027
CD3	BV786	UCHT1	2.0	BioLegend	300472
CD56	BV605	NCAM	1.0	BioLegend	318333
CD6	BV650	M-T605	2.0	BD	743448
CD57	PerCP Cy5.5	HNK-1	2.0	BioLegend	359621
NKG2A	BV421	131411	1.0	BD	747924
CD158a	PeCy7	DX27	1.0	BioLegend	312609
CD158b	PeCy7	HP-MA4	1.0	BioLegend	339511
CD158e	PeCy7	DX9	1.0	BioLegend	312720

Beckton Dickinson and Company, NJ, USA; Biolegend, CA, USA; Invitrogen, MA, USA; Miltenyi Biotec, North Rhine-Westphalia, Germany

Table S7: Flow cytometry antibodies for NK cell subsets

Antibody	Fluorochrome	Clone	Amount (uL)	Vendor	Catalog #
CD25	FITC	m-A251	1.0	BioLegend	356105
PD-1	PE	J105	2.0	Invitrogen	12-2799-42
CD95	PeCF594	DX2	1.0	BioLegend	305633
TCR a/b	PeCy 7	IP26	1.0	BioLegend	306719
CD127	APC	eBioRDR5	5.0	Invitrogen	17-1278-42
CD8	Alexa 700	RPA-T8	1.0	BioLegend	301027
TCR g/d	APC-Vio 770	11F2	2.0	Miltenyi	130-113-501
TIM 3	BV421	F38-2E2	5.0	BioLegend	345007
CD4	BV510	RPA-T4	2.0	BioLegend	300545
CD45RA	BV605	HL100	2.0	BioLegend	304133
CD6	BV650	M-T605	2.0	BD	743448
CCR7	BV711	G043-H7	5.0	BioLegend	353227
CD3	BV786	UCHT1	2.0	BioLegend	300472

Beckton Dickinson and Company, NJ, USA; Biolegend, CA, USA; Invitrogen, MA, USA; Miltenyi Biotec, North Rhine-Westphalia , Germany

Table S8: Flow cytometry antibodies for T cell subsets

Tag	Antibody	Clone	Manufacturer	Cat.no
89Y	CD45	HI30	Fluidigm	3089003B
116Cd	HLA-DR	L243	Biolegend	307651
141 Pr	CD3	UCHT1	Fluidigm	3141019B
142Nd	CD19	HIB19	Fluidigm	3142001B
143Nd	CD127/ IL-7Ra	A019D5	Fluidigm	3143012B
144Nd	CD69	FN50	Fluidigm	3144018B
145Nd	CD4	RPA-T4	Fluidigm	3145001B
146Nd	CD8	RPA-T8	Fluidigm	3146001B
147Sm	CD336/NKp44	253415	Biolegend	325121
148Nd	CD278/ ICOS	C398.4A	Fluidigm	3148019B
149Sm	CD25	2A3	Fluidigm	3149010B
150Nd	FceRI	AER-37(CRA-1)	Fluidigm	3150027B
151Eu	CD2	TS1/8	Fluidigm	3151003B
152Sm	Granzyme B	GB11	Novus Bio	NBP1-50071
153Eu	CD62L	DREG-56	Fluidigm	3153004B
154Sm	TIGIT	MBSA43	Fluidigm	3154016B
155Gd	CD279/PD-1	EH12.2H7	Fluidigm	3155009B
156Gd	CD85j	GIH/75	Fluidigm	3156020B
158Gd	CD27	L128	Fluidigm	3158010B
159Tb	CD337/NKp30	Z25	Fluidigm	3159017B
160Gd	CD14	M5E2	Fluidigm	3160001B
161Dy	CD158a,h/ KIR2DL1/DS1	MM0438-11G	Novus Bio	NBP2-11758
162Dy	CD335/NKp46	BAB281	Fluidigm	3162021B
163Dy	CD56	NCAM16.2	Fluidigm	3163007B
164Dy	CD161	HP-3G10	Fluidigm	3164009B
165Ho	TIM-3	B27	Biolegend	345019
166Er	CD314/NKG2D	ON72	Fluidigm	3166016B
167Er	NKB1	DX9	Fluidigm	3167013B
168Er	Ki-67	SK1	Fluidigm	3168007B
169Tm	CD159a/NKG2A	ON72	Fluidigm	3169013B
170Er	CD152/CTLA-4	14D3	Fluidigm	3170005B
171Yb	CD226	DX11	Fluidigm	3171013B
172Yb	NKG2C	134522	R&D	MAB1381
173YB	CD158b	DX27	Fluidigm	3173010B
174Yb	TRAIL	R4-01	Novus Bio	NBP1-45027
175Lu	Perforin	B-D48	Fluidigm	3175004B
176Yb	CD57	HCD57	Fluidigm	3176019B
209Bi	CD16	3G8	Fluidigm	3209002B

Biolegend, CA, USA; Fluidigm, CA, USA; Novus Biologicals, CO, USA; R&D systems, MN, USA

Table S9: Mass cytometry NK phenotype panel

Chapter 5

Phenotypic and functional characterization of the CD6-ALCAM T cell costimulatory pathway after allogeneic cell transplantation

Running Title: TARGETING CD6 FOR aGVHD TREATMENT

Benedetta Rambaldi[1,2], Haesook T. Kim[3], Yohei Arihara[1,4], Takeru Asano[1,5], Carol Reynolds[1], Mariah Manter[1], Max Halpern[1], Augustine Weber[1], John Koreth[1], Corey Cutler[1], Mahasweta Gooptu[1], Sarah Nikiforow[1], Vincent T. Ho[1], Joseph H. Antin[1], Rizwan Romee[1], Jeanette Ampudia[6], Cherie Ng[6], Stephen Connelly[6], Robert J. Soiffer[1] and Jerome Ritz[1]*

Affiliations

[1]Department of Medical Oncology, Dana-Farber Cancer Institute and Harvard Medical School, Boston, MA
[2]Ph.D. Program in Translational and Molecular Medicine (DIMET), University of Milano-Bicocca, Monza, Italy
[3]Department of Data Science, Dana-Farber Cancer Institute, Harvard T H Chan School of Public Health, Boston, MA
[4]Department of Medical Oncology, Sapporo Medical University
[5]Department of Hematology and Oncology, Himeji Red Cross Hospital, Hyogo, Japan 6Equillium, La Jolla, CA, USA

Synopsis

High expression of CD6 on Tcon and ALCAM on DCs and monocytes is maintained during aGVHD, representing a suitable therapeutic target. Itolizumab, an anti-CD6 monoclonal antibody, without inducing T-cell

depletion, abrogates ALCAM mediated T- cell proliferation upon TCR engagement.

Abstract

CD6 is a co-stimulatory receptor expressed on T cells that binds activated leukocyte cell-adhesion molecule (ALCAM), expressed on antigen presenting cells, epithelial and endothelial tissues. The CD6-ALCAM pathway plays an integral role in modulating T cell activation, proliferation, and trafficking. In this study we examined expression of CD6 by reconstituting T cells in 95 patients after allogeneic cell transplantation and evaluated the effects of itolizumab, an anti-CD6 monoclonal antibody, on T cell activation. CD6 T cells reconstituted early after transplant with Treg expressing lower levels of CD6 compared to Tcon and CD8 T cells. After onset of acute graft versus host disease (aGVHD), CD6 expression was further reduced in Treg and CD8 T cells compared to healthy donors, while no difference was observed for Tcon. ALCAM expression was highest in plasmacytoid dendritic cells (pDC), lowest in myeloid dendritic cells (mDC) and intermediate in monocytes and was generally increased after aGVHD onset. Itolizumab inhibited CD4 and CD8 T cell activation and proliferation in preGVHD samples, but inhibition was less prominent in samples collected after aGVHD onset, especially for CD8 T cells. Functional studies showed that itolizumab did not mediate direct cytolytic activity or antibody-dependent cytotoxicity in vitro. However, itolizumab efficiently abrogated the costimulatory activity of ALCAM on T cell proliferation, activation and maturation. Our results identify the CD6-ALCAM pathway as a potential target for aGVHD control and a phase I/II study using itolizumab as first line treatment in combination with steroids for patients with aGVHD is currently ongoing (NCT03763318).

Introduction

Acute graft versus host disease (aGVHD) continues to be an important cause of morbidity and mortality after allogeneic hematopoietic cell transplantation (HCT) (1). Steroids provide effective treatment, but most patients with severe aGVHD do not achieve a complete response (2,3). Moreover, steroid treatment is often associated with severe toxicities. Novel therapeutic options are needed and different strategies to selectively modulate alloreactive T cells and APCs have been studied for the treatment of steroid refractory GVHD. Various approaches are currently being evaluated in clinical trials including 1) targeting key inflammatory mediators (IL-6, siltuximab or tocilizumab), 2) selective depletion of alloreactive T cells (ricin-conjugated anti- CD3/CD7, anti-CD30 brentuximab, post-transplant cyclophosphamide), 3) modulation of cytokine-driven signal transduction (ruxolitinib), 4) inhibition of target organ homing (anti-integrinα4β7, vedolizumab) and 5) inhibition of costimulatory signals (abatacept) (4). Despite these advances, treatment of steroid refractory GVHD remains a challenge (5).

The costimulatory receptor CD6 is a 105-130 kDa type I transmembrane glycoprotein belonging to the highly conserved scavenger receptor cysteine-rich superfamily (SRCR-SF) (6). CD6 is expressed on the majority of T cells and minor populations of B and NK cells (7,8). CD166, activated leukocyte cell adhesion molecule (ALCAM) is the primary ligand for CD6 (9). ALCAM is expressed on APCs and various epithelial and endothelial cells (10,11). Upon ligation, the CD6-ALCAM complex helps stabilize the immunological synapse between the T cell and the APC. In this context, CD6-ALCAM binding promotes T cell activation, proliferation, maturation, and

trafficking from the intravascular space into tissues, including the central nervous system (12–17). Early studies by Soiffer and colleagues demonstrated that ex-vivo depletion of $CD6^+$ donor T cells prior to transplantation markedly decreased the incidence of aGVHD, highlighting the importance of $CD6^+$ T cells in pathogenesis of GVHD (18–21).

Itolizumab, a humanized IgG1 anti-CD6 monoclonal antibody, has been shown to block CD6 signaling, leading to a reduction in T cell activation and proliferation (22). Itolizumab therapy has been evaluated for treatment of different autoimmune disorders (9), such as severe chronic plaque psoriasis (23) and COVID-19 cytokine-release syndrome with promising results (24). However, it is not known whether blocking the CD6-ALCAM pathway with itolizumab can modulate T cell responses after allogeneic HCT in the setting of aGVHD.

In the present study, we characterized the expression of CD6 and ALCAM by reconstituting immune cells in a cohort of 95 patients who underwent allogeneic HCT and examined the effects of itolizumab on T cell responses *in vitro* in the setting of aGVHD. Our results show that T cells and dendritic cells (DCs) expressed CD6 and ALCAM, respectively early after HCT and surface expression of both structures is maintained during aGVHD. Then, we demonstrated the ability of itolizumab to inhibit *in vitro* T cell proliferation and activation in peripheral blood (PB) obtained from patients with aGVHD, in an ALCAM-dependent manner without causing T cell depletion. Our results provide new insights into the mechanisms of action of itolizumab and suggest that targeting the CD6-ALCAM costimulatory

pathway represents a novel approach for prevention and treatment of aGVHD.

Methods

Patients and sample collection

This study included 95 patients who underwent allogeneic HCT at the Dana-Farber Cancer Institute and Brigham and Woman's Hospital (Boston, MA) between September 2018 and January 2020. Blood samples were obtained at 1, 2, 3 and 6 months after transplant for analysis of CD6 and ALCAM expression. Samples from 9 healthy donors (HD) were used as controls. Samples from 9 additional patients and 9 HD were used for in vitro functional assays (**Supplemental Table S1**). Written informed consent was obtained from all patients and HD prior to sample collection, in accordance with the Declaration of Helsinki. Protocol approval was obtained from the Human Subjects Protection Committee of the Dana-Farber/Harvard Cancer Center.

Monitoring CD6 and ALCAM immune reconstitution

Immune reconstitution was evaluated by flow cytometry using fresh whole blood samples. For analysis, both percentages of positive cells and median fluorescence intensity (MFI) were considered. Two panels of directly conjugated monoclonal antibodies (**Supplemental Table S2**) were used to define the expression of CD6 and ALCAM on functionally distinct T cell and APC subsets, respectively. After staining, cells were acquired on a Fortessa LSR flow cytometer (BD) and analyzed using FlowJo and Cytobank software. Cell gating strategy

and markers used for cell subset definition are described in **Supplemental Figure S1 and S2**.

Functional activity of itolizumab *in vitro*

Frozen peripheral blood mononuclear cells (PBMC) obtained from patients who developed aGVHD after transplant (**Supplemental Table S1**) were stimulated using antiCD3/CD2/CD28 beads in the presence of itolizumab or isotype control cetuximab. T cell proliferation, activation and maturation were evaluated after 72 hours of culture using the flow cytometry panel in **Supplemental Table S3**. An example of the gating strategy used in this analysis is shown in **Supplemental Figure S3.** Detailed description of the protocol is provided in Supplemental Methods.

Complement dependent cytotoxicity (CDC), antibody direct cytotoxicity (ADC) and antibody dependent cellular cytotoxicity (ADCC) assays

The ability of itolizumab to induce CDC, ADC or ADCC was measured as the percentage of cell lysis in the presence of itolizumab compared to alemtuzumab as positive control or cetuximab as negative control. For ADCC evaluation we also measured the percent $CD107a^{+}$ cells on NK cells after 6 hours of culture (25). Detailed descriptions of CDC, ADC and ADCC protocols are provided in Supplemental Methods.

T cell stimulation using ALCAM-Fc and anti-CD3 antibody

Recombinant Human ALCAM Fc Chimera (ALCAM-Fc) and anti-CD3 Ab were resuspended in PBS overnight at 4'C in flat bottom 96

well plate. The day after, HD $CD3^+$ T cells were added and cultured in media with itolizumab or cetuximab for 96 hours. Cells were analyzed using flow cytometry (**Supplemental Table S4**). Detailed description of the protocol is provided in Supplemental Methods and **Supplemental Figure S3**.

Statistical analysis

Statistical methods are provided in Supplemental Methods.

Results

Patient characteristics

To investigate the expression of CD6 and its ligand ALCAM during immune reconstitution after allogeneic HCT, we prospectively studied a homogeneous population of 95 adult patients with hematological malignancies. Clinical characteristics of these patients are summarized in **Table 1**. Median patient age at the time of transplant was 61 years (range, 19-76). All patients received pre-transplant conditioning with busulfan and fludarabine and GVHD prophylaxis with tacrolimus and methotrexate. Half of the patients received a myeloablative conditioning regimen (50.5%) and almost all patients received PB stem cell (PBSC) grafts (97.9%). A matched unrelated donor (MUD) was used in 63 patients (66.3%). Median follow-up among survivors was 12 months (range, 4-20). Median donor T cell chimerism was 76% 1 month after HCT and 96% at 6 months (Table 2). Acute GVHD occurred in 42 patients (44.2%) at a median of 50 days after transplant (range 20-294 days).

	N (%)
Total	95 (100)
Patient Age at HCT, Median (Range), Years	61 (19-76)
Patient Sex, Male	55 (57.9)
Donor Age, Median (Range), Years	29 (18-67)
Donor Sex, Male	57 (60)
Donor type	
HLA Matched Related Donor	26 (27.4)
HLA Matched Unrelated Donor	63 (66.3)
Partially HLA Mismatched Unrelated Donor	6 (6.3)
Female Donor for Male Recipient	17 (18)
Patient or Donor CMV Serostatus, Positive	64 (67.4)
Disease	
ALL	6 (6.3)
AML	52 (54.7)
MDS	12 (12.6)
MPD	8 (8.4)
NHL	8 (8.4)
Others†	9 (9.6)
Disease Status at transplant	
Complete remission (CR)	66 (69.5)
Partial remission (PR)	2 (2.1)
Active Disease /Untreated	27 (28.4)
Cell Source	
Bone Marrow	2 (2.1)
Peripheral blood stem cells	93 (97.9)
Conditioning Intensity	
Myeloablative	48 (50.5)
Reduced intensity	47 (49.5)

Table 1. Patient characteristics. ALL, acute lymphoid leukemia; AML, acute myeloid leukemia; MDS, myelodysplastic syndrome; MPN, myeloproliferative neoplasm; NHL, non-Hodgkin lymphoma; CR, complete remission; PR, partial remission; †Chronic myeloid leukemia (CML, n=2); chronic lymphocytic leukemia (CLL, n=1); chronic myelomonocytic leukemia (CMML, n=3) and mixed myelodysplastic/ myeloproliferative neoplasm (Mixed MDS/MPN, n=3).

	N (%)
Engraftment	
ANC ≥ 500 cells/mm^3	95 (100)
% Donor T cell Chimerism - Median (Range)	
Day +30	76 (14-100)
Day +100	86 (24-100)
Day +180	96 (45-100)
Acute GVHD	42 (44.2)
Days to acute GVHD onset - Median (Range)	50 (20-294)
Maximum Grade	
1	16 (38.1)
2	17 (40.5)
3	3 (7.1)
4	6 (14.3)
Acute GVHD Sites	
Skin	31 (73.8)
Liver	6 (14.3)
Gut	17 (40.5%)
Acute GVHD patients treated systemically	34 (81%)
Steroid refractory acute GVHD	4 (11.8%)

Table 2. Engraftment, chimerism and acute GVHD outcomes.

CD6 is expressed on T cells early after transplant but expression levels vary in different T cell populations

We first examined the percent of T cells expressing CD6 as well as the level of CD6 expression on different T cell populations measured by median fluorescence intensity (MFI). While almost all T cells expressed CD6, expression level was highest in conventional CD4 T cells (Tcon) and lowest in CD4 regulatory T cells (Treg) while CD8 T cells displayed intermediate levels of CD6 expression (**Figure 1A and B**). CD6 expression was maintained at all time points after HCT and both percentage of CD6$^+$ cells and CD6 MFI were comparable between HD and patients at the different time points analyzed. The only exception was a reduction of CD6 MFI in Treg cells after transplant compared to HD. We also divided T cells into 5 maturation stages based

on the expression of CD45RA, CCR7 and CD95: Naïve ($CD45RA^+$, $CCR7^+$, $CD95^-$), Stem cell memory (SCM, $CD45RA^+$, $CCR7^+$, $CD95^+$), central memory (CM, $CD45RA^-$, $CCR7^+$), effector memory (EM, $CD45RA^-$, $CCR7^-$) and terminally differentiated effector memory (TEMRA, $CD45RA^+$, $CCR7^-$) (**Figure 1C**). As shown in the heat map in **Figure 1D**, Tcon subsets displayed the highest CD6 MFI. In both Tcon, Treg and CD8 T cells, CM T cells have the highest expression of CD6, while EM T cells express the lowest levels. CD6 expression was maintained after transplant at levels similar to HD, with the exception of lower CD6 MFI in CM and EM Treg in patients compared to HD. Finally, we examined whether CD6 was differentially expressed on PD-1 positive T cells, since PD-1 represents a marker of T cell activation and exhaustion that is upregulated after T cell receptor (TCR) engagement (26). For all 3 T cell populations, we observed that PD-1 positive T cells expressed significantly lower levels of CD6 compared to PD-1 negative T cells in both HD and patients after transplant (**Figure 1E**).

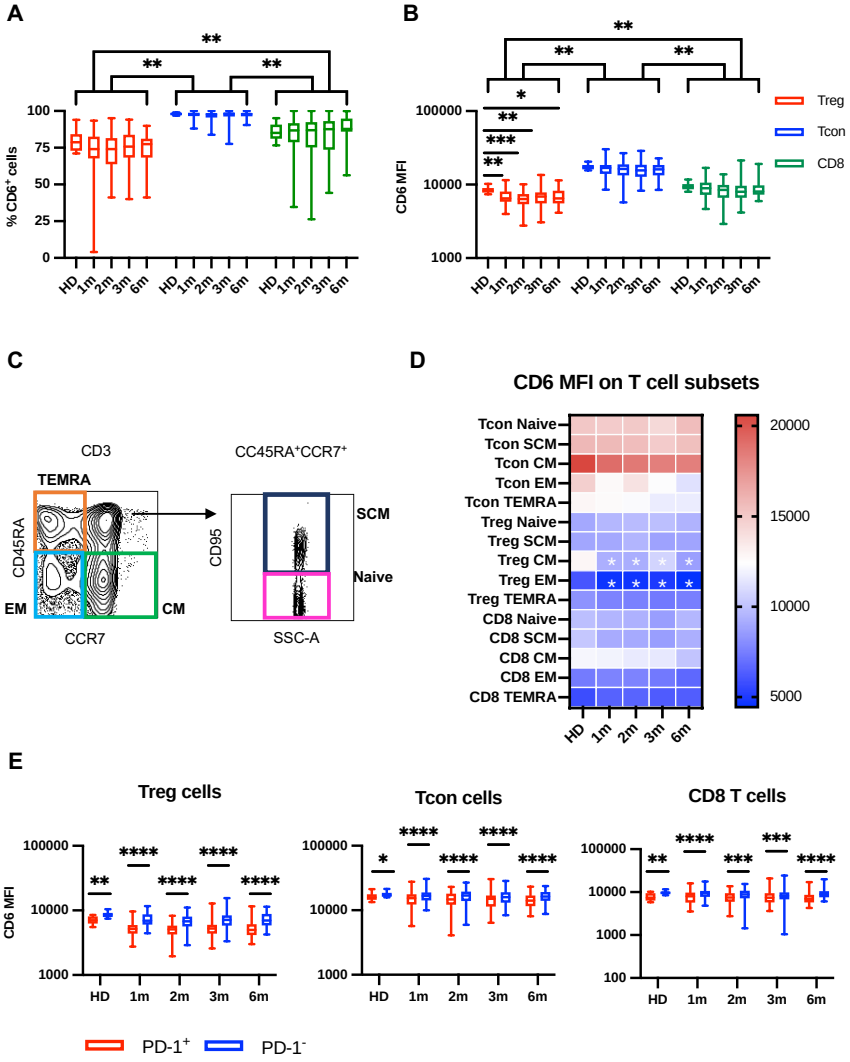

Figure 1. CD6 expression on T cells after HCT. (A) Percentage of CD6 positive cells and (B) CD6 median fluorescence intensity (MFI) on regulatory CD4 T cells (Treg, red boxes), conventional CD4 T cells (Tcon, blue boxes) and CD8 T cells (CD8, green boxes) in healthy donors (HD) and in patients at 1, 2, 3 and 6 months after HCT. Box plots indicate median, Q1 and Q3 and min and max. (C) Representative gating strategy used to define T cell subsets, based on the expression of CD45RA, CCR7 and CD95 markers. (D) Heat map summarizes the median CD6 MFI values in the different T cell subsets in HD

and in patients at 1, 2, 3 and 6 months after HCT. White stars show statistically significant differences between HD and samples after transplant (any $p<0.05$). (E) CD6 MFI on Treg, Tcon and CD8 T cells based on the expression of PD-1 in HD and in patients at 1, 2, 3 and 6 months after HCT. Statistically significant differences are noted: **** P< 0.0001; *** P< 0.001; ** P< 0.01; * P< 0.05; Wilcoxon rank-sum test.

ALCAM expression on monocytes and dendritic cells (DC) after HCT

To examine whether the CD6-ALCAM pathway represents a suitable target for aGVHD treatment, we also analyzed ALCAM expression on monocytes and DCs. DCs were divided into two major populations based on the expression of CD11c and CD123: myeloid DCs (mDCs, $CD11c^+$ and $CD123^-$) and plasmacytoid DCs (pDCs, $CD11c^-$ and $CD123^+$, **Figure 2A**). In HD, almost all monocytes and pDCs expressed ALCAM, but significantly fewer mDCs expressed ALCAM. After transplant, significantly fewer monocytes and pDCs expressed ALCAM compared to HD but the magnitude of this difference was relatively small (**Figure 2B**). ALCAM expression (MFI) was highest on pDCs, relatively low on mDCs and intermediate on monocytes (**Figure 2C**). ALCAM MFI on pDCs after transplant was similar to HD controls whereas ALCAM MFI on monocytes was significantly elevated compared to HD in the first month after transplant. In contrast, ALCAM MFI was lower in mDCs after transplant compared to HD. We also examined whether ALCAM expression on mDCs and pDCs was correlated with expression of PD-L1. As shown in **Figure 2D** and **E**, there was a weak positive correlation between ALCAM and PD-L1 expression on mDCs, while no correlation was observed for pDCs, where almost all cells uniformly express high levels of ALCAM.

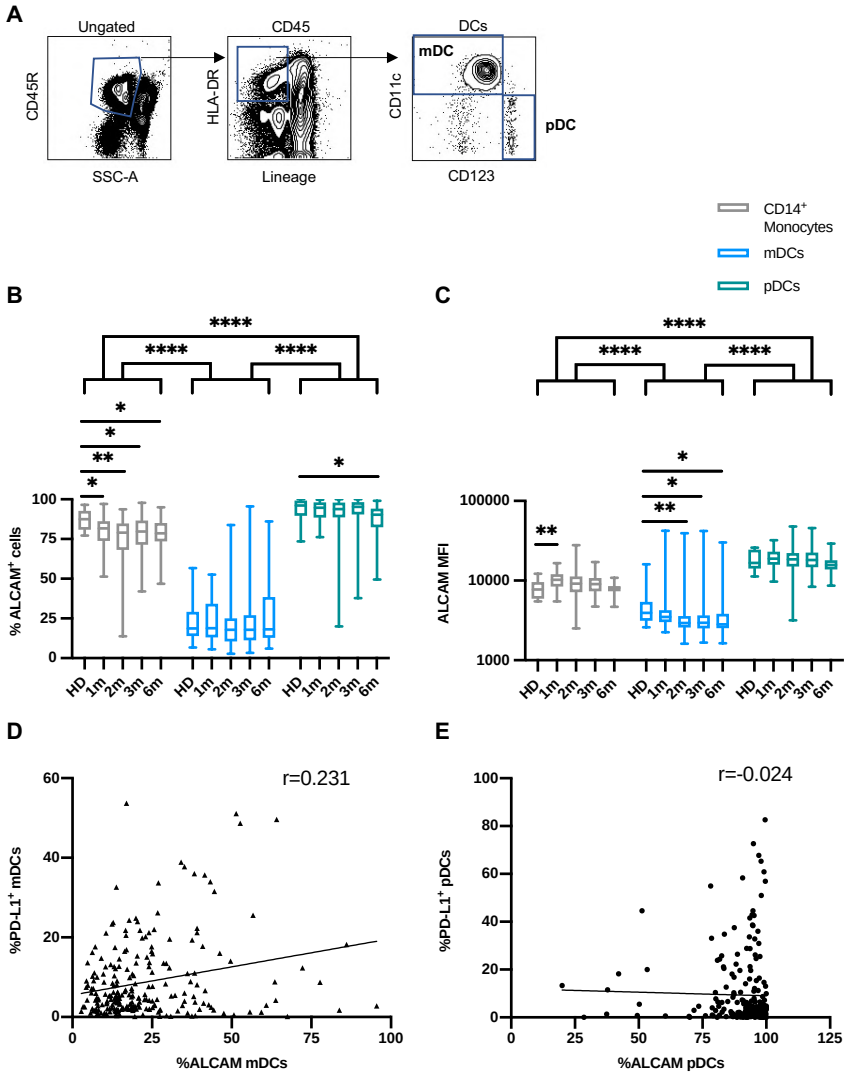

Figure 2. ALCAM expression on monocytes and DCs after HCT. (A) Representative gating strategy used to define DC subsets, based on the expression of CD11c and CD123 in flow cytometry. (B) Percentage of ALCAM positive cells and (C) levels of ALCAM expression (MFI) on $CD14^{+}$ monocytes (grey boxes), myeloid DC (mDCs, light-blue boxes) and plasmacytoid DC (pDCs, green boxes) in healthy donors (HD) and in patients at 1, 2, 3 and 6 months after HCT. Correlation of PD-L1 and ALCAM

expression on (D) mDCs and (E) pDCs. Statistically significant differences are noted: **** P< 0.0001; *** P< 0.001; ** P< 0.01; * P< 0.05; Wilcoxon rank-sum test.

CD6 and ALCAM expression are maintained during aGVHD

To examine whether CD6 and ALCAM expression were affected by the development of aGVHD, we compared CD6 and ALCAM MFI in samples obtained before (preGVHD) and after aGVHD onset (postGVHD) with samples from HD and from patients that did not develop aGVHD (noGVHD). Based on the median time of aGVHD onset, preGVHD samples were compared to noGVHD samples collected at 1 and 2 months after transplant while postGVHD samples were compared with noGVHD samples collected at 3 and 6 months after transplant. As shown in **Figure 3A**, Tcon expressed high levels of CD6 in both pre- and postGVHD samples that were similar to HD and patients who did not develop aGVHD. CD6 expression by Treg and CD8 T cells in aGVHD samples was significantly decreased compared to HD but was similar to noGVHD samples. When compared to HD, ALCAM expression was increased on CD14 monocytes preGVHD but there were no differences in expression by mDCs and pDCs (**Figure 3B**). Despite small differences, ALCAM expression was generally maintained at similar levels in monocytes, mDCs and pDCs in patients with and without aGVHD. We only observed a slightly increased ALCAM MFI on mDCs in postGVHD samples compared to noGVHD samples (**Figure 3B**).

We also compared samples from patients who developed aGVHD with patients who did not at specific time points after transplant. We observed a small decrease of CD6 MFI in Tcon and CD8 T cells in the

GVHD cohort at 1 month, compared with the noGVHD group. For ALCAM we observed a higher ALCAM MFI and percentage of ALCAM positive cells on mDCs in the GVHD cohort compared to noGVHD at 3 months after transplant (**Supplemental Figure S4 and S5**). To address the impact of systemic aGVHD treatment (steroids) on CD6 and ALCAM expression, we compared samples from patients with low grade aGVHD who only received topical therapy with patients with higher grade aGVHD who received systemic steroids. With the limitation of a low number of samples, we did not observe significant differences for CD6 expression on T cells and no clear trend was observed for ALCAM expression on monocytes and DCs (data not shown).

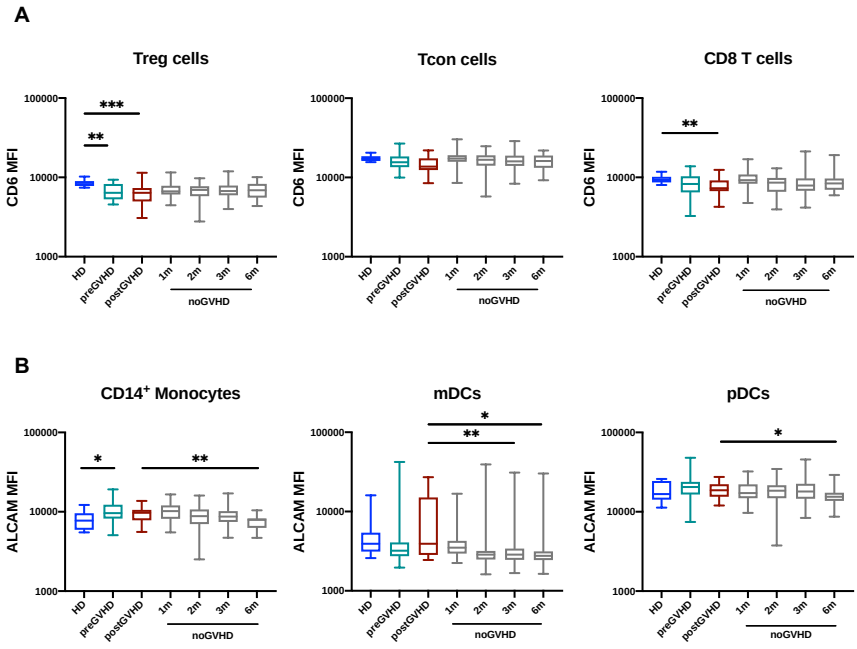

Figure 3. Expression of CD6 and ALCAM in patients after HCT with and without aGVHD. (A) Levels of CD6 expression (MFI) in Treg, Tcon and CD8 T cells. (B) Levels of ALCAM expression (MFI) in Treg, Tcon and CD8 T cells. PreGVHD samples (green boxes) and postGVHD samples (red boxes) from patients who developed acute GVHD are compared with noGVHD samples obtained at different times after transplant (grey boxes) and healthy donors (blue boxes). Statistically significant differences are noted: *** P< 0.001; ** P< 0.01; * P< 0.05; Wilcoxon rank-sum test. Healthy donor (HD, blue 13 boxes) n=9, preGVHD n=30, postGVHD n=20, noGVHD 1-month (1m) n=38, 2-months (2m) n=40, 3-months (3m) n=43 and 6-months (6m) n=21.

Itolizumab inhibits in vitro T cell proliferation, activation and maturation after TCR engagement

To test the ability of itolizumab to modulate T cell responses after TCR stimulation, cryopreserved PBMC obtained from 9 patients before (preGVHD, median time between GVHD and sample collection -24, range -32; -7 days) and after GVHD onset (postGVHD, median time between GVHD and sample collection 20, range 0; 64 days) were stimulated with antiCD3/CD2/CD28 in the presence of itolizumab or isotype control antibody (cetuximab). Clinical characteristics of these patients are summarized in **Supplemental Table S1**. Of note, postGVHD samples were collected from patients who were receiving aGVHD treatment (steroids) and one patient was also receiving ruxolitinib at the time of sample collection. Only 1 sample was collected at aGVHD onset prior to starting treatment for aGVHD. T cell proliferation, activation and maturation were evaluated 72 hours after stimulation using flow cytometry. Prior to GVHD onset, itolizumab inhibited CD4 and CD8 T cell proliferation in a similar fashion to HD control. This effect was less prominent in CD8 T cells collected after

GVHD onset (**Figure 4A**). Similar results were observed for CD25 expression, as a marker of T cell activation and CD45RO expression, as a marker of T cell maturation into memory subsets (**Figure 4B and C**). Itolizumab inhibited these other measures of T cell activation in both CD4 and CD8 T cells from healthy donors and from patients prior to aGVHD. However, increased expression of CD25 and CD45RO on T cells in postGVHD samples were no longer inhibited by itolizumab. After TCR stimulation, we also observed increased ALCAM expression on both CD4 and CD8 T cells from healthy donors and transplant patients. However, except for CD8 T cells collected preGVHD, no statistically significant inhibition was observed using itolizumab (**Figure 4D**).

Comparisons of inhibition achieved by itolizumab for each of these assays in CD4 and CD8 T cells from healthy donors and patients after transplant are shown in **Figure 4E**. In all assays, the level of inhibition induced by itolizumab in pre-GVHD T cells was similar to that achieved in healthy donors. Itolizumab induced less inhibition of proliferation in both $CD4^+$ and $CD8^+$ T cells collected after GVHD onset. Less inhibition was also noted for CD25 expression in $CD8^+$ T cells post GVHD but there were no differences in the ability of itolizumab to inhibit CD45RO and ALCAM expression in both $CD4^+$ and $CD8^+$ T cells in any groups.

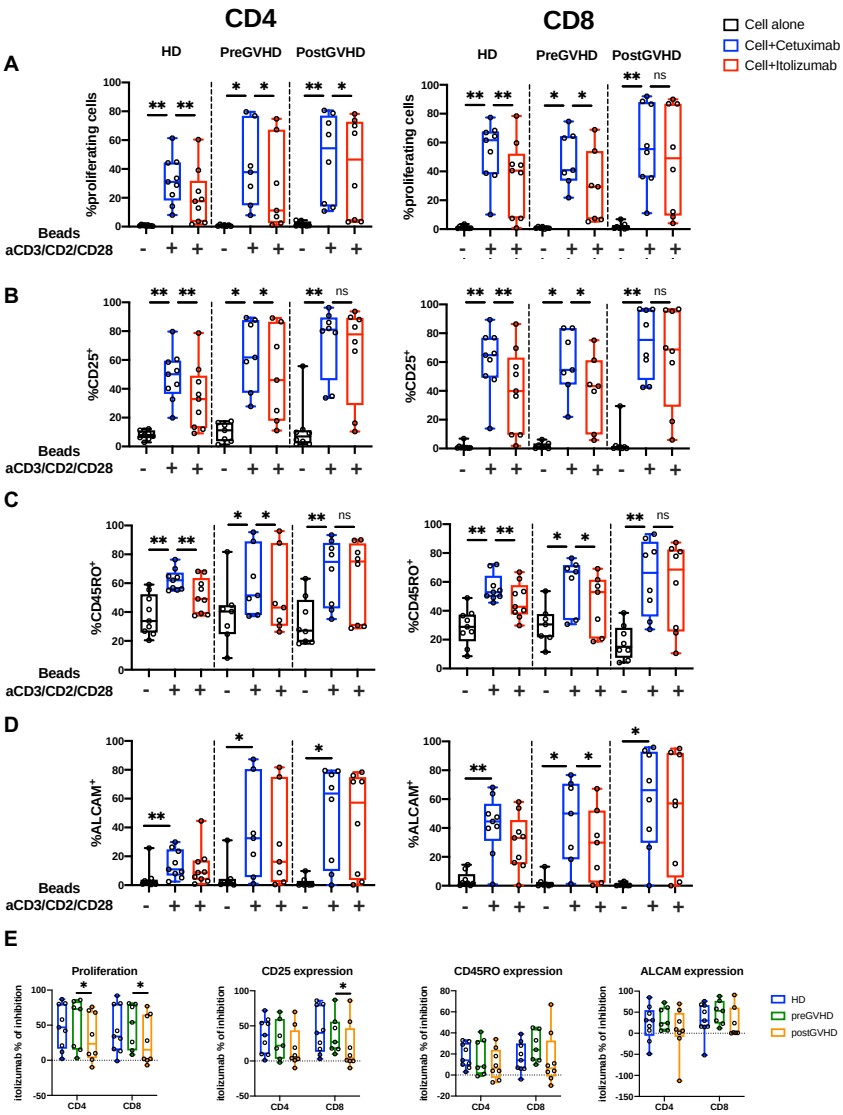

Figure 4. Inhibition of T cell proliferation, activation and differentiation by itolizumab. Cryopreserved peripheral blood mononuclear cells (PBMC) obtained from healthy donors (HD) and patients before or after aGVHD onset were stimulated with anti- CD3/CD2/CD28 beads in the presence of itolizumab or isotype control (cetuximab). (A) Proliferation of CD4 and CD8

T cells measured by CFSE dye dilution; (B) Activation of CD4 and CD8 T cells measured by expression of CD25; (C) maturation of CD4 and CD8 T cells measured by expression of CD45RO; (D) ALCAM expression is absent in resting T cells and is an additional marker of T cell activation. (E) Percent inhibition induced by itolizumab, comparing activity against HD, pre- and postGVHD samples in CD4 and CD8 T cells. Percentage inhibition was calculated using the following formula: (%cells in isotype control - %cells in itolizumab)/%cells in isotype control. If no difference was observed between isotype control and itolizumab the percentage of itolizumab inhibition equals 0%. Statistically significant differences are noted: ** P< 0.01; * P< 0.05; Wilcoxon rank-sum test. HD, n=9, preGVHD, n=7, postGVHD, n=8.

Itolizumab does not induce complement dependent cytotoxicity (CDC), antibody dependent cytotoxicity (ADC) or antibody direct cellular cytotoxicity (ADCC)

To test the ability of itolizumab to induce direct or indirect killing of target cells we evaluated the effects of itolizumab in CDC, ADC and ADCC assays. Cell lysis in the presence of itolizumab was compared to alemtuzumab as positive control or cetuximab as negative control. The gating strategy used to measure target cell lysis is shown in **Supplemental Figure S6**. Itolizumab did not mediate CDC or ADC at 6 or 24 hours. After 6 hours of incubation, itolizumab did not induce ADCC measured either by direct lysis of target cells or degranulation of CD107a on NK cells (**Figure 5**).

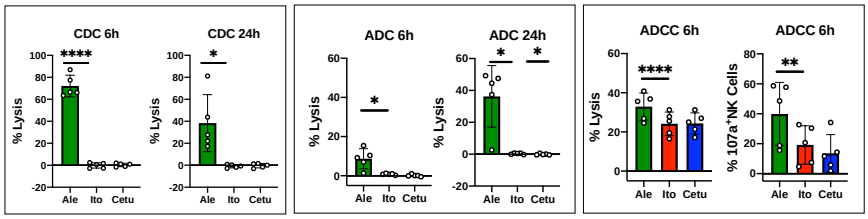

Figure 5. T esting itolizumab for complement dependent cytotoxicity (CDC), antibody dependent cytotoxicity (ADC) and antibody direct cellular cytotoxicity (ADCC). For CDC and ADC, CD3+ T cells were isolated from cryopreserved peripheral blood mononuclear cells (PBMC) from healthy donors (HD) and cultured in the presence of medium + antibody + 25% of human serum (HS) and medium + antibody, respectively. Percentage cell lysis was calculated by combining the percentage of positive cells for 7-AAD or Annexin V or both. CDC activity was calculated by subtracting the values obtained in medium + antibody from the values obtained in the culture with medium + antibody + HS. ADC activity was calculated by subtracting the values obtained in the culture with medium alone from the values obtained in the culture with medium + antibody. CDC and ADC were assessed after 6 and 24 hours of culture. For ADCC PBMC from HD were cultured in the presence of antibody for 6 hours. Both percentage cell lysis and CD107a expression on NK cells were evaluated after 6 hours of culture. The effects of itolizumab (red boxes) were compared to alemtuzumab (green boxes- positive control) and cetuximab (blue boxes - negative control). Values are expressed as mean and SD, paired t test, 2 tails was used. Statistically significant differences are noted: **** P< 0.0001; *** P< 0.001; ** P< 0.01; * P< 0.05; paired t test. HD, n=5.

Itolizumab activity is dependent on the presence of ALCAM

To test whether the inhibitory activity of itolizumab was dependent on the presence of ALCAM, T cells from HD were stimulated with anti-CD3 antibody with or without ALCAM-Fc for 96 hours. Itolizumab or isotype control cetuximab were added at the start of each culture. As shown in **Figure 6A**, the addition of cetuximab or itolizumab did not induce proliferation of CD4 or CD8 T cells alone, and anti-CD3 induced proliferation of CD4 or CD8 T cells was not inhibited by the addition of either antibody. The addition of ALCAM-Fc to anti-CD3 further enhanced CD4 and CD8 T cell proliferation. The addition of itolizumab significantly impaired this increased proliferation when compared to the addition of cetuximab. When T cells were monitored

for activation (expression of CD25, **Figure 6B**) and maturation (expression of CD45RO, **Figure 6C**), itolizumab had similar effects on both CD4 and CD8 T cells and inhibitory activity was only detected in the presence of both anti-CD3 and ALCAM-Fc. As shown **Figure 6D**, activation of CD4 and CD8 T cells with anti-CD3 also induces expression of ALCAM and this is further enhanced in the presence of ALCAM-Fc. In this setting, the presence of itolizumab inhibits increased expression of ALCAM even if ALCAM-Fc is not present.

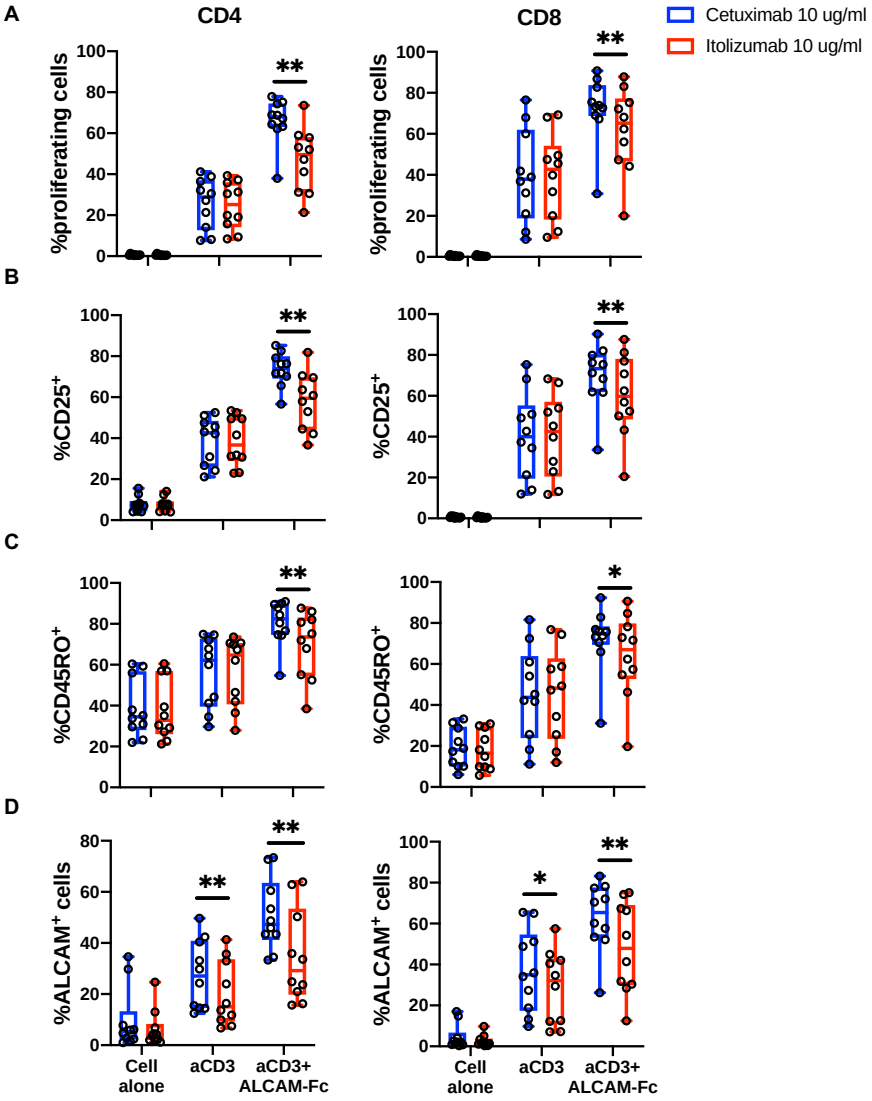

Figure 6. Itolizumab activity is dependent on the presence of ALCAM. T cells from HD were stimulated with anti-CD3 antibody with or without ALCAM-Fc for 96 hours. Itolizumab or isotype control cetuximab were added at the start of each culture. (A) Proliferation of CD4 and CD8 T cells; (B) Expression of CD25; (C) Expression of CD45RO; (D) Expression of ALCAM after stimulation with anti-CD3 antibody alone or in combination with ALC AM-Fc, in the presence of cetuximab (blue boxes) or itolizumab (red boxes).

Statistically significant differences are noted: ** P< 0.01; * P< 0.05; Wilcoxon rank-sum test. HD, n=10.

Discussion

Acute GVHD remains a frequent cause of non-relapse mortality and contributes to poor quality of life in patients who have undergone allogeneic HCT. Corticosteroids are administered as first line therapy, but steroid treatment fails to achieve complete responses in up to 50% of cases and is also associated with short and long term toxicities (5). Ideally, new treatment approaches for GVHD should be aimed at specific modulation of donor T cell alloreactivity and induction of tolerance rather than nonspecific T cell depletion or broad inhibition of T cell functions which can increase risk of tumor immune escape as well as opportunistic infections (27). In this study we demonstrate that blocking the CD6-ALCAM costimulatory pathway inhibits T cell activation and proliferation thus representing a new potential target for GVHD prevention and treatment. Indeed, CD6 is highly expressed on Tcon after HCT, and its expression is maintained at the onset of aGVHD. Moreover, expression of ALCAM, the primary ligand for CD6, is increased in DCs and monocytes in patients who develop aGVHD. In contrast, Treg express lower levels of CD6 (28–30), and targeting CD6 with itolizumab could preferentially affect Tcon while sparing Treg, thus promoting a more tolerogenic state. CD6 expression also varies as T cells undergo maturation (31). Naïve and central memory T cells express high levels of CD6 compared to more mature effector memory T cells. Previous studies have suggested that GVHD is primarily mediated by naïve T cells and these cells may also be preferentially affected by itolizumab (32–39). Similarly, we observed

that PD-1 positive T cells, that are already exposed to TCR activation (26), express lower levels of CD6 compared to PD-1 negative cells. Therefore, targeting the CD6-ALCAM pathway could potentially spare tolerogenic T cell subsets (Treg) and more mature (EM) pathogen specific T cells, leading to a more favorable balance between GVHD control and maintenances of GVL and anti-infection capabilities.

This hypothesis is supported by previous clinical studies using T12, the first anti- CD6 monoclonal antibody used in the transplant setting. T12, an IgM antibody, induced profound *ex vivo* depletion of CD6+ T cells when donor grafts were manipulated ex vivo in the presence of complement (18). Patients in these trials received myeloablative conditioning and did not receive any prophylactic immune suppressive medications. $CD3^{+}CD6^{-}$ T cells recovered rapidly after transplantation with CD6-depleted allogeneic stem cell products with very low incidence of acute or chronic GVHD (19). Functional immune recovery was not delayed and there was no increase in viral reactivation after transplant. There was also a very low incidence of graft failure and graft versus leukemia activity appeared to be preserved (20,21,40). Taken together, these previous clinical trials suggested that in vivo blockade of CD6 function might also be an effective approach for selective modulation of alloreactive T cells without affecting other critical T cell functions.

As expected, in our cohort of HCT patients, we observed mixed donor-recipient T cell chimerism in the early post-transplant period with a median donor T cell chimerism of 76% at 1 month. We are not able to distinguish CD6 expression on individual donor versus recipient T cells, but we found that CD6 expression on T cells in patients with

>95% T cell donor chimerism was similar to levels of expression in patients with <95% T cell donor chimerism. Similarly, no difference was observed for ALCAM expression on monocytes, mDCs and pDCs (**Supplemental Table S5**). This suggests that CD6 and ALCAM are equally expressed on recipient and donor cells after transplant.

Our studies also found that ALCAM expression was increased on both DCs and monocytes in patients with aGVHD compared to patients without aGVHD. In myeloid DC, ALCAM expression was positively correlated with PD-L1 expression. ALCAM is expressed at high levels on all pDCs, and this did not change when aGVHD developed. These observations support the concept that ALCAM is upregulated when DCs are activated (41). ALCAM expression on DCs is important for the promotion and maintenance of the immunological synapse and this is one of the mechanisms whereby ALCAM promotes T cell activation (13). Since immune reconstitution varies depending on the transplant setting, the expression of CD6 and ALCAM should also be explored in patients with haploidentical donors and with different GVHD prophylaxis regimens such as ATG or post-transplant cyclophosphamide.

Itolizumab, an IgG1 anti-CD6 monoclonal antibody has been evaluated in different autoimmune disorders (9), including psoriasis (23), rheumatoid arthritis (42), Sjogren syndrome (43) and in Covid-19 infection (24,44). Using PBMC from patients with aGVHD, itolizumab inhibited T cell proliferation, activation, and maturation of both CD4 and CD8 T cells. This was most evident with T cells obtained just prior to development of aGVHD and less inhibition was observed in post-GVHD T cells obtained from patients receiving immune suppressive

medications. These findings suggest that itolizumab may be more effective in early stages of GVHD in combination with steroids or as GVHD prophylaxis. Even though these *ex vivo* experiments lack GVHD target tissues and do not perfectly recapitulate aGVHD *in vivo*, using whole PBMC, we were able to mimic the alloreactive activation of T cells in the presence of ALCAM expressed on circulating APCs (monocytes and B cells) and demonstrate the inhibitory activity of itolizumab.

Infusion of itolizumab in patients with autoimmune diseases has resulted in only transient reduction of $CD6^+$ circulating T cells, suggesting that this antibody does not induce profound T cell depletion (45). This is consistent with our results demonstrating that itolizumab does not directly eliminate T cells in vitro in CDC, ADC or ADCC assays. Thus, the mechanism by which itolizumab inhibits T cell function *in vivo* is likely through its ability to prevent the interaction between CD6 on T cells and ALCAM on APCs (22). This is consistent with our *in vitro* results showing that the addition of itolizumab to activated CD3 T cells in the absence of ALCAM did not inhibit T cell proliferation, activation, or maturation. However, in the presence of ALCAM, itolizumab efficiently abrogates the costimulatory effects of this interaction and is able to suppress T cell proliferation, activation, and maturation. In contrast to other pan-T cell antibodies that either activate T cells (anti-CD3) or deplete T cells (ATG, anti-CD52), itolizumab only inhibits T cell activation in the presence of ALCAM and has no direct or indirect depleting functions.

While ruxolitinib, a JAK1/2 inhibitor, is currently the only drug approved for the treatment of steroid refractory aGVHD (46), several

drugs that target different T cell co- stimulatory molecules are currently being tested in preclinical models and in patients with aGVHD (4, 27). In this setting, itolizumab may be a promising agent for either prevention or treatment of aGVHD, due to higher expression of CD6 on naïve and central memory Tcon cells, while sparing more tolerogenic Treg and effector memory T cells, important for control of both tumor cells and opportunistic infections after transplant (37). Moreover, itolizumab may not inhibit responses to viral infections or reactivation. Indeed, different NK and T cell populations are involved in responses to CMV infection ($NKG2C^+CD8^+$ T cells) and these cells have low expression of CD6 (47).

Recently, Ruth and colleagues demonstrated that targeting CD6 may also be a novel approach to enhance cancer immunotherapy (48). This study utilized UMCD6, an anti-CD6 monoclonal antibody that binds the same CD6 domain (Domain 1) as itolizumab. UMCD6 upregulated the expression of the activating receptor NKG2D and down-regulated expression of the inhibitory receptor NKG2A on both NK cells and $CD8^+$ T cells, with concurrent increased expression of perforin and granzyme-B (48). The combined capabilities of an anti-CD6 monoclonal antibody to control autoimmunity through effects on $CD4^+$ T cells and the enhanced killing of cancer cells through distinct effects on $CD8^+$ T cells and NK cells, may represent a new approach to induce tolerance without suppressing GVL activity after HCT.

In conclusion, our studies demonstrate that functional inhibition of the CD6-ALCAM costimulatory pathway may be a novel therapeutic strategy for prevention or treatment of aGVHD. On the basis of these biological properties, a phase I/II study using itolizumab as first line

treatment in combination with steroids for patients with aGVHD is currently ongoing (NCT03763318). Future clinical studies may also test the feasibility and clinical efficacy of itolizumab for prevention of GVHD.

References

1. Zeiser R, Blazar BR. Acute Graft-versus-Host Disease — Biologic Process, Prevention, and Therapy. N Engl J Med. 2017;377(22):2167-2179.
2. MacMillan ML, Weisdorf DJ, Wagner JE, et al. Response of 443 patients to steroids as primary therapy for acute graft-versus-host disease: Comparison of grading systems. Biol Blood Marrow Transplant. 2002;8(7):387-394.
3. Levine JE, Braun TM, Harris AC, et al. A prognostic score for acute graft-versus- host disease based on biomarkers: a multicentre study. Lancet Haematol. 2015;2(1):e21-e29.
4. Watkins B, Qayed M, McCracken C, et al. Phase II Trial of Costimulation Blockade With Abatacept for Prevention of Acute GVHD. J Clin Oncol. 2021;39(17):1865-1877.
5. Toubai T, Magenau J. Immunopathology and biology-based treatment of steroid- refractory graft-versus-host disease. Blood. 2020;136(4):429-440.
6. Martínez VG, Moestrup SK, Holmskov U, Mollenhauer J, Lozano F. The Conserved Scavenger Receptor Cysteine-Rich Superfamily in Therapy and Diagnosis. Pharmacol Rev. 2011;63(4):967-1000.
7. Aruffo A, Melnick MB, Linsley PS, Seed B. The lymphocyte glycoprotein CD6 contains a repeated domain structure characteristic of a new family of cell surface and secreted proteins. J Exp Med. 1991;174(4):949-952.
8. Braun M, Müller B, ter Meer D, et al. The CD6 Scavenger Receptor Is Differentially Expressed on a CD56dim Natural Killer Cell Subpopulation and Contributes to Natural Killer-Derived Cytokine and Chemokine Secretion. J Innate Immun. 2011;3(4):420-434.
9. Consuegra-Fernández M, Lin F, Fox DA, Lozano F. Clinical and experimental evidence for targeting CD6 in immune-based disorders. Autoimmun Rev. 2018;17(5):493-503.

10. Bowen MA, Patel DD, Li X, et al. Cloning, mapping, and characterization of activated leukocyte-cell adhesion molecule (ALCAM), a CD6 ligand. J Exp Med. 1995;181(6):2213-2220.
11. Chappell PE, Garner LI, Yan J, et al. Structures of CD6 and Its Ligand CD166 Give Insight into Their Interaction. Structure. 2015;23(8):1426-1436.
12. Cayrol R, Wosik K, Berard JL, et al. Activated leukocyte cell adhesion molecule promotes leukocyte trafficking into the central nervous system. Nat Immunol. 2008;9(2):137-145.
13. Zimmerman AW, Joosten B, Torensma R, Parnes JR, van Leeuwen FN, Figdor CG. Long-term engagement of CD6 and ALC AM is essential for T -cell proliferation induced by dendritic cells. Blood. 2006;107(8):3212-3220.
14. Hassan NJ, Barclay AN, Brown MH. Frontline: Optimal T cell activation requires the engagement of CD6 and CD166. Eur J Immunol. 2004;34(4):930-940.
15. Hassan NJ, Simmonds SJ, Clarkson NG, et al. CD6 Regulates T-Cell Responses through Activation-Dependent Recruitment of the Positive Regulator SLP-76. Mol Cell Biol. 2006;26(17):6727-6738.
16. Nair P, Melarkode R, Rajkumar D, Montero E. CD6 synergistic co-stimulation promoting proinflammatory response is modulated without interfering with the activated leucocyte cell adhesion molecule interaction. Clin Exp Immunol. 42 2010;162(1):116-130.
17. Oliveira MI, Gonçalves CM, Pinto M, et al. CD6 attenuates early and late signaling events, setting thresholds for T -cell activation. Eur J Immunol. 2012;42(1):195-205.
18. Rohatiner A, Gelber R, Schlossman SF, Ritz J. Depletion of T cells from human bone marrow using monoclonal antibodies and rabbit complement. A quantitative and functional analysis. Transplantation. 1986;42(1):73-80.
19. Soiffer RJ, Bosserman L, Murray C, Cochran K, Daley J, Ritz J. Reconstitution of T-Cell Function After CD6-Depleted Allogeneic Bone Marrow Transplantation. Blood. 1990;75(10):2076-2084.
20. Soiffer RJ, Murray C, Mauch P, et al. Prevention of graft-versus-host disease by selective depletion of CD6-positive T lymphocytes from donor bone marrow. J Clin Oncol. 1992;10(7):1191-1200.
21. Soiffer RJ, Weller E, Alyea EP, et al. CD6+ Donor Marrow T-Cell Depletion as the Sole Form of Graft-Versus-Host Disease Prophylaxis in

Patients Undergoing Allogeneic Bone Marrow Transplant From Unrelated Donors. J Clin Oncol. 2001;19(4):1152-1159.
22. Bughani U, Saha A, Kuriakose A, et al. T cell activation and differentiation is modulated by a CD6 domain 1 antibody Itolizumab. PLoS One. 2017;12(7):e0180088.
23. Krupashankar DS, Dogra S, Kura M, et al. Efficacy and safety of itolizumab, a novel anti-CD6 monoclonal antibody, in patients with moderate to severe chronic plaque psoriasis: Results of a double-blind, randomized, placebo-controlled, phase-III study. J Am Acad Dermatol. 2014;71(3):484-492.
24. Kumar S, De Souza R, Nadkar M, et al. A two-arm, randomized, controlled, multicentric, open-label phase-2 study to evaluate the efficacy and safety of Itolizumab in moderate to severe ARDS patients due to COVID-19. Expert Opin Biol Ther. 2021;21(5):675-686.
25. Bologna L, Gotti E, Manganini M, et al. Mechanism of Action of Type II, Glycoengineered, Anti-CD20 Monoclonal Antibody GA101 in B-Chronic Lymphocytic Leukemia Whole Blood Assays in Comparison with Rituximab and Alemtuzumab. J Immunol. 2011;186(6):3762-3769.
26. Nishimura H, Agata Y, Kawasaki A, et al. Developmentally regulated expression of the PD-1 protein on the surface of double-negative(CD4–CD8–) thymocytes. Int Immunol. 1996;8(5):773-780.
27. Hill GR, Koyama M. Cytokines and costimulation in acute graft-versus-host disease. Blood. 2020;136(4):418-428.
28. Koreth J, Matsuoka K, Kim HT, et al. Interleukin-2 and Regulatory T Cells in Graft-versus-Host Disease. N Engl J Med. 2011;365(22):2055-2066.
29. Pierini A, Ruggeri L, Carotti A, et al. Haploidentical age-adapted myeloablative transplant and regulatory and effector T cells for acute myeloid leukemia. Blood Adv. 2021;5(5):1199-1208.
30. Garcia Santana CA, Tung JW, Gulnik S. Human treg cells are characterized by low/negative CD6 expression. Cytom A. 2014;85(10):901-908.
31. Carrasco E, Escoda-Ferran C, Climent N, et al. Human CD6 Down-Modulation following T-Cell Activation Compromises Lymphocyte Survival and Proliferative Responses. Front Immunol. 2017;8:769.
32. Anderson BE, McNiff J, Yan J, et al. Memory CD4+ T cells do not induce graft-versus-host disease. J Clin Invest. 2003;112(1):101-108.
33. Zhang Y, Joe G, Zhu J, et al. Dendritic cell–activated CD44hiCD8+ T cells are defective in mediating acute graft-versus-host disease but retain graft-versus-leukemia activity. Blood. 2004;103(10):3970-3978.

34. Chen BJ, Cui X, Sempowski GD, Liu C, Chao NJ. Transfer of allogeneic CD62L–memory T cells without graft-versus-host disease. Blood. 2004;103(4):1534-1541.
35. Dutt S, Tseng D, Ermann J, et al. Naive and Memory T Cells Induce Different Types of Graft-versus-Host Disease. J Immunol. 2007;179(10):6547-6554.
36. Chen BJ, Deoliveira D, Cui X, et al. Inability of memory T cells to induce graft- versus-host disease is a result of an abortive alloresponse. Blood. 2006;109(7):3115-3123.
37. Zheng H, Matte-Martone C, Li H, et al. Effector memory CD4+ T cells mediate graft-versus-leukemia without inducing graft-versus-host disease. Blood. 2008;111(4):2476-2484.
38. Zheng H, Matte-Martone C, Jain D, McNiff J, Shlomchik WD. Central Memory CD8+ T Cells Induce Graft-versus-Host Disease and Mediate Graft-versus-Leukemia. J Immunol. 2009;182(10):5938-5948.
39. Bleakley M, Heimfeld S, Loeb KR, et al. Outcomes of acute leukemia patients transplanted with naive T cell–depleted stem cell grafts. J Clin Invest. 2015;125(7):2677-2689.
40. Soiffer RJ, Fairclough D, Robertson M, et al. CD6-Depleted Allogeneic Bone Marrow Transplantation for Acute Leukemia in First Complete Remission. Blood. 1997;89(8):3039-3047.
41. Figdor CG. Molecular characterization of dendritic cells operating at the interface of innate of acquired immunity. Pathol Biol. 2003;51(2):61-63.
42. Rodriguez PC, Torres-Moya R, Reyes G, et al. A clinical exploratory study with itolizumab, an anti-CD6 monoclonal antibody, in patients with rheumatoid arthritis. Results Immunol. 2012;2:204-211.
43. Le Dantec C, Alonso R, Fali T, et al. Rationale for treating primary Sjögren's syndrome patients with an anti-CD6 monoclonal antibody (Itolizumab). Immunol Res. 2013;56(2):341-347.
44. Loganathan S, Athalye SN, Joshi SR. Itolizumab, an anti-CD6 monoclonal antibody, as a potential treatment for COVID-19 complications. Expert Opin Biol Ther. 2020;20(9):1025-1031.
45. Aira LE, López-Requena A, Fuentes D, et al. Immunological and histological evaluation of clinical samples from psoriasis patients treated with anti-CD6 itolizumab. MAbs. 2014;6(3):782-792.
46. Zeiser R, von Bubnoff N, Butler J, et al. Ruxolitinib for Glucocorticoid-Refractory Acute Graft-versus-Host Disease. N Engl J Med. 2020;382(19):1800-1810.

47. Sottile R, Panjwani MK, Lau CM, et al. Human cytomegalovirus expands a CD8+ T cell population with loss of BCL11B expression and gain of NK cell identity. Sci Immunol. 2021;6(63):eabe6968.
48. Ruth JH, Gurrea-Rubio M, Athukorala KS, et al. CD6 is a target for cancer immunotherapy. JCI Insight. 2021;6(5):e145662.

Acknowledgements
This work was supported by Equillium Inc and NIH grant PO1CA229092. We thank the staff of the Pasquarello Tissue Bank in Hematologic Malignancies for processing all of the clinical samples analyzed in this study.

Authorship Contributions
B.R. designed research studies, conducted experiments, acquired and analyzed data, and wrote the manuscript; H.T.K. analyzed data, performed statistical analysis, and wrote the manuscript; C.R., M.M., M.H. and A.W. acquired data; Y.A. and T.A. help in the design of functional experiments; M.G., J.K., C.C., S.N., V.T.H., J.H.A., R.R., J.A., C.N., S.C. and R.J.S. analyzed data and edited the manuscript; J.R. designed research studies, analyzed data, and wrote the manuscript.

Conflict of Interest Disclosures
B.R. received research funding from Equillium
H.T.K., Y.A., T.A., C.R., M.M., M.H., A.W., M.G., V. T. H. and R.R. have nothing to disclose
J.K., has research support from Clinigen, Miltenyi Biotec, BMS, Regeneron Scientific, advisory board for Therakos/Mallinckrodt, Cugene, and consulting for Biolojic Design, EMD Serono/Merck, Equillium, Gentibio, Moderna
C.C. has a consultancy and membership on an entity's board of directors or advisory committees for Incyte, Kadmon, Jazz, Medsenic, Generon and Mesoblast.
S.N. has membership on an entity's Board of Directors or advisory committees for Kite, Novartis, Nkarta and Iovance
J.H.A. serves on a Data Safety Monitoring Committee for CSL Behring.
J.A. has. A Current Employment at Equillium
C.N. has Current Employment and Current equity holder in private company at Equillium S.C. has Current Employment and Current equity holder in private company at Equillium

R.J.S. has a membership on an entity's board of directors or advisory committees for Kiadis and BMS and Be the Match/ National Marrow Donor Program, and consultancy for Gilead, Rheos Therapeutics, Cugene, Precision Bioscience, VOR Biopharma, Novartis, Jazz and Takeda.
J.R. receives research funding from Amgen, Equillium, Kite/Gilead and Novartis; serves on Data Safety Monitoring Committees for AvroBio and Scientific Advisory Boards for Akron Biotech, Clade Therapeutics, Garuda Therapeutics, LifeVault Bio, Novartis, Rheos Medicines, Talaris Therapeutics and TScan Therapeutics.

Corresponding author:
*Jerome Ritz, MD
Dana-Farber Cancer Institute
450 Brookline Ave,
Boston, MA 02215
Tel. 617-632-3465
Email: jerome_ritz@dfci.harvard.edu
For data sharing, contact the corresponding author: jerome_ritz@dfci.harvard.edu

Supplemental Materials

SUPPLEMENTAL METHODS

Cell processing for *in vitro* functional assays

For functional in vitro assay, PBMC were isolated from freshly drawn blood samples by density gradient centrifugation (Ficoll-Paque PLUS; GE Healthcare) and cryopreserved in RPMI 10% DMSO before being utilized. For in vitro culture of PBMC or T cells complete medium (CM) was used. CM was made using DMEM (Cat 11995-065 Gibco), 10% FBS (Heat Inactivated, Gibco 10437-028), 1% Penicillin-Streptomycin (Gibco, 100X, 15140122), HEPES 10mM (Gibco, 1M,

15630080), 1% MEM Non-ess A.A. (Gibco, 100X, 11140050) and 2-Mercaptoethanol 0.05mM (Sigma-Aldrich, 14.3M, M3148).

Functional activity of itolizumab *in vitro*

Frozen PBMC obtained from patients who developed aGVHD after transplant (**Supplemental Table S1**) were stimulated using a combination of antiCD3/CD2/CD28 beads (Treg Suppression Inspector human 2.5 ml 5x10'7 Anti-Biotin MACSiBead particles preloaded with biotinylated CD2/CD3/CD28 antibodies, Miltenyi 130-092-909) at a bead:cell ratio of 1:2 in the presence of itolizumab 10 μg/ml (Biocon Ltd, Bangalore, India) or isotype control 10 μg/ml (cetuximab Erbitux NDC 66733-948-23, LOT c1800010). To detect T cell proliferation, PBMC were stained with CFSE (Invitrogen Thermo Fisher Scientific) as per product instruction. T cell proliferation, activation and maturation were evaluated after 72 hours of culture using the flow cytometry panel in **Supplemental Table S3** and analyzed using FlowJo software. An example of the gating strategy used in this analysis is shown in **Supplemental Fig. S3**. Detailed description of the protocol is provided in Supplemental Methods.

Complement dependent cytotoxicity (CDC), antibody direct cytotoxicity (ADC)

After thawing HD PBMC, $CD3^+$ T cells were isolated using EasySep Human T-Cell isolation Kit (STEMCELL Cat 17951 Lot 17F79887) as per manufacturer's instructions. Purity of isolated $CD3^+$ T cells was assessed using flow cytometry with FITC-conjugated anti-CD3 antibody (Ab) (BioLegend, clone UCHT1, cat 300406). After T cell

isolation, we obtained a median percentage of 96.9%, $CD3^+$ cells (range 90.5-98.1%). After 15 minutes pre-incubation with itolizumab (Biocon Ltd, Bangalore, India), positive control alemtuzumab (10 μg/ml, Campath-1H, anti-CD52, human IgG1, BioVision A1105-200, Lot 4M13A11050) or negative control cetuximab (10 μg/ml, Erbitux NDC 66733-948-23, LOT c1800010), isolated $CD3^+$ T cells were cultured at a concentration of 1 x 10^6/ml in the presence of CM with (for CDC) or without (for ADC) 25% human serum. Cells were incubated at 37'C, 5% CO2 for 6 or 24 hours. At the end of cell culture, the cell plate was kept on ice to prevent further complement activity. Harvested cells were stained with 7-AAD (BD, 51-68981E' sold as 559925) and PE-conjugated Annexin V (BD, 51-65875X, sold as 556422) as per manufacturer's instructions and acquired on Fortessa LSR flow cytometer (BD). Each sample was acquired at medium velocity for 180 seconds. Analysis was performed using FlowJo software. An example of gating strategy is shown in **Supplemental Figure 4**. Percentage lysis was calculated by the average of % of 7-AAD and/or Annexin V positive cells. To detect complement-mediated cell death (CDC), percent specific lysis was calculated by subtracting the value obtained in conditions with Ab alone from the value obtained in the presence of AB+ human serum (HS). ADC activity was calculated by subtracting the values obtained in culture with medium alone from the values obtained in cultures with medium + antibody. CDC and ADC were assessed after 6 and 24 hours of culture.

Antibody dependent cellular cytotoxicity (ADCC) assay

Thawed HD PBMC were cultured at a final concentration of 1 x 10^6/ml in the presence of CM and specific ab at a concentration of 10 μg/ml. Cells were incubated at 37'C, 5% CO2 for 6 hours. Harvested cells were stained with FITC-conjugated anti-CD3 Ab (BioLegend, clone UCHT1, cat 300406), BV510-conjugated anti-CD56 Ab (BioLegend, clone HCD56 NCAM, cat 318340) and APC-conjugated anti-CD107a LAMP-1 (BioLegend, clone H4A3, cat 328620) and incubated for 30 minutes. Cells were washed two times and then stained with 7-AAD (BD, 51-68981E' sold as 559925) and PE-conjugated Annexin V (BD, 51-65875X, sold as 556422) as per manufacturer's instructions and acquired on Fortessa LSR flow cytometer (BD). Each sample was acquired at medium velocity for 180 seconds. Analysis was performed using FlowJo software. To set the positive threshold for CD107a expression an APC-conjugated isotype mouse IgG1 (BioLegend, clone MOPC-21, cat 400122) was used. An example of gating strategy is shown in **Supplemental Figure 4**.

T cell stimulation assay using ALCAM-Fc and anti-CD3 Ab

Recombinant Human ALCAM Fc Chimera (ALCAM-Fc, R&D Systems, cat 7187-AL-100) 10 μg/ml and anti-CD3 Ab 5 μg/ml (Invitrogen Thermo Fisher Scientific, clone OKT3, cat 16-0037-85) were resuspend in PBS (Gibco 10010-023, ph7.4) overnight at 4'C in flat bottom 96 well plate. Plate was washed 2 times with PBS before adding cells. After thawing HD PBMC, $CD3^+$ T cells were isolated through negative selection using the EasySep Human T-Cell isolation Kit (STEMCELL Cat 17951 Lot 17F79887) as per manufacturer's instructions. Purity of isolated CD3 T cells was assessed using

flowcytometry with FITC-conjugated anti-CD3 antibody (Ab) (BioLegend, clone UCHT1, cat 300406), median $CD3^+$ cells of 98.15%, range 94.7-99.2%. Isolated T cells were cultured in complete medium (CM) with itolizumab (10 μg/ml) or cetuximab (10 μg/ml) at 37'C, 5% CO2 for 96 hours. Cells were analyzed using flow cytometry (**supplemental Table 4**) and analyzed using FlowJo software. An example of gating strategy used is shown in **Supplemental Figure 3**.

Statistical analysis

Data analysis was primarily descriptive using the Wilcoxon rank-sum test for unpaired group comparison and the Wilcoxon signed-rank test for paired comparison. All tests were 2-sided at the significance level of 0.05 and multiple comparisons were not considered. Statistical analysis was performed using SAS version 9.2 (SAS Institute, Inc., Cary, NC) and R version 3.3.2 (the CRAN project) and Prism software (GraphPad). All graphs were made using Prism software (GraphPad). Heatmap was generated using GENE-E (http://www.broadinstitute.org/cancer/software/GENE-E).

EXP	SEX	AGE	DX	DONOR	GVHD PROPHY	GVHD GRADE	SKIN	LIVER	GUT	AGVHD TX
1	F	37	NHL	MUD	Siro/Tac/MTX	3	3	0	0	Pred/ECP
2	M	65	NHL	MUD	Siro/Tac/MTX	2	3	0	1	Pred
3	M	42	NHL	MRD	Siro/Tac/MTX	2	3	0	0	Pred
4	F	52	MM	MUD	Siro/Tac/MTX	2	0	1	1	Pred
5	F	49	NHL	MUD	Tac/MTX	1	2	0	0	Pred
6	M	71	MF	MUD	Tac/MTX	2	0	0	1	Pred
7	F	52	NHL	MUD	Tac/MTX	2	3	0	0	Pred
8	M	71	MDS	MUD	Tac/MTX	4	0	2	4	Pred /Ruxolitinib
9	M	61	AML	MUD	Tac/MTX	2	3	0	0	Pred

Table S1. Clinical characteristics of patients with aGVHD used for in vitro functional assays.

EXP, experiment number; DX, diagnosis; GVHD PROPHY, Graft versus host disease prophylaxis; aGVHD TX, acute GVHD treatment; NHL, non-Hodgkin lymphoma; MM, multiple myeloma, MF, Myelofibrosis; MDS, myelodysplastic syndrome; AML, acute myeloid leukemia; MUD, matched unrelated donor; MRD, matched related donor; Siro, sirolimus; Tac, tacrolimus; MTX, methotrexate; Pred, prednisone > 1 mg/Kg; ECP, extracorporeal photopheresis. All patients received a reduced intensity conditioning based on busulfan and fludarabine combination and a peripheral blood stem cell graft.

TUBE	TARGET	FLUOROCHROME	CLONE	COMPANY	PRODUCT
T CELL TUBE	CD45RA	BV605	HL100	BioLegend	304133
	CD279 PD-1	PE	J105	Invitrogen	12-2799-42
	CD127	APC	eBioRDR5	Invitrogen	17-1278-42
	CD25	FITC	m-A251	BioLegend	356105
	CCR7	BV711	G043-H7	BioLegend	353227
	CD4	BV510	RPA-T4	BioLegend	300545
	CD3	BV786	UCHT1	BioLegend	300472
	CD8	Alexa 700	RPA-T8	BioLegend	301027
	CD95	PeCF594 (PE Dazzle)	DX2	BioLegend	305633
	CD6	BV650	M-T605	BD	743448
APC TUBE	CD45	APC-Cy7	2D1	BD	560178
	LINEAGE:	PE-Cy7			
	CD3		SK7	BD	557851
	CD19		SJ25C1	BD	341093
	CD56		B159	BD	557747
	CD14		M5E2	BD	557742
	HLA-DR	BV510	G46-6	BD	563083
	CD11c	PE-Cy5	B-LY6	BD	551077
	CD123	FITC	AC145	Miltenyi Biotec	130-090-897
	CD166 ALCAM	BV421	3A6	BD	562936
	PD-L1	BV786	MIH1	BD	563739
	CD14	BV605	M5E2	BioLegend	301833

Table S2. Conjugated monoclonal antibodies in the flow cytometry immune monitoring panel. One tube was used for the characterization of CD6 expression on T cells (T CELL TUBE) and another tube for the characterization of ALCAM expression on monocytes and antigen presenting cells (APC TUBE).

TARGET	FLUOROCHROME	CLONE	COMPANY	PRODUCT
CD3	AF700	UCHT1	BD	557943
CD4	BV510	SK3	BD	562970
CD8	PerCP/Cy5.5	RPA-T8	BioLegend	301032
CD25	PE-CF594	M-A251	BD	562403
CD45RO	BV786	UCHL1	BD	564290
CD14	PE-Cy7	M5E2	BioLegend	301814
CD166	BV421	3A6	BD	562936
ANNEXIN V	PE	/	BD	556422
CFSE	CFSE	/	Invitrogen Thermo Fisher Scientific	C34554
ZOMBIE NIR	APC-Cy7	/	BioLegend	423105

Table S3. Conjugated monoclonal antibodies used in the T cell activation assay (Figure 4)

TARGET	FLUOROCHROME	CLONE	COMPANY	PRODUCT
CD4	BV510	SK3	BD	562970
CD8	PerCP/Cy5.5	RPA-T8	BioLegend	301032
CD25	PE-CF594	M-A251	BD	562403
CD45RO	BV786	UCHL1	BD	564290
CD166	BV421	3A6	BD	562936
CFSE	CFSE	/	Invitrogen Thermo Fisher Scientific	C34554
ZOMBIE NIR	APC-Cy7	/	BioLegend	423105

Table S4 Conjugated monoclonal antibodies used for ALCAM and T cell activation assay (Figure 6).

	Day 30 T cell chimerism at 1 month after HCT								
	<95				95-100				
	N	Median	Q1	Q3	N	Median	Q1	Q3	p-value
%CD6$^+$ Treg	56	74.25	68.11	82.68	11	69.9	58.83	80.45	0.26
%CD6$^+$ Tcon	56	98.08	97.07	98.84	11	97.42	95.98	98.1	0.25
%CD6$^+$ CD8$^+$ T cells	56	87.04	82.92	91.7	11	76	70.91	94.49	0.62
%ALCAM in CD14$^+$ monocytes	75	80.44	72.83	85.79	12	83.78	81.16	85.91	0.16
%ALCAM$^+$ mDC	75	18.74	13.51	28.61	12	16.73	10.01	21.91	0.37
%ALCAM$^+$ pDC	75	95	92.05	97.97	12	94.11	88	99.13	0.71
CD6 MFI in CD8 + T cells	56	8886	7225.8	10488	11	9149.6	6234.4	10784	0.77
CD6 MFI in Treg	56	6507.4	5936	7969.9	10	6508.4	4721.9	8022.3	0.49
CD6 MFI in Tcon	56	17057	14328	18599	11	16107	13399	17949	0.44
ALCAM MFI in CD14+ monocytes	75	10131	8379.5	11385	12	12141	8668.4	13496	0.22
ALCAM MFI in mDCs	75	3609.5	3043.6	4314.3	12	3209.7	2914.9	4103.2	0.37
ALCAM MFI in pDCs	75	18307	15962	22602	12	21176	16139	25528	0.30

Table S5. Expression of CD6 and ALCAM in patients with different levels of donor chimerism.

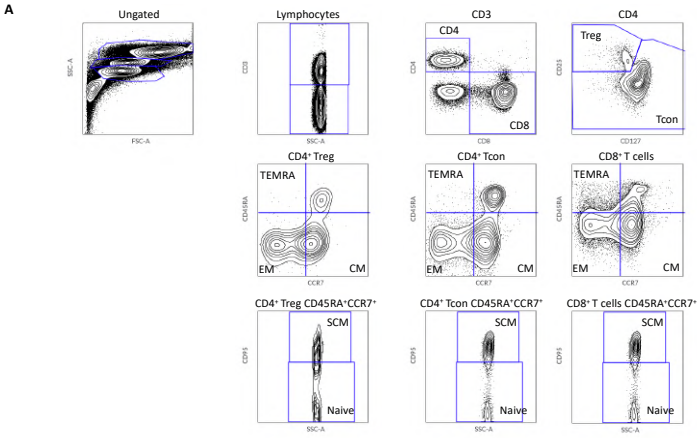

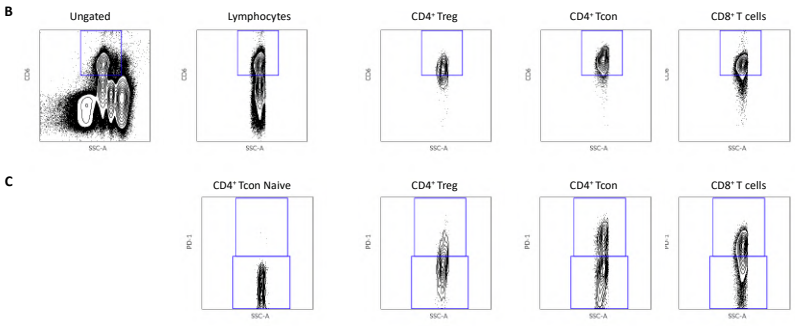

Figure S1. Gating strategy for T cell subset analysis. (A) Three major T cell populations, CD4Treg, CD4Tcon, and CD8 T cells, were defined as $CD3^+CD4^+CD8^-CD25^+CD127^-$, $CD3^+CD4^+CD8^-$ non-Treg cells and $CD3^+CD4^-CD8^+$, respectively. Within each T cell population, subsets were defined as follows: central memory (CM, $CD45RA^-CCR7^+$), effector memory (EM, $CD45RA^-CCR7^-$), terminally differentiated effector memory (TEMRA, $CD45RA^+CCR7^-$), T cells naïve ($CD45RA^+CCR7^+CD95^-$) and stem cell memory (SCM, $CD45RA^+CCR7^+CD95^+$). (B) The threshold of CD6 gate on T cell subsets was made using monocytes as internal negative control. (C) PD-1 expression was monitored on each T cell subset, using Tcon naïve cells as internal negative control. 265 peripheral blood samples were tested with this panel: n=9 HD; n=67 at 1 mo; n=76 at 2 mo; n=78 at 3 mo; n=35 at 6mo.

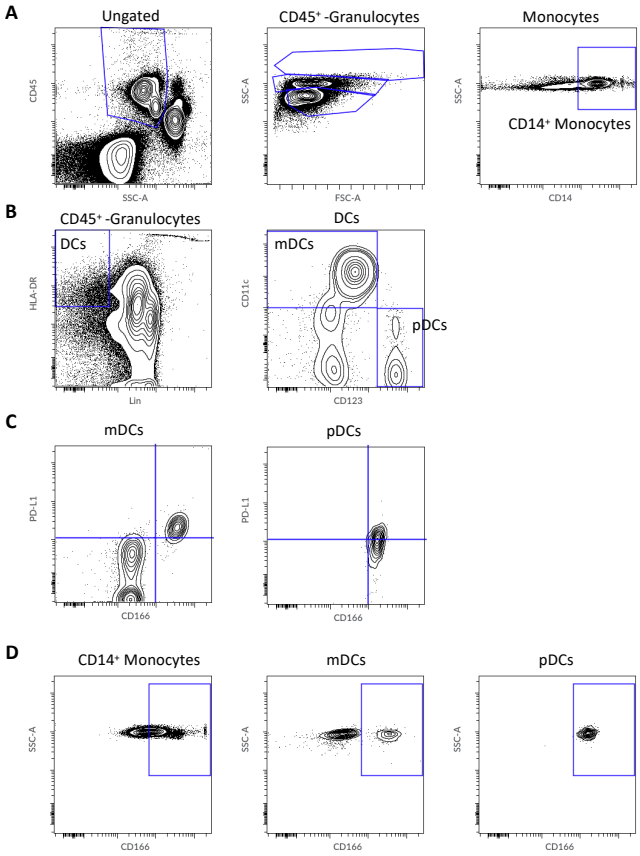

Figure S2. Gating strategy for dendritic cell subsets and monocyte analysis. (A) Monocyte were defined within the CD45$^+$ cells, after excluding granulocytes, based on the SSC-A, FSC-A and CD14 expression. (B) Dendritic cells (DCs) were defined within the CD45$^+$ cells, after excluding granulocytes, based on the positivity of HLA-DR and negativity of lineage markers (CD14, CD3, CD19 and CD56). DC subsets were defined as follows: myeloid DCs (mDCs, CD11c$^+$CD123$^-$) and plasmacytoid DCs (pDCs, CD11c$^-$CD123$^+$). (C) PD-L1 and CD166 (ALCAM) expression on both mDCs and pDCs. (D) CD166 (ALCAM) expression on CD14$^+$ monocytes, mDCs and pDCs. Samples with less than 1000 DC events were excluded from the

analysis. 236 peripheral blood samples were tested with this panel: n=9 HD; n=62 at 1 mo; n=66 at 2 mo; n=69 at 3 mo; n=30 at 6mo.

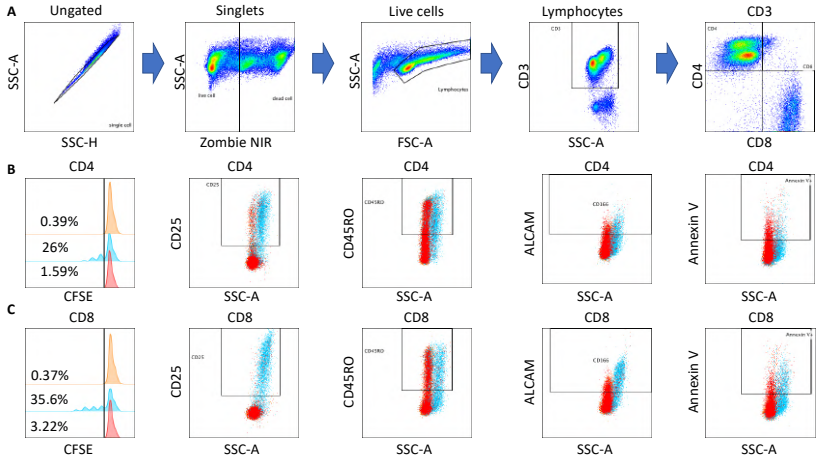

Figure S3. Gating strategy for in vitro functional assays. (A) Example of the gating strategy of $CD4^+$ and $CD8^+$ T cells, after exclusion of doublets and dead cells. Gating strategy on $CD4^+$ T cells (B) and $CD8^+$ T cells (C) for CFSE dilution (T cell proliferation), CD25 (T cell activation), CD45RO (T cell maturation), ALCAM and Annexin V (T cell apoptosis) expression. Cell alone (orange), cells+beads+cetuximab (blue), cells+beads+itolizumab (red).

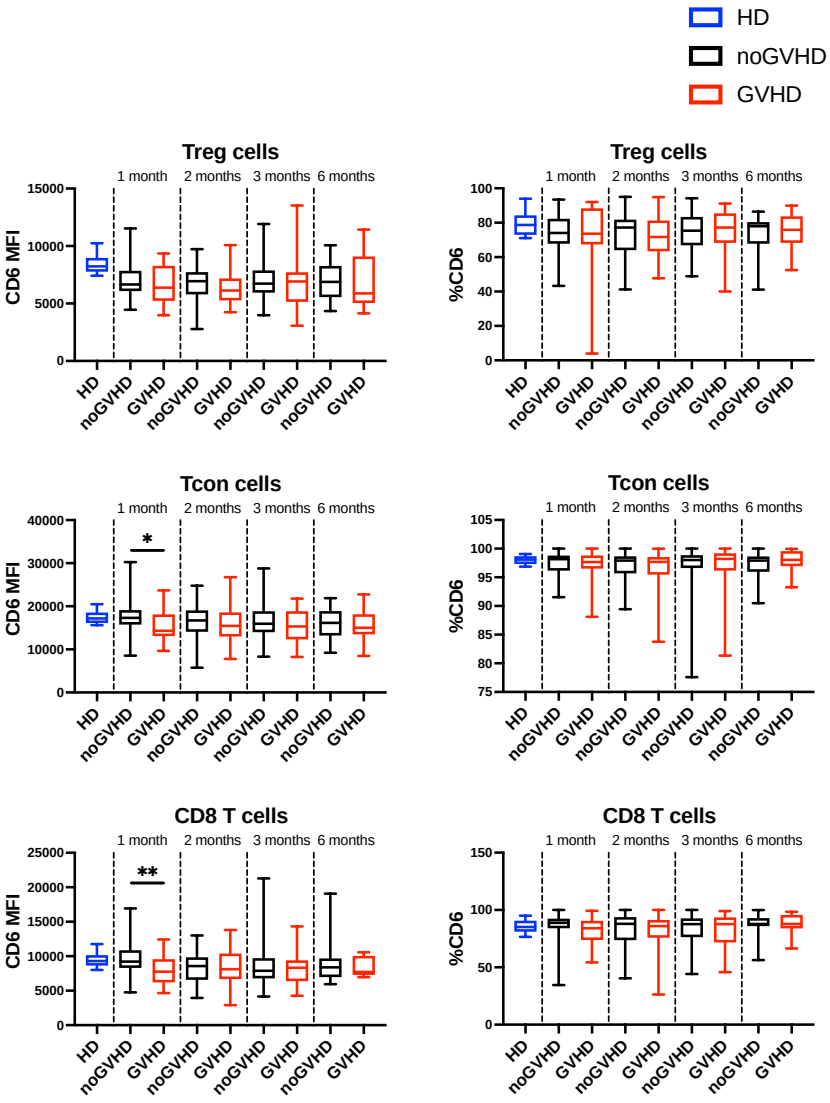

Figure S4. Comparison of CD6 expression on Treg, Tcon and CD8 T cells in patients with and without GVHD at specific time points after transplant. CD6 MFI was lower in GVHD group compared noGVHD group at 1 month after transplant in Tcon and CD8 T cells. Statistically significant differences are noted: * P< 0.05; ** P< 0.01. Wilcoxon rank-sum test. HD, n=9; noGVHD month 1, n=41; GVHD month 1, n=26; noGVHD month 2, n=40; GVHD month 2, n=36;

noGVHD month 3, n=45; GVHD month 3, n=33; noGVHD month 6, n=23; GVHD month 6, n=12.

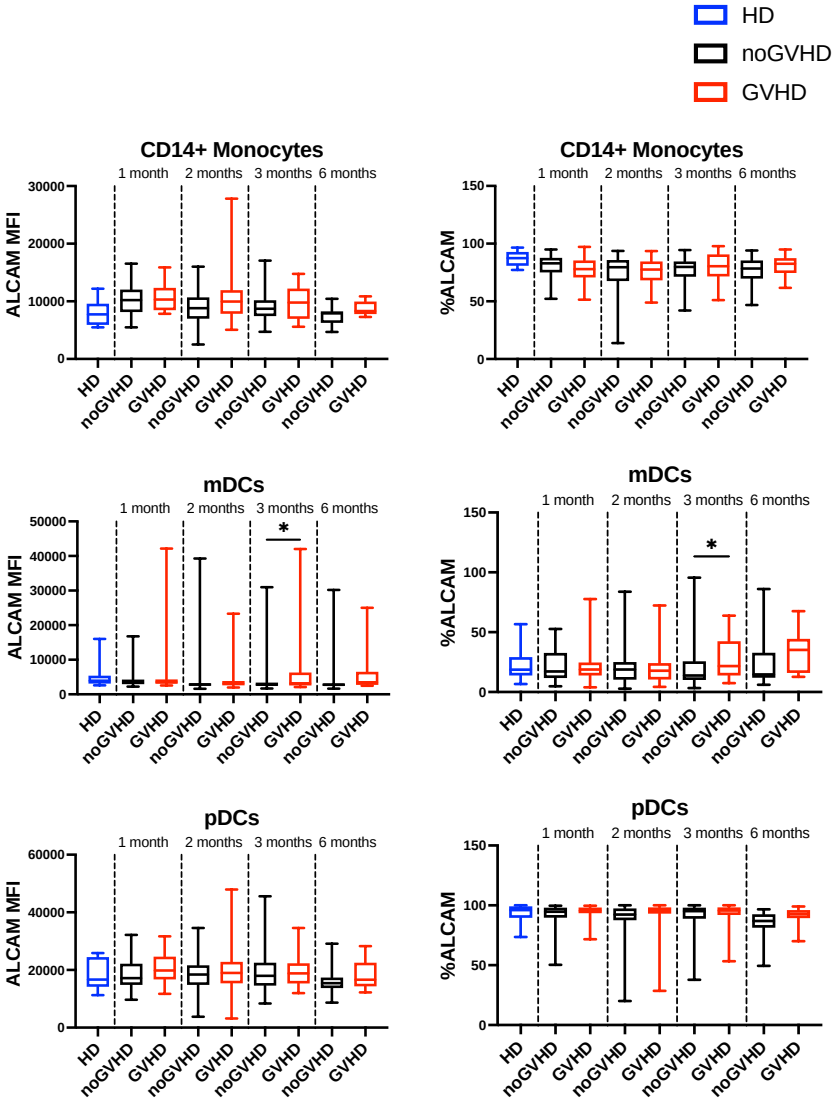

Figure S5. Comparison of ALCAM expression on CD14$^+$ Monocytes, mDCs and pDCs in patients with and without GVHD at specific time points after transplant. ALCAM MFI and % of ALCAM positive cells on mDCs was higher in the GVHD cohort

compared to noGVHD at 3 months after transplant. Statistically significant differences are noted: * P< 0.05; Wilcoxon rank-sum test. HD, n=9; noGVHD month 1, n=41; GVHD month 1, n=26; noGVHD month 2, n=40; GVHD month 2, n=36; noGVHD month 3, n=45; GVHD month 3, n=33; noGVHD month 6, n=23; GVHD month 6, n=12.

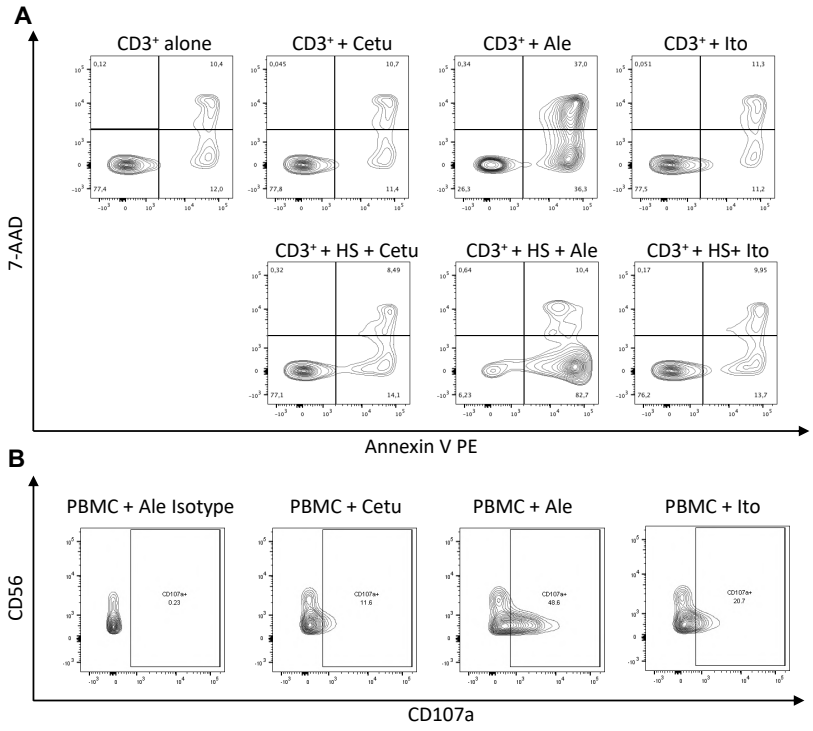

Figure S6. Gating strategy to test itolizumab complement dependent cytotoxicity (CDC), antibody dependent cytotoxicity (ADC) and antibody direct cellular cytotoxicity (ADCC) analysis.
(A) Representative example of percentage of cell lyses, based on the expression of 7-AAD and annexin V. (B) Representative example of CD107a expression on NK cells, as marker of ADCC. An APC-

conjugated mouse isotype was used to design the gate for CD107a. Percentage of cell lysis was calculated by adding the percentage of positive cells for 7-AAD or Annexin V or both. CDC activity was calculated by subtracting the values obtained in the medium + antibody from the values obtained in the culture with medium + antibody + HS. ADC activity was calculated by subtracting the values obtained in the culture with medium alone from the values obtained in the culture with medium + antibody. For ADCC PBMC form HD were cultured in the presence of antibody for 6 hours. Both percentage of cell lyses and CD107a expression on NK cells were evaluated after 6 hours of culture.

Chapter 6

General discussion

Summary, Conclusions and Future Perspectives

Immune reconstitution (IR) after HCT varies dependent of multiple factors and as reported in the review in the chapter 2 of this thesis, it can change between different HCT transplant settings and also within the same group of donors.

We showed how post-transplant cyclophosphamide (PTCy) has an impact in the T- and NK-cell reconstitution after haplo-HCT compared to matched donor (MD) HCT. We highlighted a delay in T- and NK-cell recovery in the first 3 months after haplo-HCT with PTCy compared to MD-HCT with conventional GVHD prophylaxis. Delayed recovery of naive T cells along with a significantly higher Treg-cell/Tcon-cell ratio and PD-1 expression on memory $CD4^+$ T cells likely contribute to the low incidence of cGVHD. Delayed NK-cell reconstitution, with the preferential expansion of immature $CD56^{bright}CD16^-NKG2A^+$ NK cells, may contribute to the higher rate of CMV reactivation after haplo-HCT (1). These observations are in line with a previous publication (2) in which immature NK subsets are detected early after haplo-HCT with PTCy and were associated with loss of KIR-mediated leukemia-killing. These data were confirmed also in a subsequent paper from McCurdy and colleagues (3), in which different donor sources (MD and haplo) with PTCy were analyzed for T- and NK-cell reconstitution. The authors showed, across all the donor groups, that conventional $CD4^+$ T cell recovery, their activation status,

and metabolic signatures are risk factors for aGVHD, and early NK cell recovery protects against relapse, while loss of NK and $CD8^+$ T cell inflammatory signaling predominates in relapsing patients.

Moreover, we demonstrated that the expansion of functionally impaired immature $CD56^{bright}CD16^-$ NK cells after haplo-HCT can be enhanced with *in vitro* interleukin-15 priming (1) This impairment in the NK cell reconstitution after haplo-HCT with PTCy opens the field to post-transplant cellular therapy, such as with the infusion of donor NK cells to prevent or treat leukemia relapse. One of the limitations of the use of donor-derived NK cell is the limited life span and persistence in the recipient. Different platforms were tested to overcome this limit.

Cooley and colleagues treated 42 patients with relapse/refractory myeloid malignancies in a dose-escalation study phase 1/2 trial with rhIL-15 infusion after lymphodepleting chemotherapy and haploidentical NK-cells infusion. They observed robust *in vivo* NK-cell expansion and 35% achieved complete remission. Cytokine release syndrome (CRS) was observed in 56% of patients given subcutaneously rhIL-15 (with concurrent neurologic toxicity in 5 of 9 patients) and was responsive to steroids and tocilizumab (4).

Ciurea and colleagues treated 25 patients in a phase I/II trial using mb-IL21 *ex vivo* expanded donor-derived haploidentical NK cells infused at 1×10^5 - 1×10^8 cells/kg/dose on days −2, +7, and +28 after transplant. Results were compared with an independent case-matched cohort of 160 patients from the CIBMTR database. After a median follow-up of 24 months, the 2-year relapse rate was 4% vs. 38% (p =

0.014), and disease-free survival (DFS) was 66% vs. 44% (p = 0.1) in the cases and controls, respectively (5,6).

In our work, 6 patients with myeloid malignancies, relapsed after haplo-HCT, were treated in a phase I study with donor-derived cytokine-induced memory-like (CIML) NK cells 5 to 10 million cells/kg after lymphodepleting chemotherapy, followed by systemic IL-2 for 7 doses. We observed a rapid expansion and long-term persistence of the infused CIML-NK cells with a positive safety profile (all the infusions were well tolerated, with fever and pancytopenia as the most common adverse events) and a response to therapy in 4 out of 6 patients at day 28 after infusion (7).

Another approach that combines the property of both NK and cytotoxic $CD8^+$ T cells is the use of cytokine-induced killer (CIK) cells. CIK cells showed very little GVHD in several experimental models in the presence of either minor or major histocompatibility mismatches (8). In the work by Introna and colleagues seventy-four patients who relapsed after HCT were enrolled in a phase IIA study and treated with the sequential infusion of donor lymphocyte infusion (DLI) followed by CIK cells. Overall, 12 patients (16%) developed acute aGVHD, mostly after DLI infusions. cGVHD was observed in 11 patients (15%). A complete response was observed in 26%, partial response in 4%, stable disease in 11%, early death in 3%, and disease progression in 56% (9). In our institution, an ongoing phase I/II trial aims to test the safety of haplo-CIK infusions in relapsed patients after haplo-HCT (NCT03821519).

Finally, both NK and T cells can be used as a platform to produce chimeric antigen receptor (CAR) cells against specific tumor

antigens. In the setting of disease relapse after transplant, donor derived CAR cells represent a suitable tool, but with the warning of inducing GVHD. For this reason, different strategy using off the shelf umbilical-cord-derived CAR-NK cells (10) and donor-derived CAR-CIK cells (11) were tested with promising results in terms of safety and efficacy.

Future approaches are needed especially in the field of relapsed/refractory myeloid malignancies. In this regard, we are planning to test the safety and efficacy of CIK cells armored with a dual CD33/CD123 CAR in patients affected by relapsed/refractory myeloid malignancies.

The last part of this thesis is focused on the balancing of T cell response to control GVHD occurrence. Indeed, multiple co-inhibitory and co-activating receptor regulate the T cell response and fate (12). CD6, a pan-T cell co-stimulatory receptor, helps to stabilize the immunological synapse between the T cell and the APC, upon ligation, with its ligand, antigen activated leukocyte cell adhesion molecule (ALCAM). In this context, CD6-ALCAM binding promotes T cell activation, proliferation, maturation, and trafficking from the intravascular space into tissues. In our study, we showed that CD6 T cells reconstituted early after transplant with Treg expressing lower levels of CD6 compared to Tcon and $CD8^+$ T cells. After onset of aGVHD, both CD6 and ALCAM expression was maintained. Itolizumab inhibited $CD4^+$ and $CD8^+$ T cell activation and proliferation in the setting of aGVHD in ex vivo experiments, without mediate direct cytolytic activity or antibody-dependent cytotoxicity (13).

A humanized xenograft mouse model was used to investigate the ability of itolizumab to prevent and treat GVHD. Mice were treated

with itolizumab, abatacept (CTLA4-Ig), or vehicle, starting one day prior to PBMC transplantation to investigate prevention and at day 5 post-PBMC transfer, to investigate the therapeutic effect of itolizumab. Treatment with itolizumab either for prevention or for treatment schedule, significantly decreased mortality compared to the vehicle control and this decrease was similar to the positive control group treated with abatacept (14).

Altogether, our results identify the CD6-ALCAM pathway as a potential target for aGVHD control and a phase I/II study using itolizumab as first line treatment in combination with steroids for patients with aGVHD is currently ongoing (EQUATE study, NCT03763318). The objective of this study is to evaluate the safety, tolerability, pharmacokinetics (PK), pharmacodynamics (PD, as change in CD6 surface expression on $CD4^+$ cells), and clinical activity of itolizumab in subjects with newly diagnosed aGVHD. Preliminary results were presented at the annual ASH international conference (15). Twenty-two adult subjects with Grade III-IV aGVHD who initiated steroid treatment within 7 days prior to the first dose of itolizumab have enrolled in EQUATE at 0.4 mg/kg (n=4), 0.8 mg/kg (n=9), or 1.6 mg/kg (n=9), administered IV every 2 weeks x 5 doses. The median follow-up is 146 days (range: 14-355 days). All enrolled patients had grade III or IV aGVHD and 91% had lower GI involvement. All subjects received at least one dose and 15 received at least 2 doses of itolizumab. All subjects experienced at least 1 adverse event (AE). Serious AEs occurred in 14 subjects (64%), with 9 (41%) reporting infection-related SAEs. There were 8 deaths. Six subjects (27.3%) had SAEs leading to death (3 at 0.8 mg/kg and 3 at 1.6 mg/kg): sepsis (n=1), Staphylococcal

sepsis (n=1), Klebsiella sepsis (n=1), intestinal infarction (n=1), cardiac arrest (n=1), and GVHD (n=1). Another 2 deaths occurred >100 days post-last dose due to progressive aGVHD (n=1) and primary disease relapse (n=1). Across all doses, the complete response (CR) rate was 55% at both Day 15 and Day 29, and the overall response rate (ORR) was 73% at Day 15 and 68% at Day 29. At Day 169 (n=20), non-relapse mortality (NRM) was 35%, overall survival was 65%. Of note, the 10 subjects who achieved an early CR at Day 15 had a lower rate of NRM at Day 169 (20%) compared to the 10 subjects who had a very good partial response (VGPR), partial response (PR), no response (NR), or disease progression (50%). Itolizumab substantially decreased the levels of cell surface CD6 on circulating T cells after the first dose in a dose-dependent manner and maintained that decrease throughout the treatment period. Notable findings by immunophenotyping included: (1) an increase in the ratio of T regulatory to T effector cells at 0.8 and 1.6 mg/kg dose-level by Day 15, and (2) decreases of PD-1 expression on T cells and of ALCAM on CD14+ monocytes at all dose-levels by day 8. This indicates itolizumab can reduce activation of T effector cells and monocytes. Higher itolizumab trough concentrations on day 15, achieved at higher dose-levels, correlated with a higher rate of CR at day 15 (15).

These promising data support the design and initiation of a pivotal phase 3, placebo-controlled clinical trial to assess itolizumab in combination with corticosteroids as first-line treatment of aGVHD. Our center is going to participate to this phase III trial.

While ruxolitinib, a JAK1/2 inhibitor, is currently the only drug approved for the treatment of steroid refractory aGVHD (16) several

drugs that target different T cell co-stimulatory molecules are currently being tested in preclinical models and in patients with aGVHD (12)(17). Abatacept, a CTLA-4 Ig targeting the CD28/CTLA-4-CD80/CD86 axis, has been tested for aGVHD prevention in a phase II randomized placebo-controlled trial in combination with calcineurin inhibitor and methotrexate in 8/8 and 7/8 HLA-matched HCT, showing significant lower rates of grades III-IV aGvHD (18). This favorable result led to FDA breakthrough therapy designation for the prevention of moderate to severe aGVHD in HCT from unrelated donors. In this scenario, itolizumab may be a promising agent for either prevention or treatment of aGVHD.

Moreover, Ruth and colleagues demonstrated that targeting CD6 may also be a novel approach to enhance cancer immunotherapy (19). The combined capabilities of an anti-CD6 monoclonal antibody to control autoimmunity through effects on $CD4^+$ T cells and the enhanced killing of cancer cells through distinct effects on $CD8^+$ T cells and NK cells, may represent a new approach to induce tolerance without suppressing GVL activity after HCT.

In conclusion, the results collected in this PhD thesis highlight the need of balancing the effector and tolerogenic properties of the immune system reconstituting after HCT and suggest different strategies to enhance or moderate the T and NK cells functions. Only with a better understanding of the transplant immunology it will be possible to achieve significant translational and clinical advances.

References

1. Rambaldi B, Kim HT, Reynolds C, Rai SC, Arihara Y, Kubo T, et al. Impaired T- And NK-cell reconstitution after haploidentical HCT with posttransplant cyclophosphamide. Blood Adv. 2021;5.
2. Russo A, Oliveira G, Berglund S, Greco R, Gambacorta V, Cieri N, et al. NK cell recovery after haploidentical HSCT with posttransplant cyclophosphamide: dynamics and clinical implications. Blood [Internet]. 2018;131:247–62. Available from: https://doi.org/10.1182/blood-2017-05-780668
3. McCurdy SR, Radojcic V, Tsai H-L, Vulic A, Thompson E, Ivcevic S, et al. Signatures of GVHD and relapse after posttransplant cyclophosphamide revealed by immune profiling and machine learning. Blood [Internet]. 2022;139:608–23. Available from: https://doi.org/10.1182/blood.2021013054
4. Cooley S, He F, Bachanova V, Vercellotti GM, DeFor TE, Curtsinger JM, et al. First-in-human trial of rhIL-15 and haploidentical natural killer cell therapy for advanced acute myeloid leukemia. Blood Adv [Internet]. 2019;3:1970–80. Available from: https://doi.org/10.1182/bloodadvances.2018028332
5. Ciurea SO, Schafer JR, Bassett R, Denman CJ, Cao K, Willis D, et al. Phase 1 clinical trial using mbIL21 ex vivo–expanded donor-derived NK cells after haploidentical transplantation. Blood [Internet]. 2017;130:1857–68. Available from: https://doi.org/10.1182/blood-2017-05-785659
6. Ciurea SO, Kongtim P, Soebbing D, Trikha P, Behbehani G, Rondon G, et al. Decrease post-transplant relapse using donor-derived expanded NK-cells. Leukemia [Internet]. 2022;36:155–64. Available from: https://doi.org/10.1038/s41375-021-01349-4
7. Shapiro RM, Birch GC, Hu G, Vergara Cadavid J, Nikiforow S, Baginska J, et al. Expansion, persistence, and efficacy of donor memory-like NK cells infused for posttransplant relapse. J Clin Invest [Internet]. The American Society for Clinical Investigation; 2022;132. Available from: https://doi.org/10.1172/JCI154334
8. Nishimura R, Baker J, Beilhack A, Zeiser R, Olson JA, Sega EI, et al. In vivo trafficking and survival of cytokine-induced killer cells resulting in minimal GVHD with retention of antitumor activity. Blood [Internet]. 2008;112:2563–74. Available from: https://www.sciencedirect.com/science/article/pii/S0006497120598819
9. Introna M, Lussana F, Algarotti A, Gotti E, Valgardsdottir R, Micò C, et al. Phase II Study of Sequential Infusion of Donor Lymphocyte Infusion

and Cytokine-Induced Killer Cells for Patients Relapsed after Allogeneic Hematopoietic Stem Cell Transplantation. Biol Blood Marrow Transplant [Internet]. Elsevier; 2017;23:2070–8. Available from: https://doi.org/10.1016/j.bbmt.2017.07.005

10. Liu E, Marin D, Banerjee P, Macapinlac HA, Thompson P, Basar R, et al. Use of CAR-Transduced Natural Killer Cells in CD19-Positive Lymphoid Tumors. N Engl J Med [Internet]. Massachusetts Medical Society; 2020;382:545–53. Available from: https://doi.org/10.1056/NEJMoa1910607
11. Magnani CF, Gaipa G, Lussana F, Belotti D, Gritti G, Napolitano S, et al. Sleeping Beauty–engineered CAR T cells achieve antileukemic activity without severe toxicities. J Clin Invest [Internet]. The American Society for Clinical Investigation; 2020;130:6021–33. Available from: https://doi.org/10.1172/JCI138473
12. Hill GR, Koyama M. Cytokines and costimulation in acute graft-versus-host disease. Blood [Internet]. 2020;136:418–28. Available from: https://doi.org/10.1182/blood.2019000952
13. Rambaldi B, Kim HT, Arihara Y, Asano T, Reynolds C, Manter M, et al. Phenotypic and functional characterization of the CD6-ALCAM T cell costimulatory pathway after allogeneic cell transplantation. Haematologica [Internet]. 2022; Available from: https://haematologica.org/article/view/haematol.2021.280444
14. Ng CT, Ampudia J, Soiffer RJ, Ritz J, Connelly S. Itolizumab As a Potential Therapeutic for the Prevention and Treatment of Graft Vs Host Disease. Blood [Internet]. 2019;134:5603. Available from: https://doi.org/10.1182/blood-2019-122787
15. Koreth J, Chhabra S, Pidala J, Shea TC, Jagasia M, Waller EK, et al. Equate, a Phase 1b/2 Study Evaluating the Safety, Tolerability, Pharmacokinetics, Pharmacodynamics, and Clinical Activity of a Novel Targeted Anti-CD6 Therapy, Itolizumab, in Subjects with Newly Diagnosed Acute Graft Versus Host Disease. Blood [Internet]. 2019;134:4516. Available from: https://doi.org/10.1182/blood-2019-127325
16. Zeiser R, von Bubnoff N, Butler J, Mohty M, Niederwieser D, Or R, et al. Ruxolitinib for Glucocorticoid-Refractory Acute Graft-versus-Host Disease. N Engl J Med [Internet]. Massachusetts Medical Society; 2020;382:1800–10. Available from: https://doi.org/10.1056/NEJMoa1917635

17. Gooptu M, Koreth J. Translational and clinical advances in acute graft-versus-host disease. Haematologica [Internet]. 2020;105:2550–60. Available from: https://haematologica.org/article/view/haematol.2019.240309
18. Watkins B, Qayed M, McCracken C, Bratrude B, Betz K, Suessmuth Y, et al. Phase II Trial of Costimulation Blockade With Abatacept for Prevention of Acute GVHD. J Clin Oncol [Internet]. Wolters Kluwer; 2021;39:1865–77. Available from: https://doi.org/10.1200/JCO.20.01086
19. Ruth JH, Gurrea-Rubio M, Athukorala KS, Rasmussen SM, Weber D, Randon PM, et al. CD6 is a target for cancer immunotherapy. JCI Insight [Internet]. The American Society for Clinical Investigation; 2021;6:e145662. Available from: https://doi.org/10.1172/jci.insight.145662

Chapter 7

List of publication

- Baumeister SHC, **Rambaldi B**, Shapiro RM, Romee R. Key Aspects of the Immunobiology of Haploidentical Hematopoietic Cell Transplantation. *Front Immunol.* 2020 Feb 14;11:191. doi: 10.3389/fimmu.2020.00191. eCollection 2020. PMID: 32117310
- **Rambaldi B**, Kim HT, Reynolds C, Chamling Rai S, Arihara Y, Kubo T, Buon L, Gooptu M, Koreth J, Cutler C, Nikiforow S, Ho VT, Alyea EP, Antin JH, Wu CJ, Soiffer RJ, Ritz J, Romee R. Impaired T- and NK-cell reconstitution after haploidentical HCT with posttransplant cyclophosphamide. *Blood Adv.* 2021 Jan 26;5(2):352-364. doi: 10.1182/bloodadvances.2020003005. PMID: 33496734
- Shapiro RM, Birch GC, Hu G, Vergara Cadavid J, Nikiforow S, Baginska J, Ali AK, Tarannum M, Sheffer M, Abdulhamid YZ, **Rambaldi B**, Arihara Y, Reynolds C, Halpern MS, Rodig SJ, Cullen N, Wolff JO, Pfaff KL, Lane AA, Lindsley RC, Cutler CS, Antin JH, Ho VT, Koreth J, Gooptu M, Kim HT, Malmberg KJ, Wu CJ, Chen J, Soiffer RJ, Ritz J, Romee R. Expansion, persistence, and efficacy of donor memory-like NK cells infused for posttransplant relapse. *J Clin Invest.* 2022 Jun 1;132(11):e154334. doi: 10.1172/JCI154334. PMID: 35349491
- **Rambaldi B**, Kim HT, Arihara Y, Asano T, Reynolds C, Manter M, Halpern M, Weber A, Koreth J, Cutler C, Gooptu M, Nikiforow S, Ho VT, Antin JH, Romee R, Ampudia J, Ng C, Connelly S, Soiffer RJ, Ritz J. Phenotypic and functional characterization of the

CD6-ALCAM T cell costimulatory pathway after allogeneic cell transplantation. *Haematologica*. 2022 Apr 28. doi: 10.3324/haematol.2021.280444. Online ahead of print. PMID: 35484649

Other publications published during the PhD period:

- Podda GM, Fiorelli EM, Birocchi S, **Rambaldi B**, Di Chio MC, Casazza G, Cattaneo M. Treatment of immune thrombocytopenia (ITP) secondary to malignancy: a systematic review. *Platelets*. 2022 Jan 2;33(1):59-65. doi: 10.1080/09537104.2020.1822521. Epub 2020 Sep 23. PMID: 32967527
- Farina M, Bernardi S, Gandolfi L, Zanaglio C, Morello E, Turra A, Zollner T, Gramegna D, **Rambaldi B**, Cattina F, Polverelli N, Malagola M, Russo D. Case Report: Late Onset of Myelodysplastic Syndrome From Donor Progenitor Cells After Allogeneic Stem Cell Transplantation. Which Lessons Can We Draw From the Reported Case? *Front Oncol*. 2020 Oct 14;10:564521. doi: 10.3389/fonc.2020.564521. eCollection 2020. PMID: 33178592
- Malagola M, Greco R, Santarone S, Natale A, Iori AP, Quatrocchi L, Barbieri W, Bruzzese A, Leotta S, Carotti A, Pierini A, Bernardi S, Morello E, Polverelli N, Turra A, Cattina F, Gandolfi L, **Rambaldi B**, Lorentino F, Serio F, Milone G, Velardi A, Foà R, Ciceri F, Russo D, Peccatori J. CMV Management with Specific Immunoglobulins: A Multicentric Retrospective Analysis on 92 Allotransplanted Patients. *Mediterr J Hematol Infect Dis.* 2019 Sep

1;11(1):e2019048. doi: 10.4084/MJHID.2019.048. eCollection 2019. PMID: 31528314

- **Rambaldi B**, Romee R. Inducing Fat to Feed a Natural Killer of Malignancy. *Mol Ther.* 2019 May 8;27(5):898-899. doi: 10.1016/j.ymthe.2019.04.005. Epub 2019 Apr 13. PMID: 30992190

Acknowledgments

This PhD program and the people met on this path, gave me the opportunity to understand the importance of pursuing good immunology base science at the bench side to overcome critical clinical issues at the bed side.

This work was done on the supervisor of Prof. Jerome Ritz and Prof. Rizwan Romee at Dana Farber Cancer Center Institute (DFCI), Harvard Medical School, Boston, MA with the support of Equillium founding and of the Ph.D. Program in Translational and Molecular Medicine (DIMET) with the supervision of Prof. Andrea Biondi.

I would like to thank all the members of Ritz's and Romee's Laboratory and all the doctors of the BMT unit at DFCI for the important contribution to these works, in particular: Carol Reynolds, Sharmila Chamling Rai, Takeru Asano, Yohei Arihara, Tomohiro Kubo, Yusuke Kamihara, Juliana Vergara, Roman Shapiro, Mohsin Maqbool, Mahasweta Gooptu, John Koreth, Corey Cutler, Sarah Nikiforow, Vincent T. Ho, Edwin P. Alyea, Joseph H. Antin, Robert J. Soiffer. Particularly, I would like to thank Dr. Romee for his constant support and encouragement, Dr. Soiffer for giving me the opportunity to join the institute.

A special thanks is to Dr. Ritz for taking me in his group and for being a great mentor, for teaching me a solid scientific method and for supporting me during the research path.

I would like to thank Prof. Andrea Biondi for being such a great teacher and dear friend. Prof. Biondi has inspired me, as many other students during the years, to be good scientist and at a same time good doctor, caring for patients on a daily basis.

Thank to Dr. Marta Serafini e Dr. Alice Pievani for inspiring me and for advising me to undertake the PhD adventure.

I would like to thank all the people of the Hematology Unit and of the Paolo Belli Laboratory of Papa Giovanni XXIII Bergamo, for welcoming me during the complicated time of the COVID pandemic, especially hard for Bergamo city. A particular mention to Gianmaria Borleri for teaching me how important is to make science with the enthusiasm of the beginning, to be always curious and to study every day.

Thank to my family and friends, for supporting me and inspire me to be a better human being, a good scientist, and a compassionate doctor.

A special thanks to my husband Giacomo, who has always been here for me. Thank you for being supportive, enthusiastic and ready for new adventures. Also, thank you for bringing me pizza in the Lab at 10 pm!

Finally, most importantly, I would like to thank all the patients and their family that I have the honor to meet in my path. They gave me more that I could expect and deserve. They remain my first inspiration for the present work and for the future ones.